RADIOLYSIS OF AMINO ACIDS: A STUDY USING RAMAN SPECTROSCOPY, ULTRAVIOLET-VISIBLE SPECTROPHOTOMETRY AND ELECTROSPRAY IONIZATION MASS SPECTROMETRY

A Thesis

by

JIJIE LOU

Submitted to the Office of Graduate and Professional Studies of
Texas A&M University
in partial fulfillment of the requirements for the degree of

MASTER OF SCIENCE

Chair of Committee,	Gamal Akabani
Committee Members,	Marlan O. Scully
	John R. Ford
	Lisa M. Perez
Head of Department,	Yassin A Hassan

December 2014

Major Subject: Nuclear Engineering

ABSTRACT

Amino acids are basic components of proteins and play a crucial role in the development and treatment of chronic diseases. Raman spectroscopy, as a non-destructive tool that requires little sample preparation, has been widely used *in vitro* and *in vivo* studies. In the current study, twenty amino acids in solid state and aqueous or 0.5 M hydrogen chloride (HCl) solution were irradiated to 10, 25 and 50 kGy using an electron beam and analyzed using Raman spectroscopy, ultraviolet-visible (UV-Vis) spectrophotometry and electrospray ionization mass spectrometry (ESI-MS). Raman spectroscopy revealed spectral signatures of radiolysis of amino acids, which were related to the specific molecular vibration and could be used for non-invasive analysis of radiation damage in *vivo*. Correlation between the absorbed dose and UV-Vis absorbance of amino acids was modeled using the Arrhenius equation to explain the nature of radical effects during irradiation. Finally, the results from ESI-MS revealed the modification of molecules after radiation.

The relative stability to radiolysis of twenty amino acids was estimated from the results of Raman spectroscopy, UV-Vis spectrophotometry, and ESI-MS, and compared with previous work. The ability of three techniques to identify the effects of radiolysis on amino acids in solution was evaluated. To our knowledge, this study is the first attempt to combine these three observational techniques to explore the effects of radiation on amino acids and was shown to be a promising strategy for further application *in vivo* studies.

DEDICATION

This thesis is dedicated to my family for their endless love, support and encouragement.

ACKNOWLEDGEMENTS

Thanks go to my friends and colleagues and the department faculty and staff for making my time at Texas A&M University a great experience.

I appreciate the technique assistance and support from my committee, Dr. Marlan O. Scully, Dr. John R. Ford, and Dr. Lisa M. Perez.

I want to give a special recognition to my advisor, Dr. Gamal Akabani for directing me thought my research work, guiding me through the development of my career, and for being a great friend.

I would like to thank my boyfriend Qize He for his love and support. Finally, thanks to my parents for their encouragement, patience and immeasurable love.

NOMENCLATURE

AD	Alzheimer disease
APCI	Atmospheric pressure chemical ionization
BCAA	Bbranched-chain amino acids
CHCA	α-Cyano-4-hydroxycinnamic acid
DFT	Density functional theory
DOPA	Dihydroxyphenylalanine
DSC	Differential scanning calorimetry
EMSC	Extended multiplicative signal correction
EPR	Electron spin resonance
ESI	Electrospray Ionization
ESI-MS	Electrospray Ionization Mass Spectrometry
ESI-MS	Electrospray ionization-mass spectrometry
ESR	Electron Spin Resonance
FTIR	Fourier Transform Infrared Spectrometer
GC-MS	Gas chromatography-mass spectrometry
GC-MS	Gas chromatography mass spectrometry
HAS	Human serum albumin
HCl	Hydrogen Chloride
HF	Hartree–Fock

HPLC–MS/MS	High-performance liquid chromatography associated with tandem mass spectrometry
IAsLS	Improved asymmetric least squares
Kyn	Kynurenine
mAb	Monoclonal antibody
MALDI	Matrix-assisted laser desorption/ionization
MP	Møller–Plesset perturbation
MTBSTFA	N-tert-butyldimethylsilyl-N-methyltrifluoroacetamide
NADH	Nnicotinamide adenine dinucleotide dehydrogenase
NCEBR	National Center for Electron Beam Research
NFK	N-formylkynurenine
NO	Nitric oxide
OH-Trp	Hydroxytryptophan
ORD	Optical rotatory dispersion
PD	Parkinson's disease
SERS	Surface-enhanced Raman spectroscopy
SERRS	Surface-enhanced resonance Raman spectroscopy
SOPs	Standard operating procedures
TC	Temporal cortex
UV-Vis	Ultraviolet-visible
VUV	Vacuum ultraviolet

TABLE OF CONTENTS

Page

LIST OF FIGURES

Page

LIST OF TABLES

Page

CHAPTER I

INTRODUCTION TO AMINO ACIDS

1.1 Introduction to amino acids

1.1.1 Basic concepts about amino acids

Amino acids are an important class of molecules with the same defining property: including a carboxylic acid group and an amino group both linked to the same carbon atom, which is called the α-carbon. Twenty types of amino acids are encoded directly by triple codons in the genetic code, and commonly found in proteins, each with a unique side chain attached to the α-carbon atom. The variation of chemical property of amino acids is due to the side chains attached to the α-carbons. The structures of 20 amino acids are shown in Fig. 1.1.

1.1.2 Classification of amino acids

Based on the structures of the side chains, amino acids can be assorted into seven main groups. The detailed classification of the 20 amino acids is given in the Table 1.1. Proline is an imino acid, due to lacking a primary amino group, also named as "N-alkylated alpha-amino acid".

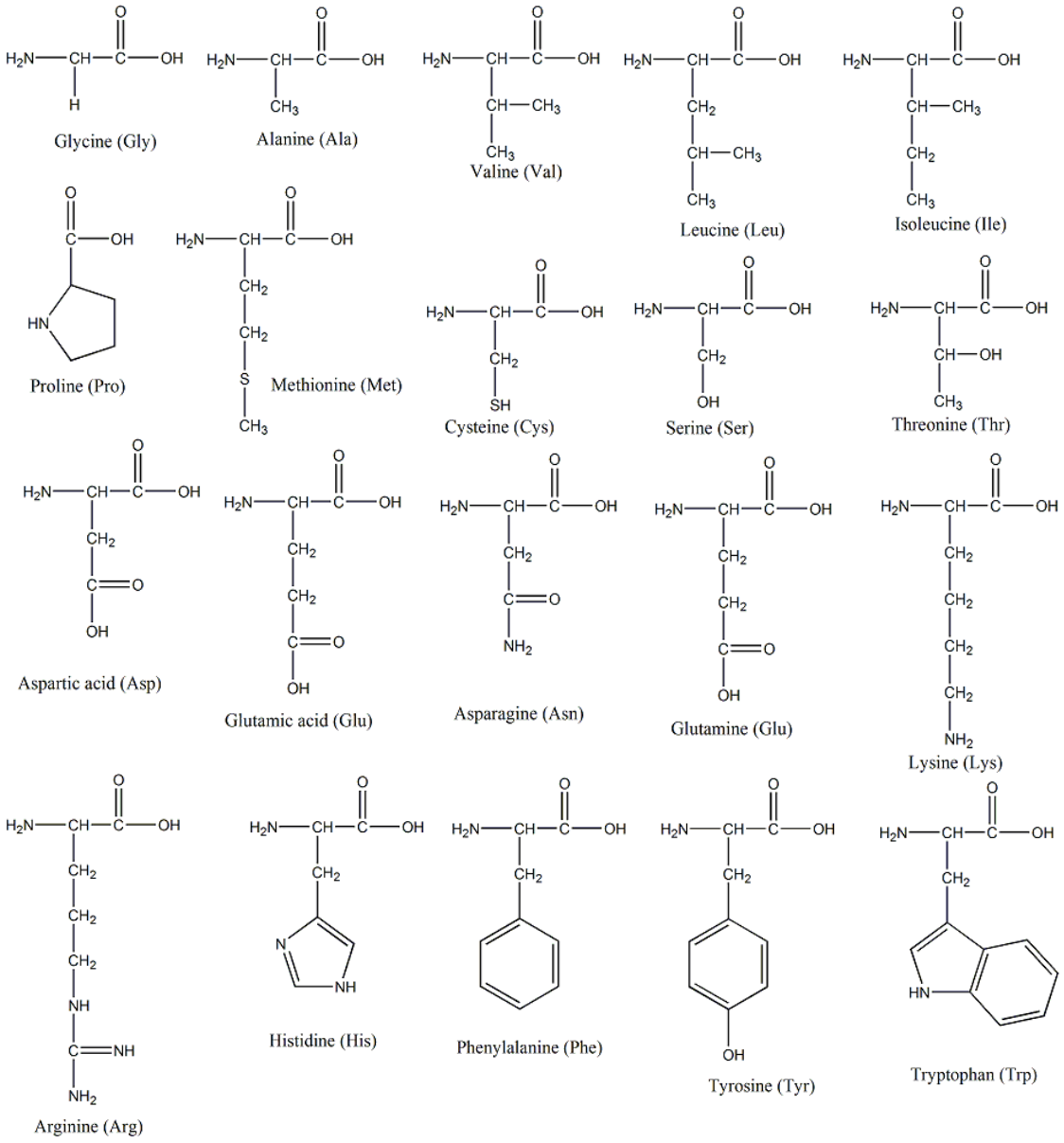

Figure 1.1. Structures and abbreviations of 20 amino acids.

Table 1.1. Classification of 20 amino acids according to their side chains	
Class	Name of amino acids
Aliphatic	Glycine, Alanine, Valine, Leucine, Isoleucine
Neutral	Serine, Threonine, Asparagine, Glutamine
Aromatic	Phenylalanine, Tyrosine, Tryptophan
Basic	Histidine, Lysine, Arginine
Acidic	Aspartate, Glutamate,
Sulfur-containing	Cysteine, Methionine
Imino acid	Proline

The phrase "branched-chain amino acids" (BCAA) refers to the amino acids having aliphatic side chains, which are non-linear, including leucine, isoleucine, and valine.

1.1.3 Structure changes of amino acids

All amino acids (except glycine) have structures as optical isomers in both *D*- and *L*-forms. The majority of carboxylate groups (-COOH) can be deprotonated to become negative carboxylates ($-COO^-$), at a pH greater than the pKa of the carboxylate ion, and amino groups ($-NH_2$) can be protonated to become positive ammonium groups ($-NH_3^+$)

at a pH lower than the pKa of the ammonium group. At a pH between the ranges, α-amino acids containing a negative carboxylate and a positive ammonium group, have net zero charge, the structure of which is known as a zwitterion. The fully neutral structure is less than 1/107 in aqueous solution. In solid phase and crystallize, amino acids exist as zwitterions.

The covalent linkage between two adjacent amino acids in a protein chain is called a peptide bond. Cells use amino acids to build proteins by the polymers of amino folding into a unique three-dimensional structure.

1.1.4 Intestinal amino acid uptake

The amino acids classified as essential or nonessential are listed in Table 1.2. Arginine, methionine and phenylalanine are only considered essential in certain cases. Arginine, the majority of which is cleaved to form urea, is synthesized at a rate insufficient to meet the growth needs. Methionine and phenylalanine are utilized by the body to produce cysteine and tyrosine, respectively, if the latter amino acids are not adequately supplied in the diet.

Table 1.2. Essential and nonessential amino acids			
Nonessential		**Essential**	
Alanine	Glutamine	Arginine*	Methionine*
Asparagine	Glycine	Histidine	Phenylalanine*
Aspartate	Proline	Isoleucine	Threonine
Cysteine	Serine	Leucine	Tyrptophan
Glutamate	Tyrosine	Lysine	Valine

* means the amino acids only consider essential in certain cases.

1.2 Relevance of amino acids in health and disease

1.2.1 The antioxidant activity and repair ability of amino acids

For years, it has been shown in epidemiological studies that there is a positive correlation between the oxidation stress and the development of chronic disease. Even though plenty of antioxidant compounds have been reported to be capable of reducing the oxidative stress in biological system, few studies have been reported examining the structural characters of those compounds which produce antioxidants. Amino acids, containing the same amine-carboxylic acid structure with the unique side chain, can function as antioxidants both as free compounds, such as glutathione, which is a cysteine-glutamic acid-glycine tripe tide, and in the active sites of antioxidant enzymes. In a recent study by Garrett *et al.*, the relationship between the repair ability and structural character of 20 amino acids has been examined using the oxygen radical absorbance capacity combining a simplest-case amino acid model.[1] The data being

collected has been successfully applied to predict the antioxidant activities of other compounds.

In another study by Milligan *et al.*, the repair ability of cystine, histidine, methionine, tryptophan, tyrosine, and their simple ester and amide derivatives were examined by reacting with guanyl radicals in plasmid DNA.[2] It was revealed that cysteine, methionine, tyrosine and particularly tryptophan derivatives reacted to repair guanyl radicals. Therefore, it can be concluded that amino acid residues in DNA binding proteins such as histones might be able to repair DNA damage produced by the direct effect of ionizing radiation.

1.2.2 Effect of sulfur-containing amino acids on body and immune system

Sulfur is one of the most abundant elements in living organisms and it is mainly provided by the intake of the methionine. Methionine controls the initiation of protein synthesis, and it governs major metabolic and catalytic activities, and may undergo reversible redox processes safeguarding protein integrity.[3] Whenever methionine is withdrawn from customary diets, it can cause great loss of lean body mass. Deprivation of sulfur increases the risk of cardiovascular disorders, which has been considered a significant risk to people with vegetarian diets. Moreover, animal studies have shown that an excess ratio of methionine in maternal diet is critical for fetal growth development, affecting both short-term reproductive function and the long-term physiology of the offspring.[4] The methionine and folic acid cycle is shown in Fig. 1.2. Methionine requirements can be affected by components in the cycle.

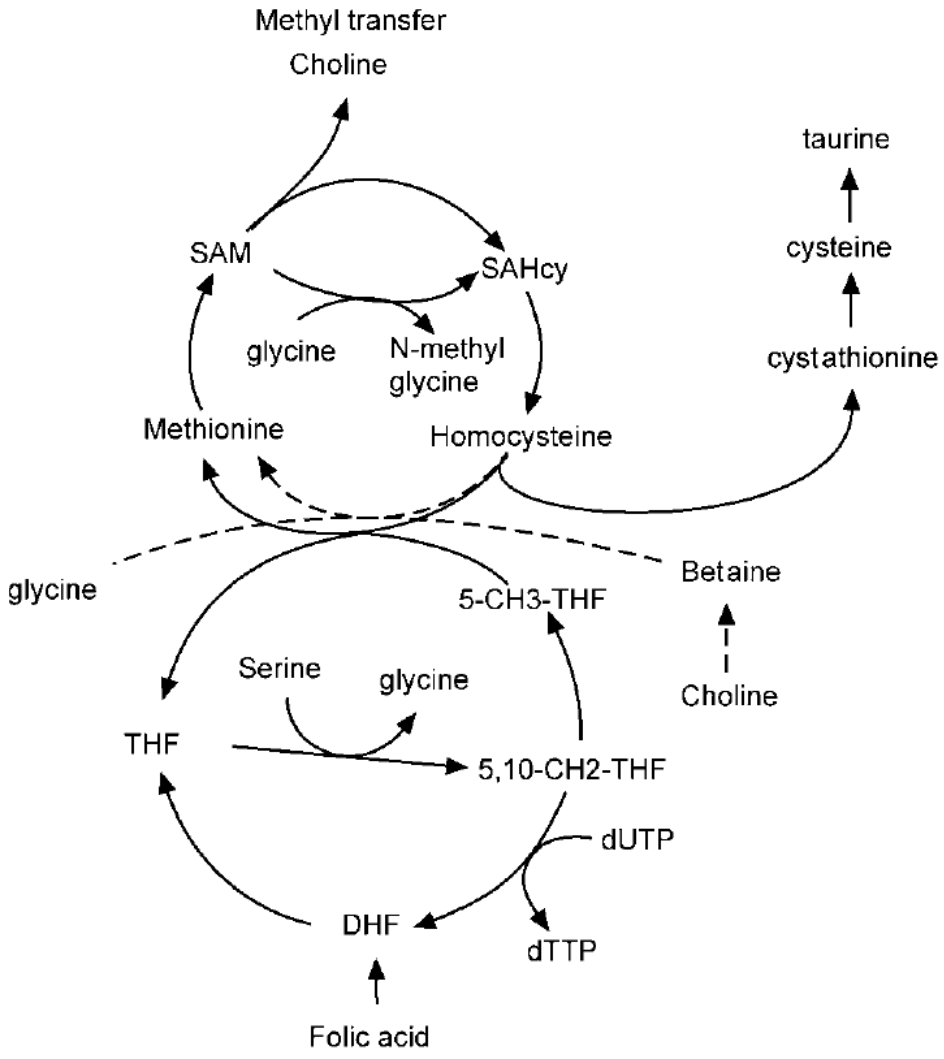

Figure 1.2. The methionine and folic acid cycle. The metabolic pathways interconnect the metabolism of methionine, folic acid, and choline. SAM, S-adenosyl methionine; SAHcy, S-adenosyl homocysteine; 5-CH_3-THF, methyl tetrahyrofolate; 5,10 CH_2-THF, methylene tetrahydrofolate; DHF, dihydrofolate; THF, tetrahydrofolate.[4]

The redundant methionine increases the demand of glycine, and also indirectly enhances fetal development by the increasing production of homocysteine or the perturbation of concentration of hormones in bloodstream. Moreover, according to the methionine and folic acid cycle, above-normal intake of methionine may increase the production of S-adenosyl methionine pools and affect the methylation of proteins and DNA according to the methionine and folic acid cycle.

Three major products of sulfur-based amino acids in the body, are homocysteine, taurine and glutathione, which influence the inflammatory aspects of the immune system, and their concentration is highly affected by the intake of methionine.[5] Although both glutathione and taurine help to improve inflammation, homocysteine acts as anti-inflammatory. It was suggested that homocysteine might affect the inflammatory aspects of aging because of the positive correlation between homocysteine and plasma neopterin, which is a marker of a Th-1–type immune response.[6]

1.2.3 Effect of arginine on the neurological and immune systems, and cancer

Arginine has multiple effects on the human body, including ammonia detoxification, hormone secretion, and immune modulation.[7, 8] Nitric oxide (NO) is produced in the arginine-citrulline pathway, and it is a signal-molecule for regulating gene expression and protein synthesis. Based on the closely correlation between arginine and NO, arginine can be used in the treatment for congestive heart failure, hypertension, coronary heart disease, preeclampsia, intermittent claudication, and erectile dysfunction.[8]

In addition, arginine has been studied for the treatment of HIV/AIDS, athletic performance, burns and trauma, cancer, diabetes and syndrome X, gastrointestinal diseases, male and female infertility, interstitial cystitis, immunomodulation, and senile dementia. [9, 10] It was revealed that the activity of myeloid cell in different states can be traced by analyzing the metabolic pathways of arginine, which is reviewed in detail by Peranzoni, E., *et al.*.[11] In myeloid cells, arginine is mainly metabolized either by arginine-citrulline pathway or by arginase, enzymes that are stimulated by T helper 1 or 2 cytokines, respectively.[12] Thus, activation of NO synthesis or arginase (or both) reflects the type of inflammatory response in disease process. And myeloid cell expressing arginase has been shown to accumulate in patients with cancer. Arginase and ornithine production are two competing process in arginine metabolism. Myeloid cell can efficiently deplete arginine and generate ornithine. Low circulating arginine has been documented in trauma and cancer, suggesting that myeloid cell may exert a systemic effect and cause a state of arginine deficiency.[12] Moreover, it was shown in a recent study in mice that dietary arginine supplementation could alter intestinal microbiota and innate immunity.[13]

1.2.4 Effect of amino acids on Parkinson's disease

The exact mechanism of Parkinson's disease (PD) is still unidentified. The fact that as age increases, the chance of PD increases, makes people believe that PD is related to age and reactive oxygen species.

Deficiency of nicotinamide adenine dinucleotide dehydrogenase (NADH) in the respiratory chain is the main cause of the unfavorable neural apoptosis generation in PD, which leads the severe damage in dopaminergic neurons. The genetic mutations of Parkinson's related proteins contribute to mitochondrial dysfunction. This dysfunction precedes reactive oxygen species formation and cause neural cell damage. It is revealed that the specific impact of mitochondrial genetic change and production of free radicals have correlation to the neurodegeneration in Parkinson's disease. [14]

The development of PD may be induced by excitotoxicity. In the central nervous system, the amino acids act as neurotransmitters and neuromodulators. A study on amino acid concentrations in different brain regions was carried out. Marked decreases in most of the amino acid concentrations in the striatum and in the cortex were detected, while the levels in the cerebellum increased significantly.[15]

1.2.5 Effect of amino acids on Alzheimer's disease

Several amino acids act as neurotransmitters and neuromodulators in central nervous system. The number of neurotransmitter can be affected by the concentration of amino acids. Abnormalities in the plasma amino acid profile have been reported in elderly persons with cognitive impairment, but no data exists for the prodromal phase of Alzheimer disease (AD).[16] A study has been carried to test the hypothesis and it was found that the ratio of arginine to other amino acids was higher in AD patients.

Similar study on brain free amino acids and their relation with dementia was carried out.[17] Temporal cortex (TC) samples obtained from AD patients and control group were used for study. The patterns of free amino acids showed significant changes in AD patient compared to the control group. Amino acids glutamate, and aspartate concentrations, appeared significantly reduced in the TC of AD patients when compared with controls.

CHAPTER II

RADIOLYSIS OF WATER

2.1 Biodosimetry

The interaction of radiation with a biological system is a common factor irrespective of the condition of planned medical treatment or accidental radiation exposure. The interaction involves deposition of energy into cellular targets either directly or indirectly by highly reactive free radicals. Efforts have been made in radiobiological research to establish the relationship between absorbed dose and the corresponding biological effect. A biological dose-response relationship can easily be influenced by genetic sensitivity and environmental factors; therefore, the level of accuracy and precision of radiation dose becomes essential in order to allow valid comparisons and reproducibility. Accurate dosimetry measurements would help determine the dose, and it is appealing to create dosimetry standard operating procedures (SOPs) for *vitro* (cell culture) and *vivo* (small and large animals) experiments and the needs for developing a formal system for coordinating standardization efforts. [18]

However, it is very unlikely that individuals will be carrying dosimeters or that their doses can be quickly and accurately calculated based on their condition. Therefore, the concept of biodosimetry has evolved and it is generally agreed to be essential. By definition, biodosimetry employs radiation-induced changes in the person's own tissues to estimate their individual exposure. The cytogenetic alterations, Electron Spin Resonance (ESR) of tooth enamel, and markers based on genomics, proteomics and

metabolomics, which show a function of absorbed dose, are considered as promising biodosimeters and discussed in recent papers.[19-21] It is unlikely that the radiation effects will be possible to associate with a single gene or protein and thus "easily" counteract. It is likely that the biomarker of the exposure will be a group of genes, proteins and metabolites altered together in response to radiation exposure. In order to counteract the radiation effects and protect human health, it is necessary to find these genes, proteins and metabolites. With modern analytical techniques to measure and identify the products, there is an increasing need for us to explore new biodosimetry and establish the relationship between the biomarkers and absorbed dose.

2.2 Radiolysis of water

In the energy range below 1 MeV, Compton and photoelectric effect are predominant. Above 1.022 MeV pair production occurs. Both the Compton and the photoelectric effect generate electrons, which may contain energy to cause further ionizations and excitations, and subsequently lose their energy. According to the Bethe equation, multiply charged and heavy particles lose their energy more effectively (densely ionizing radiation) in the same distance compared to the single charged particle.

When ionization occurs in water, a water radical cation and an electron is generated. The areas, containing a number of ionization and excitation, are called spurs. The water radical cation, produced in reaction (Eq. 2.1), immediately loses a proton to neighboring water molecules thereby forming •OH (Eq. 2.3). The electron is hydrated by water (Eq. 2.4). Electronically excited water (produced form Eq. 2.2) can decompose

into •OH and •H (Eq. 2.5). Therefore, three kinds of free radicals are formed in the spurs, •OH, e_{aq}^{-}, and •H. Since the radiolytic products can interact with each other and undergo very efficient back reactions, there is scarcely any net decomposition in the pure water. The rate constants for radical reactions in pure water can be found in the review.[22]

$$H_2O \xrightarrow{\text{Radiation}} H_2O^{\bullet+} + e^- \quad (2.1)$$

$$H_2O \xrightarrow{\text{Radiation}} H_2O^* \quad (2.2)$$

$$H_2O^{\bullet+} \rightarrow \bullet OH + H^+ \quad (2.3)$$

$$e^- + nH_2O \rightarrow e_{aq}^- \quad (2.4)$$

$$H_2O^* \rightarrow \bullet OH + \bullet H \quad (2.5)$$

In N_2O-saturated solutions enhancement in production of •OH radicals can be achieved since the reductive species (e_{aq}^-) can be easily converted to •OH radicals by the following reaction

$$e_{aq}^- + N_2O \rightarrow N_2 + O^{\bullet-}\left(+H_2O\right) \rightarrow {}^{\bullet}OH + OH^-. \quad (2.6)$$

Production of superoxide radical anions ($O_2^{\bullet-}$) is enhanced in O_2-saturated solutions containing ions ($HCOO^-$) by the following reaction:

$$e^-_{aq} + O_2 \rightarrow O_2^{\bullet-} \quad (2.7)$$

$$\bullet OH + HCOO^- \rightarrow CO_2^{\bullet-} + H_2O \quad (2.8)$$

$$\bullet H + HCOO^- \rightarrow CO_2^{\bullet-} + H_2 \quad (2.9)$$

$$CO_2^{\bullet-} + O_2 \rightarrow CO_2 + O_2^{\bullet-} \quad (2.10)$$

Ionizing radiation is absorbed by the components of a given mixture approximately proportional to the contributions by weight of the various components. This means that in moderately dilute (< 0.1M/L) aqueous solution almost all the energy is absorbed by the water and free radicals are produced by the radiolysis of water. Monte Carlo simulations are used to investigate the yield of radical produced due to the ionization and excitation of water, especially including oxygen in the tracks, in the radiolysis of pure, deaerated liquid water by using different types of radiation ($^1H^+$, $^4He^{2+}$, $^{12}C^{6+}$, and $^{20}Ne^{9+}$ ions).[23, 24]

2.3 Radiation effect and the origin of life

Laboratory studies have shown that the photolysis and radiolysis of space ice analogues can produce complex organic compounds and prebiotic molecules such as amino acids and nucleobases,[25, 26] which lead to the evolution of origin of life.

There are pressing questions related to the areas of radiation-produced free-radicals in biology and environmental research. Whenever free radicals are formed, corresponding peroxyl radicals can be formed in the presence of oxygen. The physical properties of the peroxyl radicals studied by means of radiation-chemical methods and their unimolecular and bimolecular reactions of selected examples are discussed in detailed, including radical-induced DNA damage, by von Sonntag.[27]

2.4 Radiation proteomics

As the main catalytic and structural molecules within living systems, proteins are the most likely biomolecules to be affected by radiation exposure. Proteomics, the comprehensive characterization of proteins within complex biological samples, is therefore a research approach ideally suited to assess the effects of radiation exposure on cells and tissues. However, the currently available database of radiation effects on proteomes is far too small to be useful in formulation of new hypotheses concerning health consequences of radiation exposures.[30] Consistent with history, technical advances will continue to define and mature the field of MS-based proteomics, catalyzing new milestones of achievement.[31]

CHAPTER III

EFFECTS OF RADIATION AND RADIOLYSIS ON AMINO ACIDS, PEPTIDES AND PROTEINS

3.1 Radiation on amino acid and peptide solution

Hatano studied the radiolytic deamination of amino acid and peptides in aqueous solution by gamma irradiation.[32-35] Ammonia yield (G value) by the deamination of amino acid was observed to remain almost constant for a wide range of irradiation doses, but increased with concentration of the amino acid. Radiosensitivity of α-amino acids to the deamination was proved to be larger than that of β-amino acid. ω-amino acid was revealed to be very resistant to gamma rays and amino group of amino sulfonic acid was more stable than that of amino carboxylic acid. α-Keto acid was found to be produced from its parent amino acid and peptide by gamma irradiation in the aerated aqueous solution. The yield of decomposed α-alanine was identical stoichimetrically with that of liberated ammonia, but did not correspond to the pyruvic acid. The reaction product of leucine with hydrogen peroxide or with a Fenton's reagent was different from that with gamma irradiation. The keto acid would be produced oxidatively from the corresponding amino acid, which had been produced as hydrolytic splitting products form the parent peptide. In amino sulfonic acid the deamination of the amino acids took place less readily than in amino carboxylic acid.

In the liberation of ammonia in irradiated peptide and protein solutions, not only free amino groups but also peptide bonds were proved to contribute. α-Keto acid 2, 4-

dinitrophenylhydrazones were derived from the α-keto acids. Reaction yield of α-ketoglutaric acid obtained from irradiated glutamic acid was also affected by irradiation conditions. Further decomposition of the pyruvic acid by larger doses of γ-rays, was observed in aqueous solutions. The mechanism of oxidative deamination of amino acid and peptide, was established and a scheme of radiolysis of proteins was proposed from the results, as shown in Fig. 3.1.[35] It was also revealed that by small dose of gamma irradiation, inactivation of sulfhydryl enzymes such as alcohol dehydrogenase and urease, was proved to be induced and was recovered reversibly by the addition of thiol compounds such as cysteine and glutathione. In the course of radiolysis of cysteine and sulfhydryl enzyme proteins, a measurable decrease in the amount of sulfhydryl group was found to occur, which corresponded to the lost activities of the enzymes.

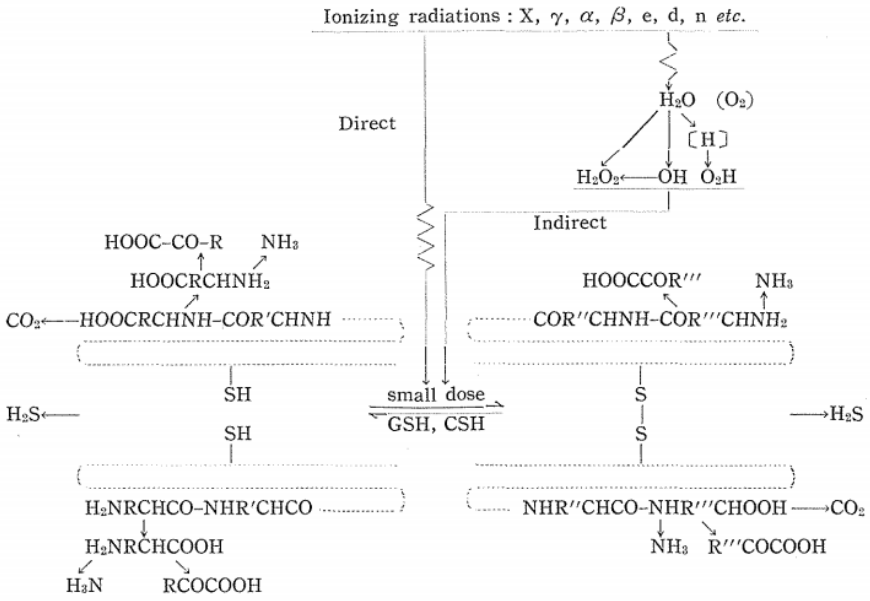

Figure 3.1. Scheme of radiolysis of proteins proposed by Hatano.

3.2 Radicals study by electron spin resonance study

Electron spin resonance (EPR) is a sensitive, specific method for the detection and identification of free radicals, and is the most commonly used analytic tool to study radical production in DNA and amino acids.

Neta *et al.* has used ESR to study the reaction of hydroxyl radical with amino acids and amines in aqueous solution at different pH.[36] It was revealed that the radical produced in acidic glycine solution was NH_2•CHCOOH, instead of NH_3^+•CHCOOH, as supported by the experiment in D_2O. However, in the basic solution, the radicals of H_2N•$CRCOO^-$ were observed in all amino acid solution. The aminoalkyl radical produced in acidic amine solution was formed by hydrogen abstraction from the carbon bearing amino group, which occurred in most cases. However, in the amine basic solution, it was proposed that there were competing hydrogen abstraction form carbon bearing amine group and amine group.

3.3 Radiolysis of amino acids by heavy and energetic cosmic ray

Glycine molecules in the crystalline zwitterion form ($^+NH_3CH_2COO^-$), have been studied by Portugal *et al*, under heavy cosmic ray analogues.[37] The samples were bombarded at two different temperatures (14 K and 300 K) by high energy $^{58}Ni1^{1+}$ ions in a high vacuum chamber, and the products were analyzed by a Fourier Transform Infrared Spectrometer (FTIR). OCN^-, CO, CO_2 and CN^- were detected after the bombardment of the sample in 14K. The results suggested possibility of peptide bonds

during irradiation, and also proved that glycine was present in space environments that suffered aqueous changes, such as the interiors of comets, meteorites and planetesimals.

3.4 Kinetics and conditions of radiation-induced cross-linking and polymerization

Polymerization of cyanides (HCN and NH_4CN) after radiation exposure was confirmed in the work of Vujošević *et al*.[38] Polymers of different masses were detected by HPLC in the experiment. The yield of major polymer products increased with cyanide concentration and absorbed dose. A saturable relationship was revealed between the yield and absorbed dose.

In the work of Fletcher *et al.* , the formation of dihydroxyphenylalanine (DOPA), which was the major product of the radiation of tyrosine aqueous solution, has been tested in amino acids mixture solution or tyrosine-containing peptide solutions.[39] It was revealed that the initial G value of DOPA remained constant. Only amino acids containing sulfur or ring structure provided protection effect on tyrosine from radiation-induced DOPA formation. The relative reactivity of amino acids was concluded from DOPA formation from tyrosine, which also provided the measurement of the reactivity of comparable exogroups of proteins.

The presence of oxygen in radiation induced reactions can increase the quantity of produced oxidations by three to six times, and also make a difference in the quality of products, which was discussed detail in the paper.[40] Under anaerobic condition, the organic free radicals could react by recombination, dimerization and dismutation, which

would all be suppressed in aerobic condition. In addition, hydroperoxides can be produced in the presence of oxygen from biological material, such as nucleic acids and amino acids. The yield of hydroperoxide and structure of amino acids have been explored. The amino acids with a tertiary carbon, such as isoleucine and valine, produced the most hydroperoxides. In addition, sample amino acids (glycine and alanine), containing a benzene ring and histidine produced the least amount of hydroperxide.

The free enthalpy of dimerization of amino acids is positive by several kJ mol^{-1} (+14.25 kJ mol^{-1} for glycine), which indicates that dimerization is energetically unfavorable, as well as the further polymerization. Considering the selectivity of the amino acids, therefore, the polymerization in a mixture of amino acids solution is not viable in thermodynamics. Amino acid adsorption and thermal reactivity of polymerization on minerals, has been discussed in the recent review.[41] The reality of the phenomenon is established, but understanding of its mechanism is very fragmentary. Coupling of thermodynamically unfavorable and favorable reactions has been proposed to explain the phenomenon. The free energy of adsorption of dimer should be more negative than two monomers and an increase in adsorption energy is requested for the further polymerizing. Moreover, the charged side chain, which can cause electrostatic repulsion, should be compensated by the electrostatic adsorption. However, specific covalent bond formation, hydrogen bonding, and other contribution for molecular recognition are still remaining for further work.

The chemical reaction of alanine and leucine in solid state induced by vacuum ultraviolet (VUV) irradiation was studied by HPLC coupled with mass spectroscopy.[42] It was revealed that efficiency of dimerization of alanine was dependent on the wavelength, and yield was proportional to the absorbed dose. In the mass spectra of alanine and leucine, deamination and decarboxylation were both observed, while dissociation of side chain was only observed in the spectra of leucine.

Radiation-induced crosslinking of polymers is one of the most popular industry applications of radiation, including upgrading of polymeric insulation on wire and cable; crosslinking of polyethylene and polypropylene foam for better foam control; crosslinking of polymers for improved stress-work resistance; vulcanization of sheet rubber; and imparting plastic memory technique, which are discussed in detail in the review.[43]

Radiation-induced DNA base-amino acid crosslinks was isolated and identified after derivatization by capillary gas chromatography-mass spectrometry (GC-MS).[44] 5-S-Cysteaminemethyluracil was formed after irradiation of a mixture of cysteamine and thymine solution.[45]

In addition, radiation-induced DNA-protein crosslinks in intact cells was detected by a filter-binding assay.[46] The production of crosslink was dose dependent and reverses due to protein synthesis. The effect of radiation and hyperthermia on the DNA-protein has been evaluated by the work of Cress *et al.*.[47] It was revealed that radiation alone caused DNA-protein, while hyperthermia in combination increased the

recovery time and phosphate to nitrogen bonding, which suggested the interactive effect of hyperthermia and radiation was more related to the rate of removal chemical bonding involved in crosslinks instead of the amount of produced crosslinks. It was also reported that guanine neutral radicals, and amino acid radicals could be employed in *vitro* synthesis of DNA-protein cross-links while the amino acid radicals were induced by photoionization.[48]

The crosslink of phenylalanine and glucagon were observed by the interaction of glucagon and phenylalanine mediated by the OH· radical.[49, 50] The result indicated that the aromatic residues, basic residues, and sulfur-containing residue, of glucagon were predominantly involved in crosslinking, which were also observed in the glucagon-glucagon crosslinking. The relative yields of induced products were dependent on the molecular ratio of phenylalanine to glucagon. It was also reported that gelatin was transformed into hydrogel by degradation and crosslink after radiation.[51]

Radical-induced DNA damage in biological system can be induced by various mechanisms, which has been reviewed in the recent paper.[52, 53] Radicals produced in the radiolysis of water can react with the heterocyclic DNA bases, which further produce adduct radicals. These include DNA base and sugar products, single- and double-strand breaks, tandem lesions, clustered sites and DNA-protein cross-links, which play an important role in the formation of numerous diseases, including cancer.

With the development of modern techniques, it is possible to detect multiple radical-induced damages in DNA, which helps disease prevention and treatment. High-

performance liquid chromatography associated with tandem mass spectrometry (HPLC–MS/MS) is considered to be the most precise and standard method.[54] DNA repair enzymes can also be used to access oxidative damage but lack specificity since cross-reactivity can occur with normal base. ESI-MS has also used to identify the cross-linking of DNA and peptide due to gamma ray irradiation,[55] which indicated the usefulness of the ESI-MS for detecting crosslink in biomolecules. However, it should be noticed that artifacts can exist in any measurement of modern techniques.

3.5 Production of volatiles from oil emulsion and amino acid polymers by irradiation

Volatile compounds produced by irradiation of emulsion have been collected and analyzed. Increasing yield of aldehyde with absorbed dose has been detected due to the accelerating oxidation of oil emulsion by irradiation.[56] New volatile compounds such as methionine and cysteine have been produced by radiolytic degradation, which indicated that the off-odor generated during the irradiation of meat may come from the radiolysis of protein.

Radiation on homopolymer has been performed. The amounts of some volatiles greatly increased, while others significantly decreased after irradiation, which indicate radiation can not only produce new volatile compounds, but also destroy existing volatile compounds.[57] Sulfur compounds were detected to be the most produced and increased compound due to the radiosensitivity of sulfur amino acid. Radical attacking side chain has been proved to occur in the product, and some volatiles come from the further degradation of attacked side chains.

CHAPTER IV

INTRODUCTION TO METHODOLOGIES

4.1 Introduction to Raman spectroscopy

4.1.1 Basic principle

When a photon interacts with matter, scattering can easily happen, if the energy of the photon does not match the difference between two energy levels and no absorption occurs.

Raman spectroscopy is the principal technique used for molecular identification. Raman spectroscopy uses a single frequency laser to irradiate a sample and the scattered photons are collected at a given angle and detected. The energy of the scattered photons is increased or decreased by one vibration energy different from the incident beam. In Raman scattering, the incident photon beam interacts with the molecule and polarizes the cloud of electrons, which induces an unstable short-lived state called a 'virtual state'. The de-excitation of the molecule yields the prompt emission of a photon. The scattering process form the ground state *m* to an excited state *n* is called Stokes, whereas scattering from an excited state *n* to the ground state *m* is called anti-Stokes. The process is shown in the Fig. 4.1. When a laser with an emission frequency v_0 interacts with a molecule, the electron cloud within the molecule is changed and dipole moment *P* is induced. If the electric field *E* of the electromagnetic wave is weak enough, *P* is proportional to *E*, expressed as:

$$P = \alpha E, \tag{4.1}$$

where α is the electric polarizability. Here, both P and E are assumed to be on one coordinate axis for simplicity. Substituting $E = E_0 \cos(2\pi \nu_0 t)$ in Eq. 4.1, we obtain

$$P = \alpha E_0 \cos(2\pi \nu_0 t). \tag{4.2}$$

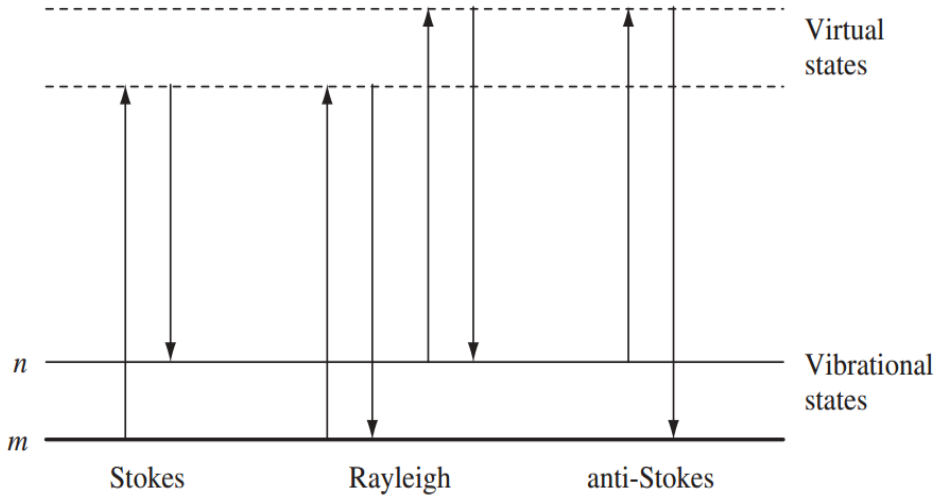

Figure 4.1. Diagram of the Rayleigh and Raman scattering process.

The polarizability α can also be divided into two parts: α_0, which remains constant despite the effect of irradiation, and another term changing with molecular vibration. Defining $Q = Q_0 \cos(2\pi \nu t)$ as the same coordinate corresponding to the vibrational displacement, we can obtain

$$\alpha = \alpha_0 + \left(\frac{\partial \alpha}{\partial Q}\right)_0 Q = \alpha_0 + \left(\frac{\partial \alpha}{\partial Q}\right)_0 Q_0 \cos(2\pi \nu t) \tag{4.3}$$

Therefore, the dipole moment can be describes as:

$$\begin{aligned} P &= \left\{\alpha_0 + \left(\frac{\partial \alpha}{\partial Q}\right)_0 Q_0 \cos(2\pi \nu t)\right\} E_0 \cos(2\pi \nu_0 t) \\ P &= \alpha_0 E_0 2\pi \nu_0 t + \frac{1}{2}\left(\frac{\partial \alpha}{\partial Q}\right)_0 Q_0 E_0 \{\cos(2\pi(\nu_0 + \nu)t) + \cos(2\pi(\nu_0 - \nu)t)\} \end{aligned} \tag{4.4}$$

The first term is the product of the constant α_0 and E, vibrating at the same frequency of the incident light. The second term contains a component vibrating at two different frequencies, $\nu+\nu_0$ and $\nu-\nu_0$, indicating the changed frequencies of scattered photon, known as Raman scattering.

Eq. 4.4 also reveals that in order for Raman scattering to occur, one condition should be met as $\left(\frac{\partial \alpha}{\partial Q}\right)_0 \neq 0$, which indicates Raman-active are only those vibration that change the polarizability associated with vibration displacement of a molecule.

4.1.2 Application of Raman Spectroscopy

Raman spectroscopy as a label-free and nondestructive technique for providing molecular structure and chemical composition has been applied to *vitro* and *vivo* studies. The changes in molecular conformation can produce qualitative changes in Raman

shifts, which can be used to analyze protein secondary structures and intramolecular interactions.

Currently, databases of band assignment in Raman spectra of bio compounds have been developed. In the Table 4.1,[61] frequencies of Raman-active vibrations in biomedical applications are summarized. Some correlation can be directly applied to protein and more complex molecules, which accelerates the interpretation of Raman spectra. The detailed discussion about Raman spectroscopy and protein can be found in recent review.[58]

Human serum albumin (HAS) is the most abundant protein in plasma. In the work of Jurasekova *et al.*, Raman spectroscopy was used to investigate the changes on HAS caused by free radicals produced by gamma irradiation. [59] It was revealed that Raman spectroscopy was capable of identifying the conformational changes of secondary structure in protein by observing decrease in α-helix content while increase in β-sheet content, and also damages occurring at sensitive amino acids sites.[59]

In a recent study by Gong *et al.*, Raman spectroscopy was used to assay the ratio between mineral and matrix, carbonate and phosphate in bone after radiation by a noninvasive fiber optic probe.[60] The results revealed that there was radiation damage on bone quality and persisted long term, which suggested that Raman spectroscopy can be a complementary approach to conventional CT.

Table 4.1. Summary of frequencies of Raman-active vibrations in biomedical applications		
Vibration	Frequencies (cm^{-1})	Indicative of …
OH	3400, 1640	Water
CH_2/CH_3, C-C	2920, 2880, 2850, 1450, 1300, 1128, 1065	Lipids, proteins
Amide I/III	1620 to 1710, 1230 to 1330	Proteins
PO_4	1090 to 1100	Nucleic acids, phospholipids
$N(CH_3)_3$	716, 875	Phosphatidylcholine and sphingomyeline
	608, 700, 1440, 1674	Cholesterol
C=O	1745	Ester group in phospholipids
Triple helix	810, 850, 930, 1240	Collagen
	620, 1004, 1208	Phenylalanine
	642, 830, 850, 1208	Tyrosine
	760, 880, 1010, 1340, 1360, 1550	Tryptophan
	498, 680, 1485, 1575	Guanine
	729, 1304, 1333, 1577	Adenine
	498, 670, 750, 780, 1370, 1666	Thymine
	780, 1256	Cytosine
	852, 931, 1048, 1085, 1127, 1340, 1382	Glycogen
	663, 740, 1250, 1561, 1582, 1620	Heme (denatured)
C=C-H, C=C	1270, 1660, 3050	Nonsaturated fatty acids
	1160, 1530	Carotene
	960	Mineralized tissue

Cancer is one of the leading causes of death and early detection of cancer is critical for successful therapy. Raman spectroscopy, as a noninvasive, nondestructive, and water-insensitive technique, is popular for detecting changes in cells and tissues that are caused by different disorders, such as cancer.

Raman spectroscopy proved to have better sensitivity and specificities in carcinoma and melanoma diagnosis, the more detailed discussion of the most investigated optical techniques for the noninvasive diagnosis of skin cancer can be found in the recent paper.[62]

In the work of Tollefson *et al.*, it was revealed that Raman spectroscopy was able to identify the biochemical differences in patients with Gleason 7 progressed to metastatic disease and without disease after treatment.[63] Moreover, Raman spectroscopy was proved to identify and characterize the murine fibroblast cell line combing with advanced statistical methods.[64]

Laser of 532 nm excitation instead of near infrared is first used to annotate colon tissue by Raman spectral histopathology in the work of Mavarani *et al.*.[65] The result successfully differentiated the example of erythrocytes and lymphocytes, while Raman scattering auto-fluorescence was observed, which provided a new label free assignment for cancer cells. In addition, circulating tumor cells as a marker of breast cancer and colorectal cancer, has been successfully differentiated from normal human mononuclear cells using Raman spectroscopy combining a state-of-the-art micro-Raman microscopic technique.[66]

It was reported that enhanced analytical sensitivity was obtained for both surface-enhanced Raman spectroscopy (SERS) and surface-enhanced resonance Raman spectroscopy (SERRS) using situ synthesis of silver colloid in a microfluidic flow structure, which can be used for pigment determination from cyanobacteria and detection of trace concentration of drugs of abuse in saliva in short time.[67, 68] In addition, it was also revealed that free-surface microfluidic and SERS detection system can provide continuous, real-time monitoring of particular vapor-phase analytes at low concentration.[69] Ashok *et al.* and Li *et al.* independently developed a portable Raman spectroscopy system embedded on a microfluidic chip.[70, 71] Both systems showed high sensitivity for the detection of analytes and environmental sensing. The current applications of microfluidics and Raman microscopy on the investigation of analytes, nano-material science, biological samples and pharmaceuticals, were discussed in detail in the recent review by Chrimes et al.[72]

Work of Raman spectroscopy on amino acids has been improved and exploited with the development of the system. Raman database of twenty amino acids were built and reported in several papers with discussion on the vibration.[73-78] In the work of Sonois *et al.*, considerable differences were observed with changes in pH of the amino acids, H/D substitution and pH dependence experiments were used to identify vibrational bands associated with the functional groups able to exchange protons.[79] The extended multiplicative signal correction (EMSC), has been applied to Raman spectra, to retrieve quantitative information from amino acids mixtures and peptides.[74] In the work of A.L. Jenkins *et al.,* Raman spectroscopy was used to investigate amino acids and

related biopolymers, which suggested further application of Raman spectroscopy for monitoring the interaction between the drug and target protein.[77]

4.2 Basic theory of Ultraviolet–visible (UV-Vis) spectroscopy

Many compounds absorb ultraviolet or visible light. When the energy of photon matches the energy difference between two electron states, the electron will be prompted from a ground state to an excited state. In a molecular, discrete electron states can be produced by rotation and vibration of atoms. Absorbance is defined by the logarithm of transmittance, and can be described by the Beer-Lambert law as

$$A = \varepsilon lc \tag{4.5}$$

where A is the absorbance (unit-less), ε is the molar extinction coefficient (L $mole^{-1}$•cm^{-1}), c is the sample concentration (mole L^{-1}), and l is the length of light path through the cuvette (cm).

UV-Vis spectroscopy as one of the oldest methods in molecular spectroscopy has been applied in multiple areas. Detailed discussion of UV-Vis spectroscopy on analytical application, investigation of equilibria and kinetics on chemical can be found in the book of H. Charlote Grinter *et al.*.[80]

4.3 Electrospray Ionization Mass spectrometry

Mass spectrometry is an analytical technique that can provide the structure change or variation in molecular concentration. John Fenn first introduced Electrospray Ionization

(ESI) in 1989. During standard electrospray ionization, the sample is dissolved in a volatile solvent and pumped through a narrow capillary at a flow rate between 1×10^{-3} and 1 L min^{-1}.[81] A high voltage between 3 and 4 kV is applied to the tip of the capillary, which produces strong electric field. The sample emerging from the tip is dispersed into an aerosol of highly charged droplets. Gas is applied to direct the molecular towards the mass spectrometer. The mechanism is given in Fig. 5.1.[82]

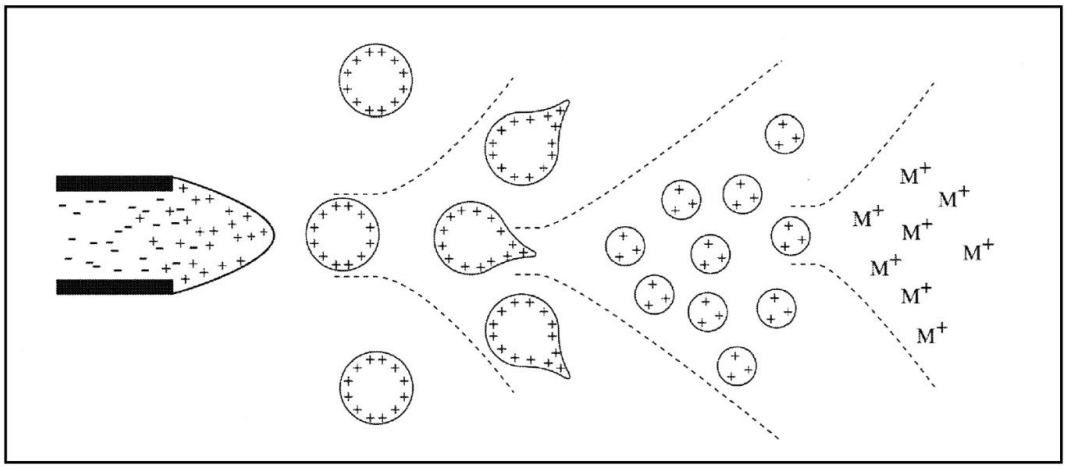

Fig 5.1. Mechanism of electrospray ionization.

Currently, ESI-MS as a soft ionization technique extensively used for production of gas phase ions is becoming an important technique in structural study or quantitative measurement for multiple areas.

In the work of Kujawinski *et al.,* ESI-MS has been proved advance of analyzing soil organic material, which is a critical component of environment process and the

global carbon cycle.[83] Ho, C., *et al.* reported the ability of ESI-MS detected metabolites in a complex biological sample, which can be used to screen for inborn errors of metabolism, identification and quantification of Hemoglobin in variants.[82, 84] ESI-MS has important supporting roles in the drug development process, including the assessment of compound purity; quantitation of absorption, distribution, metabolism and excretion; and compound-specific pharmacokinetic analyses.[85-88] In addition, it is reported that ESI was capable of identifying lead compounds on the basis of the characterization of noncovalent ligand–macromolecular target interactions.[89]

CHAPTER V

MATERIAL AND METHODS

5.1 Sample preparations

The 20 amino acids were purchased from Sigma Aldrich and each had purity of >99.9%. Sample of solid and solution forms were both prepared. Stock solutions were produced by dissolving solid amino acids in deionized water (ELGA PURELAB Flex water purifier) or 0.5 M HCl based on the solubility and stability of amino acids, as specified in Table 5.1. The final concentration of the amino acids in solution was 0.1 M.

Table 5.1. Summary of 20 amino acid solutions with a molar concentration of 0.1 M

Solute	Solvent	Molar mass ($g\ mol^{-1}$)	Solute	Solvent	Molar mass ($g\ mol^{-1}$)
Alanine	water	89.09	Leucine	0.5 M HCl	131.18
Arginine	water	174.20	Lysine	water	146.19
Asparagine	water	132.12	Methionine	water	149.21
Aspartic acid	0.5 M HCl	133.11	Phenylalanine	water	165.19
Cysteine	0.5 M HCl	121.16	Proline	water	115.13
Glutamic acid	0.5 M HCl	147.13	Serine	water	105.09
Glutamine	water	146.15	Threonine	water	119.12
Glycine	0.5 M HCl	75.07	Tryptophan	0.5 M HCl	204.23
Histidine	water	155.16	Tyrosine	0.5 M HCl	181.19
Isoleucine	water	131.18	Valine	0.5 M HCl	117.15

5.2 Electron bean irradiation of samples

Irradiation of all samples was carried out at the National Center for Electron Beam Research (NCEBR) at Texas A&M University. The samples were placed in thin polyethylene bags to ensure uniform irradiation as a function of depth. All solid and liquid samples for a particular dose were irradiated together, and six alanine dosimeter pellets were placed uniformly throughout the sample arrangement to measure the average dose received by the samples. Alanine pellets irradiated with the samples were analyzed with a Bruker e-scan Alanine Dosimetry System. The average doses administered to the irradiated samples were 10, 25, and 50 kGy.

5.3 Raman Spectroscopy of solid and solution samples

Raman spectra of the amino acid samples were collected using a Horiba Jobin Yvon spectrometer with a 532 nm laser and a 10× objective located at the Raman Spectroscopy laboratory in the physics department courtesy of Dr. Scully. Samples were placed in a quartz petri dish for data collection, as quartz had a simple Raman spectrum that is distinguishable from that of the amino acid samples. For solid samples, the laser power at the sample was 80 mW, and the spectra were collected for one second and averaged three times. For the solutions, the laser power at the sample was increased to approximately 100 mW with a collection time of 10 seconds and averaged three times. The same laser and spectrometer settings were used when spectra were collected before and after irradiation. The calibration of the system was carried out every time before

operation using silicon slide sample. The range used to obtain the Raman spectrum was from 400 to 2400 cm^{-1} for solids and 500 to 1800 cm^{-1} for solutions.

5.4 UV-Vis Spectrophotometry of solution samples

The NanoDrop 2000c UV-Vis spectrophotometer (Thermo Scientific) was used to evaluate the absorbance spectra of all amino acid solutions. All measurements were carried out using the 2 μL pedestal on the device. Deionized water or 0.5 M HCl was used as a blank reference. Given that absorbance was proportional to path length, it was deemed necessary after initial tests to use the spectrophotometer pedestal for measurement with a nominal path length of 1 mm instead of cuvette measurements due to the possibility of high absorbance obscuring results. The acquisition range of data was from 190 to 700 nm. The baseline correction for all spectra was set at 750 nm under the assumption that no absorbance should occur at this wavelength.

5.5 ESI Mass Spectroscopy of solution samples

The non-irradiated amino acid solutions (0 Gy) and those that received a dose of 50 kGy were sent to the Texas A&M University Laboratory for Biological Mass Spectroscopy for further analysis using ESI-MS in both positive and negative modes. A 10 μL sample was diluted in 990 μL of triple distilled water. Electrospray ionization (ESI) in positive and negative ion modes was carried on a quadruple ion trap mass spectrometer (LCQ-DECA, ThermoFinnigan, San Jose, CA). The sample was injected into a 10 μL-loop injection with a flow rate of 200 μl/min. The spray voltage was set at -4.0 kV. Sheath

gas and auxiliary gas flow rates were 50 and 10 arbitrary units, respectively. Transfer capillary temperature was held at 250°C. The Xcalibur 2.0 software package (ThermoFinnigan) was used for data acquisition and processing. Data was transferred to personal computers and visualized using the software mMass (Open Source Mass Spectrometry Tool, by Martin Strohalm).

5.6 Determination of sample pH of solution samples after irradiation

The pH of amino acid solution samples was determined prior to and after irradiation using a digital pH meter equipped with a standard pH electrode (Qph 70; VWR International GmbH, Darmstadt, Germany). Calibration of the pH meter was carried out using a standard buffer before operation.

CHAPTER VI

RESULTS

6.1 Qualitative changes of amino acids after irradiation

The solid amino acid samples were acquired in powder form (Sigma Aldrich, St. Louis, Mo) having a white color and solution samples were transparent before irradiation. After the solid and solution samples were irradiated at different absorbed doses, qualitative changes were observed for some amino acids samples. A summary of such qualitative changes is given in the Table 6.1.

6.2 Analysis of UV-Vis spectrum of amino acids

The solution samples were prepared under the presence of atmospheric carbon dioxide and oxygen. As a result, UV-Vis absorption became quite significant below 200 nm. Therefore, the UV-Vis range between 100 and 200 nm was usually not scanned unless special air-free techniques were employed. On those sample solutions that required the use of HCl, the UV-Vis spectra were affected near 200 nm wavelength. Therefore, all UV-Vis spectra were recorded between 220 and 400 nm. The UV-Vis spectra of the 20 amino acids in solution irradiated at different absorbed doses are shown in Appendix. The observed UV-Vis spectra for all samples are summarized in the Table 6.2. Also, a summary of the pH changes for 20 amino acids solution irradiated by different doses is shown in Table 6.3 along with the isoelectric points (pI). Because of the precision limit of the pH meter, variations of 0.1 or less were considered to be negligible.

Table 6.1. Observed changes after irradiation of amino acids in solution form

Sample	Observed qualitative changes post-irradiation
Alanine	Solid turning yellow and becoming darker with increasing dose
Cysteine	Appearance of sulfurous odors possibly due to the liberation of hydrogen sulfide Solid turning yellow and becoming darker with increasing dose
Glutamine	Solid turning yellow and becoming darker with increasing dose
Glycine	Solid turning yellow and becoming darker with increasing dose
Histidine	Solution turning yellow and becoming darker with increasing dose
Methionine	Appearance of sulfurous odors possibly due to the liberation of hydrogen sulfide
Phenylalanine	Solution exhibiting slight yellowing Solid turning yellow and becoming darker with increasing dose
Serine	Solid turning light grey and into with increasing dose
Threonine	Solution exhibiting slight yellowing Solid turning yellow and becoming darker with increasing dose
Tryptophan	Solution turning orange-red and becoming darker with increasing dose
Tyrosine	Solution exhibiting slight yellowing
All samples	Appearance of strong pungent odor due to the liberation of ammonia

Table 6.2. Summary of the UV-Vis observable changes in solution form

Sample	Observations	Figure
Alanine	No significant change	A.1
Arginine	Peak broadening at 220 nm; marginally higher absorbance with dose	A.2
Asparagine	New absorbance band at 276 nm increasing in intensity with dose	A.3
Aspartic Acid	No significant change	A.4
Cysteine	Minor increase in absorbance as function of dose	A.5
Glutamic Acid	No significant change	A.6
Glutamine	New absorbance band at 287 nm increasing in intensity with dose	A.7
Glycine	No significant change	A.8
Histidine	New absorbance band at 282 nm strongly increasing in intensity with dose	A.9
Isoleucine	No significant change	A.10

Table 6.2. (cont.) Summary of the UV-Vis observable changes in solution form

Sample	Observations	Figure
Leucine	No significant change	A.11
Lysine	No significant change	A.12
Methionine	Increase in absorbance between 270 nm and 315 nm and flattening/saturation with dose	A.13
Phenylalanine	Increase in absorbance and minor right-ward shift of peaks from 223 nm and 258 nm; absorbance increased universally with dose	A.14
Proline	No significant change	A.15
Serine	Peak broadening and increased absorption as function of dose	A.16
Threonine	Peak broadening and increased absorption as function of dose	A.17
Tryptophan	Peak broadening and increased absorption from 299 nm to 380 nm	A.18
Tyrosine	Minor peak shift and broadening from 275 nm to 284 nm with dose	A.19
Valine	No significant change	A.20

Table 6.3. Summary for pH changes in twenty amino acids in solution

Sample (Solvent)	pI at 25°C	Absorbed Dose (kGy)			
		0	10	25	50
Alanine (water)	6.11	7.46	7.16	7.11	7.01
Arginine (water)	10.76	10.94	10.66	10.57	10.53
Asparagine (water)	10.76	4.74	6.5	7.03	7.33
Aspartic Acid (0.5HCl)	2.98	0.22	0.29	0.3	0.43
Cysteine (0.5HCl)	5.02	0.31	0.28	0.29	0.35
Glutamic Acid (0.5HCl)	3.08	0.39	0.28	0.27	0.39
Glutamine (water)	5.65	4.44	5.07	6.37	7.05
Glycine (0.5HCl)	6.06	0.35	0.28	0.3	0.25
Histidine (water)	7.64	7.74	7.74	7.79	7.83
Isoleucine (water)	6.04	7.29	7.15	7.19	7.09
Leucine (0.5HCl)	6.04	0.43	0.28	0.27	0.37
Lysine (water)	9.47	10.06	9.99	9.9	9.88
Methionine (water)	5.74	7.21	7.5	7.73	7.81
Phenylalanine (water)	5.91	6.76	6.89	6.88	6.79
Proline (water)	6.30	7.93	7.44	7.16	6.89
Serine (water)	5.68	6.83	7.31	7.40	7.55
Threonine (water)	5.60	6.81	7.42	7.56	7.68
Tryptophan (0.5HCl)	5.88	0.31	0.31	0.28	0.32
Tyrosine (0.5HCl)	5.63	0.28	0.27	0.28	0.48
Valine (0.5HCl)	6.02	0.3	0.28	0.26	0.39

On those sample solutions that exhibited noticeable UV-Vis variations in absorbance, peak shifts, new peaks, or changes in pH, as a function of dose are presented in Appendix. The observed changes in UV-Vis spectra of histidine and phenylalanine was consistent with the data reported by Nakano *et al*. using femtosecond laser irradiations.[90] The analysis of the UV-Vis spectra response as a function of absorbed dose was carried out based on amino acid functional groups. Amino acids were analyzed based on their corresponding group; these were aliphatic, aromatic, neutral, acidic, basic, sulfur-containing, and imino acid classification (see Table 1.1).

In general, the absorbance intensity of a given wavelength was exponentially related to absorbed dose, which suggested that radiolytic reactions of amino acids followed first order kinetics as established by the Arrhenius formula. The absorbance of an amino acid is proportional to its molar concentration following Beer-Lambert law as

$$A = \varepsilon lc \tag{6.1}$$

where A is the absorbance (unit-less), ε is the molar extinction coefficient (L mole^{-1} cm^{-1}), c is the sample concentration (mole L^{-1}), and l is the length of light path through the cuvette (cm). The sample volume and path length were kept constant; therefore, new bands in the spectrum were caused by changes in product concentration or generation of new products. Therefore, the absorbance in the spectrum was the indication of the molar concentration of a product. We used the following equation to fit the absorbance intensity for a fixed wavelength for a new radiolytic product

$$A = A_{\max}\left(1 - e^{-D/D_0}\right) + A_0, \tag{6.2}$$

where A_0 is the initial absorbance at zero absorbed dose, and D_0 is the absorbed dose required to increase the absorbance A by $\frac{e^{-2}-e^{-1}}{e^{-1}-1}$ or 37%, which may refer to the production rate probability (kGy^{-1}) for a given wavelength, and A_{max} is the maximum increase in absorbance produced by radiation.

6.2.1 Aliphatic amino acids

There were no significant changes in UV-Vis spectra for alanine, glycine, leucine, isoleucine and valine; these are all aliphatic amino acids that do not contain N, O, and S in their side chain. On the other hand, a decrease in pH was observed for alanine and isoleucine solutions with increased absorbed dose. The solutions for glycine, leucine and valine all contained HCl, and no significant changes in pH were observed.

6.2.2 Aromatic amino acids

Aromatic amino acids are phenylalanine, tyrosine and tryptophan, all of those amino acids showed increasing absorbance as a function of absorbed dose and minor right-ward shift of peaks while pH remained constant after irradiation. The results are shown in the Fig. 6.1.

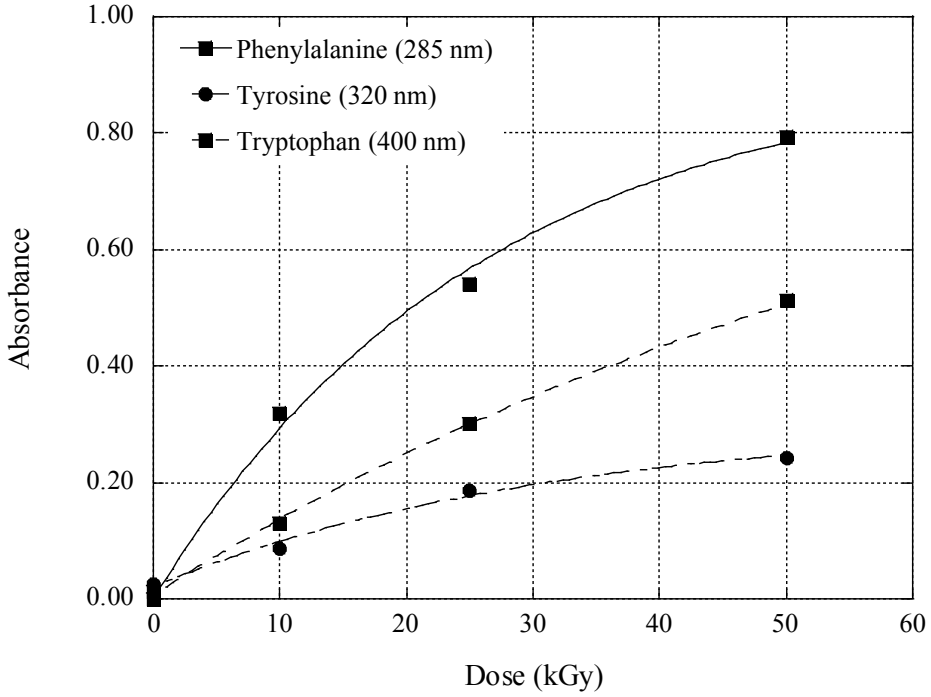

Figure 6.1. Absorbance as a function of absorbed dose for aromatic amino acids at specific wavelengths. The absorbance-dose relationship was $A_{\mathrm{Trp}}^{400} = 0.982\left(1 - e^{-0.142D}\right) + 0.0073$ for tryptophan at 400 nm, $A_{\mathrm{Tyr}}^{320} = 0.281\left(1 - e^{-0.0325D}\right) + 0.0207$ for tyrosine at 320 nm, and $A_{\mathrm{Phe}}^{285} = 0.918\left(1 - e^{-0.0285D}\right)$ for phenylalanine at 285 nm.

6.2.3 Neutral amino acids

The neutral amino acids are those with a hydroxyl or amide groups in their side-chain. These are serine, threonine, asparagine and glutamine. They all exhibited a higher pH with increasing absorbed dose, and yielded a new absorbance band increasing in

intensity with absorbed dose. The relationship of the absorbance intensity and pH with absorbed dose is plotted in the Fig. 6.2.

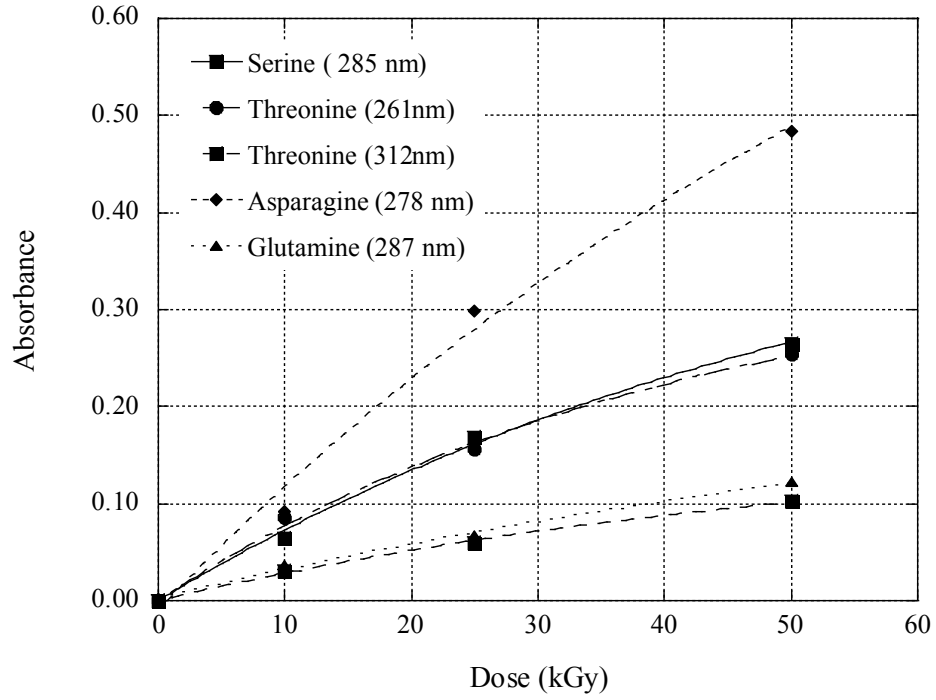

Figure 6.2. Absorbance as a function of absorbed dose for neutral amino acids at specific wavelengths. The absorbance-dose relationship was $A_{\text{Arg}}^{278} = 1.04\left(1 - e^{-0.0130D}\right) - 0.0089$ for asparagine at 278 nm, $A_{\text{Glu}}^{287} = 0.286\left(1 - e^{-0.0106D}\right) + 0.0039$ for glutamine at 287 nm, $A_{\text{Ser}}^{285} = 0.462\left(1 - e^{-0.0172D}\right)$ for serine at 285 nm, $A_{\text{Thr}}^{261} = 0.360\left(1 - e^{-0.0241D}\right)$ and $A_{\text{Thr}}^{312} = 0.167\left(1 - e^{-0.0188D}\right)$ for glutamine at 261 nm and 312 nm, respectively.

6.2.4 Acidic amino acids

For acidic amino acids (carboxylate groups in side chain), including aspartic acid and glutamic acid, no change in either UV-Vis spectrum or pH was observed. However, when it came to the aspartic acid and glutamic acid aqueous solution, there was minor increase in absorbance as a function of absorbed dose, which was similar for proline. An explanation would be that HCl had an effect on absorbance, which compensated for the difference expected to show; a blank calibration was done to do a baseline correction.

6.2.5 Basic amino acids

For basic amino acids, which include lysine, arginine, and histidine, the pH remained constant. There were no significant changes in the UV-Vis spectrum for lysine. However, for arginine there was peak broadening at 220 nm, which showed marginally higher absorbance with increased absorbed dose. In the case of histidine, a new absorbance band at 282 nm was observed with a strong increase with absorbed dose. The different appearances of the three amino acids in the UV-Vis spectrum were caused by their different side chains: arginine had a double bond between C and N, and there was an extra carbon double bond in imidazole ring in histidine. The peak broadening of arginine may be caused by the oxidation of the double bond, which leaded to the production of citrulline. The new absorbance band observed in histidine was similar to that resulting by the oxidation of an imidazole ring. The mechanism of chemical reaction would be a cycloaddition of excited oxygen to the imidazole group, which resulted in an unstable cyclic peroxide.[91] Then the aromatic system would be reformed via proton

rearrangement. The relationship of the absorbance intensity with dose is plotted and fitted in the Fig. 6.3.

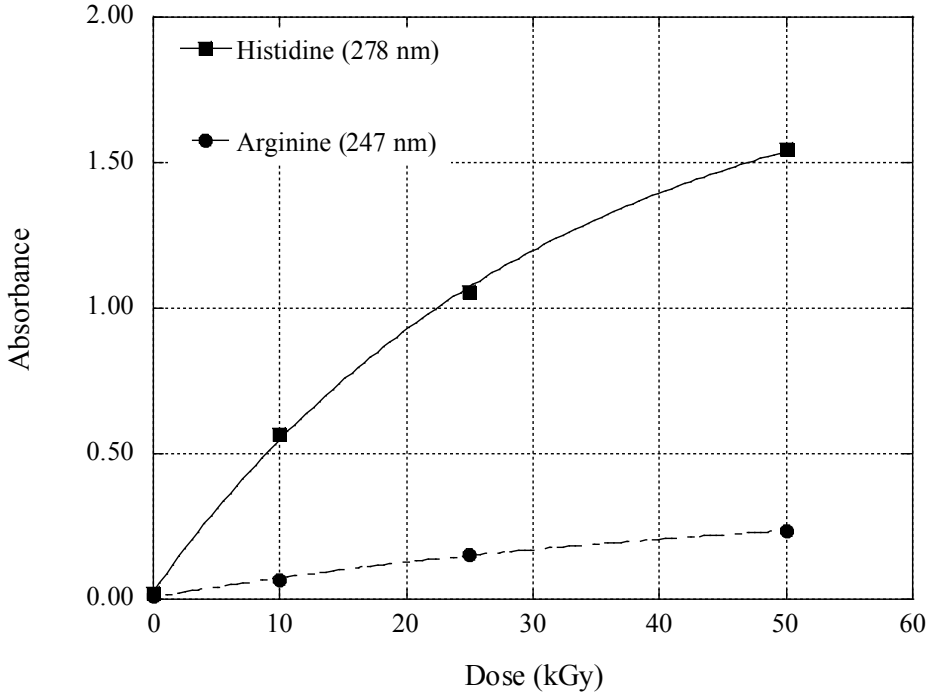

Figure 6.3. Absorbance as a function of absorbed dose for basic amino acids at specific wavelengths. The absorbance-dose relationship was $A_{\text{Arg}}^{247} = 0.353\left(1 - e^{-0.0209D}\right) + 0.0068$ for arginine at 247 nm, and $A_{\text{His}}^{278} = 1.88\left(1 - e^{-0.0325D}\right) + 0.0262$ for histidine at 278 nm.

6.2.6 Sulfur-containing amino acids

For the sulfur-containing group, there was a minor increase in absorbance as function of absorbed dose. The pH of cysteine remained constant as a function of absorbed dose, which had been affected by HCl as it was the same for aliphatic amino acids. The UV-Vis spectrum for methionine showed an increasing broad absorbance between 270 nm and 315 nm and an increase in pH with increased absorbed dose. The change in the UV-Vis spectrum could be explained as the oxidation of sulfur in the side chain. The relationship of the absorbance intensity with dose is plotted and fitted in the Fig. 6.4.

6.2.7 Imino acid

Proline is an imino acid and showed no change in UV-Vis spectrum as a function of absorbed dose; however, a decrease in pH was observed. The side chain of proline forms a closed ring with its closest carbonyl of the polypeptide backbone. More accurately, proline is an alpha amino acid that has a secondary amino group in which the nitrogen is single bonded to a hydrogen and two sp3-hybridized carbons, whereas a primary amino group is one in which the nitrogen is single bonded to two hydrogen atoms and one sp3-hybridized carbon atom. A decrease in pH with increase absorbed dose was similar to that of alanine and leucine.

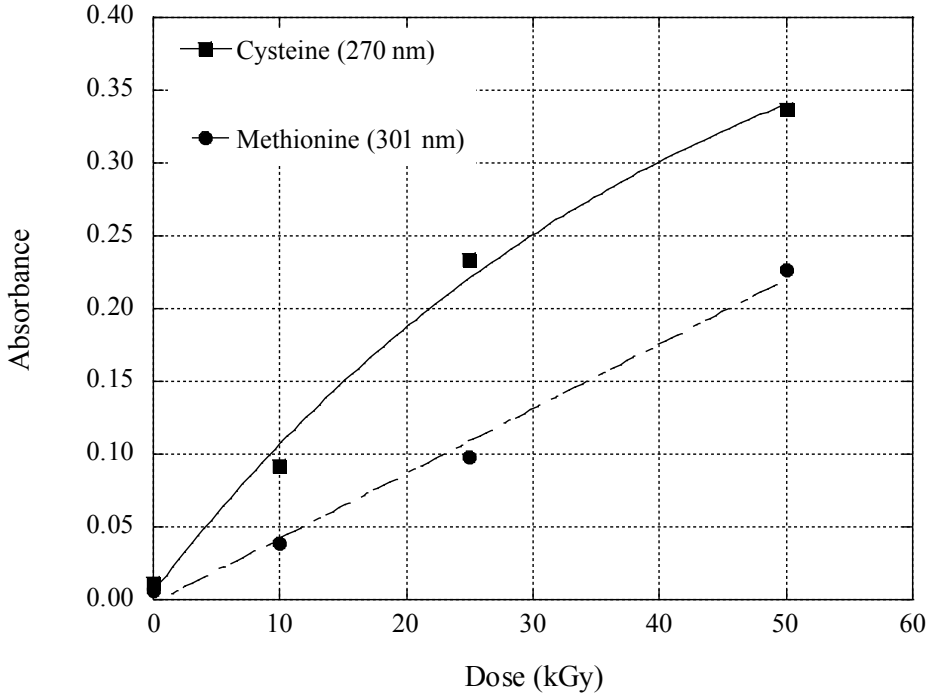

Figure 6.4. Absorbance as a function of absorbed dose for surfer-containing amino acids at specific wavelengths. The absorbance-dose relationship was $A_{\text{Cys}}^{270} = 0.485\left(1 - e^{-0.0235D}\right) + 0.0052$ for cysteine at 270 nm, and $A_{\text{Met}}^{301} = 67.926\left(1 - e^{-6.56\times10^{-5}D}\right) - 0.0024$ for methionine at 301 nm.

6.2.8 Radiosensitivity of amino acids

There are different ways to define the radiosensitivity of amino acids. Cataldo et al., concluded that the stability of amino acids to radiolysis due to radioracemization, which was measured by differential scanning calorimetry (DSC) and by optical rotatory

dispersion (ORD) spectroscopy for solid and dry state amino acids for a total absorbed dose of 3.2 MGy of gamma rays.[92] Amino acids in solid and solution forms can be used to examine the direct and indirect effect of radiation. In solution form most of the energy will be absorbed by water producing free radicals, which react with amino acids. Based on the fitting results of Eq. 6.2, a connection between the amount of primary amino acid and the corresponding product was determined; this is shown in Fig. 6.5, where *A* is the primary amino acid, and *B* is the corresponding product.

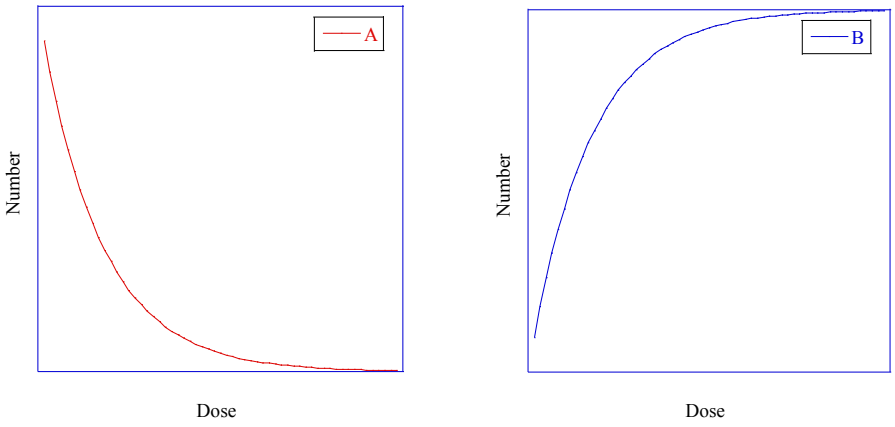

Figure 6.5. Schematic mechanism for an amino acid reaction to radiolysis, $A \xrightarrow{D} B$, yielding new products. We assume that product *B* is insensitive to radiation.

Then, the amounts of primary amino acid *A* and corresponding radiolytic product *B* could be described by Eq. 6.3 and Eq. 6.4 based on the reaction mechanism $A \xrightarrow{D} B$.

$$N_A = \frac{V}{\varepsilon_B l} A_{\max} e^{-D/D_0} \tag{6.3}$$

$$N_B = \frac{V}{\varepsilon_B l}\left(A_{\max}\left(1 - e^{-D/D_0}\right) + A_0\right) \tag{6.4}$$

where N_A and N_B are the number of amino acid and corresponding product (mole^{-1}), respectively, ε_B is the molar extinction coefficient of the product (L mole^{-1}·cm^{-1}), V is the volume of the sample (L^{-1}), l is the length of light path through the spectrophotometer (cm). Here we assume that the radiolytic product B is insensitive to radiation or as a combination of products that behave under the Arrhenius formula. Therefore, the radiosensitivity of amino acids in the current study is defined as

$$R_A = -\frac{1}{N_A}\frac{dN_A}{dD} = \frac{1}{D_0} \tag{6.5}$$

where R_A is the radio-sensitivity of the amino acid for a given wavelength.

Our UV-Vis observations indicated that in general aliphatic amino acids, acidic amino acids and imino acid were the most stable or radioresistant among all twenty amino acids. Moreover, the UV-Vis spectrum of acidic amino acids and imino acid in aqueous solution showed slight increase absorbance as a function of absorbed dose. Considering the secondary amino group in proline, the relative radiosensitivity of these three groups would be acidic amino acids > imino acid > aliphatic amino acids. The remaining amino acids are aromatic, neutral, basic, and sulfur-containing amino acids showed significant changes in their UV-Vis spectra. The UV-Vis experimental data for

selected wavelengths was fit to Eq. 6.2. The values for D_0 and $A_{\max}$ obtained from fitting the data are listed in the Table 6.4. However, methionine showed a linear absorbance-dose response with a non-saturable absorption for the range of absorbed doses in this study. For aromatic amino acids, the wavelength of new peaks, and D_0 increased with molecular weight. The same phenomenon was observed for the sulfur-containing amino acids. However, for serine and threonine, asparagine and glutamine, while the wavelength increases with molecular weight, D_0 decreased. For histidine and arginine, D_0 increased with mass, while the wavelength decreased. The values for A_{max} of histidine and asparagine were higher when compared with other amino acids, which was consistent with the fact that isolated arising new peaks were observed in the spectra.

The order in radiosensitivity among selected amino acids is given in Table 6.4. Comparing result of phenylalanine and tyrosine illustrated the fact tyrosine had not been reported as component of the mixture of amino acids found in meteorites, as tyrosine was formed in later stages of the chemical evolution as a derivative of phenylalanine as experimentally demonstrated.[93]

Table 6.4. Summary D_0 and A_{max} from fitting result of new band intensity in UV-Vis spectrum for selected amino acids

Sample	Classification	Wavelength (nm)	D_0 (kGy)	A_{max}
Phenylalanine (water)	Aromatic	285	25.97	0.918
Histidine (water)	Basic	278	30.77	1.882
Tyrosine (0.5HCl)	Aromatic	320	30.77	0.282
Threonine (water)	Neutral	261	41.49	0.361
		312	53.19	0.167
Cysteine (0.5HCl)	Sulfur-containing	270	42.37	0.485
Arginine (water)	Basic	247	47.85	0.353
Serine (water)	Neutral	285	58.14	0.462
Glutamine (water)	Neutral	287	61.35	0.286
Tryptophan (0.5HCl)	Aromatic	400	70.42	0.962
Asparagine (water)	Neutral	278	76.92	1.042
Methionine (water)*	Sulfur-containing	301	$>1.5\times10^{7}$	67.926

*Methionine showed a linear absorbance-dose relationship yielding a very low radiosensitivity.

As the components of the same neutral group, threonine and serine were more sensitive than asparagine and glutamine to radiation, which proved that the hydroxyl group is more easily attacked by free radicals than the amide group. Both threonine and glutamine showed a higher radiosensitivity when compared to serine and asparagine,

which could be accounted for by the extra statured carbon in the side chain of threonine and glutamine.

6.3 Analysis of Raman spectra of amino acids

Raman scattering is a photon emission process. The intensity of the Raman scattered photon is determined by the molecular vibrational frequency but is affected by many factors, such as the frequency and power of the excitation laser, the concentration of the sample, noise form system and software, and the operation temperature. In order to eliminate systematic differences among measurements, peak intensity normalization was performed. Baseline correction was performed before normalization using 7^{th} order polynomial fit. Min-/Max-normalization was applied, which is defined by Eq. 6.6, where I is the intensity of the Raman peak.

$$I_{\text{norm}} = \frac{I - I_{\text{min}}}{I_{\text{max}}} \qquad (6.6)$$

For amino acids, there was only one band of interest in the range from 1800 to 2850 cm^{-1}, the thiol SH stretching, at 2560 – 2590 cm^{-1}.[77] Therefore, the spectrum range for solid samples was 400 – 1800 cm^{-1}, solution simples was 500 – 1800 cm^{-1} because of the intense peak generated by quartz near 464 cm^{-1}. As a reference, the Raman spectra were collected from all samples, in solid and solution form, prior to irradiation. The results were in good agreement with previously reported results of amino acid Raman spectra.[73-75, 77, 79] The intensity normalized Raman spectra of the 20

amino acids in both, solid and solution form, irradiated at different absorbed doses are described in Appendix. A short operating time was needed to obtain the Raman spectrum for the tryptophan in solid form; otherwise the laser would burn the solid sample. For the case of histidine and tryptophan solutions, a significant change in color was observed after irradiation. We were not able to acquire Raman spectra of these amino acid solutions due to high fluorescence which overshadowed the Raman signal. The Raman spectra from aqueous solutions were acquired using a quartz dish, which generated strong peaks between 600 and 796 cm^{-1}. Moreover, an intense peak was observed at 1625 cm^{-1}, which was caused by water.

6.3.1 Aliphatic amino acids

The observed peaks for aliphatic amino acids are listed in Table 6.5 along with their relative intensities. Also, Table 6.6 lists the vibrational mode assignments for the Raman peaks that were identified in the open literature.

For alanine, the Raman shifts for the solid sample located at 842, 1299, 1352, 1401, and 1456 cm^{-1} could be found at 842, 1299, 1351, 1408 and 1457 cm^{-1} in the aqueous sample respectively, which could be considered as markers for alanine. It was noticed that the relative intensity of the Raman peaks in aqueous solution at 1298, 1352, 1401, and 1456 cm^{-1} were different from that in solid. The most intense peak in the solution was found at 1405 cm^{-1} and at 1352 cm^{-1} in solid form, which indicated a structural change altering the vibrational strength. Comparing the spectra of samples irradiated at different absorbed doses, there were no new peak appearances or

disappearances; however, an increase in intensity for the peak at 1482 cm^{-1} was observed for the solid sample irradiated at 25 kGy, which was caused by an incomplete baseline correction. This should be considered a measurements artifact and not an effect of radiation. In the spectra of solid samples, it was noticed that the peak at 842 cm^{-1}, which corresponded to a C-C stretching, displayed an increase in intensity with increased dose, which is listed in the Table 6.19. The same effect was observed in the solution sample for peak at 1621 cm^{-1} with an increase in intensity with increased absorbed dose.

Table 6.5. Baseline experimental Raman shifts for aliphatic amino acids in solid and solution forms			
Amino acid	Form	Observed Raman bands (cm^{-1})	Figure
Alanine	Solid	471(vw) 526(w) 642(vw) 764(w) 842(s) 914(w) 1014(m) 1106(w) 1139(m) 1229(vw) 1298(s) 1352(s) 1401(m) 1456(m) 1482(sh) 1496(sh) 1546(sh) 1593(m) 1621(sh)	A.22
	Sol. (H_2O)	604(solv) 785(solv) 842(s) 994(vw) 1106(vw) 1299(m) 1351(m) 1408(s) 1457(m) 1628(solv)	
Glycine	Solid	488(m) 596(w) 690(vw) 884(s) 1025(m) 1101(vw) 1130(vw) 1314(s) 1404(m) 1437(m) 1514(w) 1567(w) 1670(w)	A.29
	Sol. (0.5 M HCl)	604(solv) 701(br) 797(br) 872(s) 1042(br) 1435(m)	
Isoleucine	Solid	415(br) 479(w) 527(m) 664(w) 702(w) 741(br) 818(w) 842(w) 866(sh) 916(m) 982(m) 1022(m) 1079(w) 1127(m) 1181(w)1257(w) 1321(s) 1348(s) 1388(w) 1412(sh) 1443(s) 1511(w) 1625(w)	A.31
	Sol. (H_2O)	521(sh)604(solv) 748(sh) 811(br) 868(w) 912(vw) 981(w) 1025(w) 1067(sh)1126(vw) 1167(sh)1253(w)1332(m) 1409(m) 1440(w) 1453(sh)	

Abbreviations. solv: solvent, vw: very weak, w: weak, m: medium, s: strong, br: broad, sh: shoulder. Excitation laser: 532 nm.

Table 6.5. (cont.) Baseline experimental Raman shifts for aliphatic amino acids in solid and solution forms			
Amino acid	Form	Observed Raman bands (cm^{-1})	Figure
Leucine	Solid	447(s) 523(s) 664(w) 761(vw) 821(s)834(s) 913(m) 941(w) 948(w) 1028(w) 1071(m) 1124(m) 1179(m) 1230(vw) 1290(vw) 1307(vw) 1332(s) 1405(m) 1455(s) 1516(vw) 1624(w)	A.32
	Sol. (0.5 M HCl)	720(m) 821(br) 843(br)886(m) 955(m) 1127(m)1168(w) 1344(m) 1448(m) 1454(sh)	
Valine	Solid	455(w) 530(s) 647(vw) 701(w) 738(vw) 767(m) 811(w) 838(m) 888(w) 936(m) 1023(w) 1056(w) 1115(w) 1171(w) 1260(m) 1340(s) 1387(m) 1417(vw) 1445(s) 1510(m) 1614(m)	A.41
	Sol. (0.5 M HCl)	604(solv) 722(m) 805(br) 871(br) 937(w) 1057(w)1335(br) 1442(w) 1466(w)	

Abbreviations. solv: solvent, vw: very weak, w: weak, m: medium, s: strong, br: broad, sh: shoulder. Excitation laser: 532 nm.

Table 6.6. Assignment of Raman peaks for aliphatic amino acids (solid)					
Alanine		Glycine		Isoleucine	
Raman shift (cm^{-1})	Assignment	Raman shift (cm^{-1})	Assignment	Raman shift (cm^{-1})	Assignment
761	ω(CO2)	590	δ(COOH), δ(NCCO)	741	δ(CO_2-)
842	ν(CC)	685	δ(NH2)	842	r(CH_3)
1010	ν(CN)	883	τ(NH2), τ(CH2)	982	ν(CC)
1103	ν(CN)	1025	ν(CN)	1022	ν(CC)
1137	δ(CH) in plane	1314	τ(NH2), τ(CH2)	1127	r(NH_2)
1296	ν(CO)	1405	CH2 scissoring	1181	r(NH_2)
1352	δs(CH3)	1510	δ(CH_2), δ(OH)	1321	δ(CH)
1455	δas(CH3)	1670	δas(NH2)	1348	δ(CH)
1484	δs(CH3)			1410	νs(CO_2^-)
1494	δs(NH3)			1443	δas(CH_3)

Table 6.6. (cont.) Assignment of Raman shifts for aliphatic amino acids (solid)			
Leucine		Valine	
Raman shift (cm^{-1})	Assignment	Raman shift (cm-1)	Assignment
834	γ(COO)	767	δ(COO)
916	ν(CC)	838	γ(COO)
933	ν(CC)	889	ν(CC)
952	ν(CC)	936	ν(CC)
1075	ν(CN)	1340	δ(CH), δ(CH3)
1123	r(NH3)	1389	δ(CH), δ(CH3)
1174	r(NH3)	1451	δas(CH3)
1332	δ(CH)	1510	ν(CN)
1400	δs(CH3)		

δ= bending, ν= stretching, τ= twisting, r= rocking, ω= wagging, γ= out of plane vibration, as= asymmetric, s=symmetric

Glycine is the simplest amino acid, which contains no asymmetric carbon atoms. The bands located at 884 and 1437 cm^{-1} in the spectra of solid glycine could be found at 872 and 1435 cm^{-1} in the spectra of solution, respectively, which could be considered as markers of glycine. With increasing dose, a new peak appeared at 1455 cm^{-1}, and then combined with the peak at 1437 cm^{-1} into a large broadened peak. The peak intensity at

691 and 1670 cm^{-1} increased with dose. In the glycine solution spectrum, a peak at 647 cm^{-1} was observed with increase dose.

For isoleucine, the Raman shifts located at 527, 916, 982, 1022, 1079, 1127, 1181, and 1257 cm^{-1} from the solid sample spectra were observed at 521, 912, 981, 1025, 1067, 1126, 1167 and 1253 cm^{-1} in the solution spectra, respectively, which could be considered as markers for isoleucine. The broad peak observed at 741 cm^{-1} in the solid sample was divided into two distinct weak peaks increasing with absorbed dose. The peak at 604 cm^{-1} decreased while a new peak was formed at 640 cm^{-1} with increased dose. In the Raman spectrum of irradiated 10 kGy isoleucine solution sample, the intensities of peaks at 600, 800cm^{-1}, which were caused by quartz, increased sharply. This could be caused by the low focus depth of the laser.

For leucine, the Raman shifts located at 821, 834, 1124, 1179, 1342, and 1455 cm^{-1} in the solid sample were observed at 821, 843, 1127, 1168, 1344, and 1448 cm^{-1} in the spectrum from the solution sample, respectively, which could all be considered as the markers for leucine. With increase of dose, the two strong peaks at 821 and 843 cm^{-1} evolved into one strong peak, while the peaks at 941 and 948 cm^{-1} were combined into a broadened peak. No significant changes were observed in the spectrum of leucine solution sample after irradiation. There was abnormal behavior of the irradiated 25 kGy solution spectrum.

For valine, the Raman shifts located at 1340, 1417, and 1445 cm^{-1} in the spectra of solid could be found at 1335, 1442, and 1466 cm^{-1} in the spectra of solution

respectively, which could be considered as markers for valine in the Raman spectrum. No significant change was observed for the spectra of valine solid and solution after radiation.

6.3.2 Aromatic amino acids

The observed Raman shifts for aromatic amino acids are listed in Table 6.7 along with their relative intensities. Also, Table 6.8 lists the vibrational mode assignments for the Raman peaks that were identified in the open literature.

For phenylalanine, the Raman shifts located at 994, 1024, 1152, 1210, 1403, and 1439 cm^{-1}, in the spectrum of solid could be found at 1000, 1024, 1150, 1196, 1401, and 1438 cm^{-1} in the spectrum of solution respectively. The first three peaks were all caused by the bending of the aromatic ring, which could be considered as markers for phenylalanine. There was a weak peak shown with increase of dose at 845 cm^{-1}. The peak and new appeared shoulder at 819 and 845 cm^{-1}, were also observed in the spectrum of tyrosine. A new peak was formed in the spectrum of the sample irradiated to 25 kGy, while combined with the near peak into a larger peak in the spectrum of irradiated 50 kGy sample. No significant change was observed in the spectrum of the phenylalanine solution sample. The larger peaks at 604 and 800 cm^{-1} were caused by the low focus depth of the laser which leaded strong signal from quartz.

Table 6.7. Baseline experimental Raman shifts for aromatic amino acids in solid and solution forms.			
Amino Acid	Form	Observed Raman bands (cm^{-1})	Figure
Phenylalanine	Solid	453(w) 509(vw) 604(w) 733(w) 817(m) 900(vw) 938(vw) 994(s) 1024(m) 1152(w) 1176(w) 1210(m) 1306(w) 1333(br) 1403(vw) 1439(vw) 1606(m)	S.35
	Sol. (H_2O)	604(solv) 800(br) 1000(s)1024(m) 1150(w) 1196(m) 1334(br) 1401(vw) 1438(vw)	
Tryptophan	Solid	531(w) 620(br) 696(w) 751(s) 870(m) 966(vw) 1006(s) 1071(w) 1248(br) 1337(s) 1350(s)1431(m) 1546(s) 1577(vw) 1616(w)	S.39
	Sol. (0.5 M HCl)	528(br) 616(w) 696(w) 749(s) 793(w) 868(s) 974(vw) 1004(s) 1060(w) 1106(w) 1224(m) 1241(sh) 1332(s) 1349(sh) 1415(m) 1449(w) 1484(sh) 1555(s) 1575(sh) 1615(m)	
Tyrosine	Solid	419(w) 475(br) 521(vw) 637(m) 708(w) 731(vw) 786(w) 819(s) 841(sh) 975(m) 1037(w) 1170(m) 1198(m) 1257(m) 1318(s) 1359(w) 1432(w) 1520(br) 1609(s)	S.40
	Sol. (0.5 M HCl)	635(m) 707(w) 786(w) 819(s) 839(sh) 1069(w) 1171(w) 1200(s) 1256(br) 1347(m) 1441(w)	

Abbreviations. solv: solvent, vw: very weak, w: weak, m: medium, s: strong, br: broad, sh: shoulder. Excitation laser: 532 nm.

Table 6.8. Assignment of Raman shifts for aromatic amino acids (solid)					
Phenylalanine		Tryptophan		Tyrosine	
Raman shift (cm^{-1})	Assignment	Raman shift (cm^{-1})	Assignment	Raman shift (cm^{-1})	Assignment
610	δ(OCO)	747	indole(C8H7N) ring breathing	786	ω(NH2)
740	δring(CH), γring	867	H scissoring on indole ring	819	ring breathing
995	δring	1000	indole ring breathing	974	r(CH2)
1026	δring	1224	H rocking benzene	1035	ν(CH2)
1207	δring , γ(CH)	1351	δ(CH2)	1195	sym stretch parasubstitute benzene
		1417	indole ring stretching	1256	δ(OH) ring in plane
		1449	δ(CH2)		

δ= bending, ν= stretching, τ= twisting, r= rocking, ω= wagging, γ= out of plane vibration, as= asymmetric, s=symmetric

For tryptophan, the Raman shifts located at 696, 751, 867, 1337, and 1350 cm^{-1} in the spectrum of the solid could be found at 696, 749, 868, 1332, and 1349 cm^{-1} in the spectrum of the solution respectively, which could be considered as markers for tryptophan. With increase of dose, the peak at 1337 cm^{-1} evolved into a shoulder.

For tyrosine, the Raman shifts located at 637, 708, 786, 819, 843, 1170, 1198, and 1520 cm^{-1} in the spectra of solid could be found at 635, 707, 786, 819, 839, 1171, 1200 and 1511 cm^{-1} in the spectrum of solution respectively, which could be considered as markers for tyrosine. No significant change was observed for the spectrums of tyrosine solid. In the spectra of tyrosine solution, there was intensity increase at 604 and 786 cm^{-1} while decrease at 819 and 841 cm^{-1} after radiation.

6.3.3 Neutral amino acids

The observed Raman peaks for neutral amino acids are listed in Table 6.9 along with their relative intensities. Also, Table 6.10 lists the vibrational mode assignments for the Raman peaks that were identified in the open literature.

For asparagine, the Raman shifts located at 867, 931, and 977 cm^{-1} in the spectrum of solid could be found at 865, 920 and 975 cm^{-1}, the intensity of which three were interpreted by the quartz. The Raman shifts located at 1321, 1348, and 1408 cm^{-1} in the spectrum of solid could be found at 1322, 1350 and 1410 cm^{-1} in the spectrum of solution respectively, which could be considered as the markers for asparagine. Comparing the spectra of solid samples, there was a new peak appearance and a peak disappearance for 10 kGy and 25 kGy at 772 and 1150 cm^{-1}, respectively, the intensity of the new peak increased with dose. For 50 kGy irradiated solid samples, there was a new peak at 829 cm^{-1}. The intensity of Raman shift at 604 cm^{-1} increased with absorbed dose in the spectra of asparagine solution.

Table 6.9. Baseline experimental Raman shifts for neutral amino acids in solid and solution forms			
Amino Acid	Form	Observed Raman shifts (cm^{-1})	Figure
Asparagine	Solid	440(w) 531(m) 570(vw)650(sh) 747(m)796(vw) 867(m) 931(s) 977(w) 1063(m) 1103(m) 1150(s) 1252(w) 1321(s) 1348(sh) 1408(s) 1495(vw) 1159(w) 1617(m)	S.24
	Sol. (H_2O)	604(solv) 791(sh) 815(sh) 865(br) 920(sh)975(sh) 1322(w) 1350(m) 1410(m) 1628(solv)	
Glutamine	Solid	438(br) 532(vw) 610(w) 640(sh) 764(vw) 839(s) 887(m) 988(vw) 1047(vw) 1087(m) 1127(w) 1153(w) 1193(vw) 1279(sh) 1322(s) 1409(m) 1442(sh) 1496(w) 1544(vw) 1605(m) 1683(vw)	S.28
	Sol. (H_2O)	604(solv) 700(sh) 791(br) 850(m) 896(m) 1069(w) 1116(br) 1341(s) 1419(s)	
Serine	Solid	501(s) 598(m) 804(m) 846(s) 911(vw) 960(w) 1000(m) 1117(w) 1212(w) 1291(w) 1318(m) 1412(br) 1460(m)	S.37
	Sol. (H_2O)	604(solv) 799(s) 840(s) 900(s)964(w) 1044(m) 1338(m) 1400(w) 1460(w)	
Threonine	Solid	430(w) 478(vw) 552(s) 692(w) 734(w) 768(sh) 861(s) 893(w) 921(m) 1031(w) 1106(s) 1188(w) 1244(vw) 1330(s) 1408(s) 1450(m) 1547(w) 1598(w) 1639(w)	S.38
	Sol. (H_2O)	604 (solv) 772(br) 857(br) 917(w) 1332(m) 1398(m) 1445(w)	

Abbreviations. solv: solvent, vw: very weak, w: weak, m: medium, s: strong, br: broad, sh: shoulder. Excitation laser: 532 nm.

Table 6.10. Assignment of Raman shifts for neutral amino acids (solid)			
Asparagine		Gutamine	
Raman shift (cm^{-1})	Asgmt	Raman shift (cm^{-1})	Asgmt
570	$\delta(CO_2^-)$	614	δ(NH3)
603	δs(CONH2)	765	$\delta(CO_2^-)$
867	ν(CC)	841	ν(CC)
1063	ν(CN)	1087	r(NH2)
1103	ν(NH3+)	1125	r(NH4)
1150	ν(NH2)	1278	ω(CH2)
1252	τ(CH2)	1320	δ(CH2)
1348	δ(CH)	1438	δ(CH2)
1408	δ(CN)		

Asgmt: Assignment, δ= bending, ν= stretching, τ= twisting, r= rocking, ω= wagging, γ= out of plane vibration, as= asymmetric, s=symmetric

Table 6.10. (cont.) Assignment of Raman shifts for neutral amino acids (solid)			
Serine		Threonine	
Raman shift (cm-1)	Asgmt	Raman shift (cm-1)	Asgmt
602	δ(COO)	552	r(CO2)
804	νs(CCO)	696	νs (CO2-)
843	νs(CCN)	737	δ(CO2-)
1001	δ(COH)	861	ν(CCN)
1290	γ(CH)	893	ν(CCN)
1317	ω(CH2)	1031	δ(OH)
1406	νs(COO)	1106	r(NH3+)
1444	δ(CH)	1330	δ(CH)
1462	δ(CH)	1408	νs(CO2-)

Asgmt: Assignment, δ= bending, ν= stretching, τ= twisting, r= rocking, ω= wagging, γ= out of plane vibration, as= asymmetric, s=symmetric

For glutamine, the Raman shifts located at 764, 839, 887, 1322 and 1409 cm^{-1} in the spectrum for the solid sample could be found at 764, 850, 896, 1340 and 1419 cm^{-1} in the spectrum of the solution sample, respectively, which could be considered as the markers for glutamine. With increasing of dose, the peak shoulders at 1350 and 1628 cm^{-1} evolved into a weak peak in the spectra of 25 and 50 kGy irradiated solid samples of glutamine. It was noticed that the peak at 896 cm^{-1} evolved into broad peak with increased dose.

For serine, the Raman peaks located at 846, 1412, 1460 cm^{-1} in the solid sample spectrum could be found at 840, 1400, 1460 cm^{-1} in the spectrum of the solution sample, respectively, which could be considered as the markers for serine in Raman spectroscopy. The intensity of peaks at 507 and 604 cm^{-1} increased as a function of absorbed dose, and the intensity of the peak at 501 cm^{-1} increased faster, which leaded the relative intensity of two peaks reversed for high dose. There was sharp intensity increase at 1318 cm^{-1} in the spectrum of irradiated 10 kGy serine solid sample. The intensity of peak at 800 cm^{-1} increased rapidly after radiation in the spectra of serine solution.

For threonine, the Raman peaks located at 861, 893, 921, 1330, 1408, and 1450 cm^{-1}, in the solid spectra could be found at 857, 892, 922, 1332, 1398, and 1445 cm^{-1} in the solution spectrum, respectively, which could be considered as the markers for threonine in Raman spectroscopy. No significant changes were observed for the threonine spectra between the solid and aqueous solution.

6.3.4 Acidic amino acids

The observed peaks for acidic amino acids are listed in Table 6.11 along with their relative intensities. Also, Table 6.12 lists the vibrational mode assignments for the Raman peaks that were identified in the open literature.

Table 6.11. Baseline experimental Raman peaks for acidic amino acids in solid and solution forms			
Amino Acid	Form	Observed Raman shifts (cm^{-1})	Figure
Aspartic acid	Solid	453(w) 539(w) 587(vw)650(vw) 741(m) 770(m) 862(m) 893(vw)931(s) 982(vw) 1073(w) 1109(vw) 1242(w) 1327(s) 1416(s) 1507(vw)1550(vw)1614(vw)1688(m)	S.25
	Sol. (0.5 M HCl)	604(solv) 816(br)918(w)	
Glutamic acid	Solid	446(vw) 490(w) 529(s) 696(vw) 753(m) 793(m) 857(s) 910(m) 933(s) 959(w) 1077(m) 1117(vw) 1138(w) 1203(vw) 1301(m) 1341(m) 1398(s) 1428(m) 1509(m) 1655(m)	S.27
	Sol. (0.5 M HCl)	604(solv) 790(s) 847(sh) 908(w) 1060(br) 1411(br)	

Abbreviations. solv: solvent, vw: very weak, w: weak, m: medium, s: strong, br: broad, sh: shoulder. Excitation laser: 532 nm.

Table 6.12. Assignment of Raman peaks for acidic amino acids (solid)			
Aspartic Acid		Glutamic Acid	
Raman shift (cm^{-1})	Assignment	Raman shift (cm^{-1})	Assignment
647	δ(COOH)	793	r(CH2)
770	γ(OCO)	857	r(CH2)
889	r(CH2)	910	ν(CN), ν(CC)
929	γ(OH)	933	γ(OH)
978	ν(CN), ν(CC)	1077	ν(CN), ν(CC)
1077	ω(NH3)	1188	r(NH3)
1109	ω(NH3)	1307	ω(CH2)
1245	τ(CH2)	1342	δ(CH)
1327	δ(CH)	1431	δ(CH2)
1414	ν(CO2)		

δ= bending, ν= stretching, τ= twisting, r= rocking, ω= wagging, γ= out of plane vibration, as= asymmetric, s=symmetric.

For aspartic acid, the Raman shift located at 931 cm^{-1} in the solid spectra was found at 916 cm^{-1} in solution spectra. There was limited information obtained from the Raman spectrum of the solution. The spectrum of irradiated to 25 kGy sample behaved so abnormally that most peaks were not matched with the ones in other solid aspartic acid samples. Moreover, a check was carried out with the spectra of other amino acids samples to exclude the possibility of sample mislabeling. Therefore, the comparison of

irradiated solid aspartic acid sample excluded the 25 kGy spectrum. The intensity of peaks at 931 and 1416 cm^{-1} increased with dose, which corresponded to the function group –COOH; while at 1327 cm^{-1}, intensity decreased with dose. There was no significant change in the spectra of aspartic acids solution.

For glutamic acid, the Raman shifts located at 857, 1398, and 1428 cm^{-1} in the spectrum of the solid were found at 847, 1411 and 1446 cm^{-1} in the spectrum of the solution, respectively, which could be considered as the markers for glutamine acid in Raman spectroscopy. There was no significant change in the spectra of glutamic acid between as a function of absorbed doses for both solid and solution forms.

6.3.5 Basic amino acids

The observed peaks for basic amino acids are listed in Table 6.13 along with their relative intensities. Also, Table 6.14 lists the vibrational mode assignments for the Raman peaks that were identified in the open literature.

Table 6.13. Baseline experimental Raman peaks for Basic amino acids in solid and solution forms			
Amino Acid	Form	Observed Raman bands (cm^{-1})	Figure
Lysine	Solid	438(w) 536(m) 615(m) 695(w) 776(m) 866(m) 895(m) 965(m) 1057(s) 1142(w) 1243(vw) 1294(m) 1607(s)	S.33
	Sol. (H_2O)	528(sh)703(w)778(m) 832(br) 871(br) 967(vw)1055(m) 1138(w) 1236(vw)1408(sh) 1437(m)	
Arginine	Solid	476(vw) 539(w) 564(sh) 604(w) 785(vw) 839(vw) 872(vw) 909(w) 977(s) 1022(vw) 1059(s) 1089(m) 1186(m) 1252(vw) 1290(m) 1320(m) 1428(s) 1468(w) 1617(sh)1708(vw)	S.23
	Sol. (H_2O)	536(w) 604(solv) 707(vw)786(br) 870(br) 971(m) 1065(s) 1162(w) 1310(m) 1354(m) 1406(sh) 1432(s) 1628(solv)	
Histidine	Solid	532(w) 621(sh) 643(vw) 721(vw) 766(w) 796(vw) 844(w) 913(w) 964(w) 1058(vw) 1080(m) 1107(w) 1133(w) 1167(m) 1214(vw) 1243(sh) 1263(m) 1310(s) 1339(sh) 1400(w) 1424(w) 1493(m) 1566(m)	S.30
	Sol. (H_2O)	604(solv) 618(m) 699(w) 794(m) 850(br) 975(w) 1060(w) 1150(m) 1239(sh) 1261(m) 1312(s) 1340(sh) 1430(m) 1491(m) 1568(m)	

Abbreviations. solv: solvent, vw: very weak, w: weak, m: medium, s: strong, br: broad, sh: shoulder. Excitation laser: 532 nm.

Table 6.14. Assignment of Raman shifts for basic amino acids (solid)			
Arginine		Lysine	
Raman shift (cm^{-1})	Assignment	Raman shift (cm^{-1})	Assignment
836	ν(CC)	615	ω(COO)
906	δ(NH2)	895	ν(CC)
1019	δ(OH)	965	ν(CC)
1057	ν(CC)	1057	ν(CN)
1095	ν(CN)	1142	ω(NH)
1177	ν(CN)	1294	ω(CH2)
1317	νs(COO)		
1434	νas(NCN)		
1460	δas(CH3)		
Histidine			
Raman shift (cm^{-1})	Assignment	Raman shift (cm^{-1})	Assignment
912	δ(CH) in plane	1262	δ(CH), ν(CN)
1079	δ(CH), ν(CN)	1309	δ(CH), ν(CN)
1169	δ(CH), γ(CH2)	1425	νs(CO2)
1244	δ(CH), ν(CN)	1492	δ(NH), ν(CN)
1388	δs(CH3)		

Abbreviations. δ= bending, ν= stretching, τ= twisting, r= rocking, ω= wagging, γ= out of plane vibration, as= asymmetric, s=symmetric

For arginine, the Raman shifts located at 977, 1290, 1428, and 1468cm^{-1} in the spectrum of solid could be found at 971, 1299, 1406 and 1432 cm^{-1} in the spectrum of solution respectively, which could be considered as markers for arginine. The peak broadening at 870 cm^{-1} and intense peak at 1065 cm^{-1} in the solution were caused by the two peaks 839 and 872 cm^{-1}, 1059 and 1089 cm^{-1} in the sold, respectively. There was little change found in the spectra of solid and solution samples. The abnormal behavior of the spectrum for irradiated 10 kGy solution sample and irradiated 50 kGy solid sample could be accounted for by the low focus depth of the laser and incompleteness of baseline correction. Similar abnormal observation could be found in the spectrum of the irradiated 10 kGy lysine solid sample and the irradiated 50 kGy isoleucine and proline solid sample. There was a new arising peak at 645 cm^{-1} in the spectra of arginine solid after irradiation.

For histidine, the Raman shifts located at 1243, 1263, 1310, 1322, 1339, 1400, 1424, 1493, and 1566 cm^{-1} from the solid sample were also be found at 1239, 1261, 1312, 1340, 1408, 1430, 1491 and 1568 cm^{-1} in the solution sample, respectively, which were all caused by the bending and stretching of C-H and C-N bonds except for the peak at 1424 cm^{-1}, and could all be considered as markers for histidine. There was no new peak appearance or peak disappearance in the spectra of histidine solid samples.

For lysine, the Raman shifts for the solid sample located at 536, 695, 776, 965, 1057, 1142, and 1243 cm^{-1} were observed at 528, 703, 778, 967, 1055, 1138, and 1236 cm^{-1} in the solution sample, respectively, which could all be considered as markers for

lysine. It was noticed an intense peak around 1500 cm^{-1} in the solid sample; however, no peak was observed in the spectrum of solution sample, which might be caused by the intense peak of water in 1610 cm^{-1} also shown in the spectra of other amino acids. There was no significant change in the spectra of lysine solid sample. There was abnormal behavior of the irradiated 25 kGy solution spectrum.

6.3.6 Sulfur-containing amino acids

The observed peaks for sulfur-containing amino acids are listed in Table 6.15 along with their relative intensities. Also, Table 6.16 lists the vibrational mode assignments for the Raman peaks that were identified in the open literature.

Table 6.15. Baseline experimental Raman shifts for sulfur-containing amino acids in solid and solution forms			
Amino Acid	Form	Observed Raman bands (cm^{-1})	Figure
Cysteine	Solid	435(m) 528(m) 631(s) 682(s) 765(m) 800(sh) 814(m) 858(m) 935(w) 999(vw) 1061(w) 1099(vw) 1135(vw) 1190(m) 1261(vw) 1285(m) 1338(s) 1389(m) 1417(s)1525(w)1579(w)	A.26
	Sol. (0.5 M HCl)	604(solv) 673(s) 775(br) 860(m) 927(w) 985(w) 1060(w) 1327(br) 1417(m)	
Methionine	Solid	406(vw) 438(vw) 535(m) 637(m) 674(w) 710(s) 756(w) 797(w) 867(m) 946(vw) 980(vw) 1020(vw) 1064(vw) 1114(vw) 1145(vw) 1168(vw) 1239(vw) 1259(vw) 1314(m) 1345(m) 1408(sh) 1438(s) 1513(w) 1618(w)	A.34
	Sol. (H_2O)	604(solv) 643(w) 691(m) 713(m) 800(br) 868(w) 1055(br) 1336(m) 1418(m)	

Abbreviations. solv: solvent, vw: very weak, w: weak, m: medium, s: strong, br: broad, sh: shoulder. Excitation laser: 532 nm.

Table 6.16. Assignment of Raman peaks for sulfur-containing amino acids (solid)			
Cysteine		Methionine	
Raman shift (cm^{-1})	Assignment	Raman shift (cm^{-1})	Assignment
680	ν(CS)	710	νas(CS)
762	r(CH2)	752	r(CH2)
812	δ(CO2)	869	ν(CC), r(CH2)
860	ν(CC)	1311	ω(CH2)
936	δ(SH)	1346	ω(CH2), δ(CH2) in plane
1001	δ(SH)	1438	δas(CH3)
1061	ν(CN)		
1094	τ(CH2)		
1190	τ(CH2)		
1264	r(CH2)		
1285	ω(CH2)		
1338	r(CH2)		
1389	δs(CO2-)		
1420	δ(CH2)		

Abbreviations. δ= bending, ν= stretching, τ= twisting, r= rocking, ω= wagging, γ= out of plane vibration, as= asymmetric, s=symmetric.

For cysteine, the Raman shifts located at 682, 858 and 1417 cm^{-1} in the spectrum of solid could be found at 685, 860 and 1417 cm^{-1} in the spectrum of solution respectively, which could be considered as markers for cysteine. There was no new peak appearance or peak disappearance in the spectra of cysteine solid and solution samples.

For methionine, the Raman shifts in the solid sample located at 637, 867, and 1064 cm^{-1} in were observed at 643, 868, 1055 cm^{-1} in the solution sample, respectively. The most intense peak at 710 cm^{-1} observed in the solid spectrum, corresponding to the C-S bond stretching, was divided into two peaks in the solution spectrum. With increasing absorbed dose, the shoulder peak at 1408 cm^{-1} evolved into a distinct peak. Intensities of two peaks at 1513 and 1618 cm^{-1}, decreased with increasing dose. The changes after radiation were also reported in the recent paper.[63] Both changes corresponded to stretching of COOH and NH_2, which proved the decarboxylation and deamination during the ionization. No significant change was observed in the spectrum of methionine solution sample.

6.3.7 Imino acids

The observed peaks for imino acids are listed in Table 6.17 along with their relative intensities. Also, Table 6.18 lists the vibrational mode assignments for the Raman peaks that were identified in the open literature.

Table 6.17. Baseline experimental Raman peaks for Imino acids in solid and solution forms			
Amino Acid	Form	Observed Raman bands (cm^{-1})	Figure
Proline	Solid	437(s) 560(vw) 631(s) 779(w) 833(s) 890(s) 942(w) 977(m) 1025(m) 1045(w) 1073(s) 1167(m) 1230(s) 1251(sh) 1280(w) 1366(m) 1444(m) 1545(m) 1622(w)	S.36
	Sol. (H_2O)	604 (solv) 694(br) 779(m) 847(s) 900(s) 978(w) 1032(m) 1066(sh) 1163(w) 1229(w) 1326(m) 1400(m) 1451(m)	

Abbreviations. solv: solvent, vw: very weak, w: weak, m: medium, s: strong, br: broad, sh: shoulder. Excitation laser: 532 nm.

Table 6.18. Assignment of Raman peaks for Imino acids (solid)			
Proline			
Raman shift (cm^{-1})	Assignment	Raman shift (cm^{-1})	Assignment
631	ω(CO2-)	1025	ν(CCN), ν(CC)
779	Skeletal bend	1073	ω(CH2)
833	r(CH2)	1167	τ(CH2)
890	r(NH2)	1230	τ(CH2)
942	ν(CCN), ν(CC)	1444	δ(CH2)
977	ν(CCN), ν(CC)		

Abbreviations. δ= bending, ν= stretching, τ= twisting, r= rocking, ω= wagging, γ= out of plane vibration, as= asymmetric, s=symmetric

For proline, the Raman shifts located at 785, 833, 910, 1167, and 1444 cm^{-1} in the spectrum of the solid could be found at 782, 847, 902, 1163, and 1451 cm^{-1} in the spectrum of the solution respectively, which could be considered as markers for proline in the Raman spectrum. The broadened peak at 910 cm^{-1} evolved into a weak peak, the intensity of which increased with dose. The intensity of the peak at 779 cm^{-1} increased after irradiation in the spectra of proline solution.

It was noticed that abnormal spectra were obtained for different samples for the same absorbed dose. These abnormalities in spectra were observed for leucine and lysine in solution irradiated at 25 kGy. We adjudicate these abnormalities to potential instability of the laser.

Table 6.19. Summary of representative Raman shifts showing significant change as a function of absorbed dose					
Sample	Raman shift (cm^{-1})	Relative intensity of the peak for corresponding irradiated sample (kGy)			
		0	10	25	50
Alanine (solid)	842	0.752	0.783	0.842	0.971
Alanine (solution)	1621	0.525	0.614	0.795	0.942
Asparagine (solution)	603	0.128	0.233	0.259	0.323
Aspartic Acid (solid)	930	0.629	0.792	NA	0.936
	1327	0.881	0.670	NA	0.473
	1414	0.632	0.938	NA	1.000
Glycine (solid)	690	0.082	0.088	0.121	0.221
	1670	0.074	0.091	0.119	0.156
Methionine (solid)	1512	0.199	0.177	0.145	0.118
	1617	0.203	0.195	0.164	0.163
Proline (solid)	910	NA	0.375	0.429	0.529
Serine (solid)	507	0.140	0.314	0.655	0.840
	604	0.193	0.324	0.498	0.598
Serine (solution)	800	0.386	0.855	0.880	0.970

The summary of intensities of Raman peaks as a function of absorbed dose are shown in Table 6.19, there was no doubt that Raman spectroscopy was capable of detecting the effects of radiolysis in amino acids, however, whether it could give quantitative information based on the data needed to be further examined.

The relationship between the intensity of Raman shifts and absorbed dose listed in the Table 6.19 are plotted in Fig.6.6 to Fig. 6.10, according to the classification of amino acids.

In Fig. 6.6, the relative intensity of the Raman shift at 842 cm^{-1} in alanine solid increased almost linearly with absorbed dose, which indicated new molecule produced containing strong stretching of C-C bond and the quantity of this molecule was proportional to dose. The Raman shift at 1621 cm^{-1} in alanine solution was corresponding to combination of various vibrations, the intensity of which increased with absorbed dose and saturation existed for higher absorbed dose. The reason for this change should be further examined. The Raman shift at 690 and 1670 cm^{-1} were corresponding to NH_2 bending and NH_2 asymmetric bending, the slight increase with absorbed dose indicated the change of $-NH_2$ in glycine.

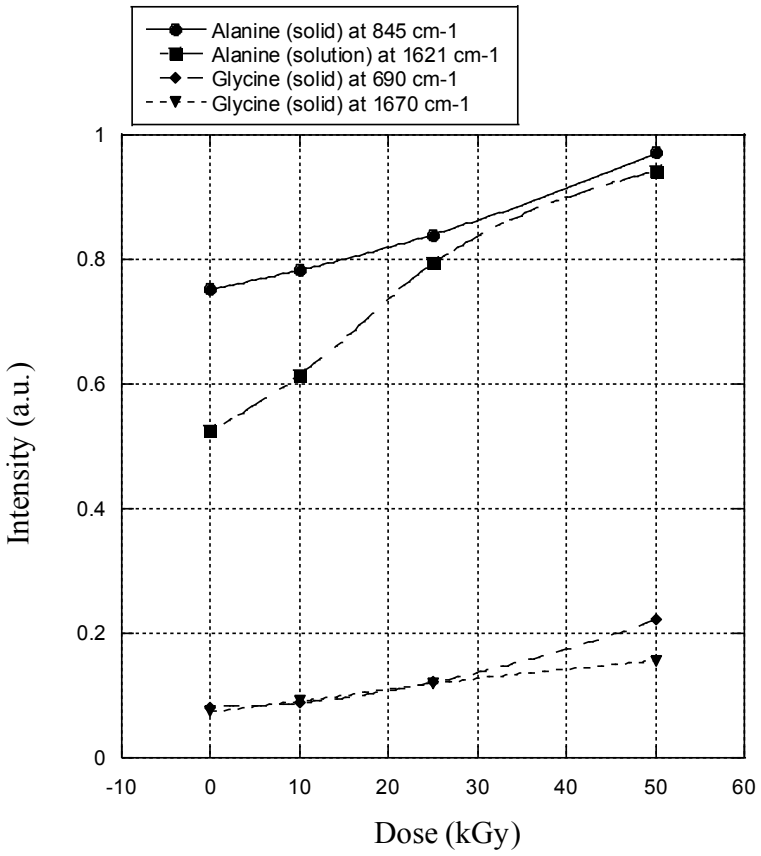

Figure 6.6. Relative intensities of Raman shifts as a function of absorbed dose for aliphatic amino acids.

In Fig. 6.7, the slight increase of relative intensity of the Raman shift at 603 cm^{-1}, indicated production of molecules containing stronger asymmetric bending of $CONH_2$. Both Raman shifts at 604, 800 cm^{-1} in serine solid were corresponding to the bending of COO and stretching of CCO, respectively. Those bands were all related to the carboxyl

acid and α carbon, which meant the new formed molecular should be an acidic molecular.

In Fig. 6.8, the relative intensity of Raman shift at 1327 cm^{-1} corresponding to CH bending suggested the potential band breakage between the α-carbon and hydrogen, which might be cause by the oxidation of carbon. Raman shifts at 930 and 1414 cm^{-1} were related to out of plane vibration of OH bond and stretching of COO bond, respectively. The intensities of both Raman shifts increased with absorbed dose and saturation existed for high dose, which suggested the amount of new formed molecules also depended on the dose.

In Fig. 6.9, the relative intensity of Raman shift at 1512 cm^{-1}, first decreased then remained constant, which suggested that there was a new molecule produced after radiation, and the new product was radiolytic resistance. The Raman shift at 1617 cm^{-1} was corresponding to the in-plane bending of NH_2; the decrease in intensity suggested the deamination of methionine during radiation.

In Fig. 6.10, a peak formed after radiation of Raman shift at 910 cm^{-1}, suggested the production of a new molecule.

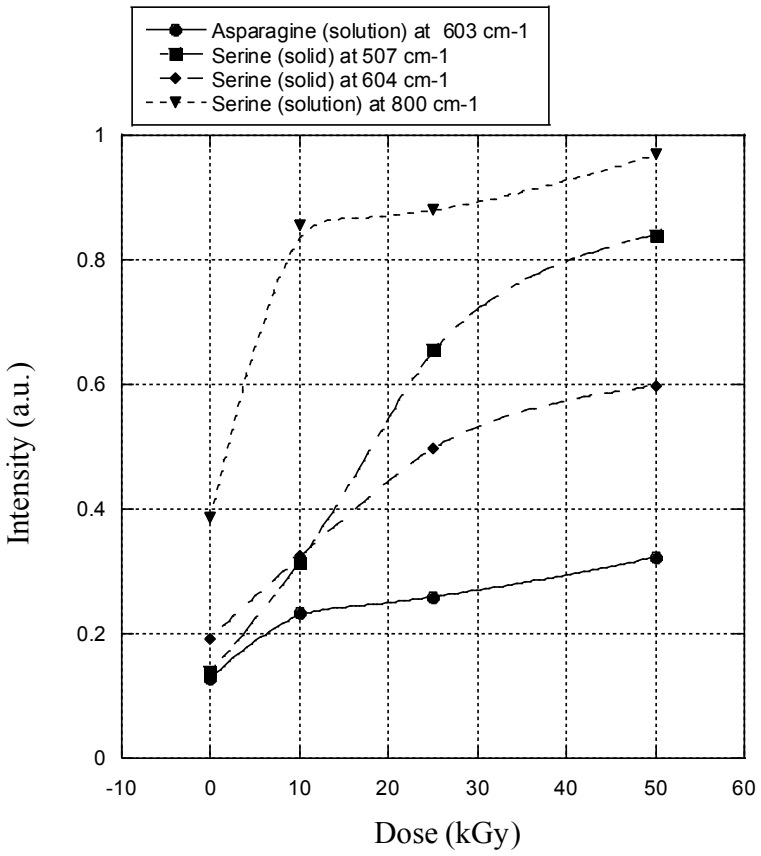

Figure 6.7. Relative intensities of Raman shifts as a function of absorbed dose for neutral amino acids.

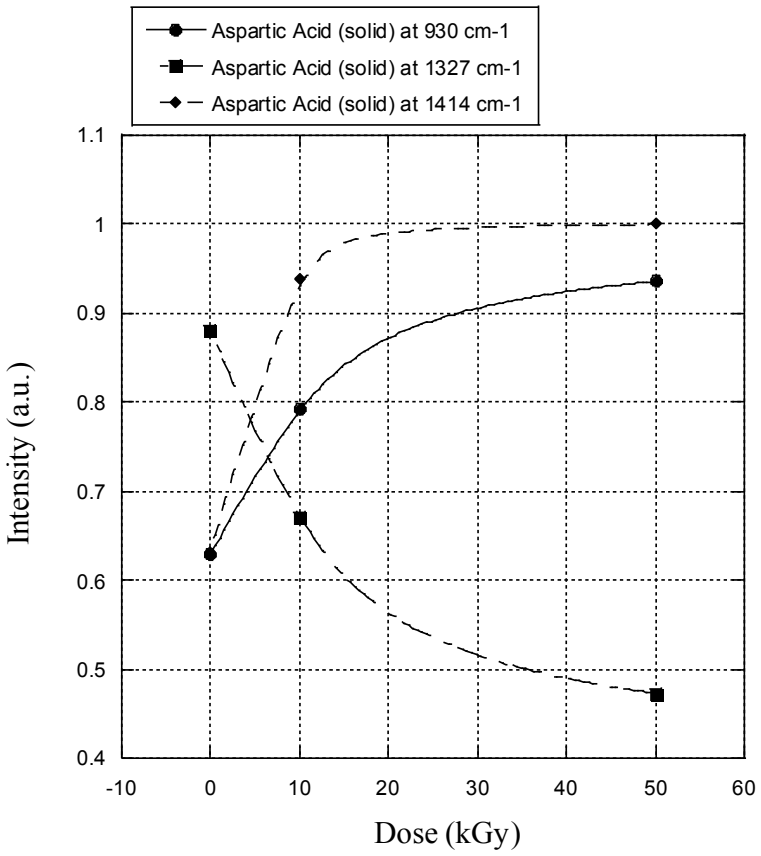

Figure 6.8. Relative intensities of Raman shifts as a function of absorbed dose for acidic amino acids.

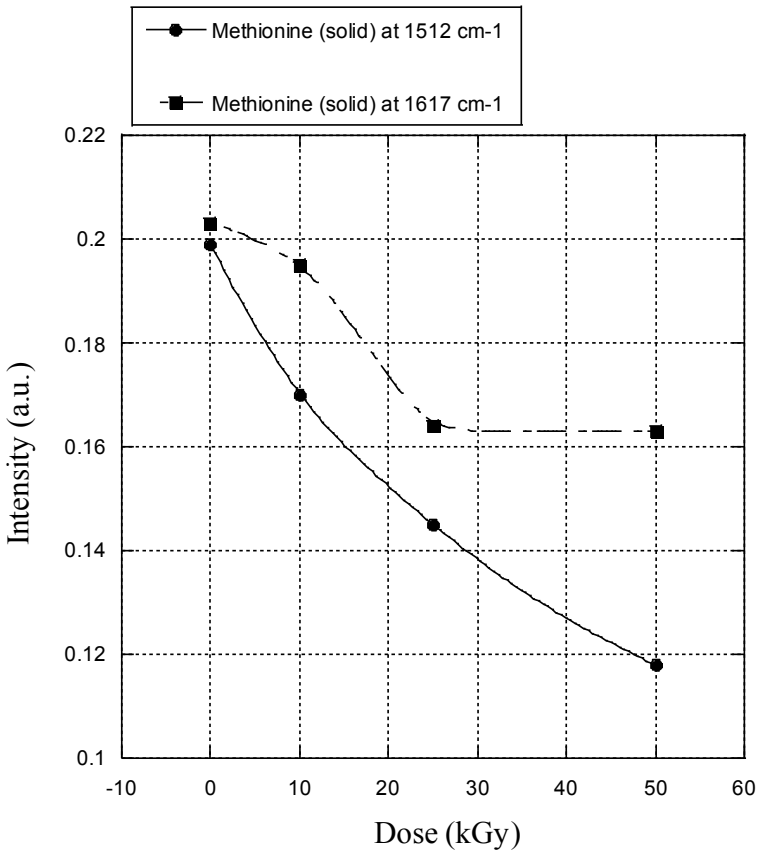

Figure 6.9. Relative intensities of Raman shifts as a function of absorbed dose for sulfur-containing amino acid.

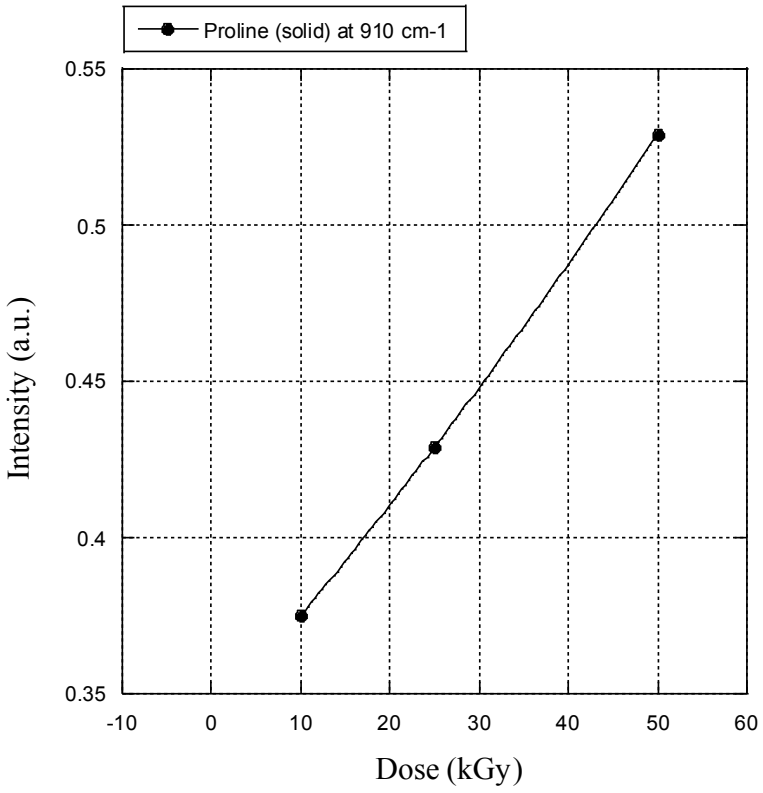

Figure 6.10. Relative intensities of Raman shifts as a function of absorbed dose for imino acid.

6.4 Electrospray ionization mass spectrometry (ESI-MS)

The ESI-MS spectra in both negative and positive modes of 20 amino acids, for the control and 50-kGy irradiated solution samples, are shown in Appendix (Figures S42-S81). Because of the noise from the ionization in the negative mode, the description of the result came from the positive mode and the mass spectrum of negative mode would be supportive information, which was seen in other literature.[94] Possible structure of the

new peaks was shown, however, unless the MS/MS was done, the exact structure would not be decided. Because of the limitation, the minimum mass for the detector was 50, therefore, small molecules such as NH_3, HS, and CO_2, which have been detected in the literature [33-35], might not be shown on the spectrum.

6.4.1 Aliphatic amino acids

There was no significant change in the ESI-MS spectrum for glycine and valine of positive mode before and after irradiation. There was one new peak at 263 (*m*/*z*) in the spectrum of leucine in positive mode, which was caused by (leu+leu)+H+. For isoleucine, there was one new very small peak at 246 in the spectrum of positive mode. The MS continuum in the spectrum for glycine in negative mode was also found in cysteine, leucine, and valine. This continuum was caused by the presence of HCl in the amino acid solutions, since Cl- can be attached to other molecules during the ionization process.

For alanine, the mass spectrum was very clean in positive mode except for two new peaks at 162 and 177, which were also verified by peaks at 160 and 175 in the negative mode spectrum. The peak at 177 was caused by the dimer of alanine. The continuum in the MS spectrum of alanine in negative mode was also observed in the MS spectra of other small amino acids, such as threonine and serine. The structure for the new peak at 73 in the negative mode spectrum was associated with CH_3CH_2COOH. The

widely used crystalline alanine dosimetry is based on the radical $CH_3\dot{C}HCOOH$ generated by ionizing radiation.

6.4.2 Aromatic amino acids

For phenylalanine (m: 165), there was no change observed in the spectrum in positive mode, while in negative mode, three new peaks were observed at 180, 345 and 363. The new peak at 180 could be explained by the generation ·OH radical-nucleophilic aromatic substitution during radiolysis. However, the new peak at 345 was caused by generation of (phe-OH+phe)-H^- during the ionization process by ESI-MS. For tyrosine and tryptophan, there was no change observed in the spectra in positive or negative mode. The two large peaks in the spectrum of tryptophan in negative mode at 443 and 445 were caused by (trp+trp)+Cl^- during the ionization process in the ESI-MS.

6.4.3 Neutral amino acids

There was no significant change in the spectrum of threonine and glutamine of positive modes. The identified new peak in the spectrum of serine was the one at 296 in the positive mode. There were two new peaks at 189 and 204 in the spectrum of asparagine in the positive mode.

6.4.4 Acidic amino acids

There was no significant change in the spectrum of aspartic acid and glutamic acid in both modes for both zero and 50 Gy irradiated samples, except one peak at 151 in the spectrum of aspartic acid in negative mode for the sample irradiated at 50 Gy.

6.4.5 Basic amino acids

Two new peaks at 130 and 262 were observed in the spectrum of arginine in positive mode. The possible structure for peak 130 was $NH_2C(NH)NHCH_2CH_2CH_2CHO$. The product causing peak 262 could be the case of change in the UV-Vis spectrum. There was new peak at 326 in the negative mode of histidine while no change was observed in the positive mode, which might be accounted for the appearance of the new band in the UV-Vis spectrum and the color change. Two new peaks at 86 and 169 were observed in the spectrum of lysine in positive mode.

6.4.6 Sulfur-containing amino acids

Two new peaks at 89 and 106 (*m/z*) were observed in the spectrum of methionine in positive mode. The peaks were caused by $CH_3CH_2CH_2COOH$ and $CH_3SCH_2CH_2CH_2NH_2$, respectively. The dimer of methionine was observed in the spectrum. No significant changes were observed in the spectrum of cysteine in positive mode. The dimer of cysteine connected by disulfide bond was observed in the spectrum

at peak 239 in negative mode, the amount of which increased sharply after radiation. The peaks at 275 and 276 were caused by the dimer+Cl^-.

6.4.7 Imino amino acids

No significant changes were observed in the ESI-MS spectra of proline in either mode.

CHAPTER VII

DISCUSSION

7.1 Radiation chemistry

Although the reactions of radiolysis of amino acids have been reported in different works [2, 32-35, 42, 55, 95-103], not all the products of radiolysis were detected in the current study. Therefore, the analysis of the undergoing reactions was only based on the detected products from the current study.

7.1.1 Basic reaction of amino acids by radiolysis

Deamination and decarboxylation of amino acids have been reported in a plethora of articles [42, 63, 104-108]; the general reaction mechanism is given in Fig 7.1. The hydroxyl radical removed the hydrogen atom in the carboxyl group, and a double bond was formed between carbon and oxygen in order to meet the octet rule. An amine was produced and CO_2 is liberated. Meanwhile, the hydrogen radical attacked the nitrogen which had two free electrons and the single bond between the nitrogen and α-carbon were broken. A carboxylic acid was produced and ammonia was liberated. As an example the new peak by the radiolysis of alanine was caused by deamination (see Figure S42).

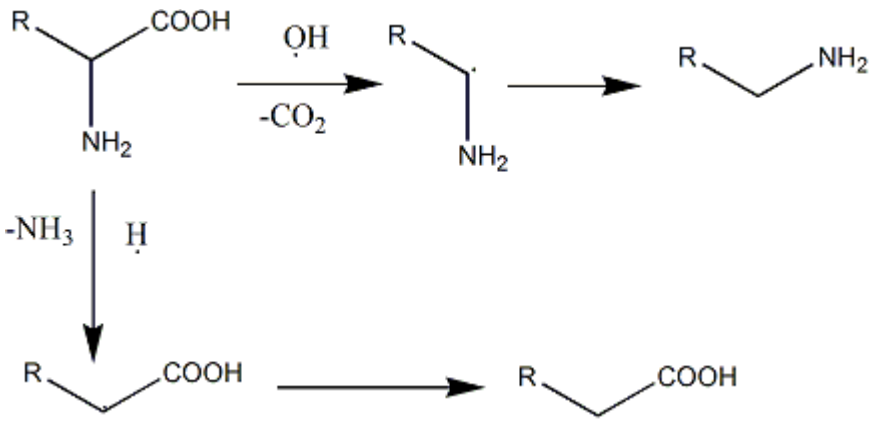

Figure 7.1. Reaction mechanism of deamination and decarboxylation of amino acids by radiolysis.

7.1.2 Aromatic amino acids

It was expected that ESI-MS results could not reveal the whole radiation process and gave no explanation for the color change and new bands observed in UV-Vis spectra. In a recent study, characterization by HPLC, UV-Vis spectroscopy and MS/MS was done on the degradation products, which were responsible for color change in near UV-visible light-irradiated and heat-stressed monoclonal antibody (mAb) drug product in liquid formulation.[109] It was revealed that color change was caused by the formation of chromophores. Moreover, major tryptophan oxidation products were identified as kynurenine (Kyn), N-formylkynurenine (NFK), and hydroxytryptophan (OH-Trp), the absorption band of which shifted to the longer wavelength in the order of OH-Trp < NFK < Kyn. However, none of these products were detected in the MS spectrum. It was also proved by the work of JM Dyer *et al.*, the photon-oxidation products within photo-

yellowed wool proteins were caused by the tryptophan and tyrosine derived chromophores.[110] The proposed routes of tryptophan and tyrosine photon-oxidation to gave yellow chromophoric species are shown in the Fig. 7.2 and Fig. 7.3. Tyrosine was oxidized by the hydroxyl radical substitution, producing dihydroxyphenylalanine (DOPA). Dityrosine was formed by the hydrogen radical attacking the aromatic ring, and bonded between two attacked aromatic rings. By the oxidation of dityrosine, hydroxydityrosine was formed, which was also the final product of DOPA in the radiolysis. Tryptophan was oxidized by the hydroxyl radical substitution, producing hydroxytroptophan. N-formylkynurenie was formed by the oxidation of the carbons double bond in tryptophan. Be removing the hydrogen atom in aldehyde function group, kynurenine was formed and CO was liberated. Further oxidation of kynurenine produced hydroxykynurenine.

The new peak at 180 in the ESI-MS spectrum of phenylalanine was caused by the radiolysis of tyrosine, the reaction mechanism of which is given in Fig. 7.4. The hydroxyl radical attacked the aromatic ring of phenylalanine and substituted the hydrogen, which produced tyrosine.

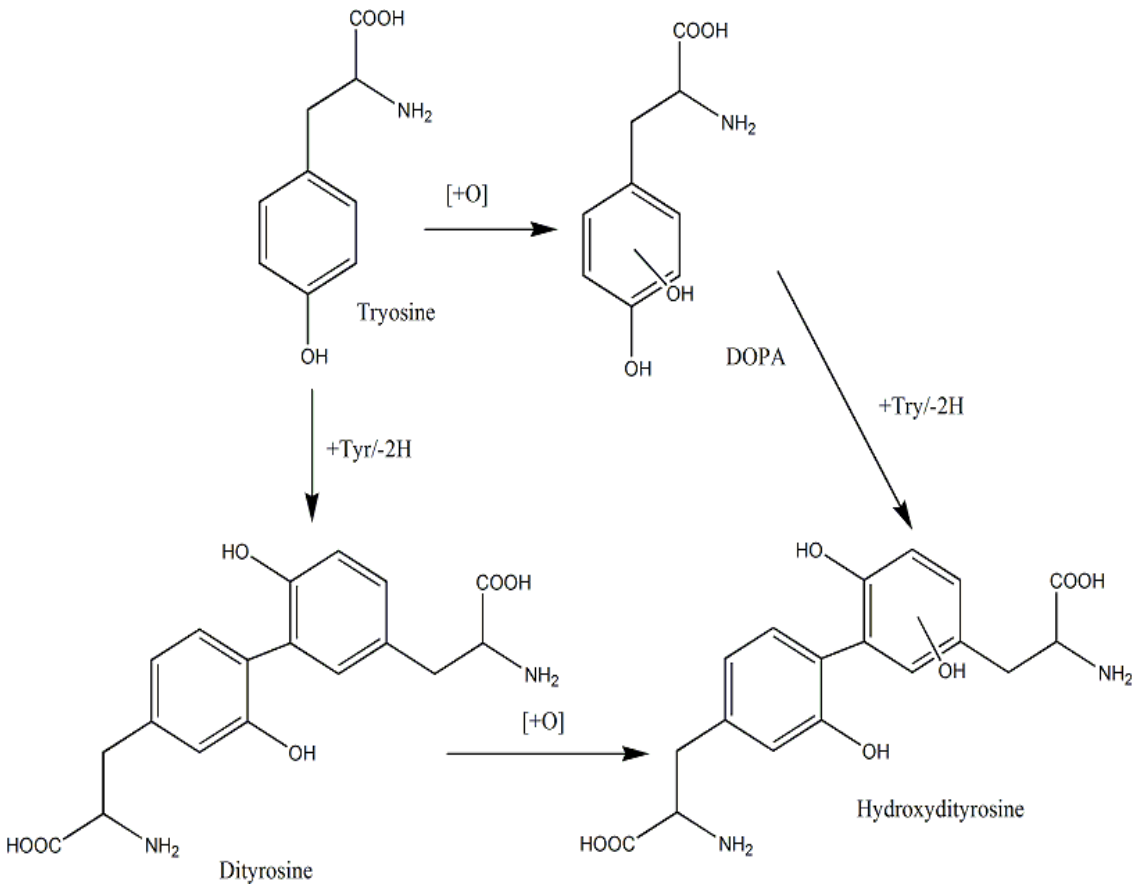

Figure 7. 2. Proposed route for tyrosine to give the yellow chromophoric species.

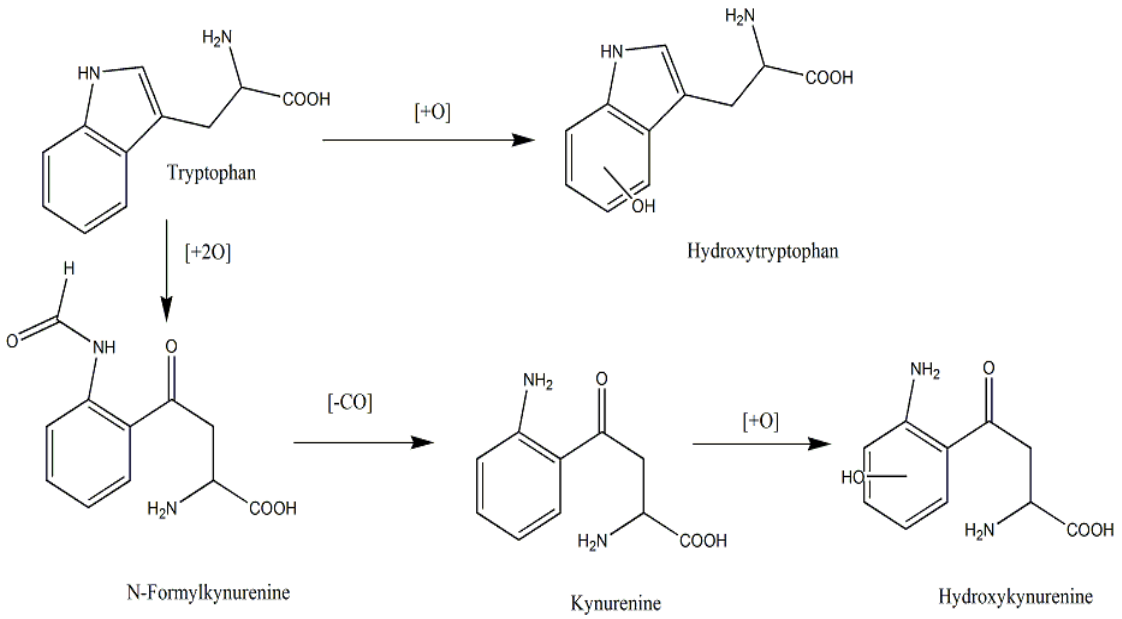

Figure 7.3. Proposed route for tryptophan to give the yellow chromophoric species.

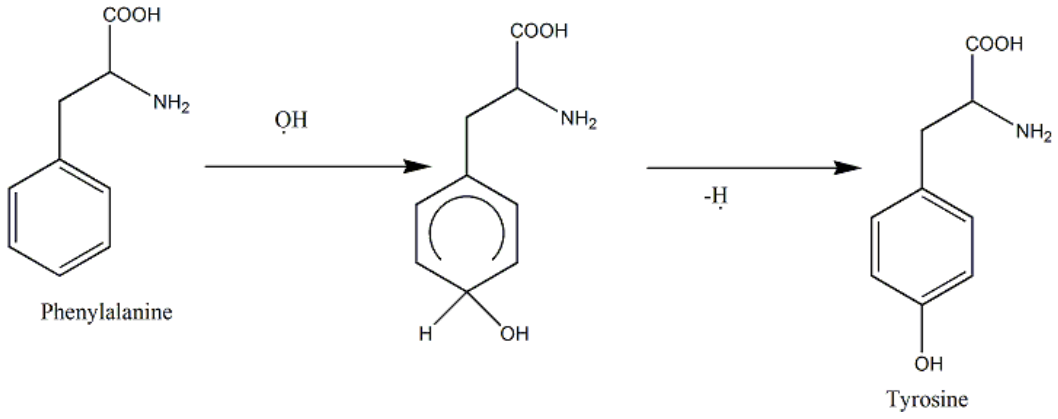

Figure 7.4. Reaction mechanism of phenylalanine current experiment.

7.1.3 Sulfur-containing amino acids

Since GC-MS and atmospheric pressure chemical ionization (APCI) were also tested on the methionine, α-aminobutyric acid and methionine sulfoxide were detected in the irradiated sample, respectively. Therefore, the reaction mechanisms of methionine solution in this experiment are shown in Fig. 7.5. The result was consistent with the work of Torreggiani et al, where methionine solution was irradiated by γ radiation, and $MTPNH_2$, methionine sulfoxide and serine were detected.[63]

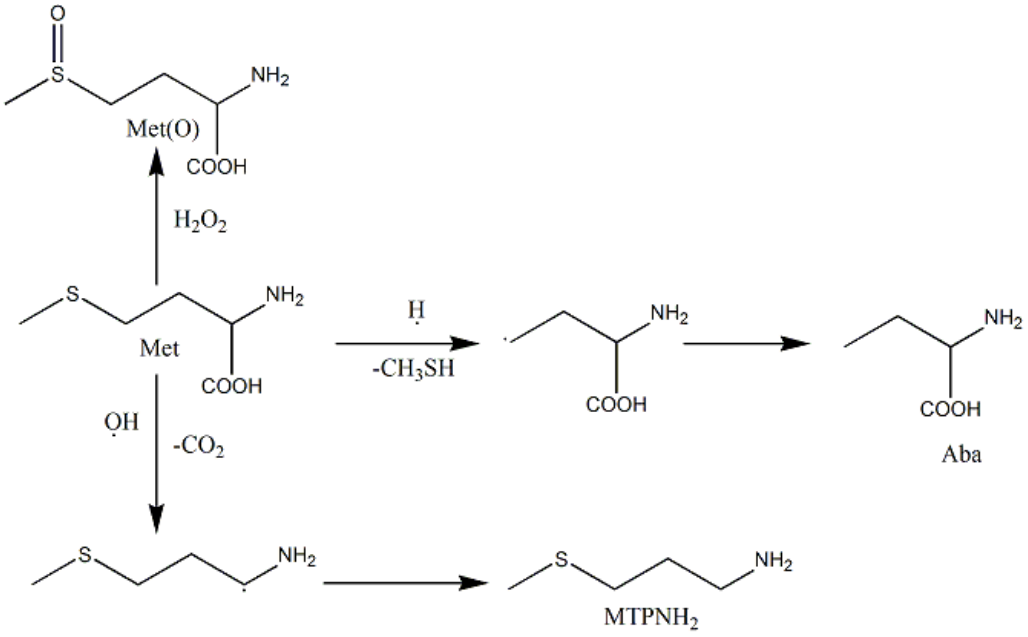

Figure 7.5. Reaction mechanism of methionine in current experiment.

GC-MS had been carried out on cysteine solution, where alanine was detected. Alanine was produced by the breakage of C-S bond. And there was new peak appearance caused by dimer detected by ESI-MS. Therefore, the reaction mechanism of cysteine in this experiment is shown in Fig. 7.6.

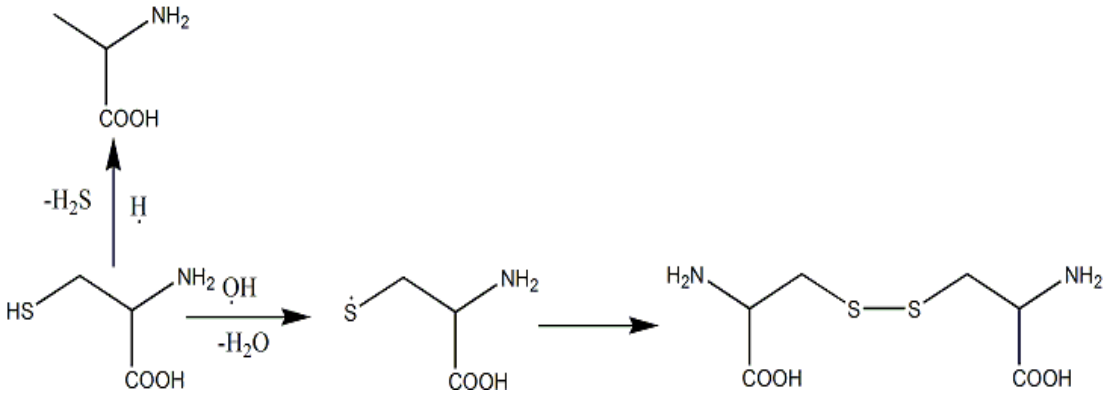

Figure 7.6. Reaction mechanism of cysteine in current experiment.

7.2 Discussion of results

7.2.1 UV-Vis spectroscopy

In the analysis of UV-Vis spectrum, we used an Arrhenius equation to fit the dose and absorbance intensity, which matched well with the experimental data. This provided another option for biodosimetry, especially for the amino acids which showed increasing absorbance intensity with dose. In term of A_{max} in the equation, the relative expected

absorbance intensity for the new product after large dose would be methionine > histidine > asparagine > tryptophan > phenylalanine > cysteine > serine > threonine > arginine > glutamine > tyrosine. However, when we did the simulation, we made the assumption that product was directly produced from amino acid by radiolysis. The possibility existed that the product, which caused the difference in the UV-Vis spectra, was not directly produced from the radiolysis of amino acids, or the changes in UV-Vis spectra were caused by the mixture of products from the radiolysis of amino acids.

It was reported that the effects of radiation on aqueous system under aerobic and anaerobia condition was totally different, for a more completed study, experiment conducted on aerobic condition should also be conducted.[40] During the irradiation, samples were contained in the polyethylene bags; air was expelled from the bags as much as possible in order to make sure samples received the same dose. However, whether the amount of air during the radiation, especially the oxygen, would dramatically affect the result needed to be examined.

Another consideration was when the absorbance intensities of the new product were picked up from the spectra; it was done manually because the exact wavelength of the new product was unknown. This might cause error especially when the peak of the new product was not isolated from the original peak. More accurate results could be concluded if all new products which caused the change in the UV-Vis spectrum could be identified. In this way, exact wavelengths could be obtained and a database could be built for application.

7.2.2 Raman spectroscopy

In Raman spectroscopy, samples were placed in a quartz petri dish for data collection, as quartz had a simpler spectrum compared to glass and plastic. However, during the analysis of Raman spectra for liquid samples, suppression effect of the signal from quartz couldn't be ignored especially at the peak 604 cm^{-1}, and 800 cm^{-1}. It was of importance to find other materials of simple Raman spectrum in order to provide clearer spectra. Another option would be lyophilization of the solution sample. [111] However, it will require large amount of solution sample considered the solubility of amino acids, and a freeze-drier machine, which sharply increase the expense.

Baseline shifts exist in many types of Raman spectrometers. Acquired spectra normally contain the desired signals as well as undesirable elements such as background noise. It is necessary to find the balance between extracting the background as much as possible while retaining the important information. In this experiment, baseline correction was performed using 7th order polynomial fit, which worked well but not perfectly for all amino acids. In the work of He *et al*., an improved asymmetric least squares (IAsLS) method has been proposed based on the advantage of AsLS and polynomial fitting. [112] An extensive literature review has been provided by Eilers and Schulze *et al*., [113, 114] which summarized the preprocessing methods for typical spectral backgrounds, without focusing on any particular instrumental method. Moreover, another option for intensity normalization exists, such as vector normalization, which makes the new spectrum vector have a length of 1. Whether different data processing

will affect the result dramatically, especially the relationship between the peak intensity and dose, need to be examined.

Plenty of works have been reported on the simulation of Raman spectra of amino acids by Gaussian using different quantum theories.[115-134] Hartree–Fock (HF), density functional theory (DFT) and Møller–Plesset perturbation (MP) theory were tried on glycine and alanine solid and solution. Further work need to be done in order to obtain better simulation results since it is helpful to analyze the experimental data and understand the vibrational modes of each peak.

7.2.3 ESI-MS

Matrix-assisted laser desorption/ionization (MALDI), GC-MS and ESI-MS were all tried in this study. MALDI is a soft ionization technique employed for the analysis of biomecules and large organic molecules. [135-138] MALDI is similar to ESI but produces far fewer multiply charged ions. However, the matrix suppression effect is an important consideration which limits its application for small molecules. In our case, α-Cyano-4-hydroxycinnamic acid (CHCA) was employed as the matrix which protected the molecules from breaking into fragments. The signal of the matrix in the low mass range (m/z: 100-300) was so overwhelming that little information could be found for the tested sample. GC-MS combines the features of gas-liquid chromatography and mass spectrometry to differentiate and identify molecules within the same sample. Applications of GC-MS include drug detection, fire investigation, environmental analysis, explosives investigation, and identification of unknown samples. [44, 129, 139, 140]

The polar nature of amino acids requires derivatization prior to GC analysis. The silylation reagent N-tert-butyldimethylsilyl- N-methyltrifluoroacetamide (MTBSTFA) for the derivatization of amino acids has been tried in this experiment. While it helped to identify the amino acids in each sample, it did not work for the new radiolysis products which could be explained the pretty similar structure and boiling point of the sample and new products. In the case of cysteine and methionine, alanine and α-Aminobutyric acid have been detected in the irradiated sample, respectively by GC-MS, but not in ESI.

7.2.4 Comparisons with literature

Comparing with literature results shows a few discrepancies. Hitoshi *et al.* did the femtosecond laser irradiation of phenylalanine, methionine and histidine, while there were changes in the UV-Vis absorbance of histidine and phenylalanine as a function of dose, no result was reported for methionine.[90] However, in the work of Yiming Li *et al.*, which was to explore the reason for color change of monoclonal antibody, it was reported that a new absorption band was observed for tryptophan, neither for methionine nor histidine in both light-irradiated and heat-stressed monoclonal antibody sample. In the current study, changes in the UV-Vis absorbance were observed for 11 amino acids, including arginine, asparagine, cysteine, glutamine, histidine, methionine, phenylalanine, serine, threonine, tryptophan, and tyrosine.

In the conclusion of relative radiolysis of twenty amino acids based on the radioracemization by Cataldo *et al.*[141], asparagine, aspartic acid, histidine were classified as the most stable, which was opposite to the result in the current study.

Arginine, proline and tyrosine were irradiated to 3.2 MGy in solid state, and analyzed by ESI-MS in positive mode by Cristina *et al.*[141]. New peak at 117, 132 and 160 were observed in the spectrum of irradiated arginine, new peaks at 100, 118, 185 and 199 were noticed in the spectrum of irradiated proline, and new peak at 138 and 165 was recorded in the spectrum of irradiated tyrosine. Most peaks were caused by bond breakages by direct irradiation. However, none of those new peaks were observed in the spectra of the irradiated solution samples which may indicate the different effect of radiation on solution and solid sample.

In the work of Torreggiani *et al.*, Raman spectroscopy and ESI-MS were used to study the radical-based modification of methionine.[63] In particular, homoserine was detected in the irradiated methionine solution by ESI-MS. It was shown in the study that Raman spectroscopy was useful in revealing the radical-induced modifications in the sulphur-containing moiety. More peak intensity changes were observed, however in the current experiment, more strict conditions were applied since only peaks intensity changes as a function of doses were considered to indicate the changes caused by radiation instead of random variation.

7.3 Comparison of the three techniques for detecting new chemical species by radiolysis

The ability of the three techniques employed in this study to detect new chemical species by radiolysis is evaluated on the following aspects: sample preparation, operation and data processing, and result analysis.

Raman spectra can be acquired for nearly all samples containing true molecular bonding. Although gases cannot be analyzed using Raman spectroscopy, the concentration of molecules in a gas is typically very low, so specialized equipment such as higher power lasers and long path length sample cells are necessary. For normal solid and solution samples, there is no need for sample preparation. In most cases, UV-Vis spectroscopy and ESI-MS only works for solution sample, while sample dilution is need for ESI-MS based on the sample.

For solution samples, it is easy to operate the UV-Vis spectroscopy and ESI-MS, which are automatically controlled and no data processing is required. For Raman spectroscopy, the depth of focus can be different each time, which leads variation in the spectra. Baseline correction is needed before normalization.

Both UV-Vis spectroscopy and ESI-MS give information about new molecules, which is indicated by the new peak in the spectrum. While Raman spectroscopy is based on the vibration mode of the molecules, the formation of new molecules is indicated by the relative intensities change or peak appearance and disappearance, which requiers more careful analysis.

In the current study, the result from UV-Vis spectroscopy was more consistent with the observational change and structure of amino acids. However, limited information about new products could be obtained from the spectra. In order to apply Raman spectroscopy to detect the radiolysis change, a more detailed database of band change needed to be built, which required exact structures of the new products. Even in some case, ESI-MS was able to give the mass peaks of new products; it was not capable of showing all the changes after irradiation. For example, no signal was found in the spectra of tryptophan and tyrosine to explain the color change after radiation.

7.4 Application of the result

7.4.1 Biodosimetry

The application of amino acids to a successful and versatile free-radical method of dosimetry depends on the magnitude of radical yield per unit absorbed dose and on the lifetime of the radicals. Crystalline alanine fulfills these criteria, which is widely used as a dosimeter.

In the current study, the Arrhenius equation successfully fitted the experimental data in the UV-Vis spectra. Therefore, if the relationship is also proven for other doses, new biodosimeters can be developed based on the 11 amino acids, whose absorbance changed as a function of dose.

7.4.2 New imaging and detection method

There was no question that Raman spectroscopy was effective at detecting molecules since the spectra of each amino acid are different. What was also confirmed in the current experiment was that Raman spectroscopy was capable of revealing the radical-induced modifications and direct ionization of amino acids. Thus, some band patterns useful for building a library of spectra-structure correlation for radical-based degradation and direct ionization were identified. Altogether, with the improvement more efficient detection technology, which could help to identify the formed products during radiation, combined results would be able to produce a set of spectroscopic markers of the main processes occurring as a consequence of radical stress exposure, which could be used in a spectroscopic protocol for providing a first assessment of amino acids modifications in more complex systems such as peptides and proteins, and monitoring their impact on protein structure.

Different works have been reported on the utilization of either two technologies: utilization of UV-vis and Raman spectroscopy to measure the state of a solid in a multiphase reactor;[142] combination of Raman spectroscopy and ESI-MS on the radical based modification of methionine;[63] utilization of UV-Vis spectroscopy and ESI-MS on the characterization and degradation products of a color-changed monoclonal antibody. [109] However, to our knowledge, this was the first attempt to combine those three technologies and apply them in the radiolysis of amino acid, which offered a new imaging method for further study.

7.5 Future work

Several questions remain to be to be answered in this study. These are, what caused the color change in Histidine? What are the structures from new and arising peaks after radiation? And how to quantitatively interpret the Raman spectra of amino acids after irradiation? In addition, even though the deamination and decarboxylation of different amino acids during irradiation has been reported before,[33-35] and odor of amine has been noticed after radiation, only the mass spectrum of alanine showed the corresponding product. Whether those reactions are truly happening in other amino acids in present experiments was not detected by ESI-MS because of the small amount sampled, or there were other competing reactions that need to be tested.

Even though research on radiation effects on biological system have been carried out for more than 50 years, it is important to conduct further research to identify the radiolysis products and draw a complete paradigm of radiation effects in the amino acids. Not only because amino acids are the basic components of biological system, but also the reported correlation between the amino acids and chronic diseases.

Raman spectroscopy is popular in vitro and vivo study nowadays. [61, 143-151] However, the Raman spectra of biological materials always exhibit complex profiles, constituting several peaks and or bands which arise due to the large variety of biomolecules. Experiments on amino acids mixture should be carried in order to simulate the exact situation in biological system. In this way, the makers of each amino acid summarized in this study can be tested, and exploration can be done on

mathematical tool to retrieve quantitative information, which is reported to be feasible.[74]

CHAPTER VIII

CONCLUSION

In the current study, twenty amino acids in solid state and aqueous/0.5 M hydrogen chloride (HCl) solution were previously irradiated to 10, 25 and 50 kGy by electron beam and analyzed using Raman spectroscopy, ultraviolet-visible (UV-Vis) spectrophotometry and electrospray ionization mass spectrometry (ESI-MS). Works on the radiolysis of amino acid by different techniques have been reported from 1950 until 2014, to our knowledge, the current study was the first attempt to combine three distinctive techniques with substantially different capabilities for assessing the effect of radiolysis on amino acids.

A semi-quantitative response to conformational changes as a function of absorbed dose for those radiosensitive amino acids following the Arrhenius equation was found in UV-Vis spectrophotometry and summarized, however limited information could be obtained for the detailed structure change of the radiolysis of amino acids.

Raman spectroscopy provided a fingerprint for each amino acid in both solid and liquid forms, and revealed spectral signatures of radiolysis of amino acids which related to the specific molecular vibration. Database of Raman spectra of twenty amino acids was built based on the current study, however, result needs to be further improved by better system and proper data processing.

ESI-MS provided some basic chemical information regarding new byproducts of radiolysis of amino acids. However, ESI-MS has its limitations in sensitivity and noise

from multiply charged ions produced. For more detailed analysis, MS/MS need to be run on the unidentified structure molecules.

Radio-sensitivity of amino acids was concluded based on the absorbance-absorbed dose response fitted by Arrhenius equation. Methionine could be considered as a new biodosimetry which showed linear absorbance-absorbed dose.

The ability of three techniques to identify and analyze the effects of radiolysis of amino acids in solution was evaluated. It was revealed that those three techniques are competing and complementary, and promising for further application *in vivo* studies.

REFERENCES

1. Garrett, A.R., et al., *A novel method for predicting antioxidant activity based on amino acid structure.* Food chemistry, 2014. 158: p. 490-496.

2. Milligan, J.R., et al., *Repair of oxidative DNA damage by amino acids.* Nucleic acids research, 2003. 31(21): p. 6258-6263.

3. Ingenbleek, Y. and H. Kimura, *Nutritional essentiality of sulfur in health and disease.* Nutrition reviews, 2013. 71(7): p. 413-432.

4. Rees, W.D., F.A. Wilson, and C.A. Maloney, *Sulfur amino acid metabolism in pregnancy: the impact of methionine in the maternal diet.* The journal of nutrition, 2006. 136(6 Suppl): p. 1701S-1705S.

5. Grimble, R.F., *The effects of sulfur amino acid intake on immune function in humans.* The journal of nutrition, 2006. 136(6 Suppl): p. 1660S-1665S.

6. Bianchi, G., et al., *Synthesis of glutathione in response to methionine load in control subjects and in patients with cirrhosis.* Metabolism, 2000. 49(11): p. 1434-1439.

7. Bendich, A. and R. Zilberboim, *Drug–nutrient interactions and immune function*, Handbook of drug-nutrient interactions, 2010. Springer. p. 665-736.

8. Appleton, J., *Arginine: clinical potential of a semi-essential amino acid..* Alternative medicine review : a journal of clinical therapeutic, 2002. 7(6): p. 512-522.

9. Nieves, C. and B. Langkamp-Henken, *Arginine and immunity: a unique perspective.* Biomedicine & pharmacotherapy, 2002. 56(10): p. 471-482.

10. Kirk, S.J. and A. Barbul, *Role of arginine in trauma, sepsis, and immunity.* JPEN. Journal of parenteral and enteral nutrition, 1990. 14(5 Suppl): p. 226S-229S.

11. Peranzoni, E., et al., *Role of arginine metabolism in immunity and immunopathology.* Immunobiology, 2007. 212(9-10): p. 795-812.

12. Popovic, P.J., H.J. Zeh, and J.B. Ochoa, *Arginine and immunity.* The journal of nutrition, 2007. 137(6 Suppl 2): p. 1681S-1686S.

13. Ren, W., et al., *Dietary arginine supplementation of mice alters the microbial population and activates intestinal innate immunity.* The journal of nutrition, 2014. 144(6): p. 988-995.

14. Zuo, L. and M.S. Motherwell, *The impact of reactive oxygen species and genetic mitochondrial mutations in Parkinson's disease.* Gene, 2013. 532(1): p. 18-23.

15. Klivenyi, P., et al., *Effects of mitochondrial toxins on the brain amino acid concentrations.* Neurochemical research, 2005. 30(11): p. 1421-1427.

16. Ravaglia, G., et al., *Plasma amino acid concentrations in patients with amnestic mild cognitive impairment or Alzheimer disease.* The American journal of clinical nutrition, 2004. 80(2): p. 483-488.

17. Gueli, M.C. and G. Taibi, *Alzheimer's disease: amino acid levels and brain metabolic status.* Neurological sciences, 2013. 34(9): p. 1575-1579.

18. Desrosiers, M., et al., *The importance of dosimetry standardization in radiobiology.* Journal of research of the national institute of standards and technology, 2013. 118: p. 403-418.

19. Pandey, B.N., et al., *Radiobiological basis in management of accidental radiation exposure.* International journal of radiation biology, 2010. 86(8): p. 613-635.

20. Williams, B.B., et al., *Physically-based biodosimetry using in vivo EPR of teeth in patients undergoing total body irradiation.* International journal of radiation biology, 2011. 87(8): p. 766-775.

21. Pernot, E., et al., *Ionizing radiation biomarkers for potential use in epidemiological studies.* Mutation research, 2012. 751(2): p. 258-286.

22. Buxton, G.V., et al., *Critical review of rate constants for reactions of hydrated electrons, hydrogen atoms and hydroxyl radicals (· OH/·O−) in aqueous solution.* Journal of physical and chemical reference data, 1988. 17(2): p. 513-886.

23. Meesungnoen, J. and J.-P. Jay-Gerin, *High-LET ion radiolysis of water: oxygen production in tracks.* Radiation research, 2009. 171(3): p. 379-386.

24. Meesungnoen, J. and J.-P. Jay-Gerin, *High-LET radiolysis of liquid water with 1H+, 4He2+, 12C6+, and 20Ne9+ ions: effects of multiple ionization.* The journal of physical chemistry. A, 2005. 109(29): p. 6406-6419.

25. Bernstein, M.P., et al., *Racemic amino acids from the ultraviolet photolysis of interstellar ice analogues.* Nature, 2002. 416(6879): p. 401-403.

26. Woon, D.E., *Pathways to glycine and other amino acids in ultraviolet-irradiated astrophysical ices determined via quantum chemical modeling.* The astrophysical journal letters, 2002. 571(2): p. L177.

27. von Sonntag, C. and H.P. Schuchmann, *The elucidation of peroxyl radical reactions in aqueous solution with the help of radiation‐chemical methods.* Angewandte chemie international edition in English, 1991. 30(10): p. 1229-1253.

28. von Sonntag, C., *Radiation chemistry in the 1990s: pressing questions relating to the areas of radiation biology and environmental research.* International journal of radiation biology, 1994. 65(1): p. 19-26.

29. Box, H.C. and E.E. Budzinski, *Oxidation and reduction of amino acids by ionizing radiation.* The journal of chemical physics, 2003. 55(5): p. 2446-2449.

30. Leszczynski, D., *Radiation proteomics: a brief overview.* Proteomics, 2014. 14(4-5): p. 481-488.

31. Van Riper, S.K., et al., *Mass spectrometry-based proteomics: Basic principles and emerging technologies and directions*, in Radiation Proteomics. 2013, Springer. p. 1-35.

32. Hatano, H., *Studies on radiolysis of amino acids and proteins I. On radiolytic oxidation of sulfhydryl groups.* Journal of radiation research, 1960. 1(1): p. 23-27.

33. Hatano, H., *Studies on radiolysis of amino acids and proteins II. On radiolytic deamination of amino acids in aqueous solutions by gamma irradiation.* Journal of radiation research, 1960. 1(1): p. 28-37.

34. Hatano, H., *Studies on radiolysis of amino acids and proteins III. On radiolysis of peptides and proteins in aqueous solutions by gamma irradiation.* Journal of radiation research, 1960. 1(1): p. 38-45.

35. Hatano, H., *Oxidative radiolysis of amino acids, peptides and proteins in aqueous solutions by gamma irradiation (special issue on physical, chemical and biological effects of gamma radiation, II).* Bulletin of the institute for chemical research, Kyoto University, 1961. 39(2): p. 120-132.

36. Neta, P. and R.W. Fessenden, *Electron spin resonance study of radicals produced in irradiated aqueous solutions of amines and amino acids.* The journal of physical chemistry, 1971. 75(6): p. 738-748.

37. Portugal, W., S. Pilling, and P. Boduch, *Radiolysis of amino acids by heavy and energetic cosmic ray analogues in simulated space environments: α-glycine zwitterion form.* Monthly notices of …, 2014.

38. Vujošević, S.I., A. Negrón-Mendoza, and Z.D. Draganić, *Radiation-induced polymerization in dilute aqueous solutions of cyanides.* Origins of life and evolution of the biosphere : the journal of the international society for the study of the origin of life, 1990. 20(1): p. 49-54.

39. FLETCHER, G.L. and S. OKADA, *Radiation-induced formation of dihydroxyphenylalanine from tyrosine and tyrosine-containing peptides in aqueous solution.* Radiation research, 1961. 15: p. 349-354.

40. Weiss, J., *Effects of radiations on aqueous systems under aerobic and anaerobic conditions.* The international journal of applied radiation and isotopes, 1959. 6: p. 52-58.

41. Lambert, J.-F., *Adsorption and polymerization of amino acids on mineral surfaces: a review.* Origins of life and evolution of the biosphere : the journal of the international society for the study of the origin of life, 2008. 38(3): p. 211-242.

42. Tanaka, M., et al., *Fragmentation and dimerization of aliphatic amino acid films induced by vacuum ultraviolet irradiation.* Radiation physics and chemistry, 2008. 77(10): p. 1164-1168.

43. Tabata, Y., *Radiation-induced crosslinking.* Radiation physics and chemistry (1977), 1979. 14(1): p. 235-243.

44. Dizdaroglu, M., *The use of capillary gas chromatography-mass spectrometry for identification of radiation-induced DNA base damage and DNA base-amino acid cross-links.* Journal of chromatography, 1984. 295(1): p. 103-121.

45. Grachev, S.A., E.V. Kropachev, and G.I. Litvyakova, *Radiation-Induced Crosslinking of Thymine with Cysteamine: Cysteamine Attachment to the Methyl Group of Thymine.* High energy chemistry, 2002. 36(5): p. 290-293.

46. Cress, A.E., et al., *The crosslinking of nuclear protein to DNA using ionizing radiation.* Journal of cancer research and clinical oncology, 1990. 116(4): p. 324-330.

47. Cress, A.E. and G.T. Bowden, *Covalent DNA-protein crosslinking occurs after hyperthermia and radiation.* Radiation research, 1983. 95(3): p. 610-619.

48. Uvaydov, Y., N.E. Geacintov, and V. Shafirovich, *Generation of guanine-amino acid cross-links by a free radical combination mechanism.* Physical chemistry chemical physics : PCCP, 2014. 16(23): p. 11729-11736.

49. Kim, H.J., et al., *Binding-site specificity of the radiolytically induced crosslinking of phenylalanine to glucagon.* Radiation research, 1984. 98(1): p. 26-36.

50. Mee, L.K., et al., *Gamma-radiation-induced interactions between amino acids and glucagon.* Radiation research, 1984. 97(1): p. 36-47.

51. Cataldo, F., et al., *Radiation-induced crosslinking of collagen gelatin into a stable hydrogel.* Journal Of radioanalytical and nuclear chemistry, 2008. 275(1): p. 125-131.

52. Dizdaroglu, M. and P. Jaruga, *Mechanisms of free radical-induced damage to DNA.* Free radical research, 2012. 46(4): p. 382-419.

53. Dizdaroglu, M., et al., *Free radical-induced damage to DNA: mechanisms and measurement.* Free radical biology and medicine, 2002. 32(11): p. 1102-1115.

54. Cadet, J., et al., *Measurement of oxidatively generated base damage to nucleic acids in cells: facts and artifacts.* Bioanalytical reviews, 2012. 4(2-4): p. 55-74.

55. Shi, W.-Q., et al., *Identification of radiation-induced cross-linking between thymine and tryptophan by electrospray ionization-mass spectrometry.* Journal of mass spectrometry : JMS, 2006. 41(9): p. 1205-1211.

56. Jo, C. and D.U. Ahn, *Production of volatile compounds from irradiated oil emulsion containing amino acids or proteins.* Journal of food science, 2000. 65(4): p. 612-616.

57. Ahn, D.U., *Production of volatiles from amino acid homopolymers by irradiation.* Journal of food science, 2002. 67(7): p. 2565-2570.

58. Benevides, J.M., S.A. Overman, and G.J. Thomas, *Raman spectroscopy of proteins.* Current protocols in protein science / editorial board, John E. Coligan ... [et al.], 2004. Chapter 17: p. Unit 17.8.

59. Jurasekova, Z., A. Tinti, and A. Torreggiani, *Use of Raman spectroscopy for the identification of radical-mediated damages in human serum albumin.* Analytical and bioanalytical chemistry, 2011. 400(9): p. 2921-2931.

60. Gong, B., et al., *Raman spectroscopy demonstrates prolonged alteration of bone chemical composition following extremity localized irradiation.* Bone, 2013. 57(1): p. 252-258.

61. Krafft, C., et al., *Raman and coherent anti-Stokes Raman scattering microspectroscopy for biomedical applications.* Journal of biomedical optics, 2012. 17(4): p. 040801.

62. Calin, M.A., et al., *Optical techniques for the noninvasive diagnosis of skin cancer.* Journal of cancer research and clinical oncology, 2013. 139(7): p. 1083-1104.

63. Torreggiani, A., S. Barata-Vallejo, and C. Chatgilialoglu, *Combined Raman and IR spectroscopic study on the radical-based modifications of methionine.* Analytical and bioanalytical chemistry, 2011. 401(4): p. 1231-1239.

64. Salman, A., et al., *Detection and identification of cancerous murine fibroblasts, transformed by murine sarcoma virus in culture, using Raman spectroscopy and advanced statistical methods.* Biochimica et biophysica acta, 2013. 1830(3): p. 2720-2727.

65. Mavarani, L., et al., *Spectral histopathology of colon cancer tissue sections by Raman imaging with 532 nm excitation provides label free annotation of lymphocytes, erythrocytes and proliferating nuclei of cancer cells.* The analyst, 2013. 138(14): p. 4035-4039.

66. Ranc, V., et al., *Discrimination of circulating tumor cells of breast cancer and colorectal cancer from normal human mononuclear cells using Raman spectroscopy.* The analyst, 2013. 138(20): p. 5983-5988.

67. Wilson, R., et al., *Signal enhancement of surface enhanced Raman scattering and surface enhanced resonance Raman scattering using in situ colloidal synthesis in microfluidics.* Analytical chemistry, 2010. 82(5): p. 2119-2123.

68. Andreou, C., et al., *Rapid detection of drugs of abuse in saliva using surface enhanced Raman spectroscopy and microfluidics.* ACS nano, 2013. 7(8): p. 7157-7164.

69. Piorek, B.D., et al., *Free-surface microfluidics/surface-enhanced Raman spectroscopy for real-time trace vapor detection of explosives.* Analytical chemistry, 2012. 84(22): p. 9700-9705.

70. Ashok, P.C., et al., *Fiber probe based microfluidic raman spectroscopy.* Optics express, 2010. 18(8): p. 7642-7649.

71. Li, H., et al., *Note: Mobile micro-Raman analyzer integrated with a lab-on-a-chip.* Review of scientific instruments, 2013. 84(5): p. 056105.

72. Chrimes, A.F., et al., *Microfluidics and Raman microscopy: current applications and future challenges.* Chemical society reviews, 2013. 42(13): p. 5880-5906.

73. Zhu, G., et al., *Raman spectra of amino acids and their aqueous solutions.* Spectrochimica acta. Part A, Molecular and biomolecular spectroscopy, 2011. 78(3): p. 1187-1195.

74. Candeloro, P., et al., *Raman database of amino acids solutions: a critical study of extended multiplicative signal correction.* The analyst, 2013. 138(24): p. 7331-7340.

75. De Gelder, J., et al., *Reference database of Raman spectra of biological molecules.* Journal of Raman spectroscopy, 2007. 38(9): p. 1133-1147.

76. Gargaro, A.R., L.D. Barron, and L. Hecht, *Vibrational Raman optical activity of simple amino acids.* Journal of Raman spectroscopy, 2005. 24(2): p. 91-96.

77. Jenkins, A.L., R.A. Larsen, and T.B. Williams, *Characterization of amino acids using Raman spectroscopy.* Spectrochimica acta. Part A, Molecular and biomolecular spectroscopy, 2005. 61(7): p. 1585-1594.

78. Susi, H., D.M. Byler, and W.V. Gerasimowicz, *Vibrational analysis of amino acids: cysteine, serine, β-chloroalanine.* Journal of molecular structure, 1983. 102(1): p. 63-79.

79. Sonois, V., et al., *Raman study and DFT calculations of amino acids.* NSTI-nanotech 2008, 2008. 1: p. 352-355.

80. Perkampus, H.-H., H.C. Grinter, and T. Threlfall, *UV-VIS Spectroscopy and its Applications*. 1992: Springer.

81. Yamashita, M. and J.B. Fenn, *Electrospray ion source. Another variation on the free-jet theme.* The journal of physical chemistry, 1984. 88(20): p. 4451-4459.

82. Ho, C., et al., *Electrospray ionisation mass spectrometry: principles and clinical applications.* The clinical biochemist reviews, 2003. 24(1): p. 3.

83. Kujawinski, E.B., et al., *The application of electrospray ionization mass spectrometry (ESI MS) to the structural characterization of natural organic matter.* Organic geochemistry, 2002. 33(3): p. 171-180.

84. Rashed, M.S., et al., *Diagnosis of inborn errors of metabolism from blood spots by acylcarnitines and amino acids profiling using automated electrospray tandem mass spectrometry.* Pediatric research, 1995. 38(3): p. 324-331.

85. Jiang, Y., et al., *Integrated plastic microfluidic devices with ESI-MS for drug screening and residue analysis.* Analytical chemistry, 2001. 73(9): p. 2048-2053.

86. Souverain, S., S. Rudaz, and J.-L. Veuthey, *Protein precipitation for the analysis of a drug cocktail in plasma by LC–ESI–MS.* Journal of pharmaceutical and biomedical analysis, 2004. 35(4): p. 913-920.

87. Mazzarino, M., X. de la Torre, and F. Botrè, *A screening method for the simultaneous detection of glucocorticoids, diuretics, stimulants, anti-oestrogens, beta-adrenergic drugs and anabolic steroids in human urine by LC-ESI-MS/MS.* Analytical and bioanalytical chemistry, 2008. 392(4): p. 681-698.

88. Rosu, F., et al., *Positive and negative ion mode ESI-MS and MS/MS for studying drug–DNA complexes.* International journal of mass spectrometry, 2006. 253(3): p. 156-171.

89. Hofstadler, S.A. and K.A. Sannes-Lowery, *Applications of ESI-MS in drug discovery: interrogation of noncovalent complexes.* Nature reviews drug discovery, 2006. 5(7): p. 585-595.

90. Nakano, H., et al., *Change in the UV-VIS absorbance of amino acids as a result of femtosecond laser irradiation.* Journal of laser micro/nanoengineering, 2007. 2(1): p. 100.

91. Verweij, H., T.M. Dubbelman, and J. Van Steveninck, *Photodynamic protein cross-linking.* Biochimica et biophysica acta (BBA)-biomembranes, 1981. 647(1): p. 87-94.

92. Cataldo, F., et al., *Radiolysis and radioracemization of 20 amino acids from the beginning of the Solar System.* Rendiconti lincei, 2011. 22(2): p. 81-94.

93. Taguchi, M., et al., *Yields of tyrosines in the radiolysis of aqueous phenylalanine solutions by energetic heavy ions.* Radiation physics and chemistry, 2001. 60(4): p. 263-268.

94. Cherubini, C., et al., *Mass spectrometric analysis of selected radiolyzed amino acids in an astrochemical context.* Journal of radioanalytical and nuclear chemistry, 2014. 300: p. 1061-1073.

95. Chatgilialoglu, C., et al., *Radiation-induced reductive modifications of sulfur-containing amino acids within peptides and proteins.* Journal of proteomics, 2011. 74(11): p. 2264-2273.

96. Maclot, S., et al., *Ion-induced fragmentation of amino acids: effect of the environment.* Chemphyschem : a European journal of chemical physics and physical chemistry, 2011. 12(5): p. 930-936.

97. Sagstuen, E., A. Sanderud, and E.O. Hole, *The solid-state radiation chemistry of simple amino acids, revisited.* Radiation research, 2004. 162(2): p. 112-119.

98. Schaich, K.M., *Free radical initiation in proteins and amino acids by ionizing and ultraviolet radiations and lipid oxidation--Part I: ionizing radiation.* Critical reviews in food science and nutrition, 1980. 13(2): p. 89-129.

99. Schaich, K.M., *Free radical initiation in proteins and amino acids by ionizing and ultraviolet radiations and lipid oxidation--Part II: ultraviolet radiation and photolysis.* Critical reviews in food science and nutrition, 1980. 13(2): p. 131-159.

100. Schaich, K.M., *Free radical initiation in proteins and amino acids by ionizing and ultraviolet radiations and lipid oxidation--part III: free radical transfer from oxidizing lipids.* Critical reviews in food science and nutrition, 1980. 13(3): p. 189-244.

101. Talbi, S., et al., *EPR study of gamma induced radicals in amino acid powders.* Spectrochimica acta. Part A, Molecular and biomolecular spectroscopy, 2004. 60(6): p. 1335-1341.

102. Thomas, A.H., et al., *Tryptophan oxidation photosensitized by pterin.* Free radical biology & medicine, 2013. 63: p. 467-475.

103. Buxton, G.V., et al., *Critical Review of rate constants for reactions of hydrated electrons, hydrogen atoms.* Journal of physical and chemical reference data, 1988. 17(2): p. 513.

104. Zhou, Y. and W.H. Nelson, *EPR, ENDOR, and DFT study of free radicals in L-lysine·HCl·2H2O single crystals X-irradiated at 298 K.* The journal of physical chemistry. A, 2011. 115(42): p. 11566-11578.

105. Gerakines, P.A., et al., *< i> In situ</i> measurements of the radiation stability of amino acids at 15–140K.* Icarus, 2012. 220(2): p. 647-659.

106. Strzelczak, G., et al., *EPR spectroscopy and theoretical study of gamma-irradiated asparagine and aspartic acid in solid state.* Biophysical chemistry, 2007. 125(1): p. 92-103.

107. Xu, G. and M.R. Chance, *Radiolytic modification of acidic amino acid residues in peptides: probes for examining protein-protein interactions.* Analytical chemistry, 2004. 76(5): p. 1213-1221.

108. Zhou, Y. and W.H. Nelson, *Free radicals in L-arginine x HCl x H2O single crystals X-irradiated at 66K- EPR, ENDOR, EIE and DFT studies.* The journal of physical chemistry B, 2010. 114(16): p. 5567-5582.

109. Li, Y., et al., *Characterization of the degradation products of a color-changed monoclonal antibody: tryptophan-derived chromophores.* Analytical chemistry, 2014. 86(14): p. 6850-6857.

110. Dyer, J., S. Bringans, and W. Bryson, *Characterisation of photo-oxidation products within photoyellowed wool proteins: tryptophan and tyrosine derived chromophores.* Photochemical & photobiological sciences, 2006. 5(7): p. 698-706.

111. Yu, N.-T., *Comparison of protein structure in crystals, in lyophilized state, and in solution by laser Raman scattering. III.. alpha.-Lactalbumin.* Journal of the American chemical society, 1974. 96(14): p. 4664-4668.

112. He, S., et al., *Baseline correction for Raman spectra using an improved asymmetric least squares method.* Analytical methods, 2014. 6(12): p. 4402-4407.

113. Schulze, G., et al., *Investigation of selected baseline removal techniques as candidates for automated implementation.* Applied spectroscopy, 2005. 59(5): p. 545-574.

114. Eilers, P.H. and H.F. Boelens, *Baseline correction with asymmetric least squares smoothing.* Leiden university medical centre report, 2005.

115. Alam, M.J. and S. Ahmad, *Anharmonic vibrational studies of l-aspartic acid using HF and DFT calculations.* Spectrochimica Acta Part A: Molecular and biomolecular spectroscopy, 2012. 96: p. 992-1004.

116. Castro, J., et al., *Vibrational spectra of 3-phenylpropionic acid and L-phenylalanine.* Journal of molecular structure, 2005. 744: p. 887-891.

117. Chandra, S., et al., *The spectroscopic (FT-IR, FT-Raman), NCA, first order hyperpolarizability, NBO analysis, HOMO and LUMO analysis of l-cysteine by ab inito HF and density functional method.* Spectrochimica Acta Part A: Molecular and biomolecular spectroscopy, 2011. 78(5): p. 1515-1524.

118. Chuang, C.H. and Y.T. Chen, *Raman scattering of L‐tryptophan enhanced by surface plasmon of silver nanoparticles: vibrational assignment and structural determination.* Journal of Raman spectroscopy, 2009. 40(2): p. 150-156.

119. Contreras, C., et al., *Hydration of l-tyrosine in aqueous medium. An experimental and theoretical study by mixed quantum mechanical/molecular mechanics methods.* Vibrational spectroscopy, 2011. 57(1): p. 108-115.

120. Derbel, N., et al., *Vibrational analysis of amino acids and short peptides in hydrated media. I. L-glycine and L-leucine.* The journal of physical chemistry B, 2007. 111(6): p. 1470-1477.

121. Ebenezar, I., S. Ramalingam, and C.R. Raja, *Precise spectroscopic [IR, Raman and NMR] investigation and gaussian hybrid computational analysis (UV-Visible, NIR, MEP Maps and Kubo Gap) on L- ....* J theor comput …, 2013.

122. Faria, J., et al., *Polarized Raman spectra of L-arginine hydrochloride monohydrated single crystal.* Brazilian journal of physics, 2010. 40(3): p. 288-294.

123. Gunasekaran, S., et al., *Experimental and semi-empirical computations of the vibrational spectra of methionine, homocysteine and cysteine.* Archives of physics research, 2010. 1(1): p. 12-26.

124. Hernández, B., et al., *Vibrational analysis of amino acids and short peptides in hydrated media. VI. Amino acids with positively charged side chains: L-lysine and L-arginine.* The journal of physical chemistry B, 2009. 114(2): p. 1077-1088.

125. Hernández, B., et al., *Vibrational analysis of amino acids and short peptides in hydrated media. IV. Amino acids with hydrophobic side chains: L-alanine, L-*

valine, and L-isoleucine. The journal of physical chemistry B, 2009. 113(10): p. 3169-3178.

126. Kumar, S., et al., *Infrared, Raman and electronic spectra of alanine: A comparison with ab intio calculation.* Journal of molecular structure, 2006. 791(1): p. 23-29.

127. Kumar, S., et al., *Infrared and Raman spectra of histidine: an ab initio DFT calculations of histidine molecule and its different protonated forms.* Indian journal of physics, 2010. 84(5): p. 563-573.

128. Mary, Y.S., et al., *FT-IR, FT-raman and SERS spectra of L-proline.* Journal of the iranian chemical society, 2009. 6(1): p. 138-144.

129. Navarrete, J.L., et al., *Ab initio self-consistent reaction field calculations on amino acids: asparagine zwitterions in polar medium and gas phase.* Theoretical chemistry accounts, 1997. 98(1): p. 5-15.

130. Pawlukojć, A., et al., *Neutron scattering, infra red, Raman spectroscopy and ab initio study of l-threonine.* Spectrochimica acta Part A: Molecular and biomolecular spectroscopy, 2001. 57(12): p. 2513-2523.

131. Ramirez, F., I. Tunon, and E. Silla, *Amino acid chemistry in solution: Structural study and vibrational dynamics of glutamine in solution. An ab initio reaction field model.* The journal of physical chemistry B, 1998. 102(32): p. 6290-6298.

132. Ramırez, F., I. Tunón, and E. Silla, *Amino acid chemistry in solution: structural properties and vibrational dynamics of serine using density functional theory and a continuum solvent model.* Chemical physics, 2004. 303(1): p. 85-96.

133. Sonois, V., et al., *Raman study and DFT calculations of amino acids.* NSTI-nanotech, 2008. 1: p. 352-355.

134. Sumayya, A., et al., *Vibrational spectroscopic studies and AB initio calculations of L-glutamic acid 5-amide.* Rasayan journal of chemistry, 2008. 1: p. 548-555.

135. Gogichaeva, N.V. and M.A. Alterman, *Amino acid analysis by means of MALDI TOF mass spectrometry or MALDI TOF/TOF tandem mass spectrometry.* Methods in molecular biology (Clifton, NJ), 2012. 828: p. 121-135.

136. Gogichaeva, N.V., T. Williams, and M.A. Alterman, *MALDI TOF/TOF tandem mass spectrometry as a new tool for amino acid analysis.* Journal of the American society for mass spectrometry, 2007. 18(2): p. 279-284.

137. Kuznetsova, E.S., A.K. Buryak, and G.A. Petukhova, *HPLC off-line mass spectrometry MALDI of amino acids in carbon sorbents.* Chromatographia, 2011. 73(1): p. 55-65.

138. Pan, S., et al., *Single peptide-based protein identification in human proteome through MALDI-TOF MS coupled with amino acids coded mass tagging.* Analytical chemistry, 2003. 75(6): p. 1316-1324.

139. Fuciarelli, A.F., et al., *Quantitative measurement of radiation-induced base products in DNA using gas chromatography-mass spectrometry.* Radiation research, 1989. 119(2): p. 219-231.

140. Su, C.-Y., et al., *Oxygen partial pressure effect on the preparation of nanocrystalline tungsten oxide powders by a plasma arc gas condensation technique.* International journal of refractory metals & hard materials, 2008. 26(5): p. 423-428.

141. Cherubini, C., et al., *Mass spectrometric analysis of selected radiolyzed amino acids in an astrochemical context.* Journal of radioanalytical and nuclear chemistry, 2014. 300(3): p. 1061-1073.

142. Stemmet, C., J. Schouten, and T. Nijhuis, *In-situ UV− Visible and Raman spectroscopy for gas− liquid− solid systems.* Industrial & engineering chemistry research, 2009. 48(17): p. 8205-8210.

143. Harkness, L., et al., *Identification of abnormal stem cells using Raman spectroscopy.* Stem cells and development, 2012. 21(12): p. 2152-2159.

144. Huang, Z., et al., *Raman spectroscopy of in vivo cutaneous melanin.* Journal of biomedical optics, 2004. 9(6): p. 1198-1205.

145. Ji, M., et al., *Rapid, label-free detection of brain tumors with stimulated Raman scattering microscopy.* Science translational medicine, 2013. 5(201): p. 201ra119.

146. Jiang, C., et al., *A chemically reactive Raman probe for ultrasensitively monitoring and imaging the in vivo generation of femtomolar oxidative species as induced by anti-tumor drugs in living cells.* Chemical communications (Cambridge, England), 2013. 49(59): p. 6647-6649.

147. Krishna, H., et al., *In vivo Raman spectroscopy for detection of oral neoplasia: A pilot clinical study.* Journal of biophotonics, 2013.

148. Meade, A.D., et al., *Growth substrate induced functional changes elucidated by FTIR and Raman spectroscopy in in-vitro cultured human keratinocytes.* Analytical and bioanalytical chemistry, 2007. 387(5): p. 1717-1728.

149. Schroeder, P., et al., *Infrared radiation-induced matrix metalloproteinase in human skin: implications for protection.* The journal of investigative dermatology, 2008. 128(10): p. 2491-2497.

150. Short, K.W., et al., *Raman spectroscopy detects biochemical changes due to proliferation in mammalian cell cultures.* Biophysical journal, 2005. 88(6): p. 4274-4288.

151. Thakor, A.S., et al., *Oxidative stress mediates the effects of Raman-active gold nanoparticles in human cells.* Small (Weinheim an der Bergstrasse, Germany), 2011. 7(1): p. 126-136.

APPENDIX

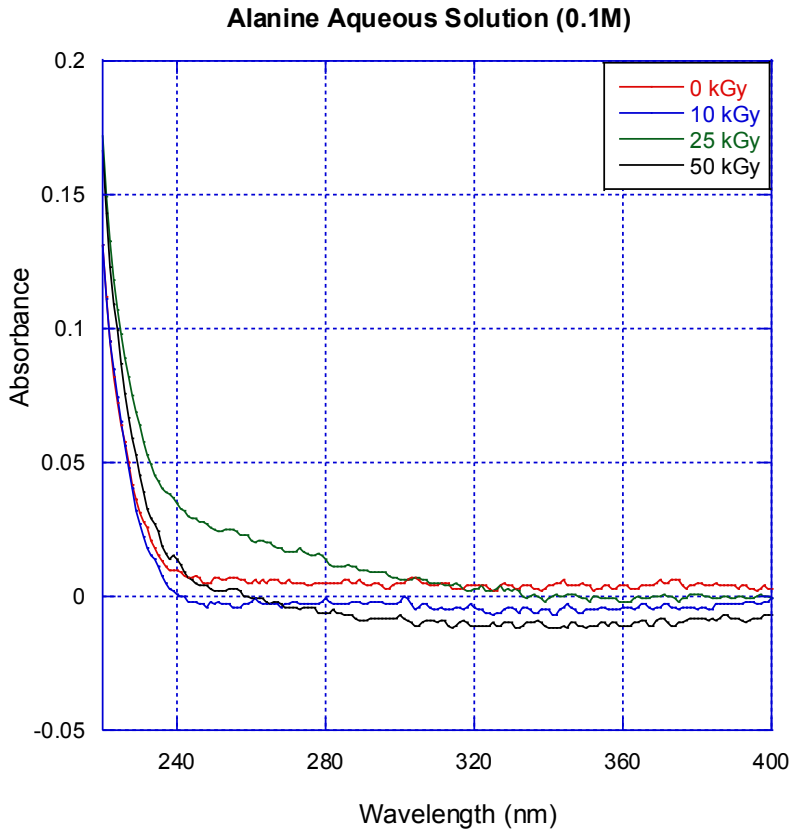

Figure A.1. UV-VIS absorbance spectra for alanine aqueous solution (0.1M)

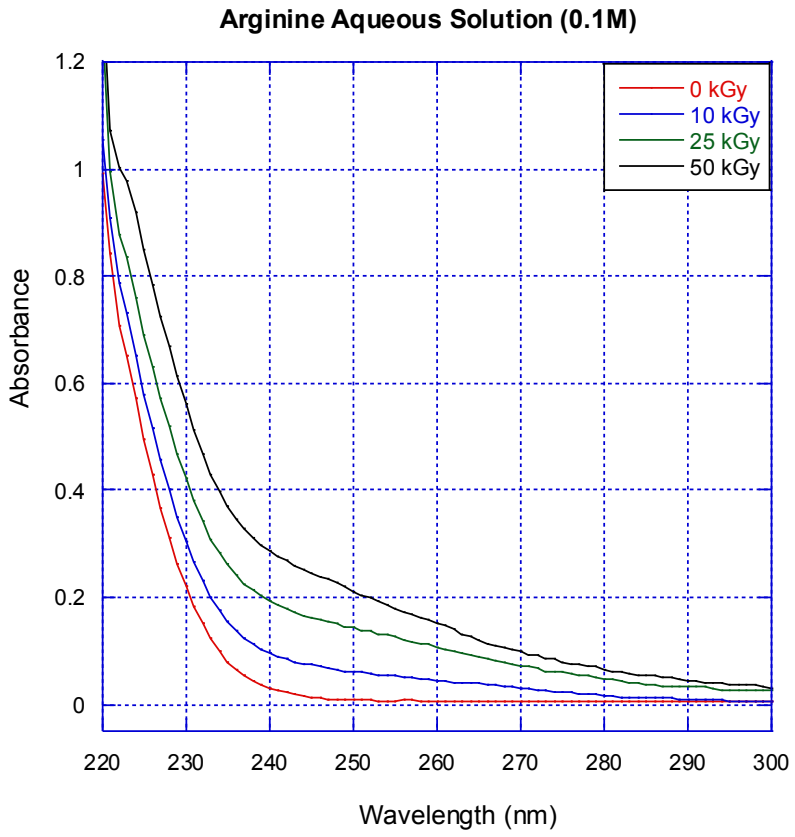

Figure A.2. UV-VIS absorbance spectra for arginine aqueous solution (0.1M)

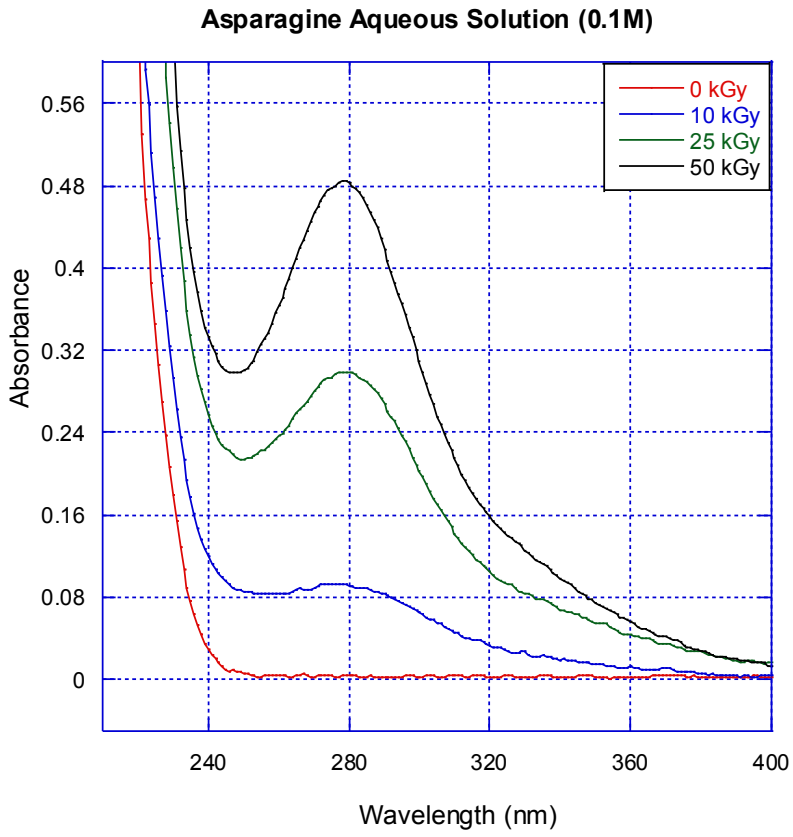

Figure A.3. UV-VIS absorbance spectra for asparagine aqueous solution (0.1M)

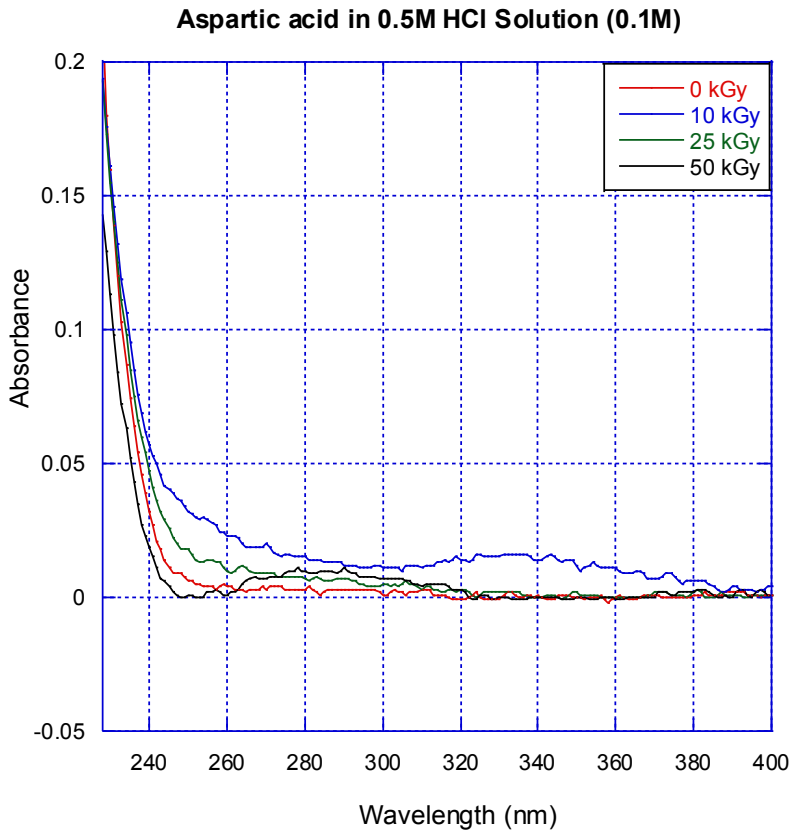

Figure A.4. UV-VIS absorbance spectra for aspartic acid in 0.5M HCl solution (0.1M)

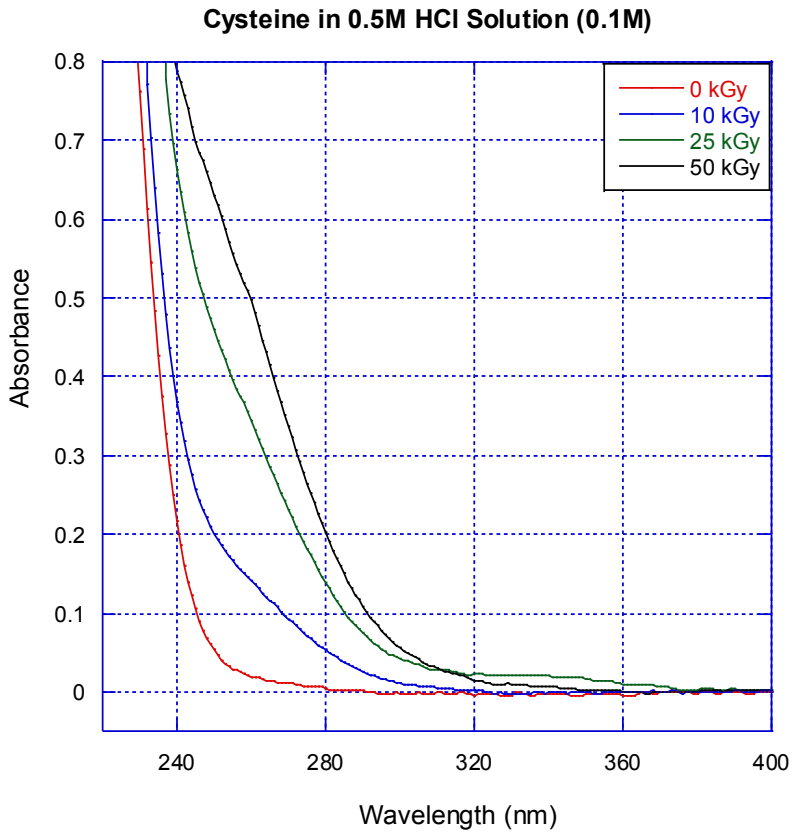

Figure A.5. UV-VIS absorbance spectra for cysteine in 0.5M HCl solution (0.1M)

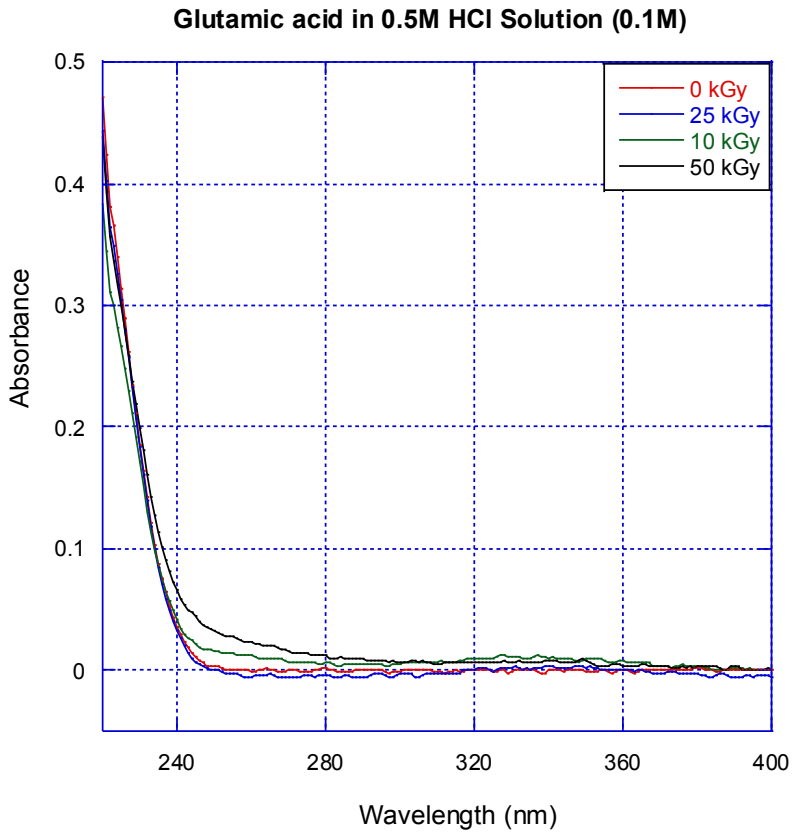

Figure A.6. UV-VIS absorbance spectra for glutamic acid in 0.5M HCl solution (0.1M)

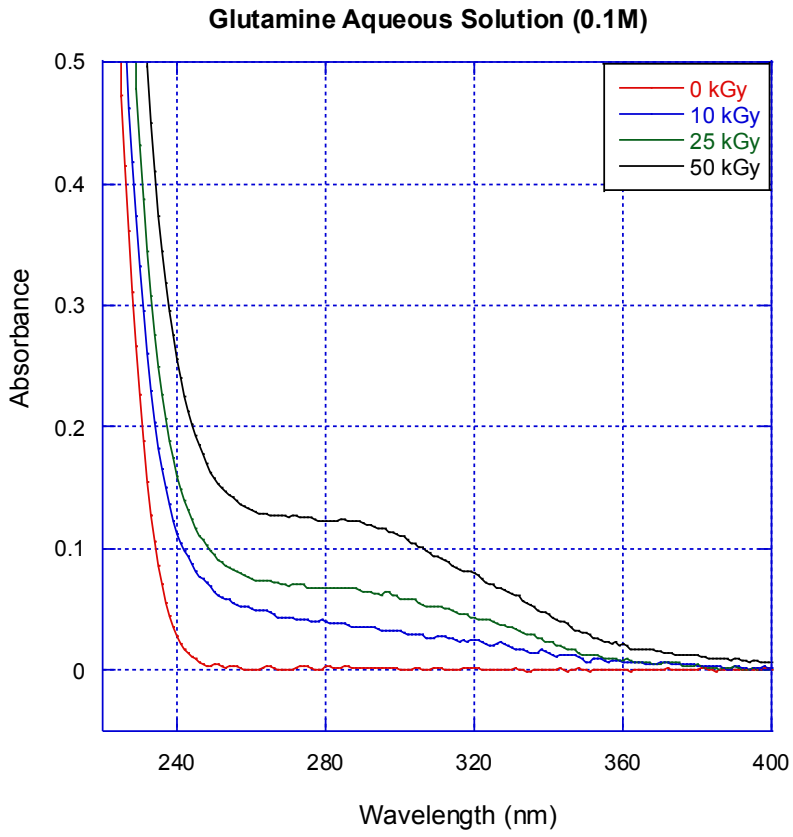

Figure A.7. UV-VIS absorbance spectra for glutamine aqueous solution (0.1M)

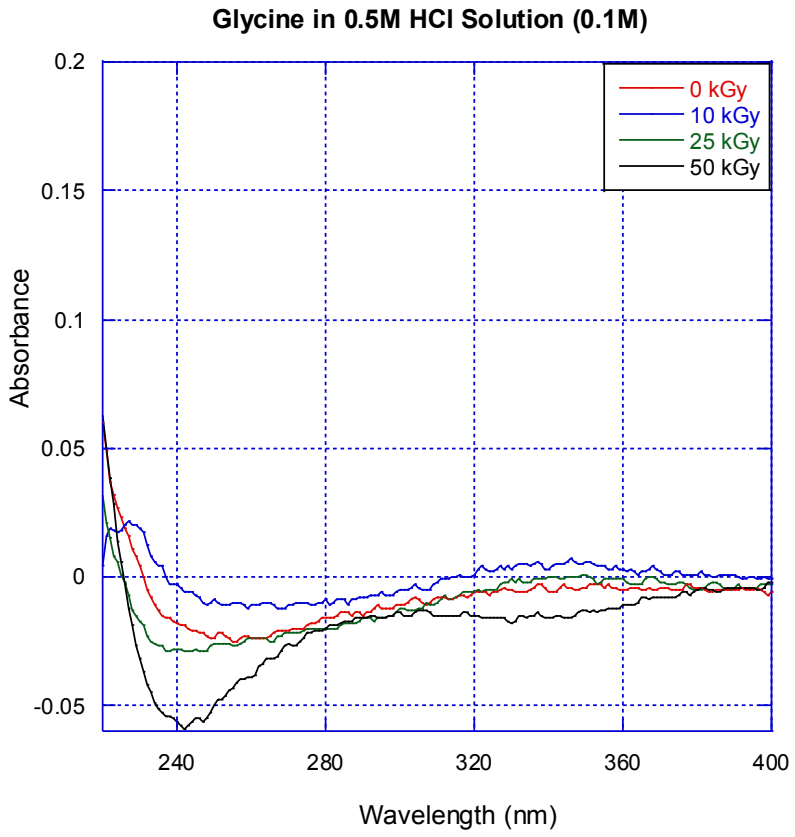

Figure A.8. UV-VIS absorbance spectra for glycine in 0.5M HCl solution (0.1M)

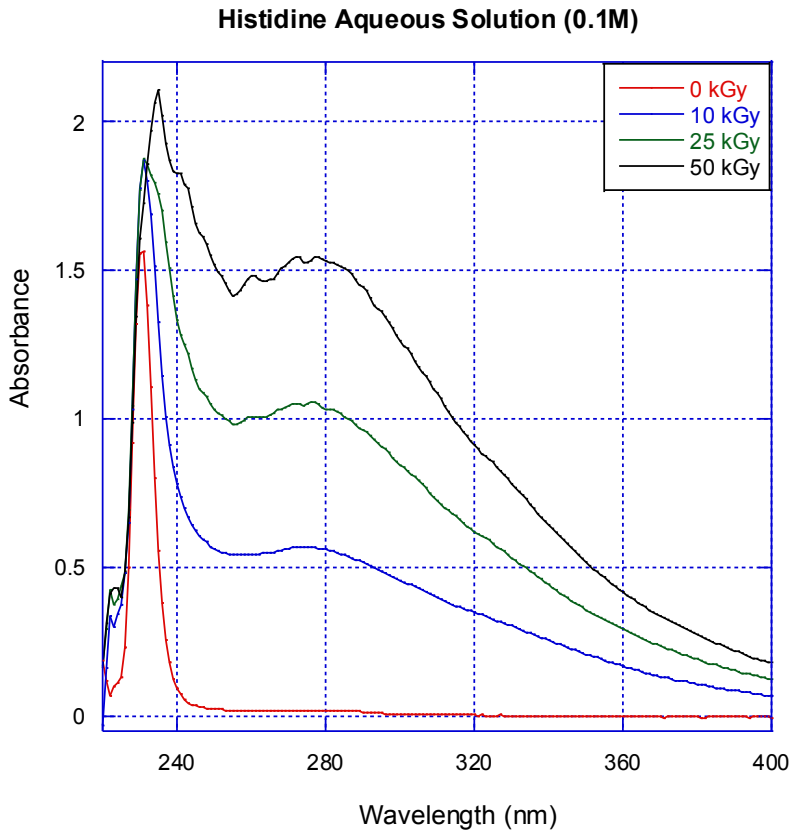

Figure A.9. UV-VIS absorbance spectra for histidine solution (0.1M)

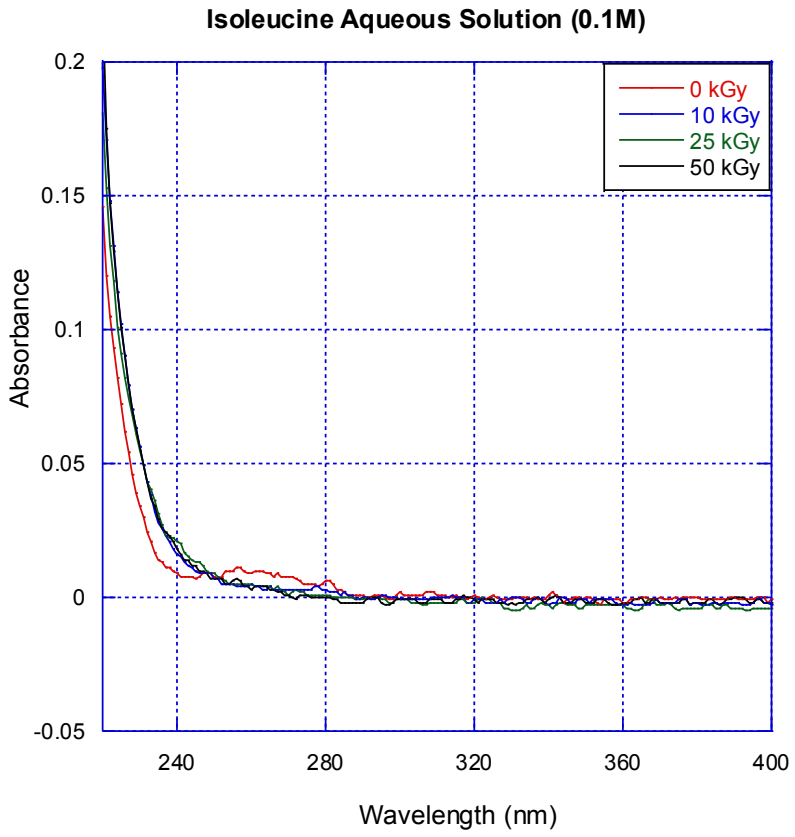

Figure A.10. UV-VIS absorbance spectra for isoleucine aqueous solution (0.1M)

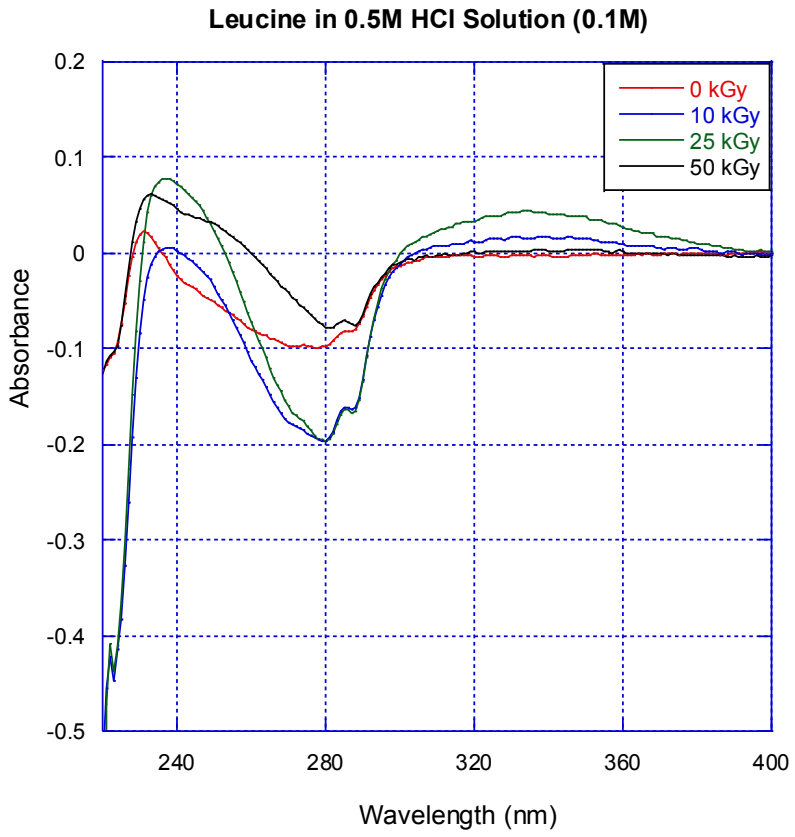

Figure A.11. UV-VIS absorbance spectra for leucine in 0.5M HCl solution (0.1M)

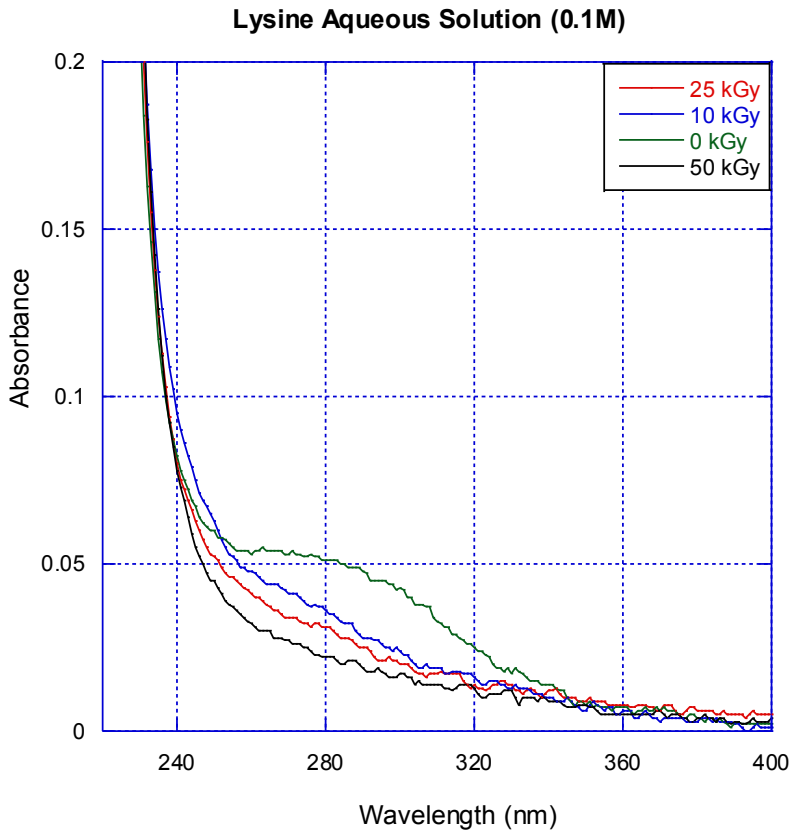

Figure A.12. UV-VIS absorbance spectra for lysine aqueous solution (0.1M)

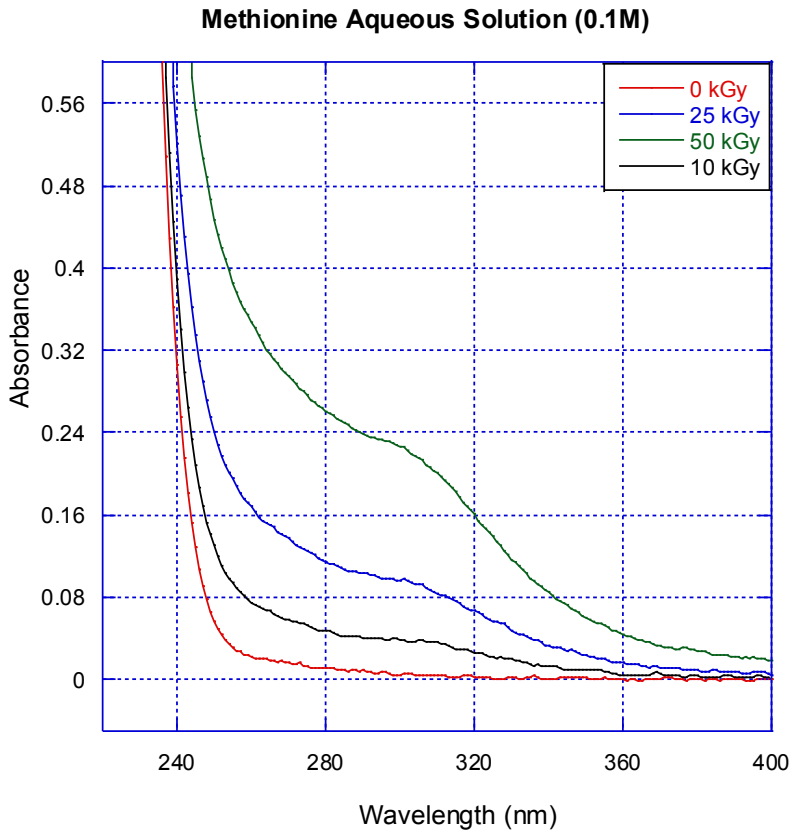

Figure A.13. UV-VIS absorbance spectra for methionine aqueous solution (0.1M)

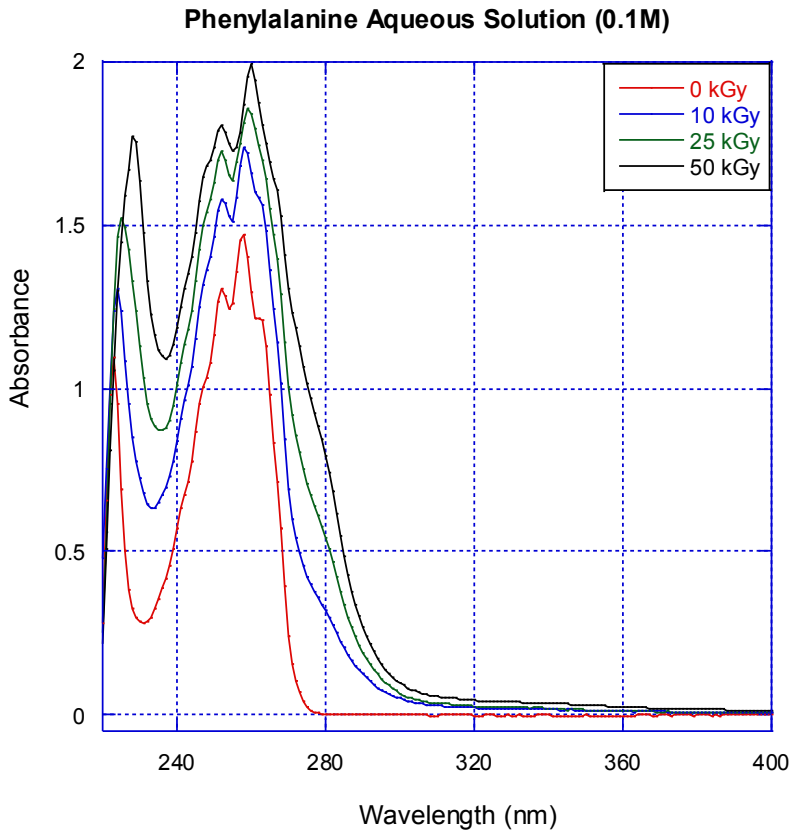

Figure A.14. UV-VIS absorbance spectra for phenylalanine aqueous solution (0.1M)

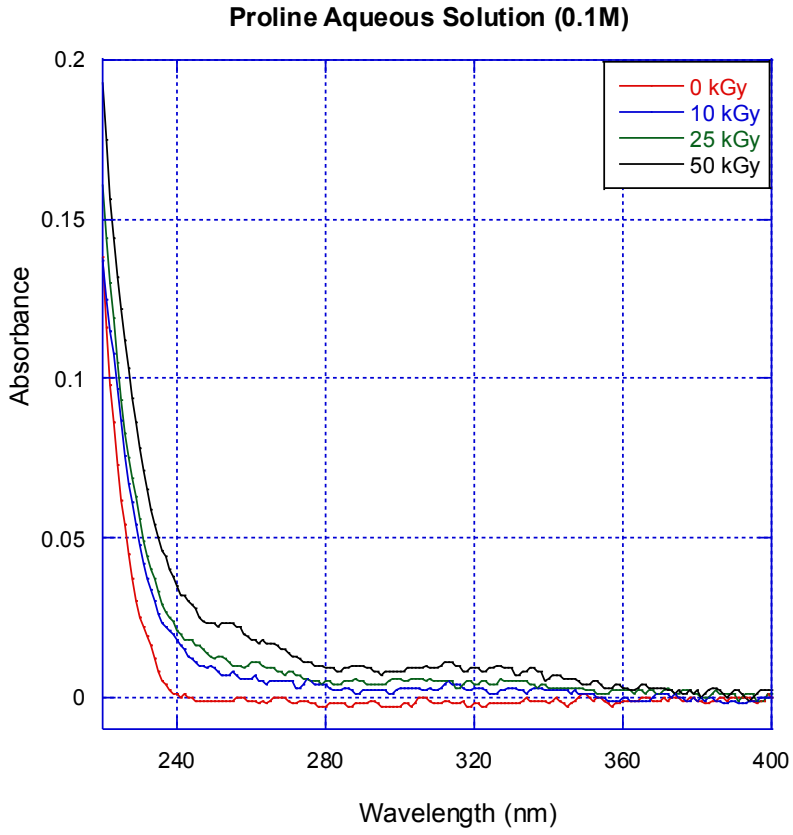

Figure A.15. UV-VIS absorbance spectra for proline aqueous solution (0.1M)

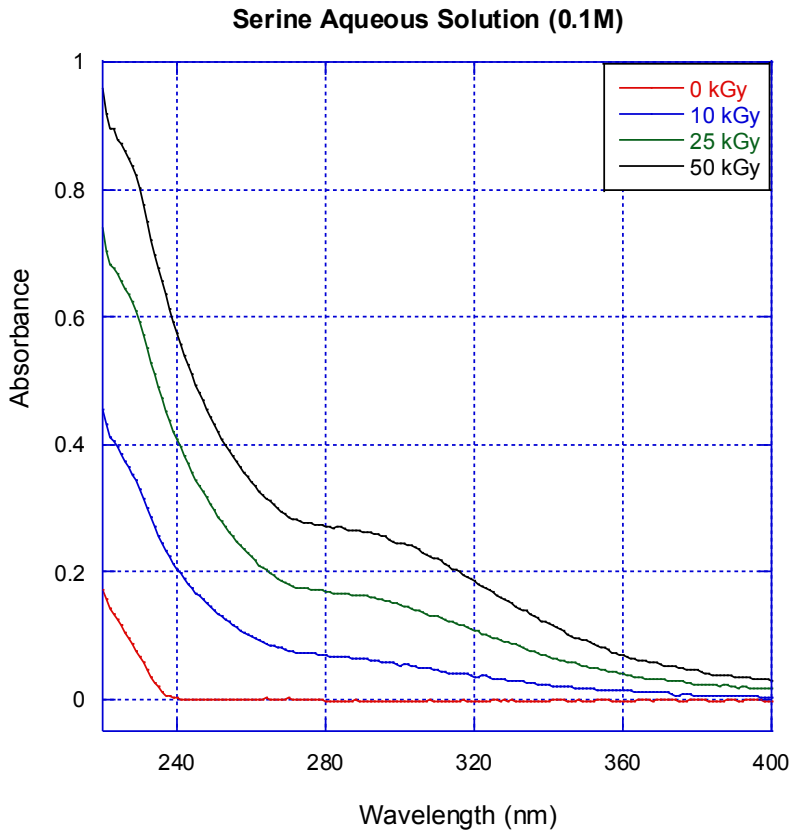

Figure A.16. UV-VIS absorbance spectra for serine aqueous solution (0.1M)

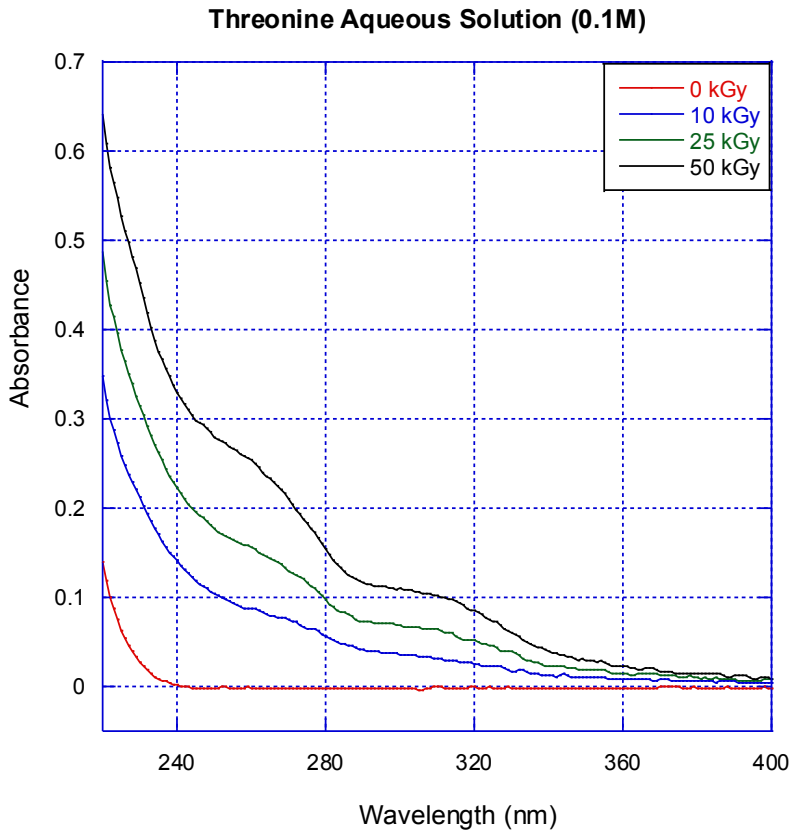

Figure A.17. UV-VIS absorbance spectra for threonine aqueous solution (0.1M)

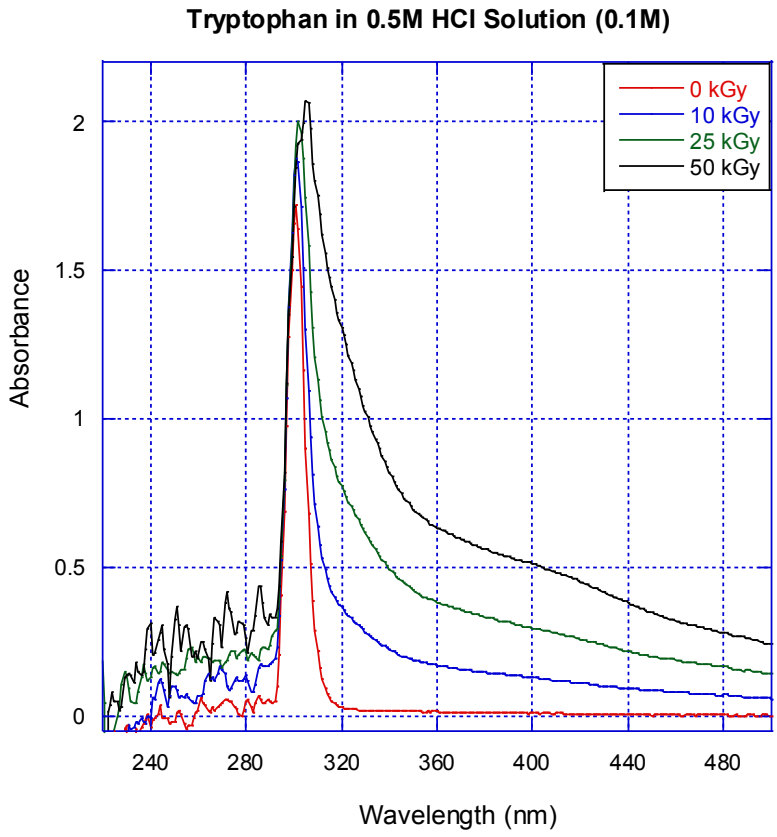

Figure A.18. UV-VIS absorbance spectra for tryptophan in 0.5M HCl solution (0.1M)

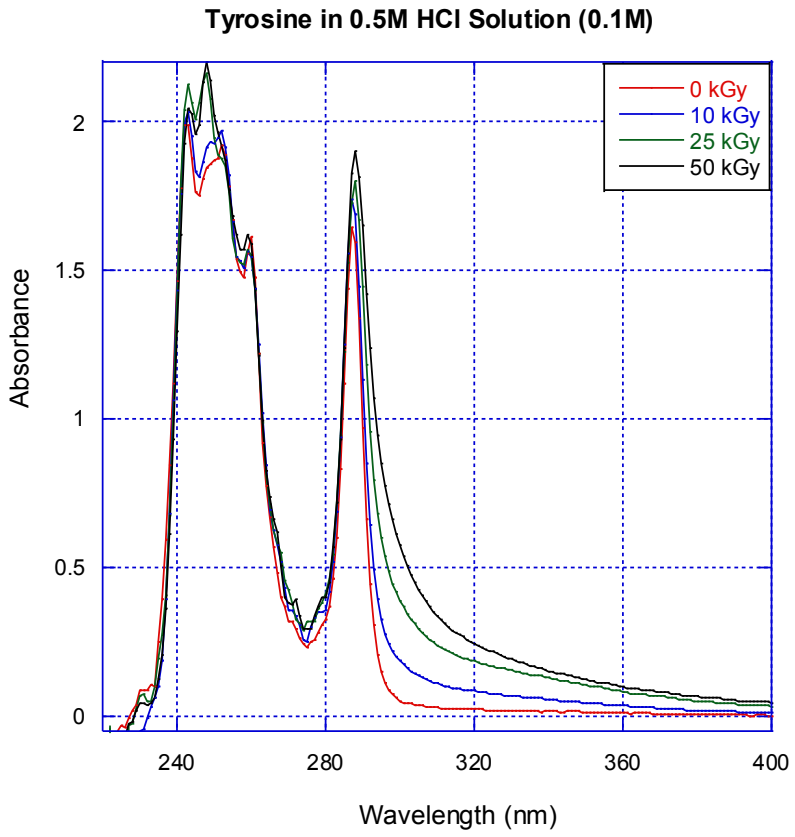

Figure A.19. UV-VIS absorbance spectra for tyrosine in 0.5M HCl solution (0.1M)

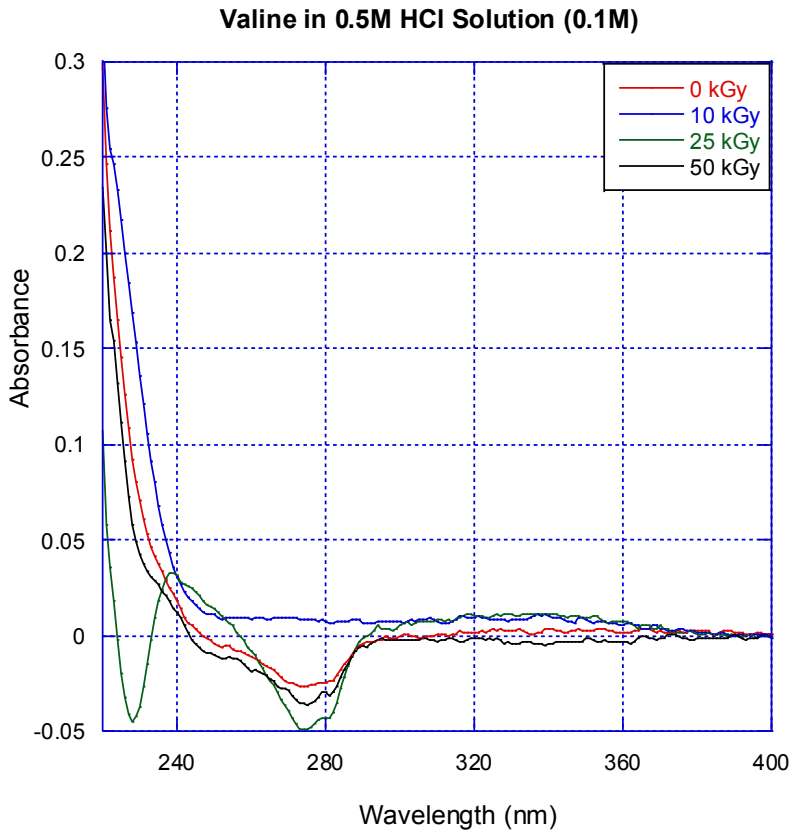

Figure A.20. UV-VIS absorbance spectra for valine in 0.5M HCl solution (0.1M)

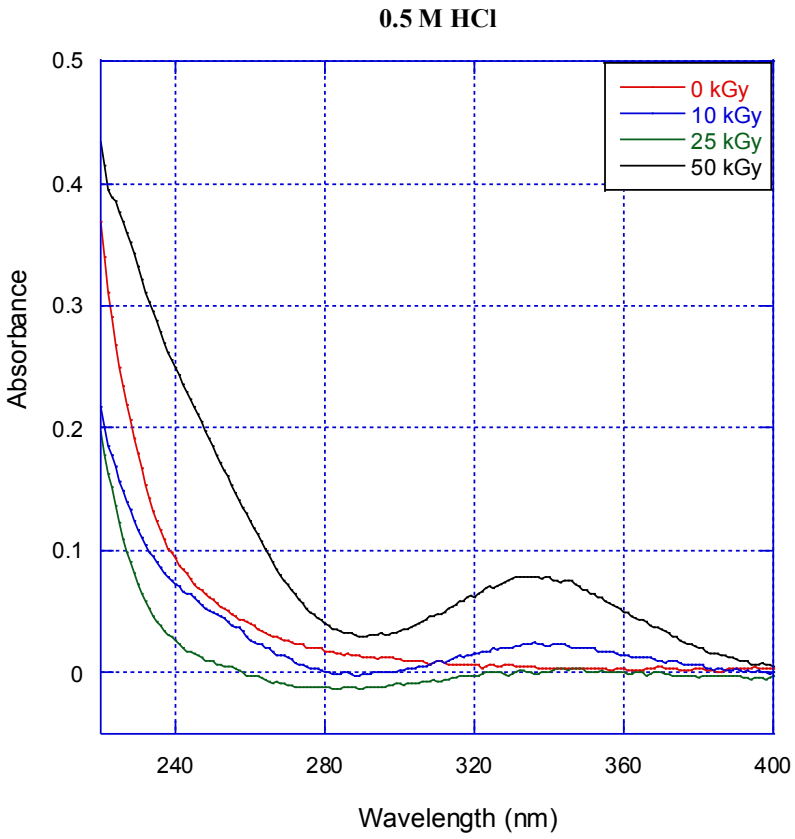

Figure A.21. UV-VIS absorbance spectra for valine in 0.5 M HCl solution

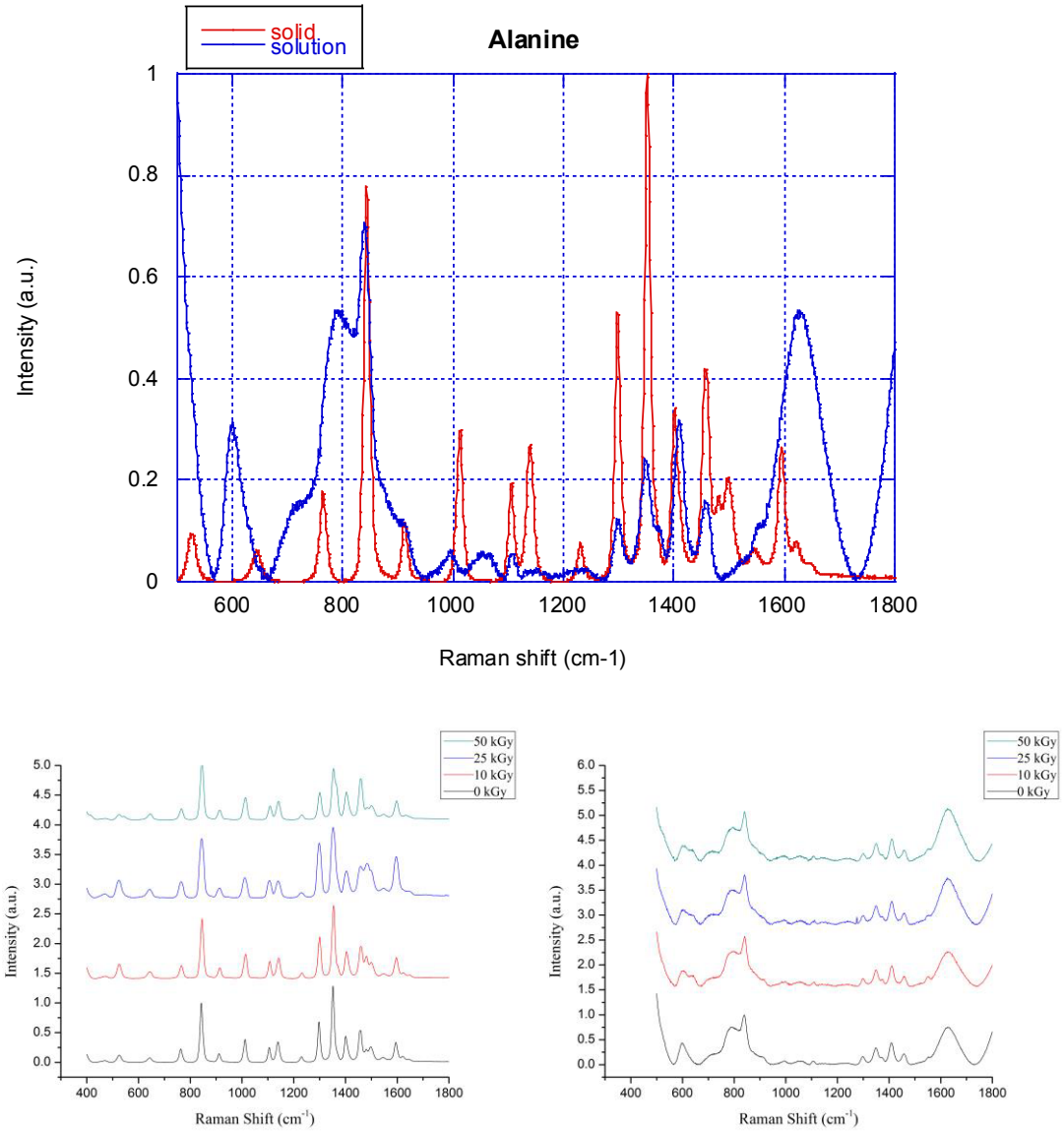

Figure A.22. Raman spectrum for alanine solid and aqueous solution (0.1M)

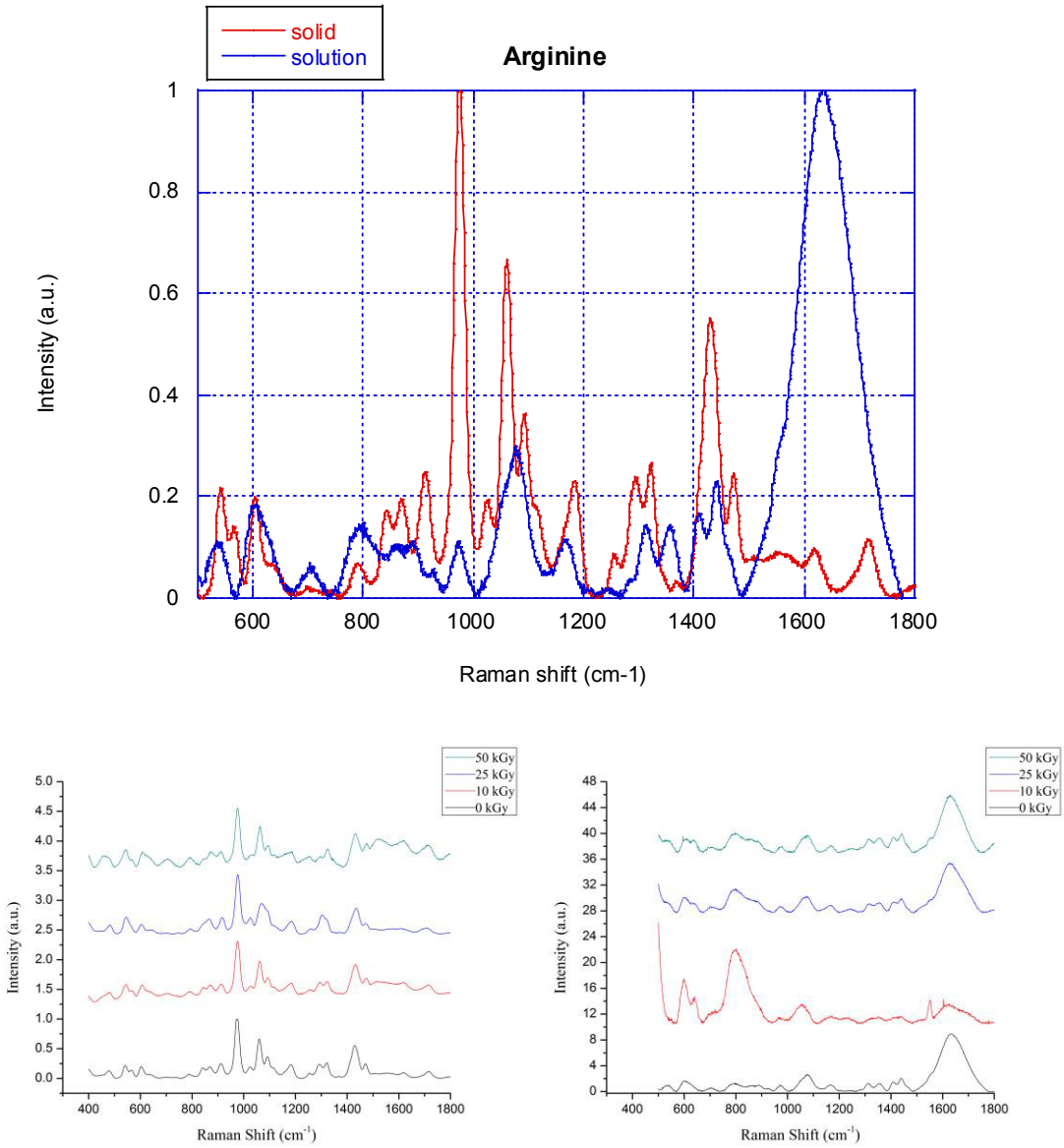

Figure A.23. Raman spectrum for arginine solid and aqueous solution (0.1M)

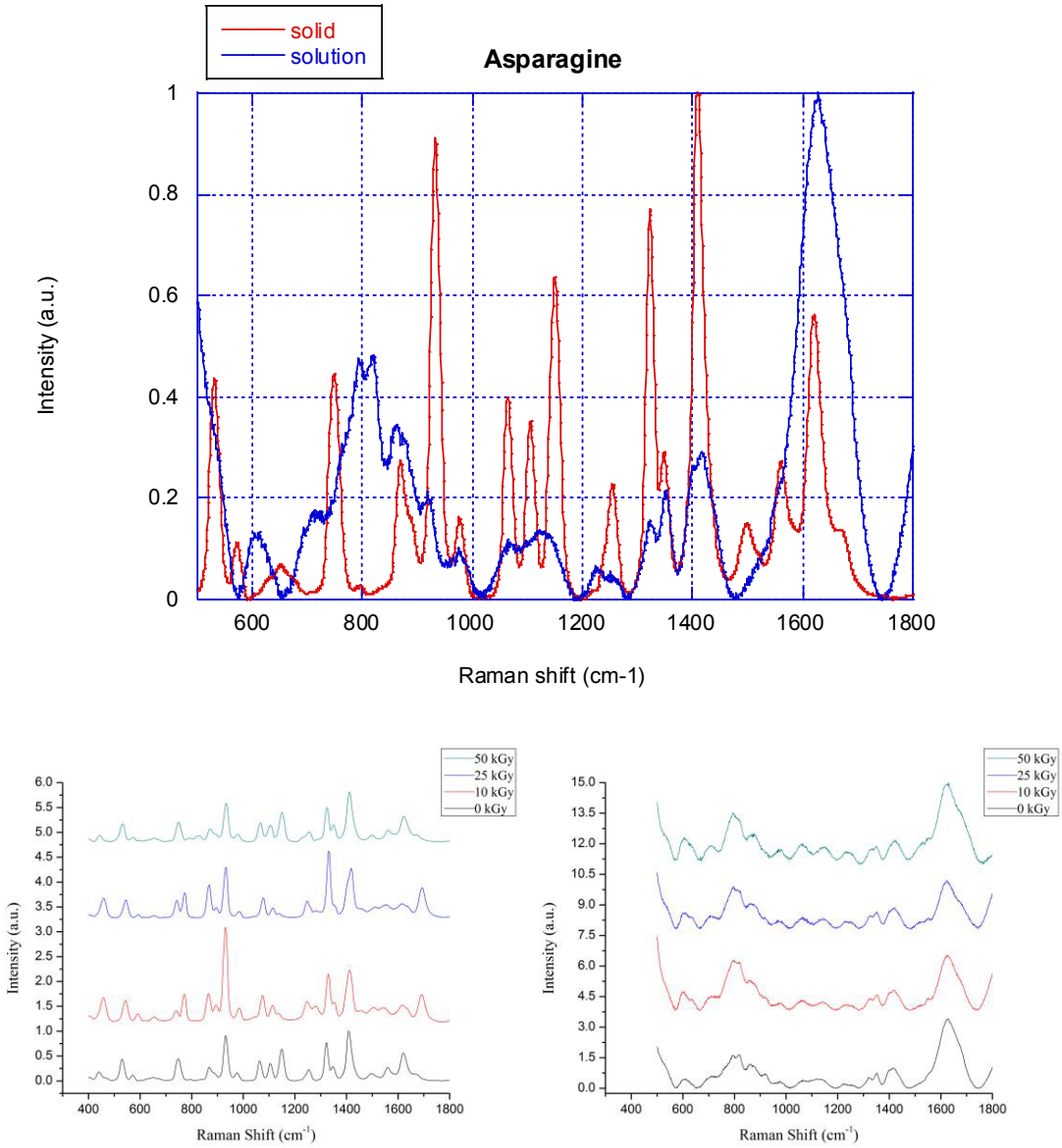

Figure A.24. Raman spectrum for asparagine solid and aqueous solution (0.1M)

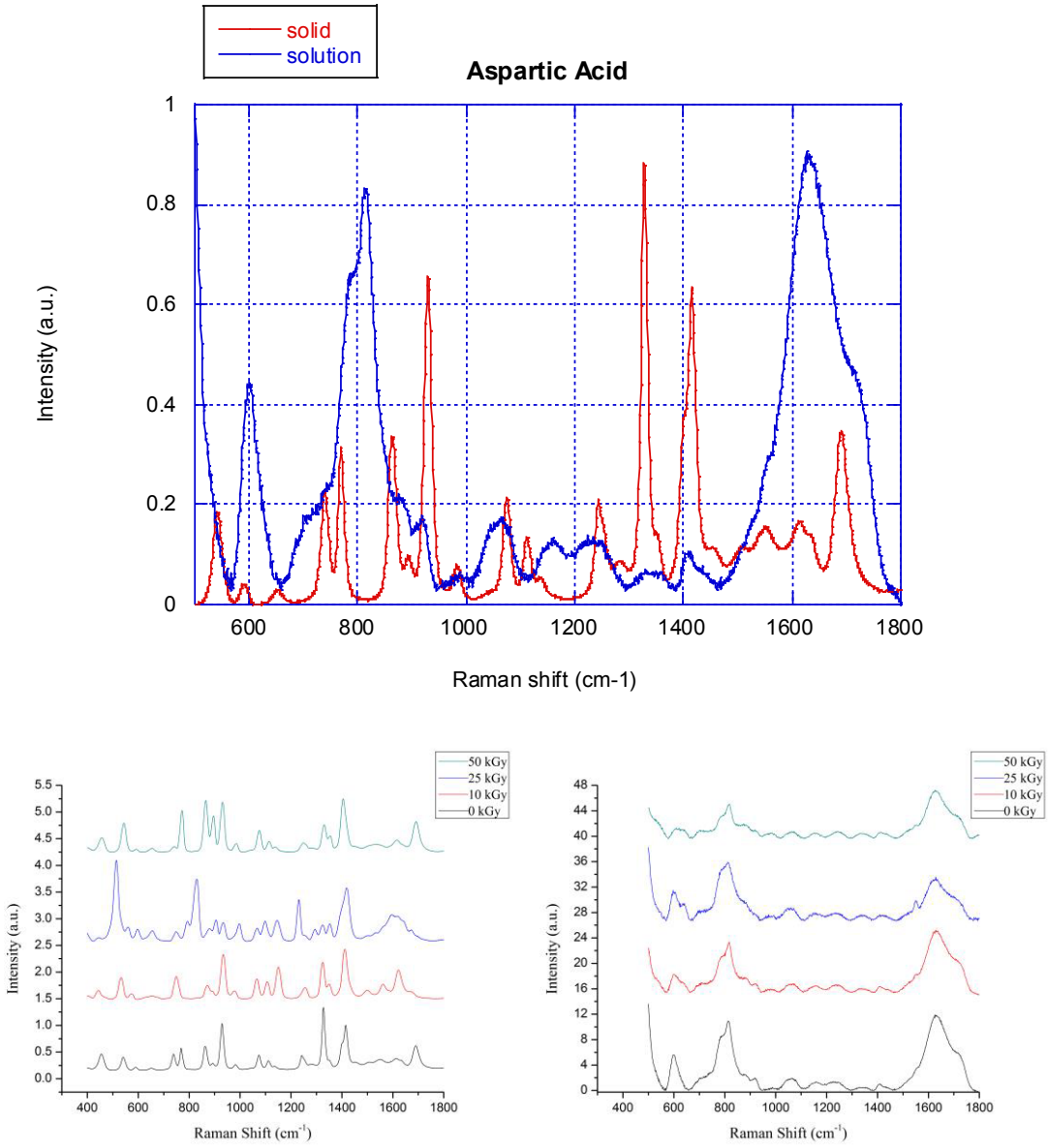

Figure A.25. Raman spectrum for aspartic acid solid and aqueous solution (0.1M)

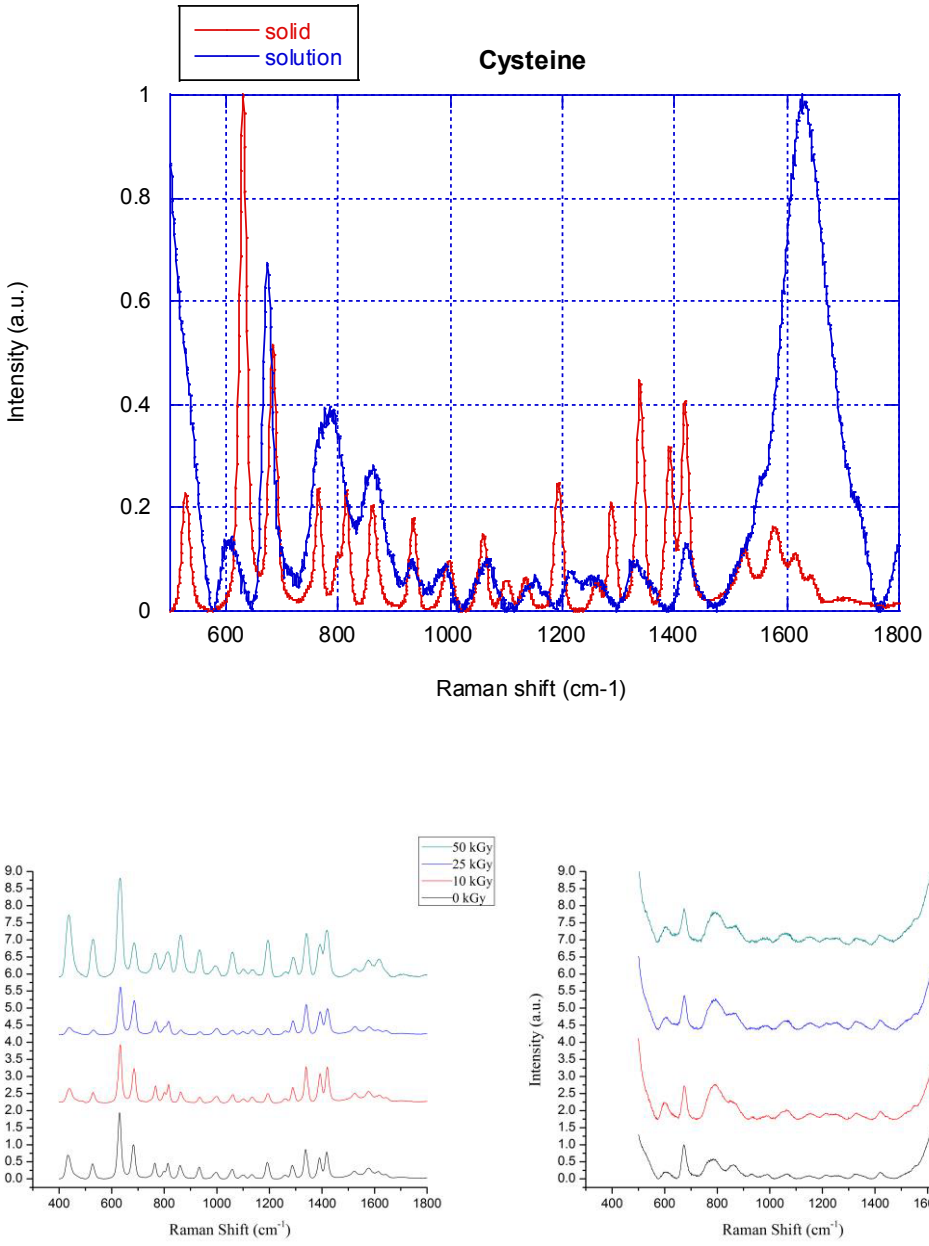

Figure A.26. Raman spectrum for cysteine solid and aqueous solution (0.1M)

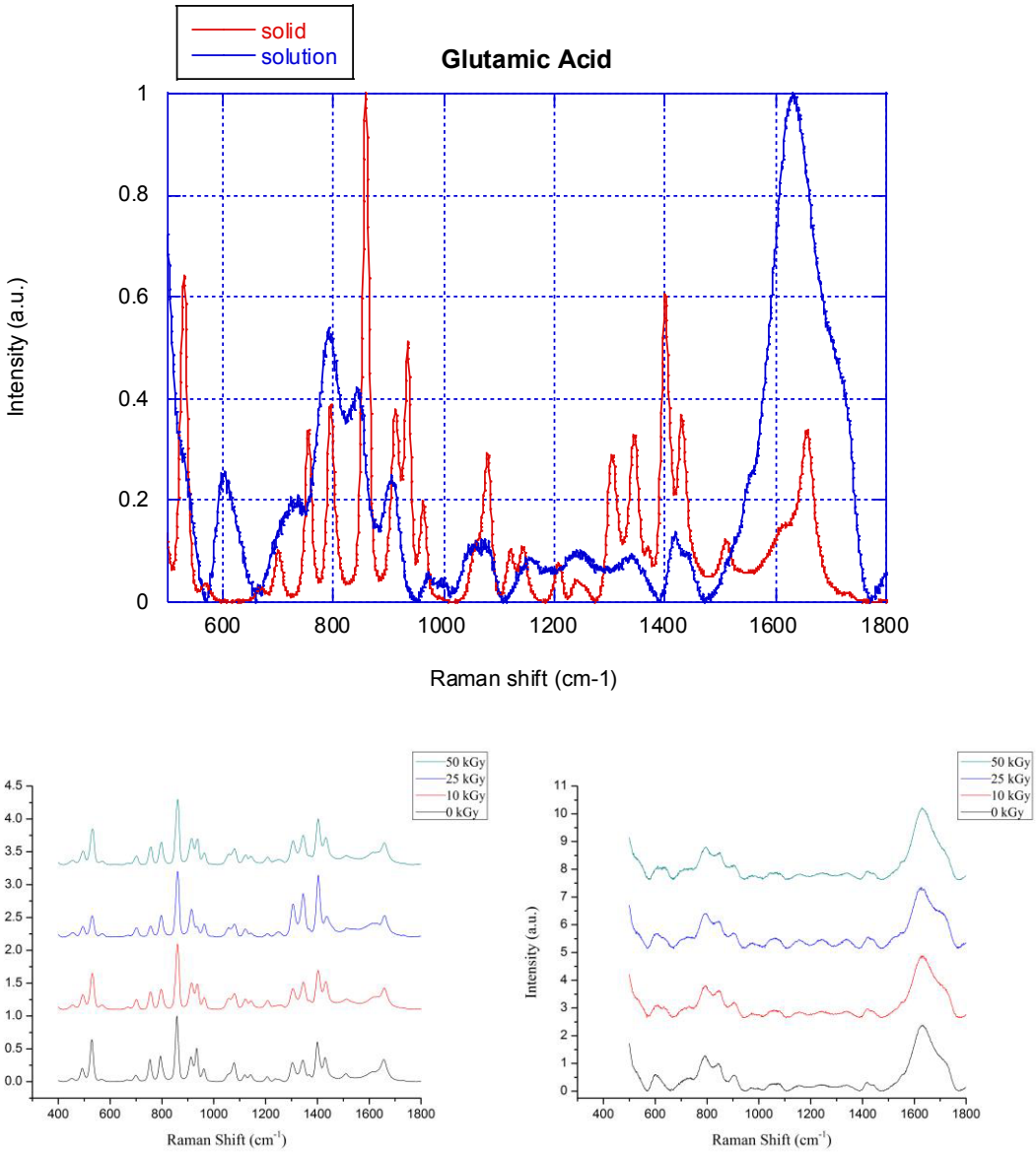

Figure A.27. Raman spectrum for glutamic acid solid and aqueous solution (0.1M)

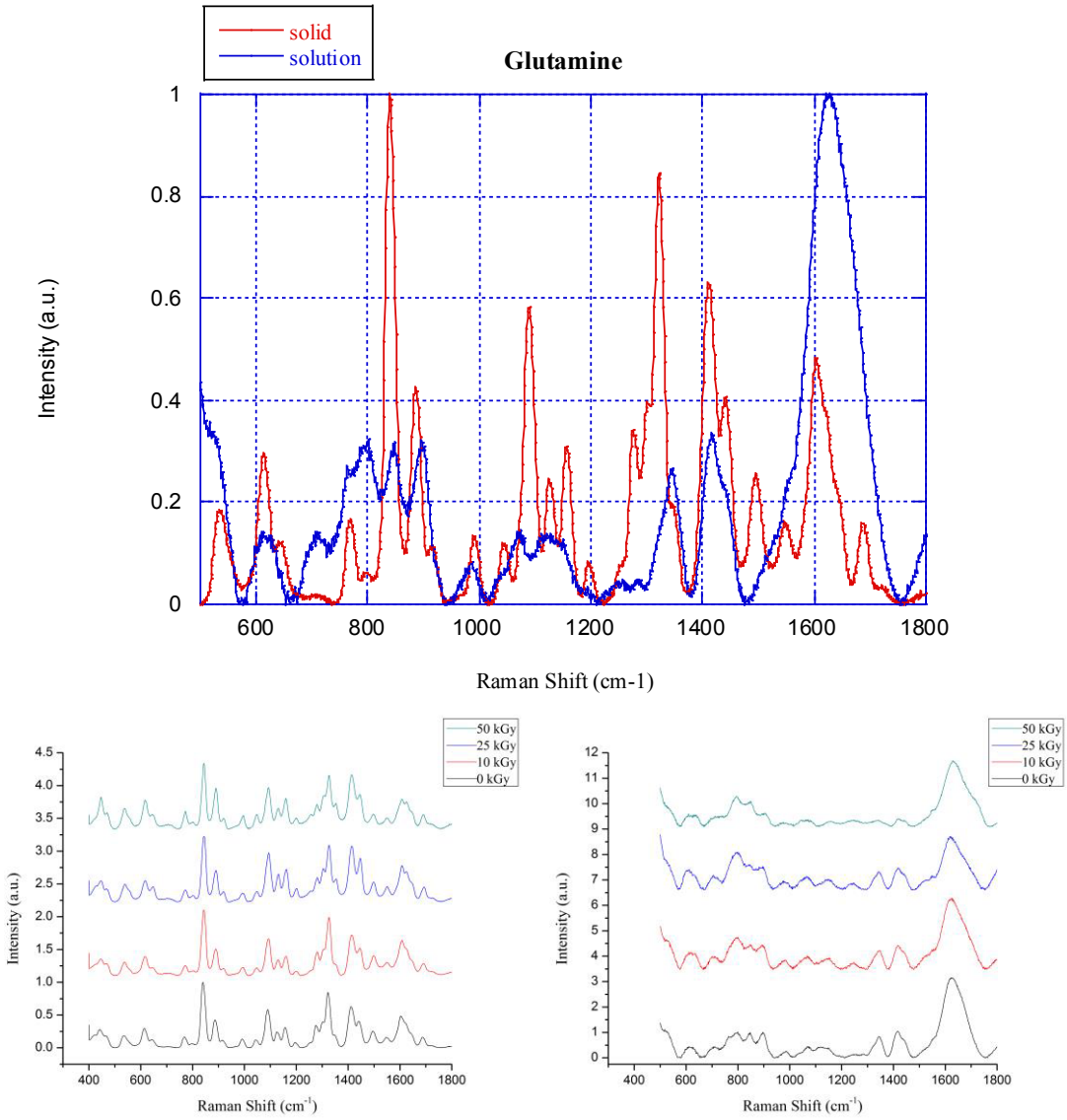

Figure A.28. Raman spectrum for glutamine solid and aqueous solution (0.1M)

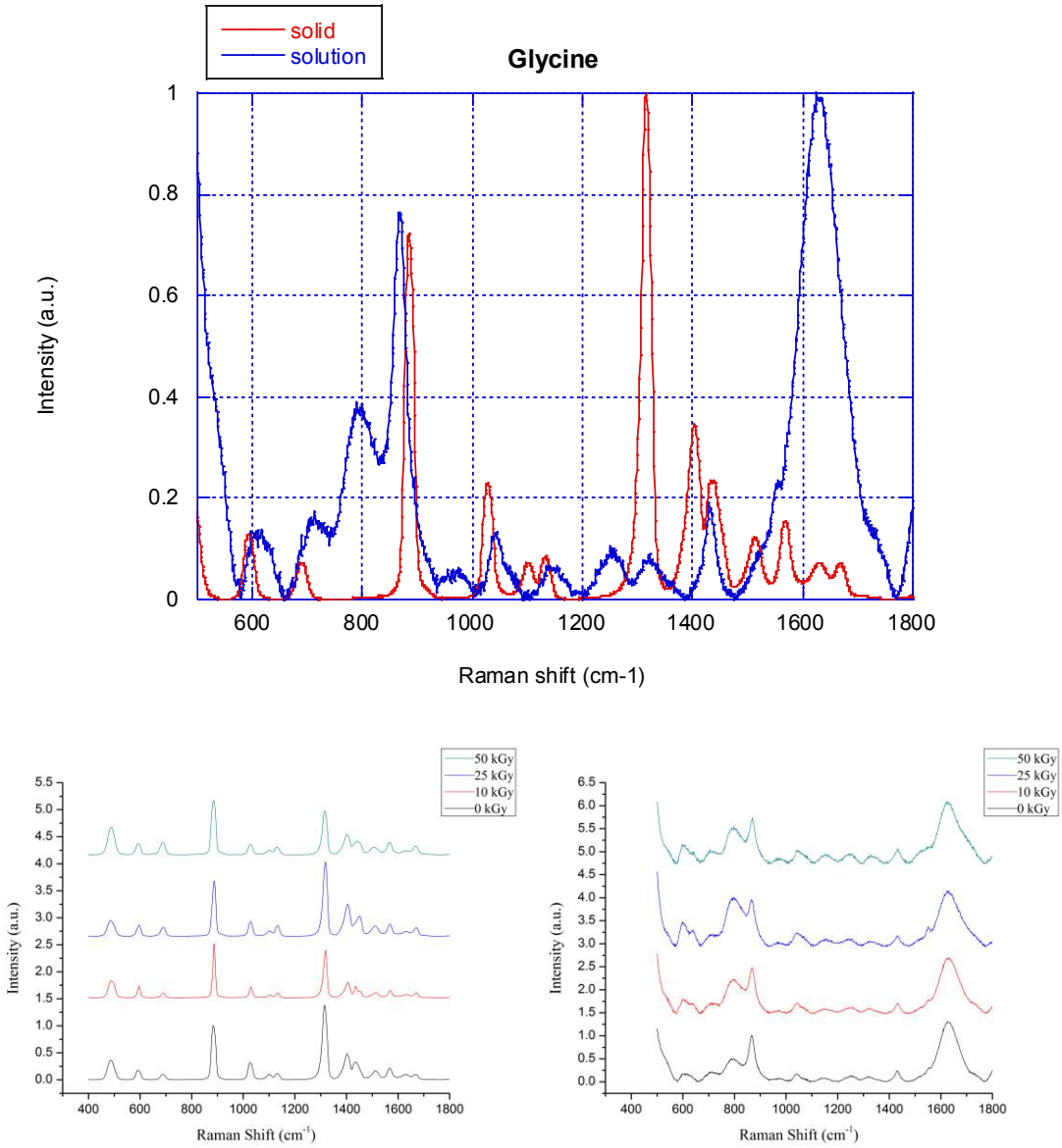

Figure A.29. Raman spectrum for glycine solid and aqueous solution (0.1M)

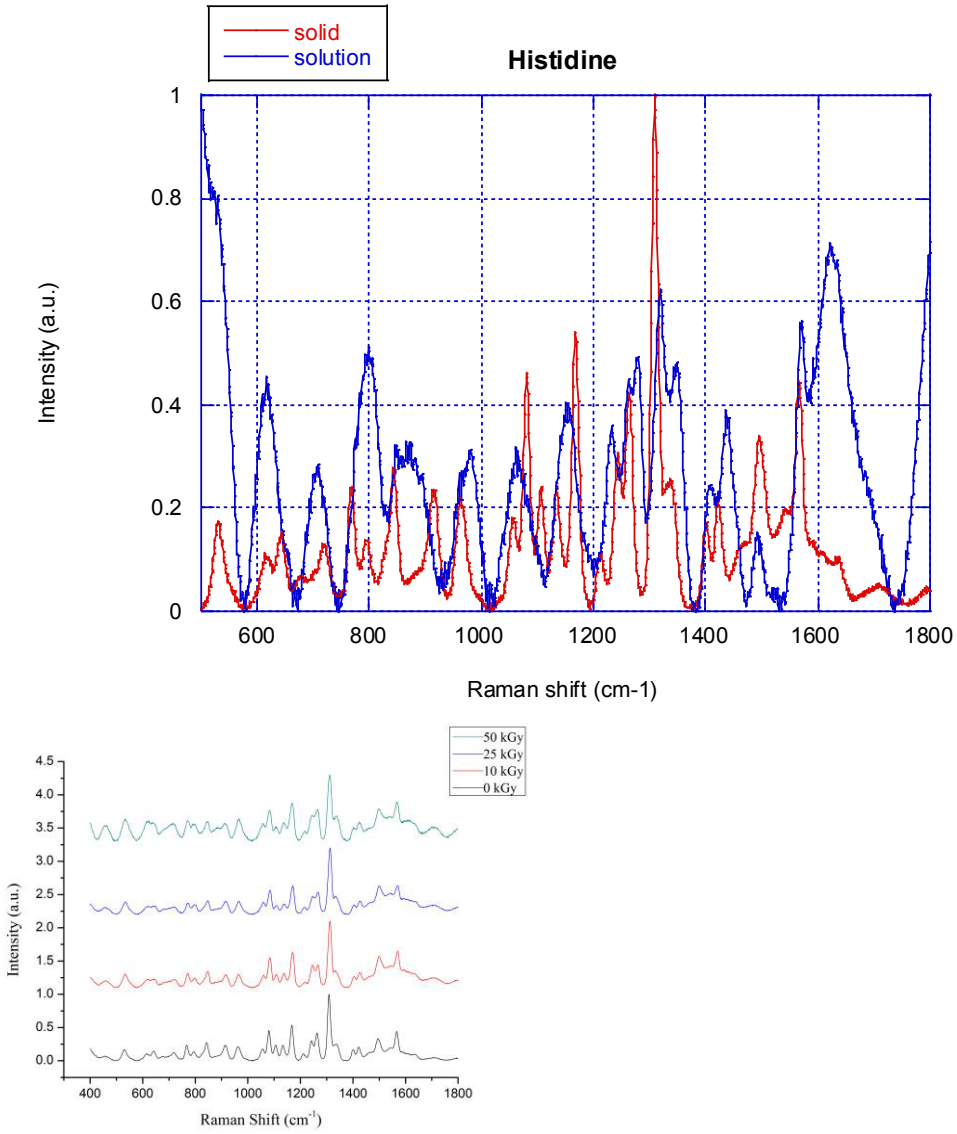

Figure A.30. Raman spectrum for histidine solid and aqueous solution (0.1M)

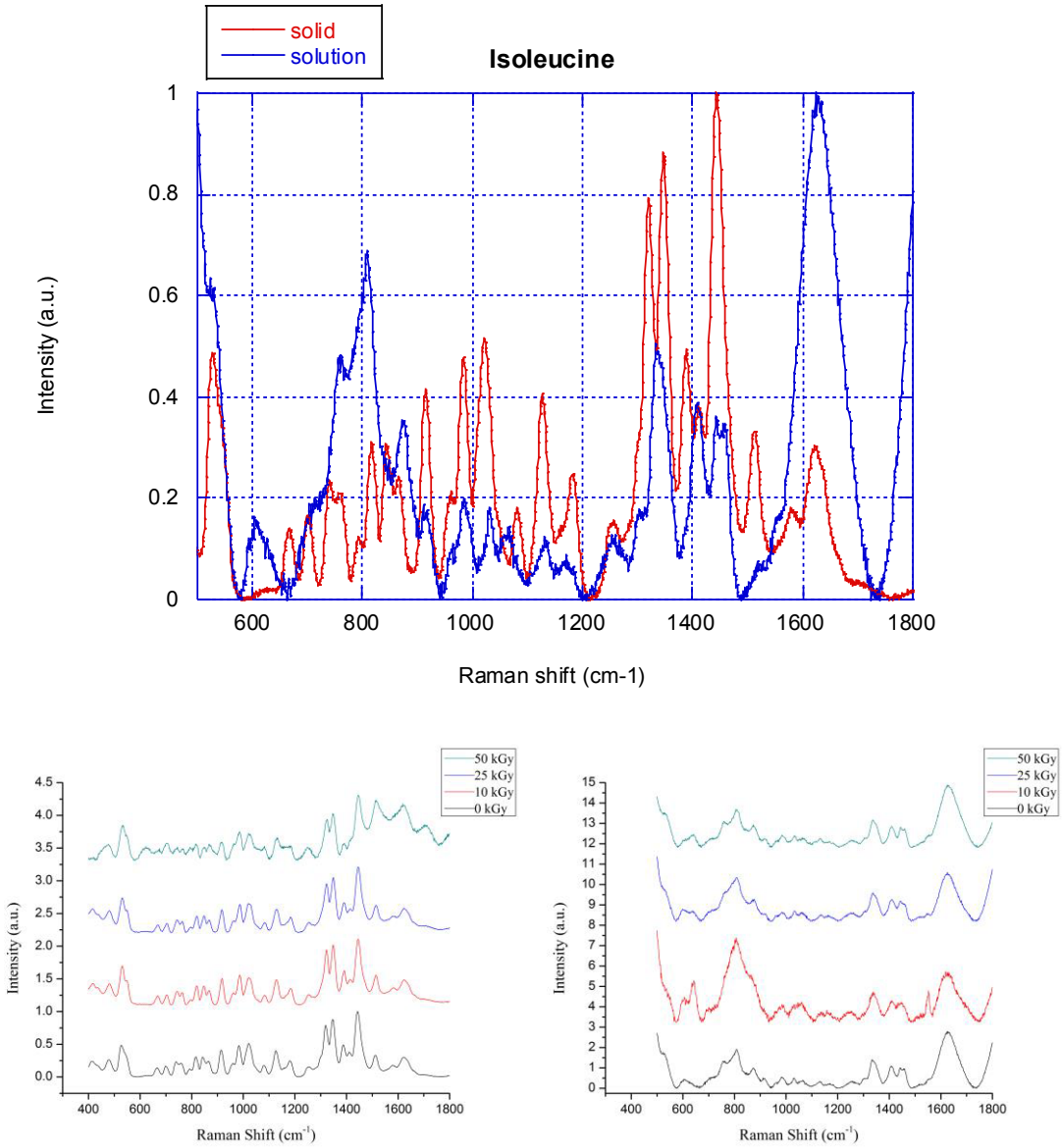

Figure A.31. Raman spectrum for isoleucine solid and aqueous solution (0.1M)

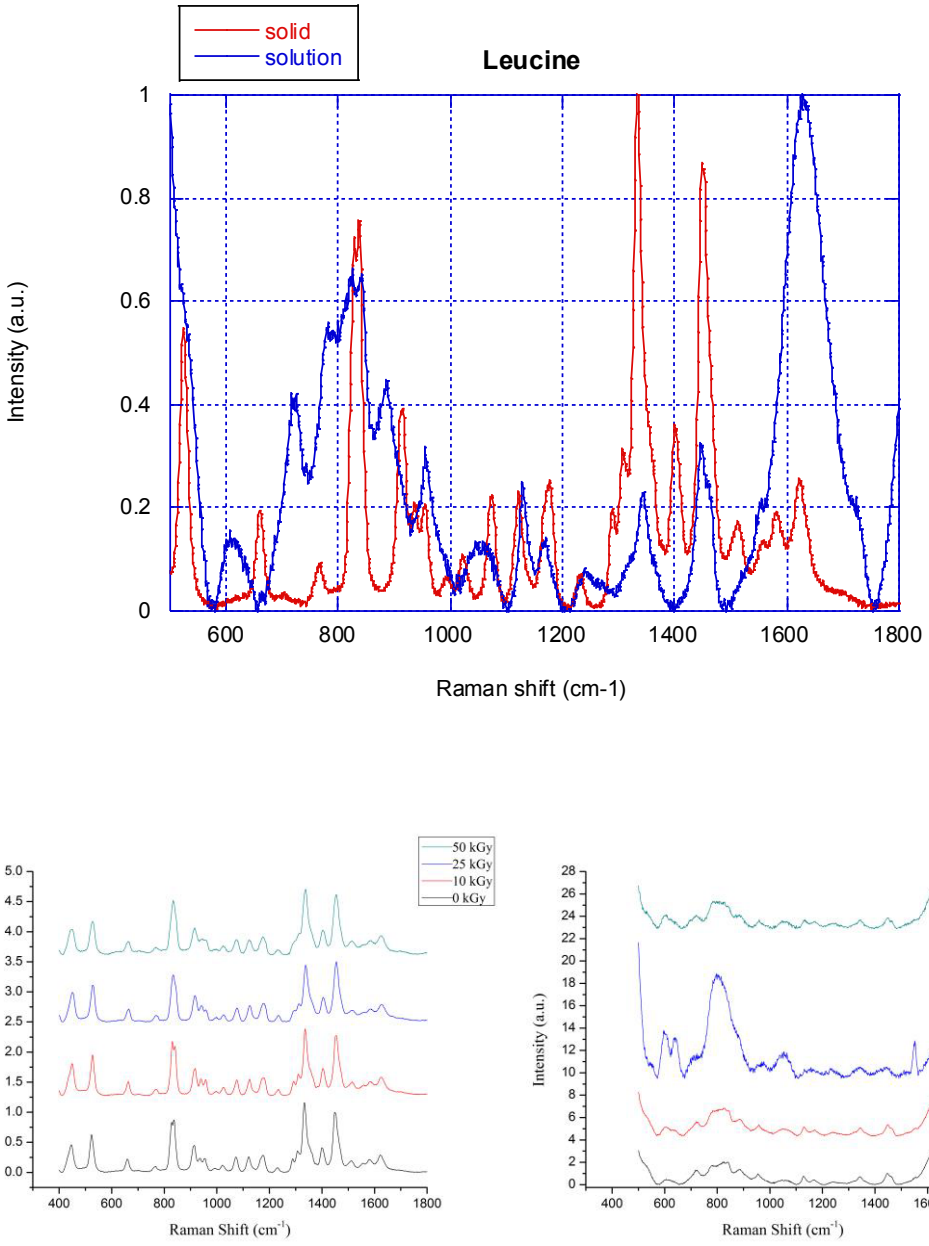

Figure A.32. Raman spectrum for leucine solid and aqueous solution (0.1M)

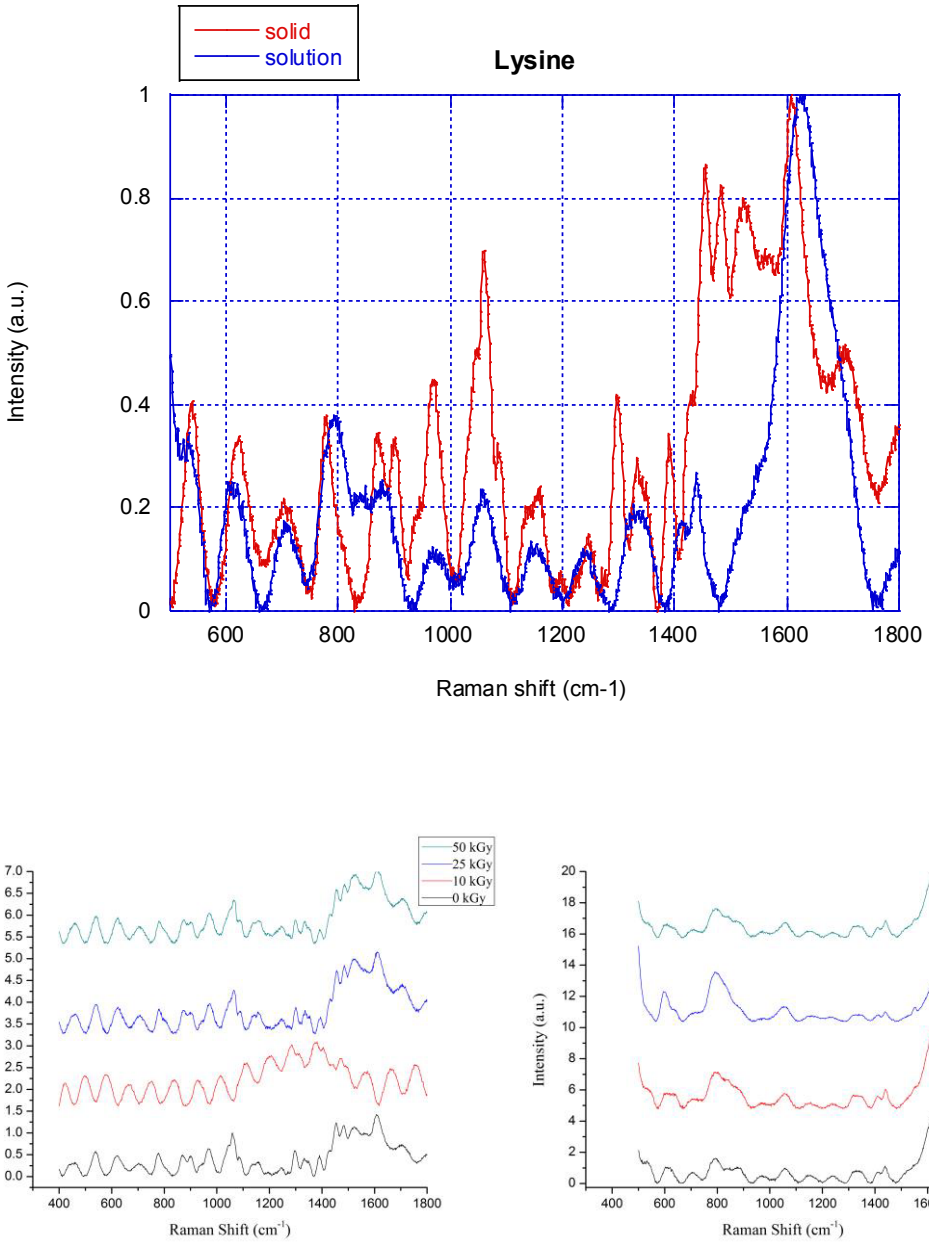

Figure A.33. Raman spectrum for lysine solid and aqueous solution (0.1M)

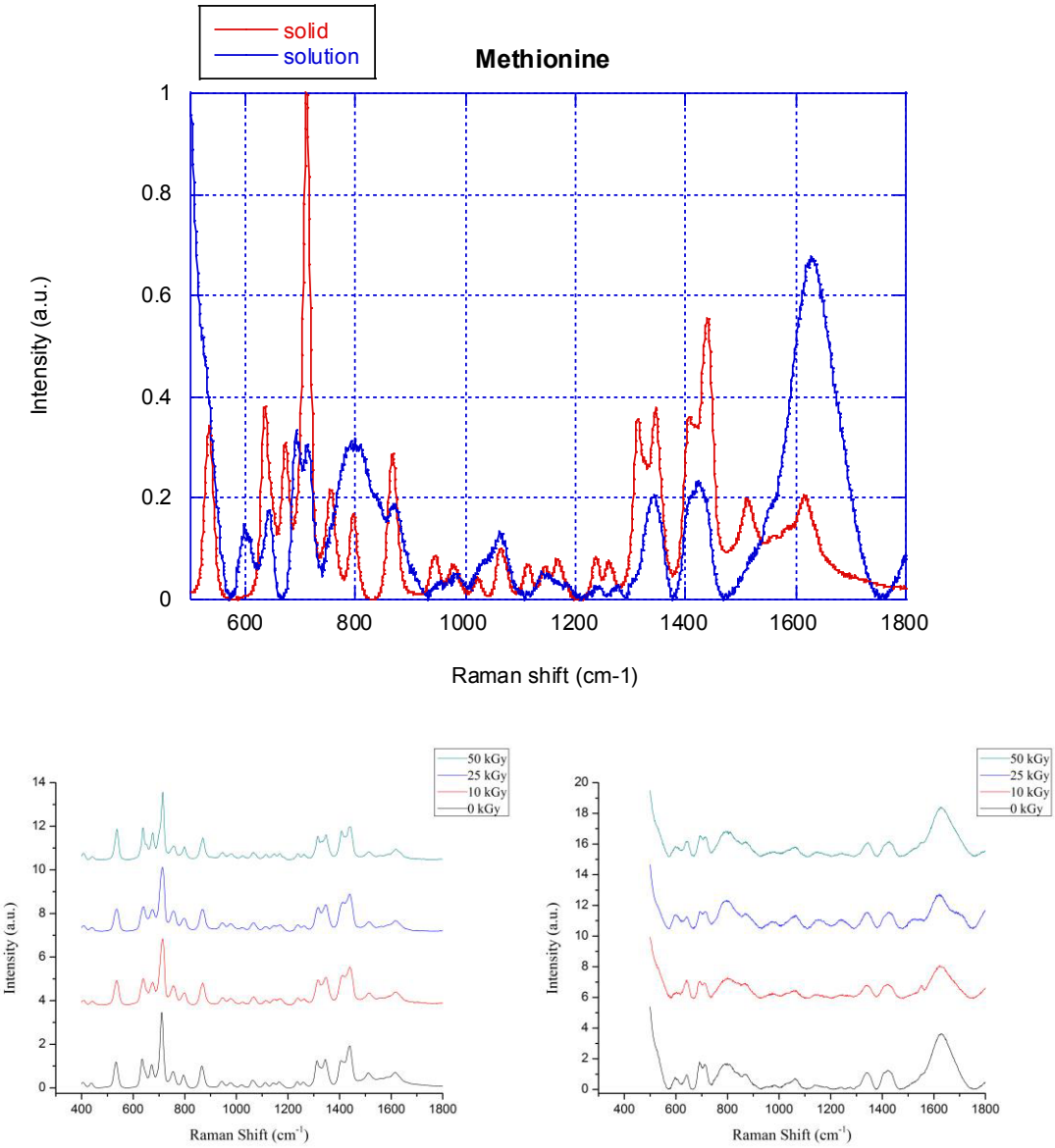

Figure A.34. Raman spectrum for methionine solid and aqueous solution (0.1M)

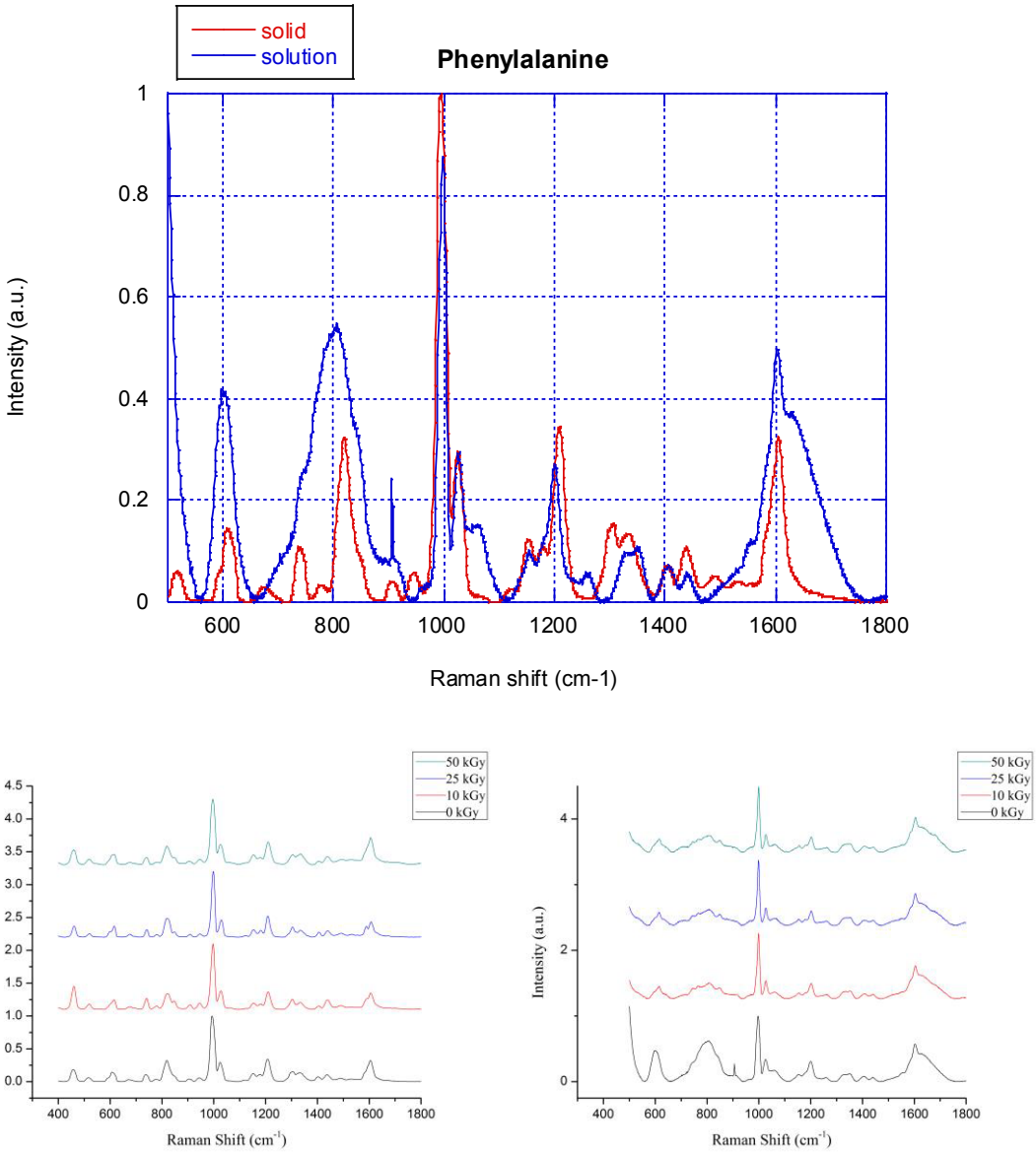

Figure A.35. Raman spectrum for phenylalanine solid and aqueous solution (0.1M)

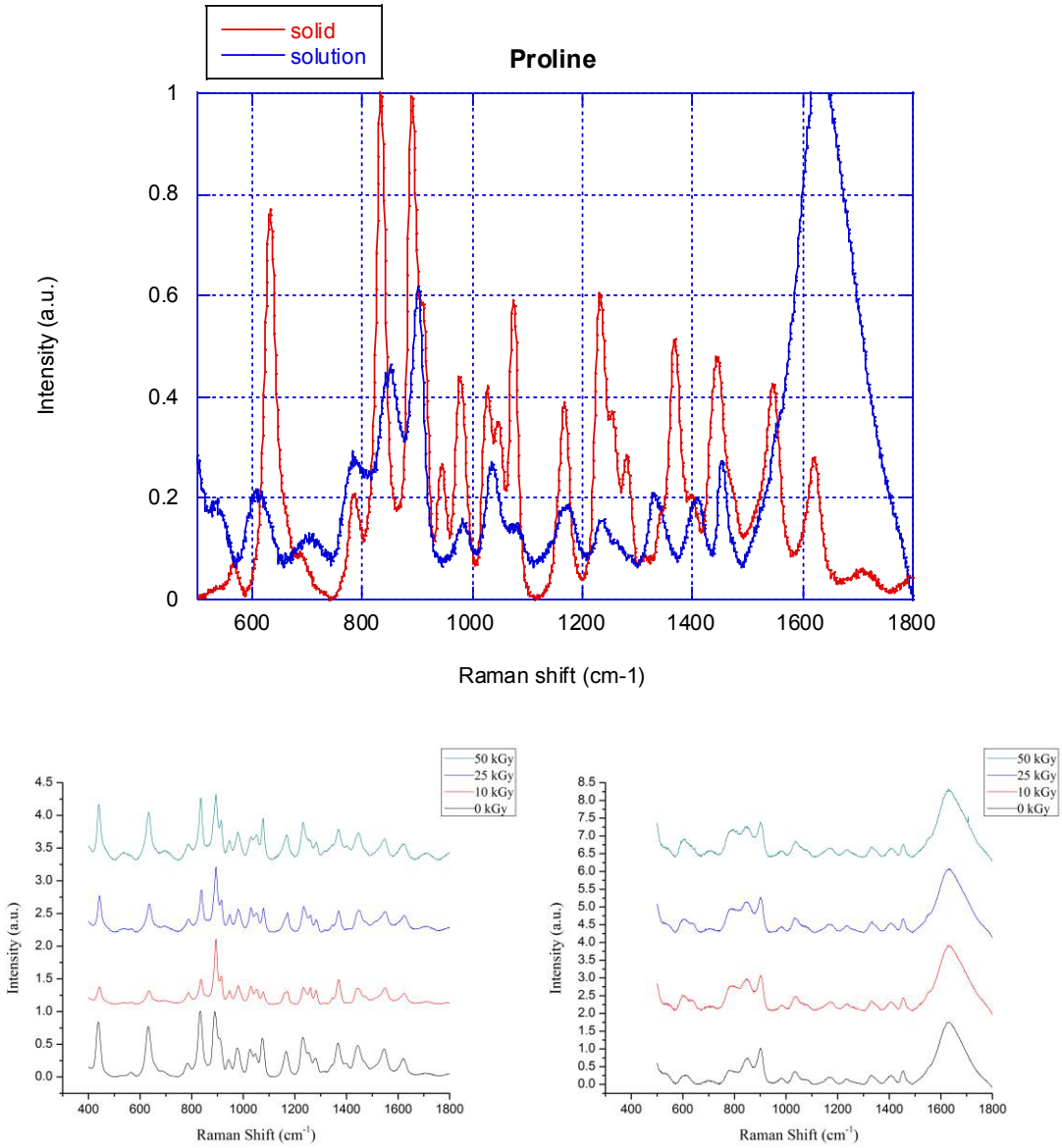

Figure A.36. Raman spectrum for proline solid and aqueous solution (0.1M)

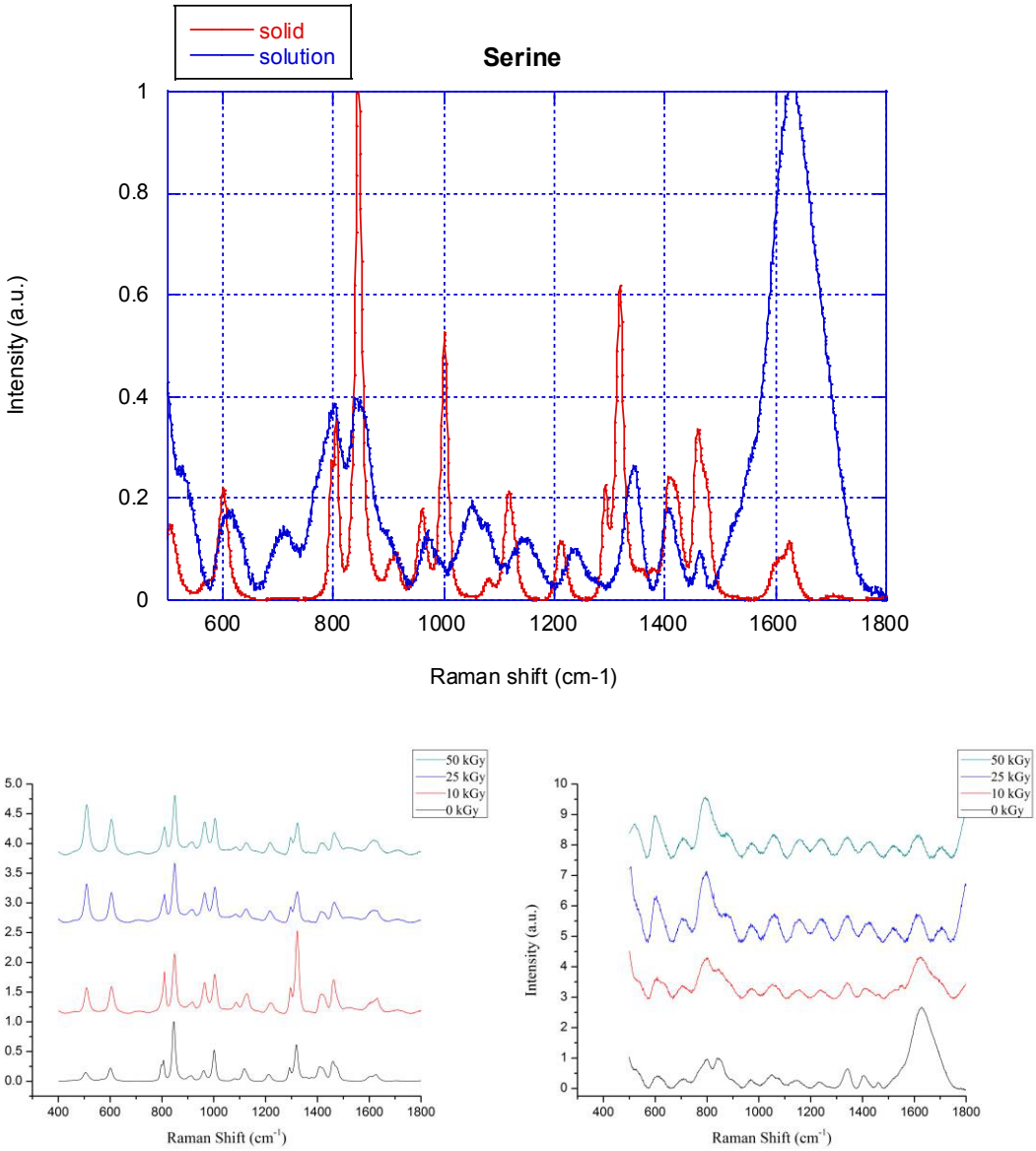

Figure A.37. Raman spectrum for serine solid and aqueous solution (0.1M)

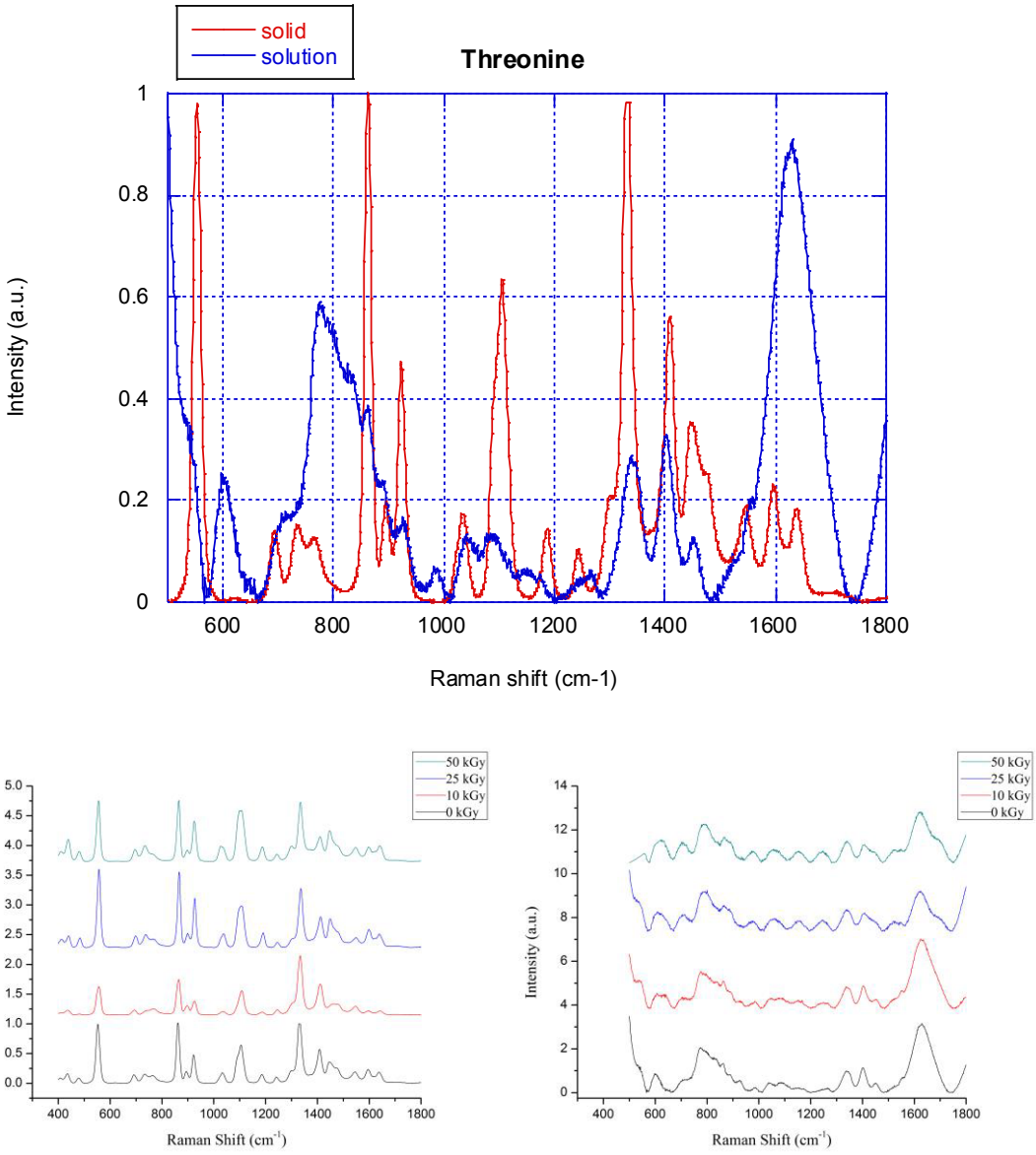

Figure A.38. Raman spectrum for threonine solid and aqueous solution (0.1M)

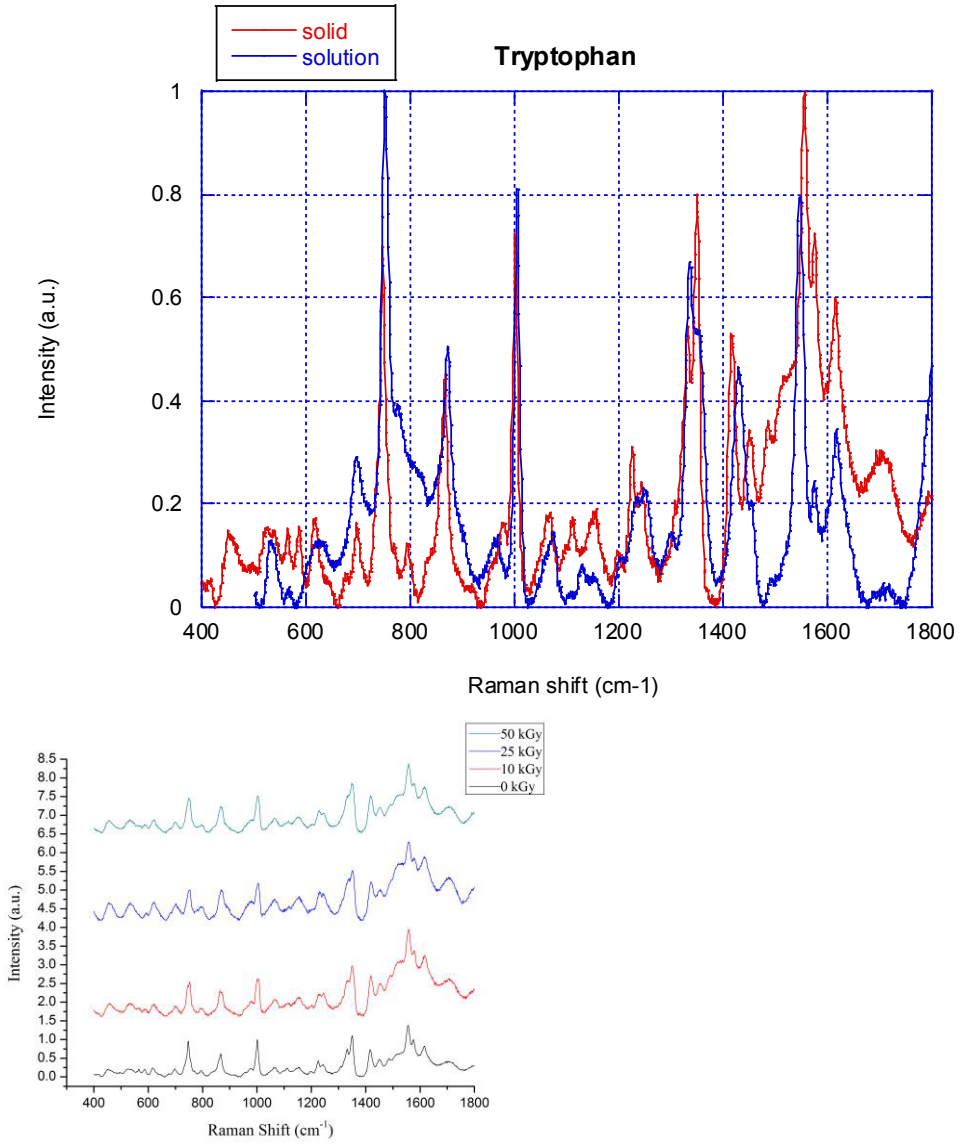

Figure A.39. Raman spectrum for tryptophan solid and aqueous solution (0.1M)

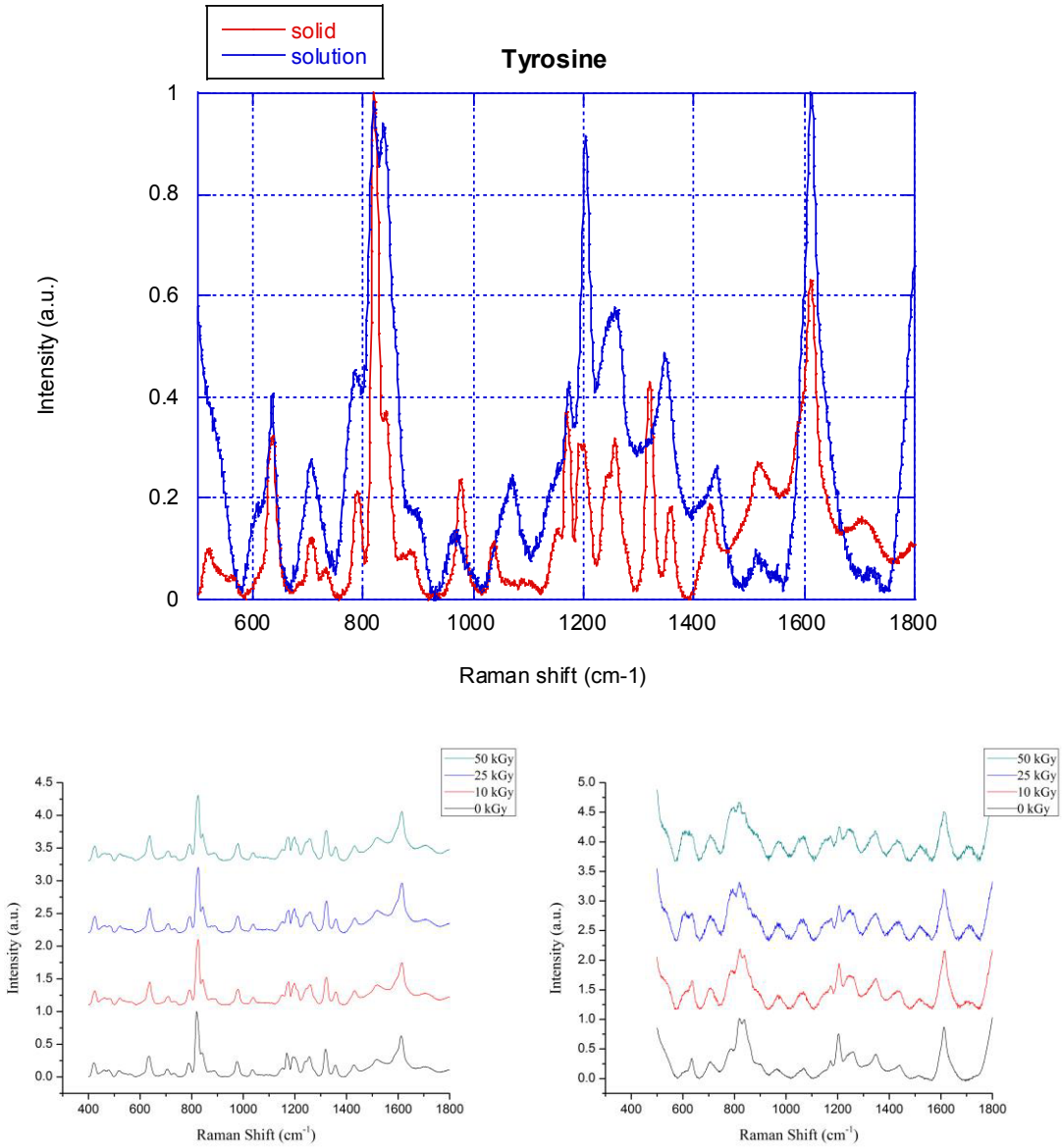

Figure A.40. Raman spectrum for tyrosine solid and aqueous solution (0.1M)

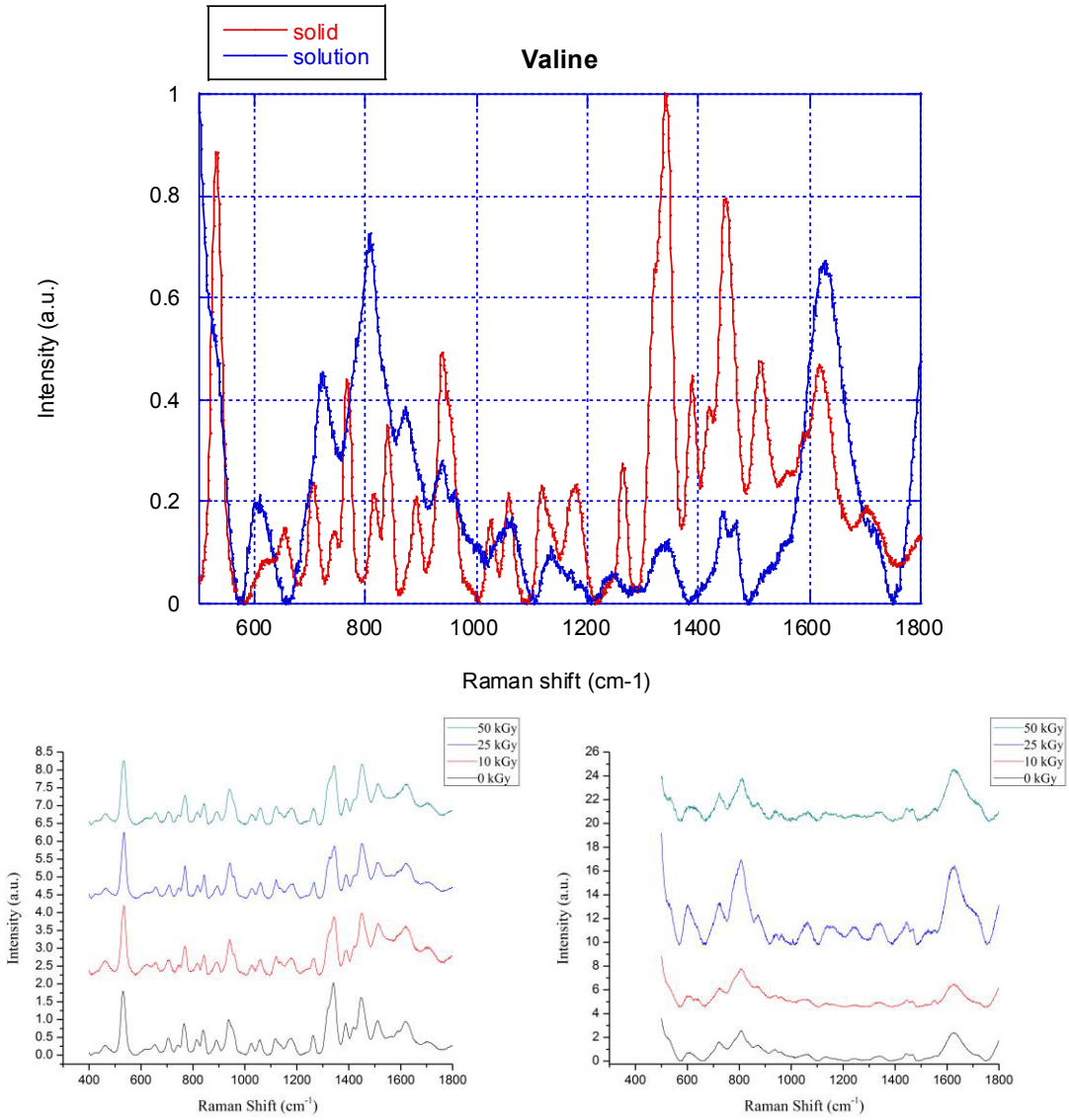

Figure A.41. Raman spectrum for valine solid and aqueous solution (0.1M)

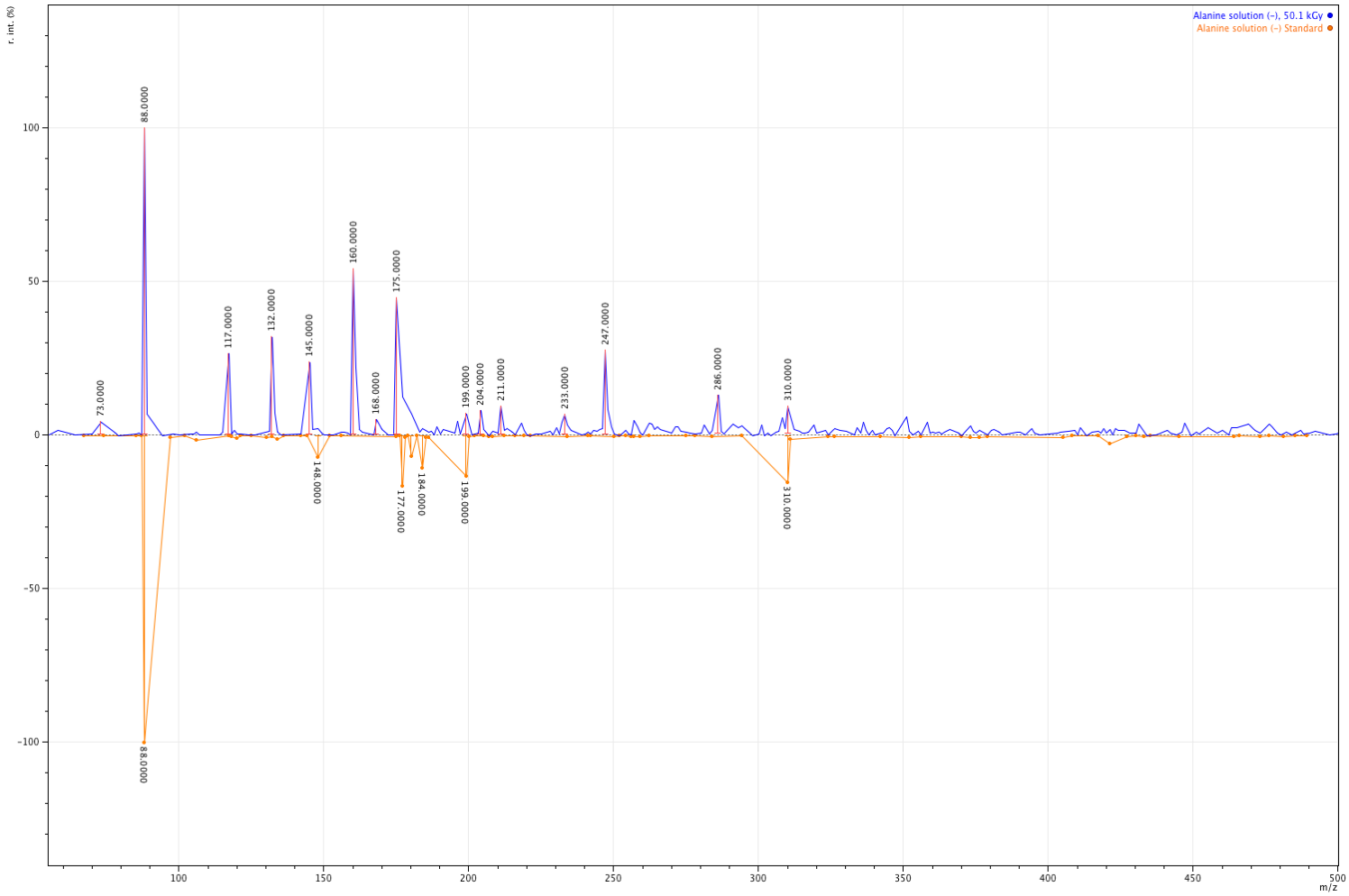

Figure A.42. ESI-MS spectrum of alanine in aqueous solution for control and irradiated 50kGy samples: negative mode

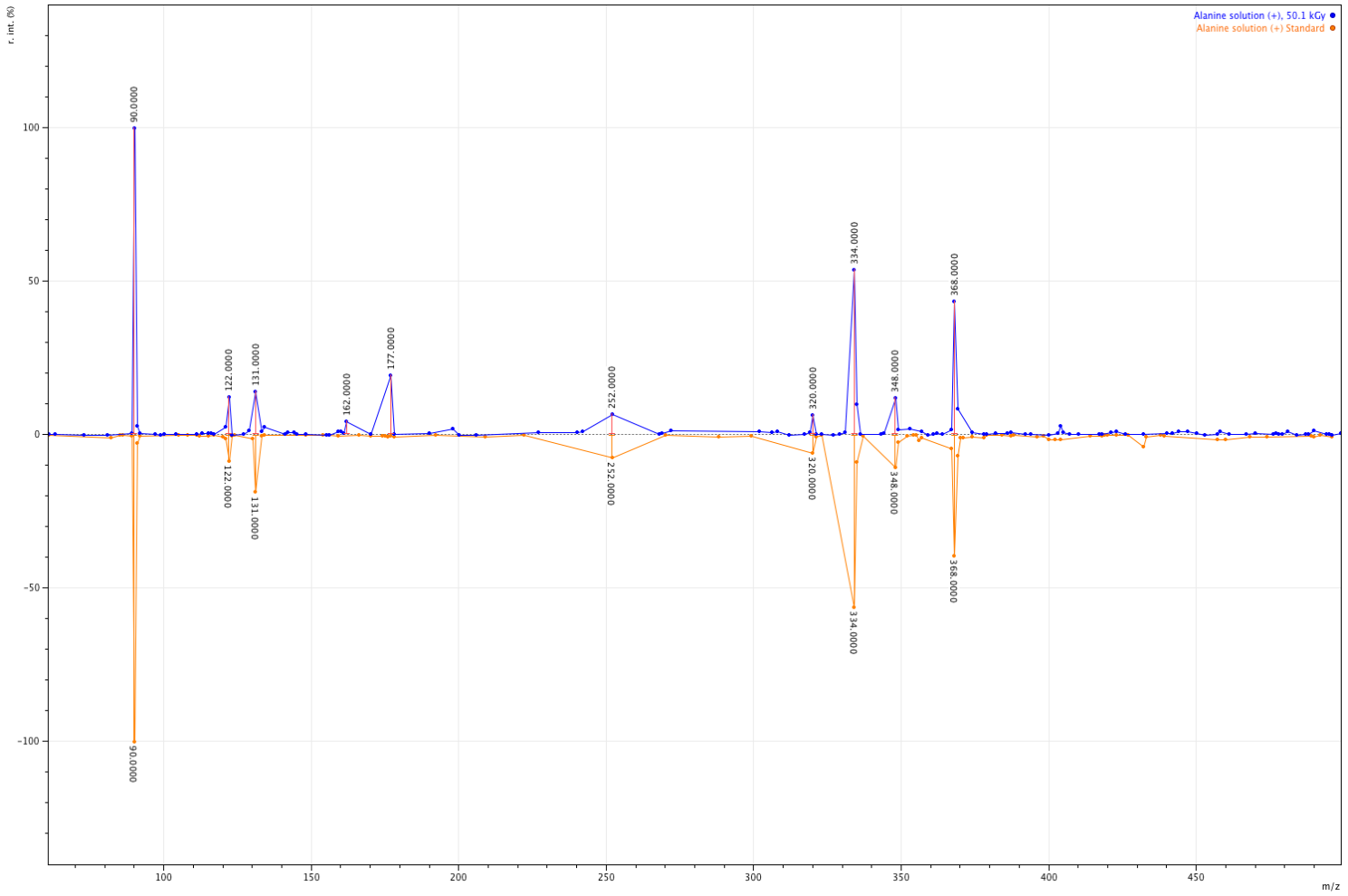

Figure A.43. ESI-MS spectrum of alanine in aqueous solution for control and irradiated 50kGy samples: positive mode

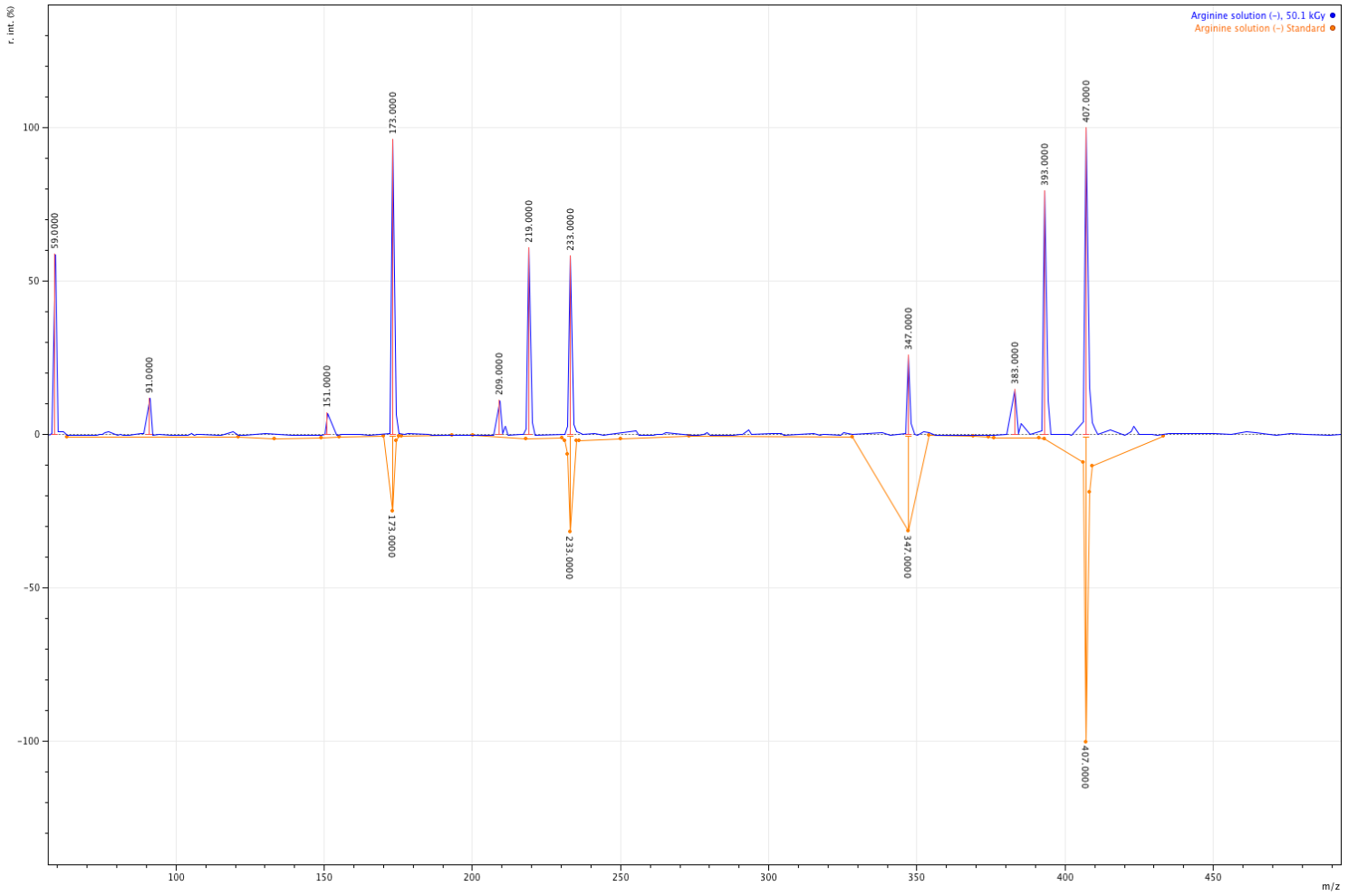

Figure A.44. ESI-MS spectrum of arginine in aqueous solution for control and irradiated 50kGy samples: negative mode

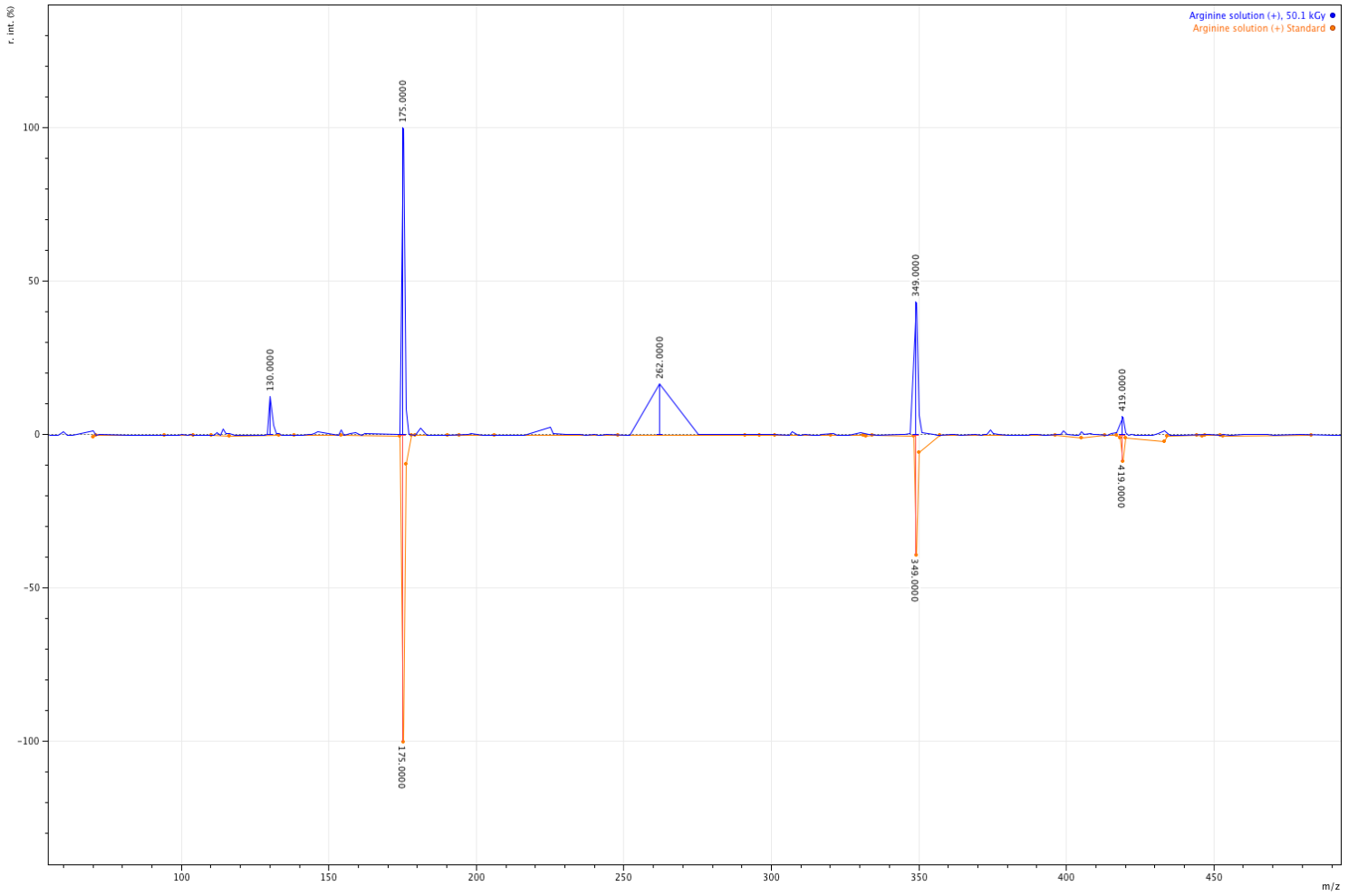

Figure A.45. ESI-MS spectrum of arginine in aqueous solution for control and irradiated 50kGy samples: positive mode

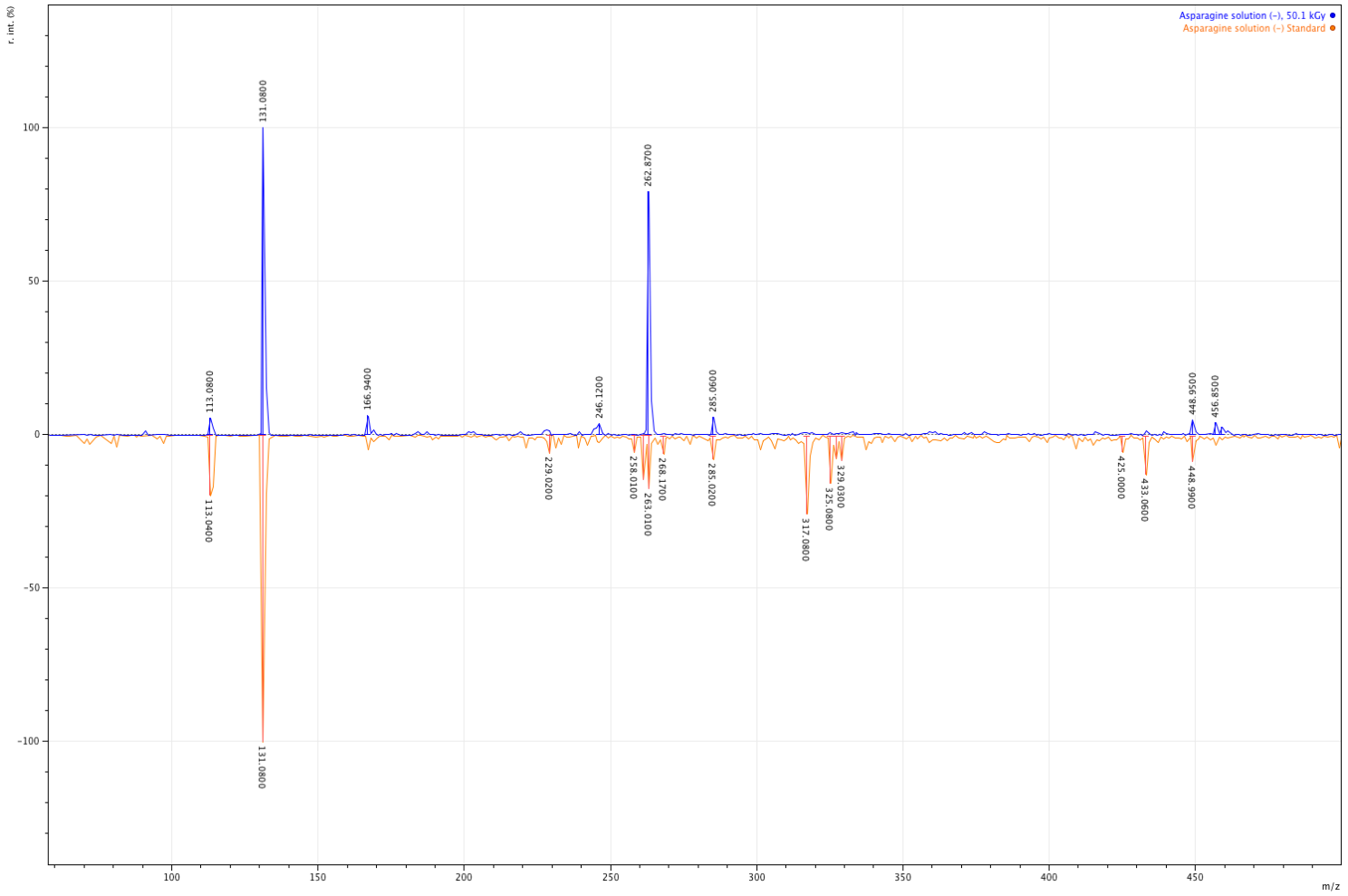

Figure A.46. ESI-MS spectrum of asparagine in aqueous solution for control and irradiated 50kGy samples: negative mode

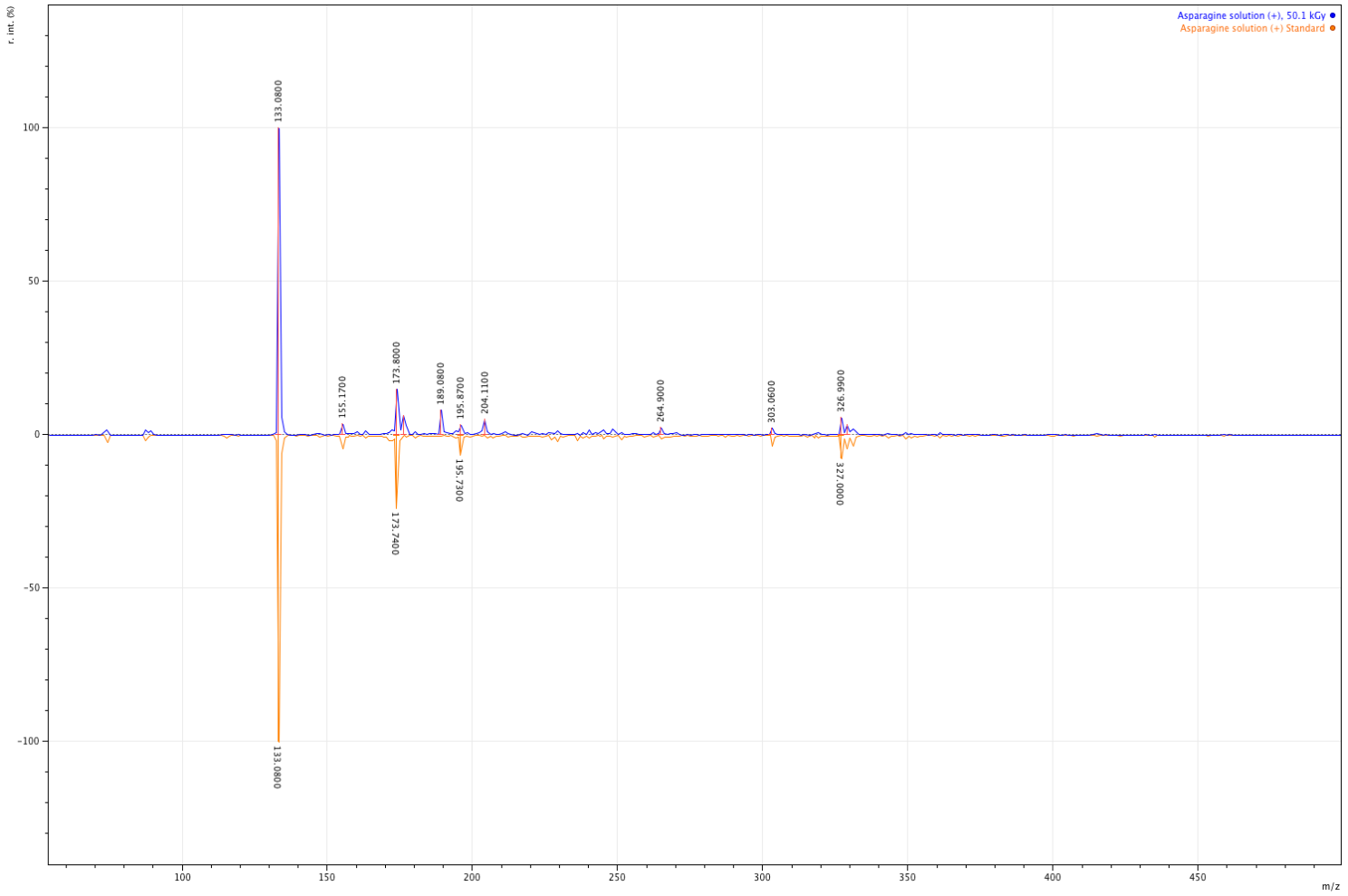

Figure A.47. ESI-MS spectrum of asparagine in aqueous solution for control and irradiated 50kGy samples: positive mode

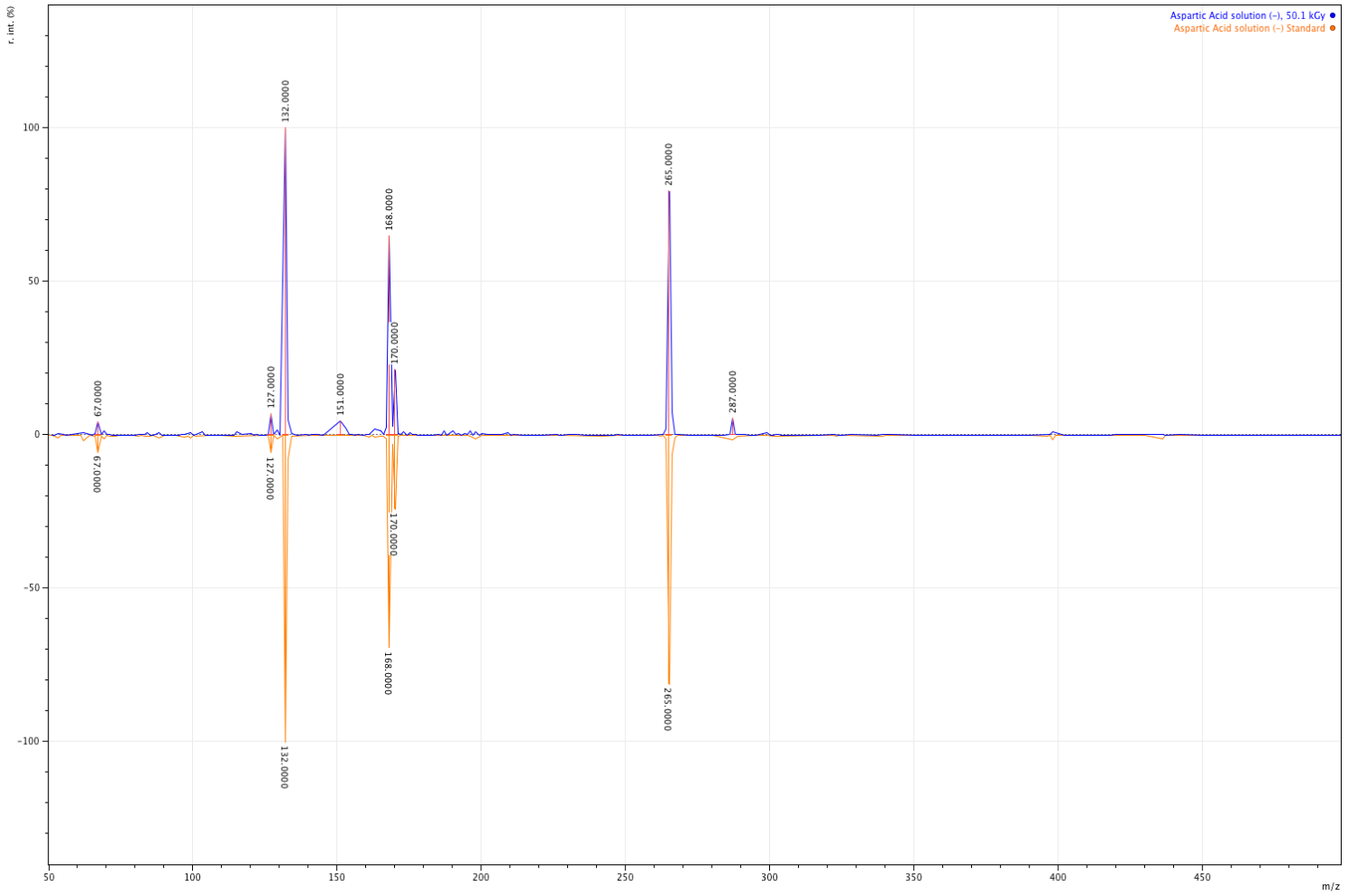

Figure A.48. ESI-MS spectrum of aspartic acid in aqueous solution for control and irradiated 50kGy samples: negative mode

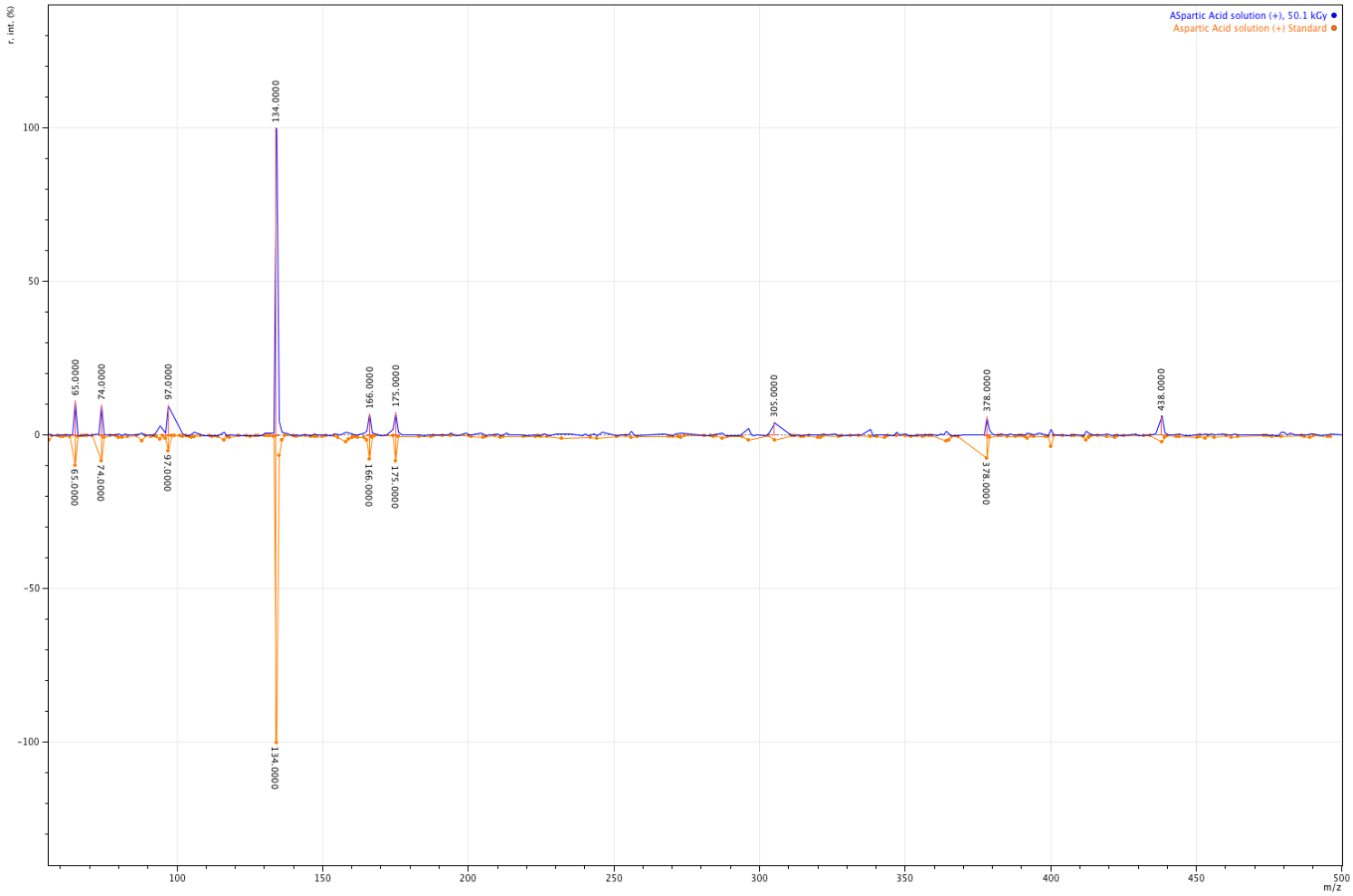

Figure A.49. ESI-MS spectrum of aspartic acid in aqueous solution for control and irradiated 50kGy samples:positive mode

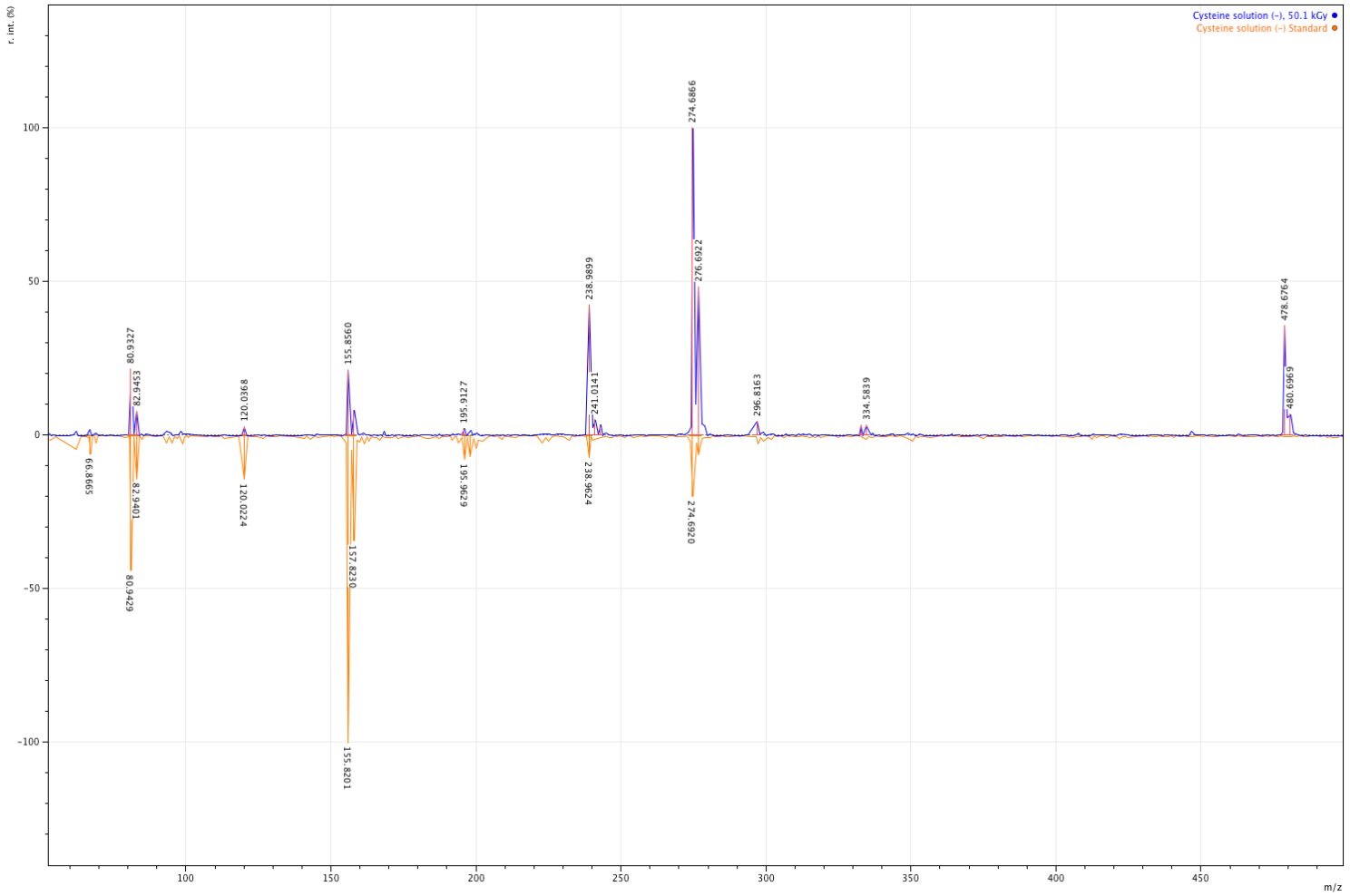

Figure A.50. ESI-MS spectrum of cysteine in aqueous solution for control and irradiated 50kGy samples: negative mode

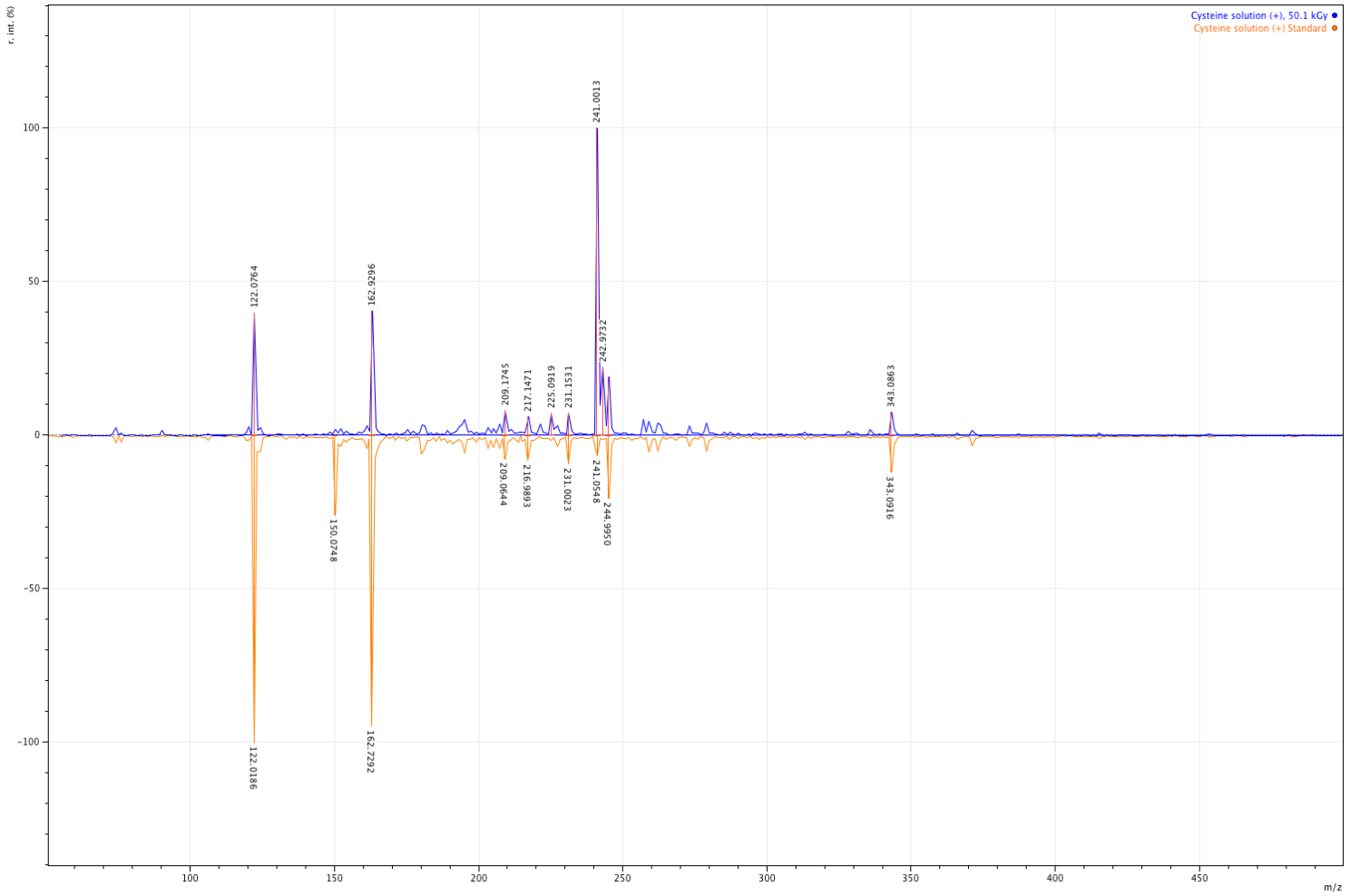

Figure A.51. ESI-MS spectrum of cysteine in aqueous solution for control and irradiated 50kGy samples: positive mode

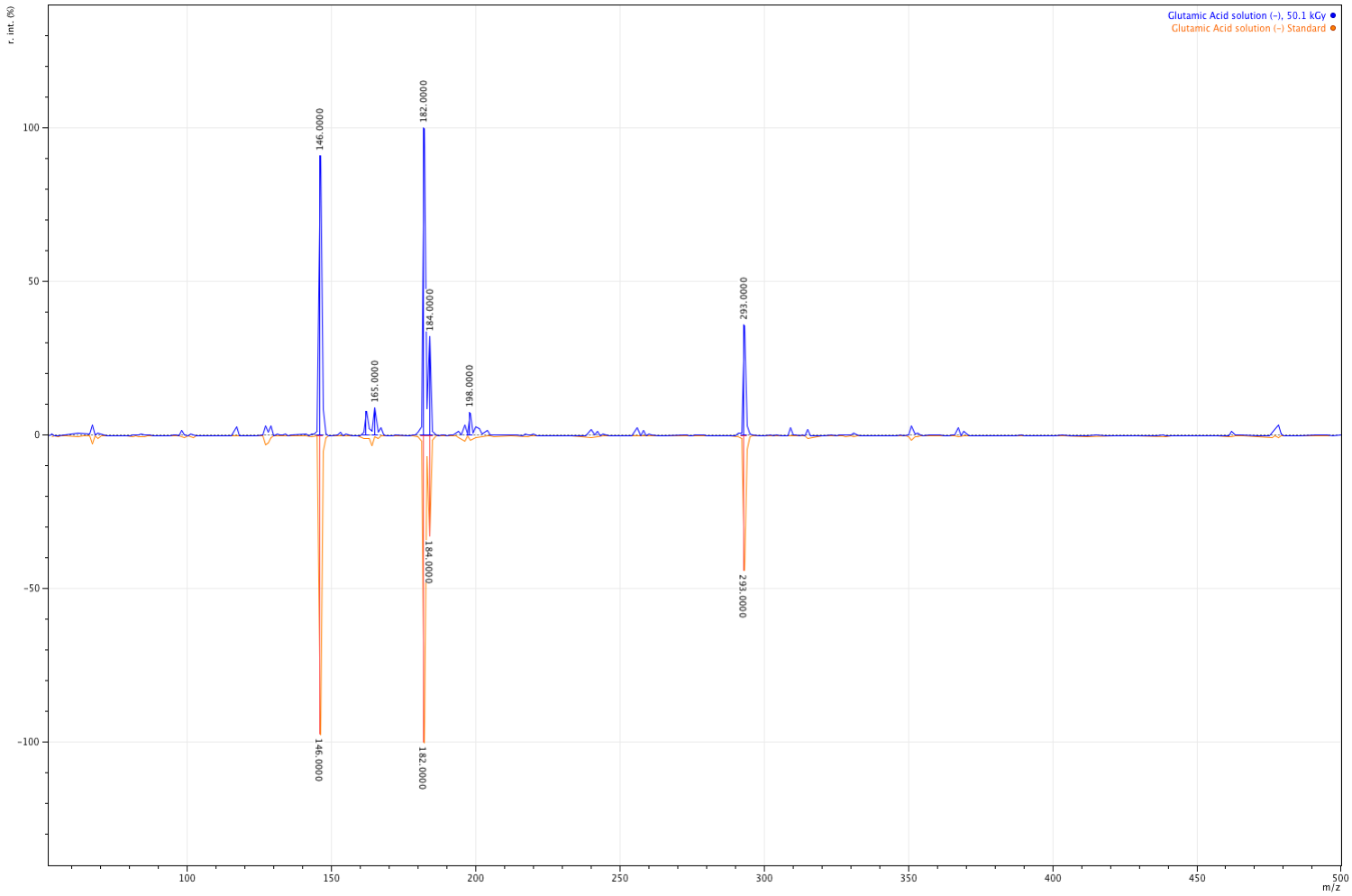

Figure A.52. ESI-MS spectrum of glutamic acid in aqueous solution for control and irradiated 50kGy samples: negative mode

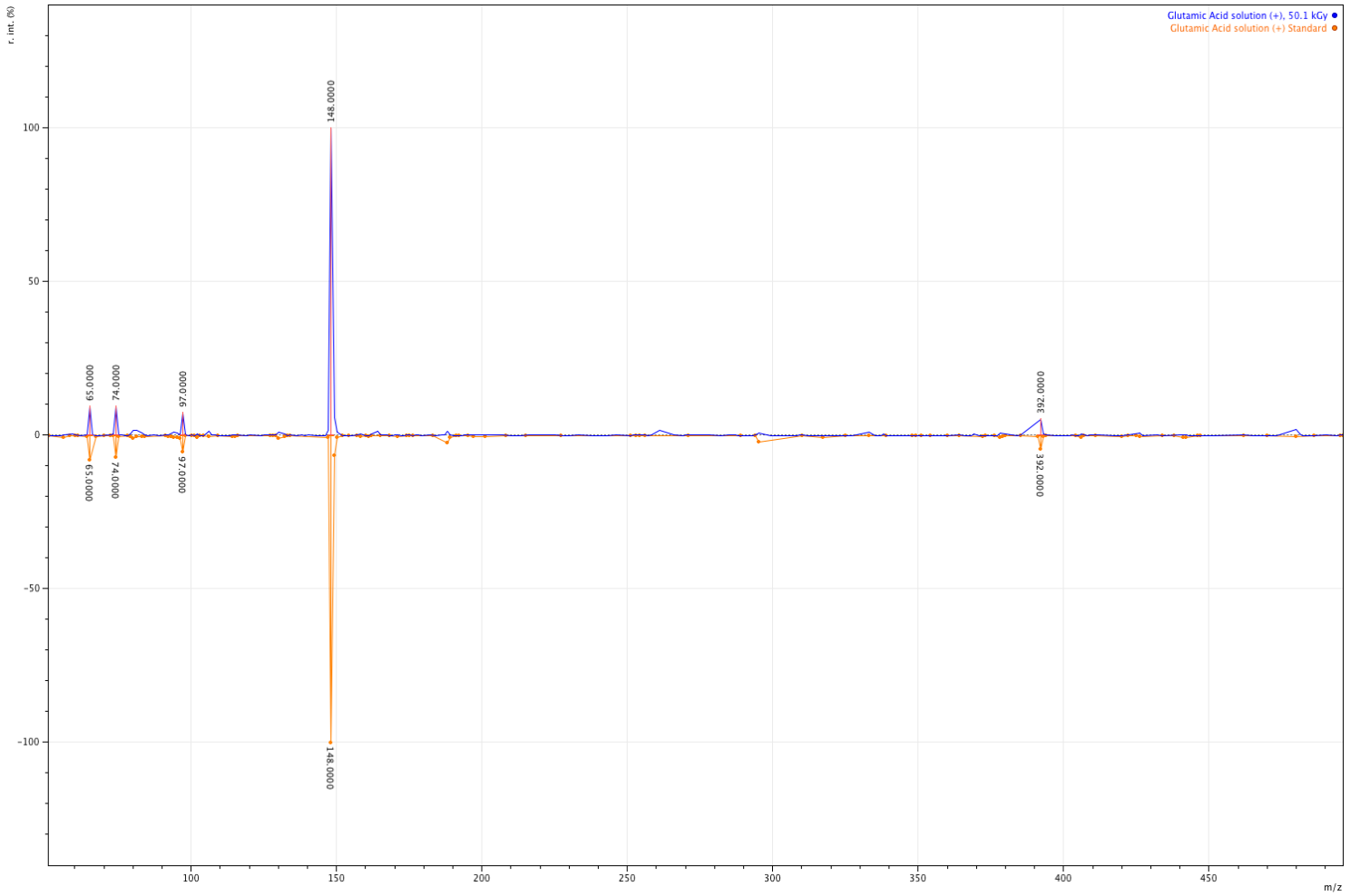

Figure A.53. ESI-MS spectrum of glutamic acid in aqueous solution for control and irradiated 50kGy samples: positive mode

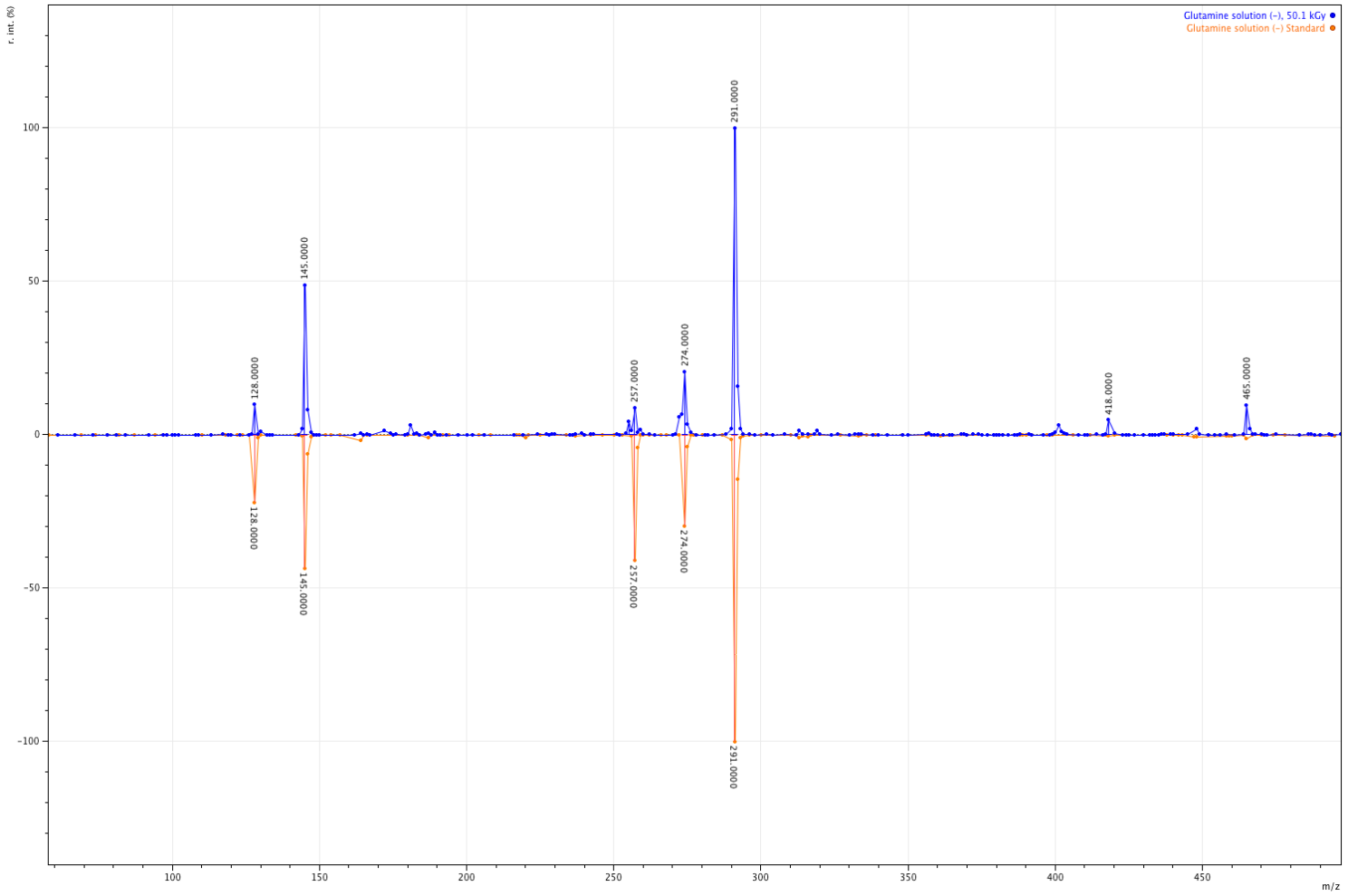

Figure A.54. ESI-MS spectrum of glutamine in aqueous solution for control and irradiated 50kGy samples: negative mode

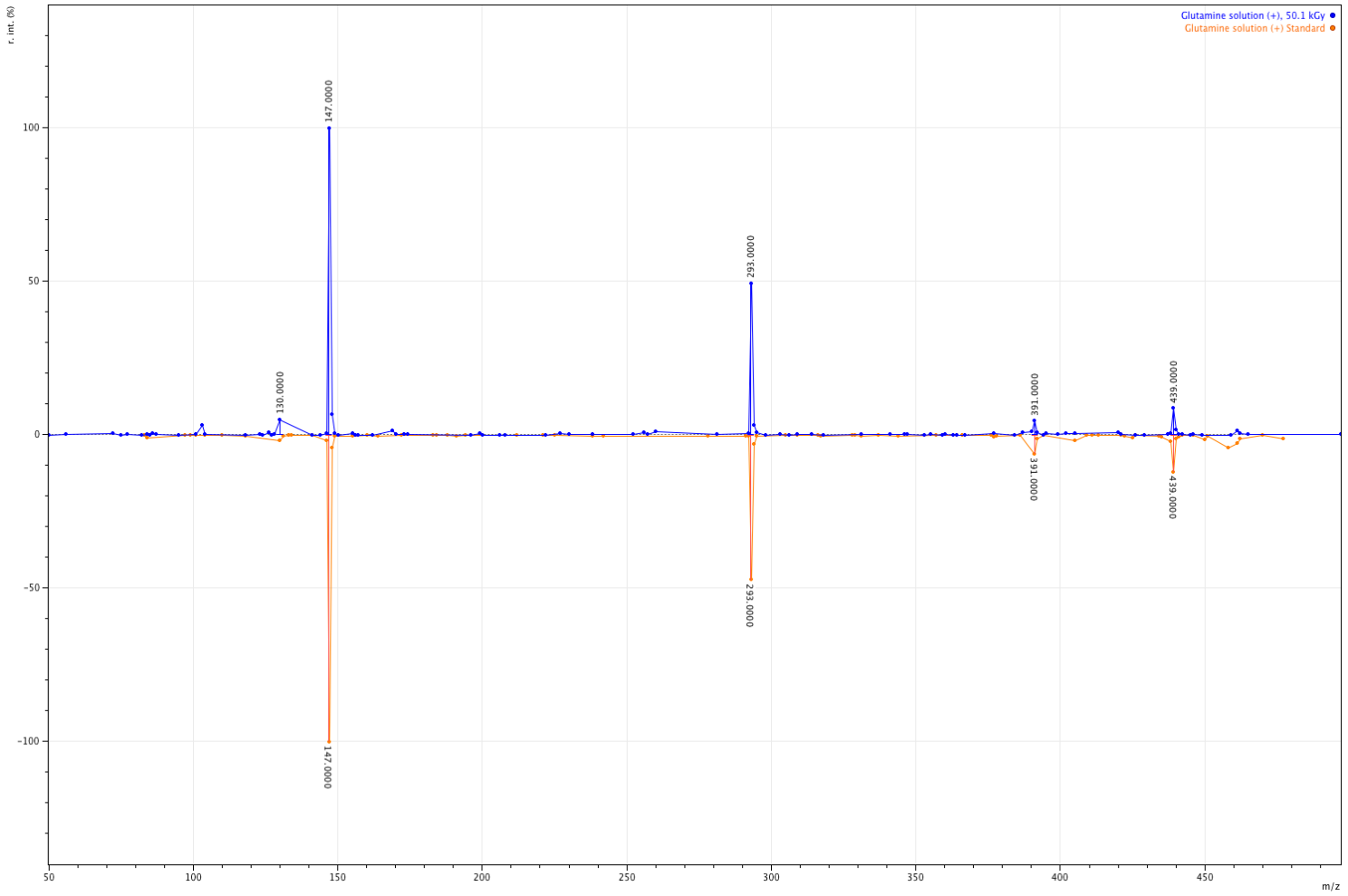

Figure A.55. ESI-MS spectrum of glutamine in aqueous solution for control and irradiated 50kGy samples: positive mode

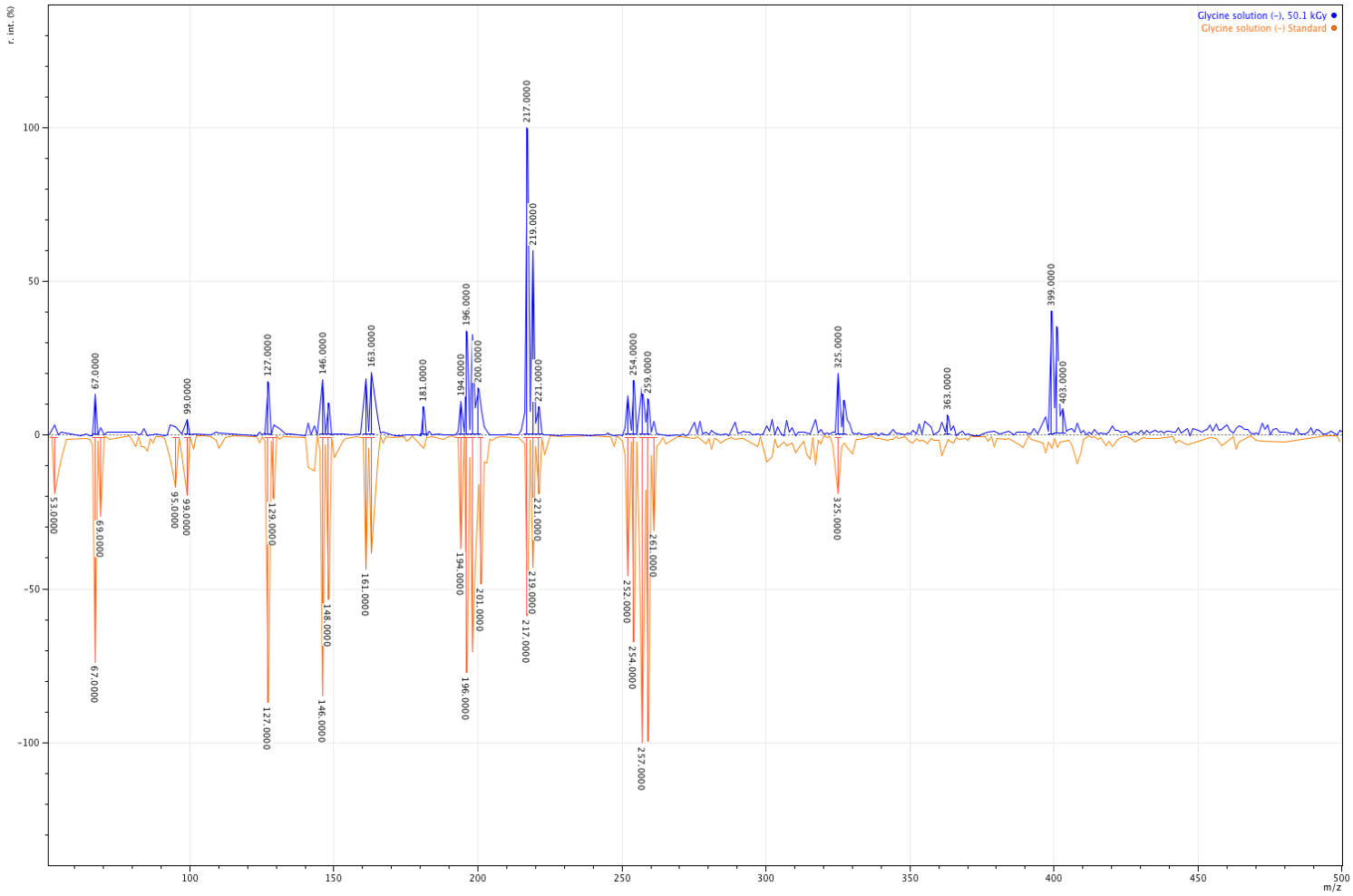

Figure A.56. ESI-MS spectrum of glycine in aqueous solution for control and irradiated 50kGy samples: negative mode

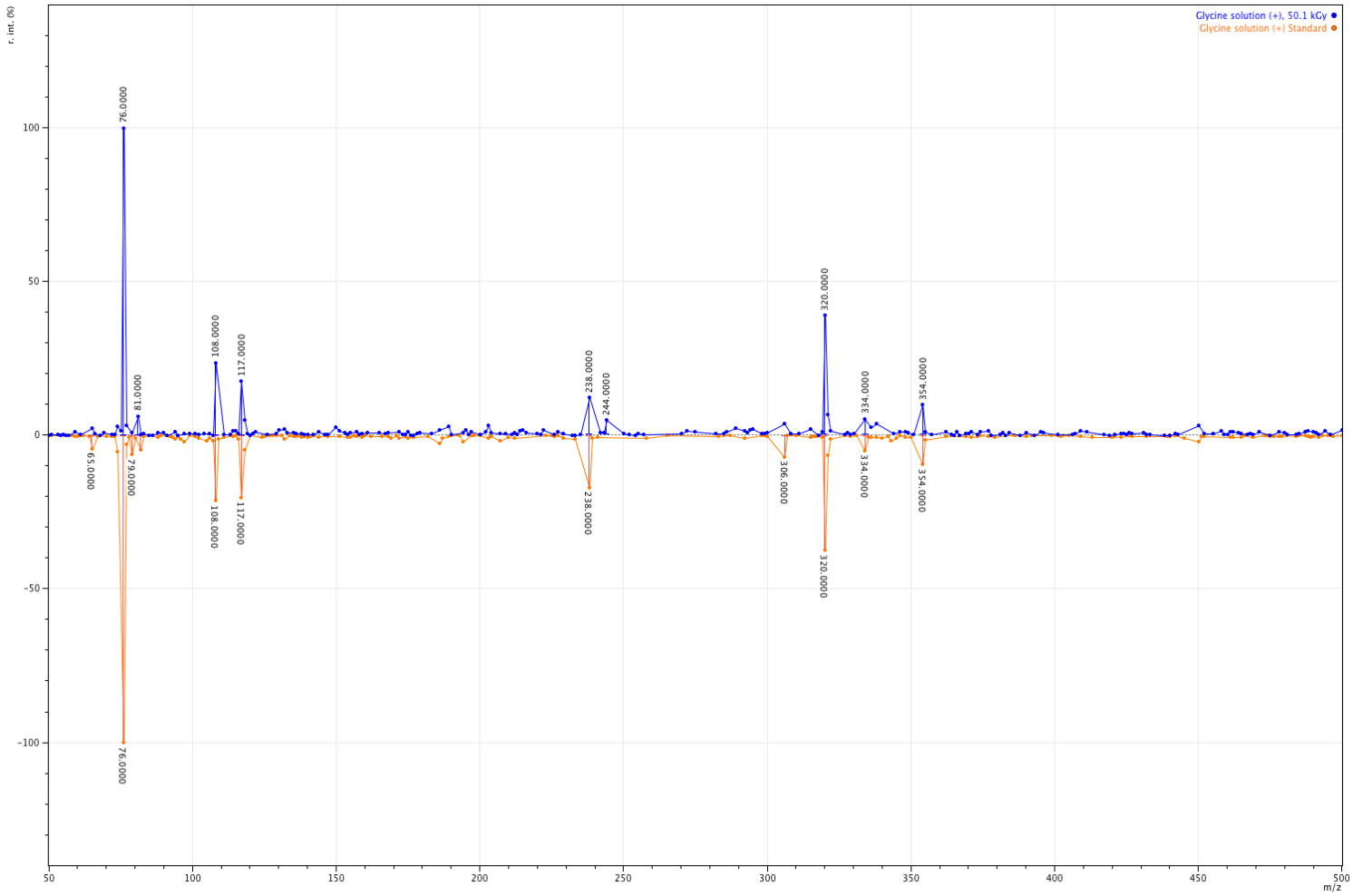

Figure A.57. ESI-MS spectrum of glycine in aqueous solution for control and irradiated 50kGy samples: positive mode

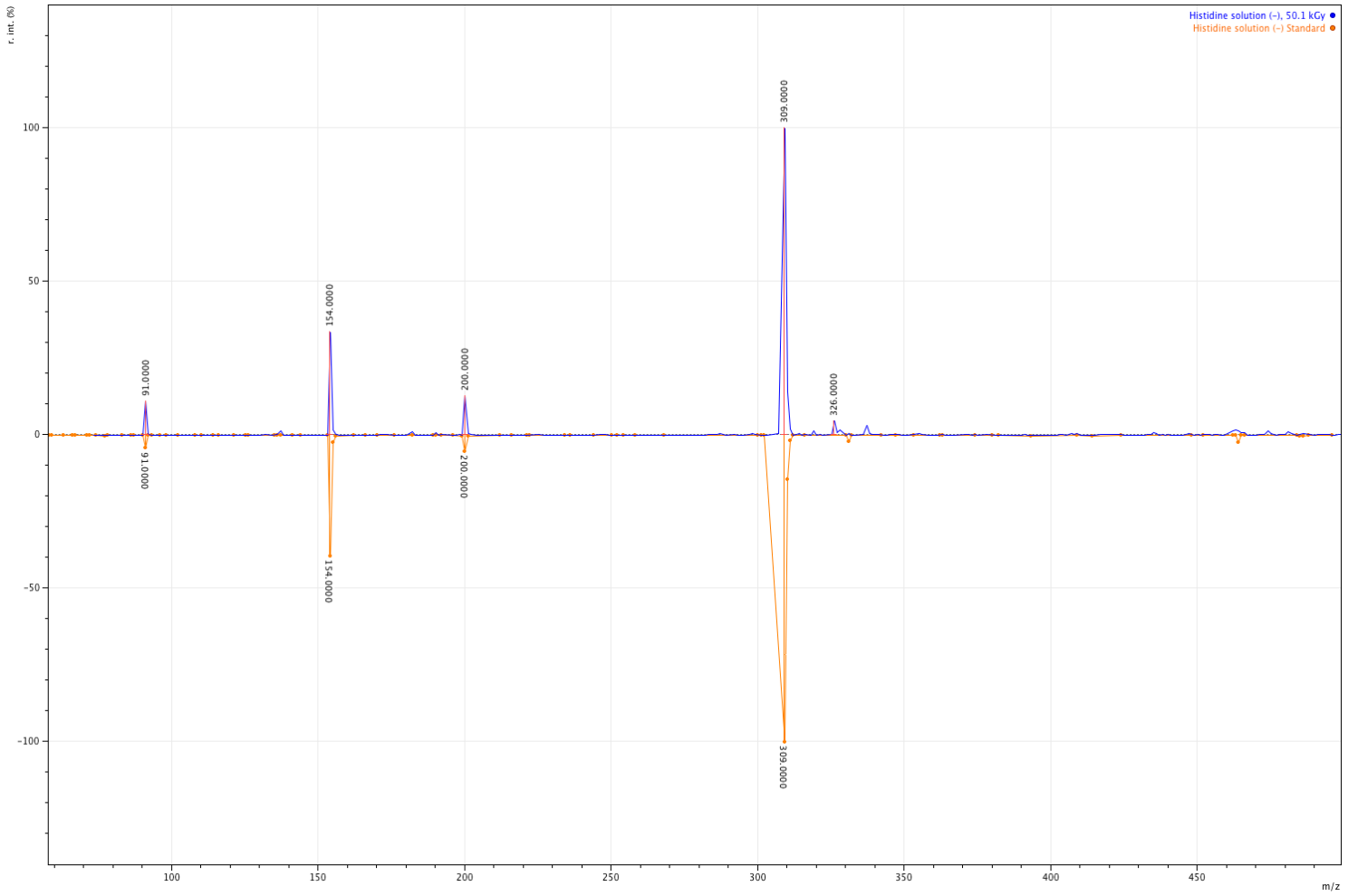

Figure A.58. ESI-MS spectrum of histidine in aqueous solution for control and irradiated 50kGy samples: negative mode

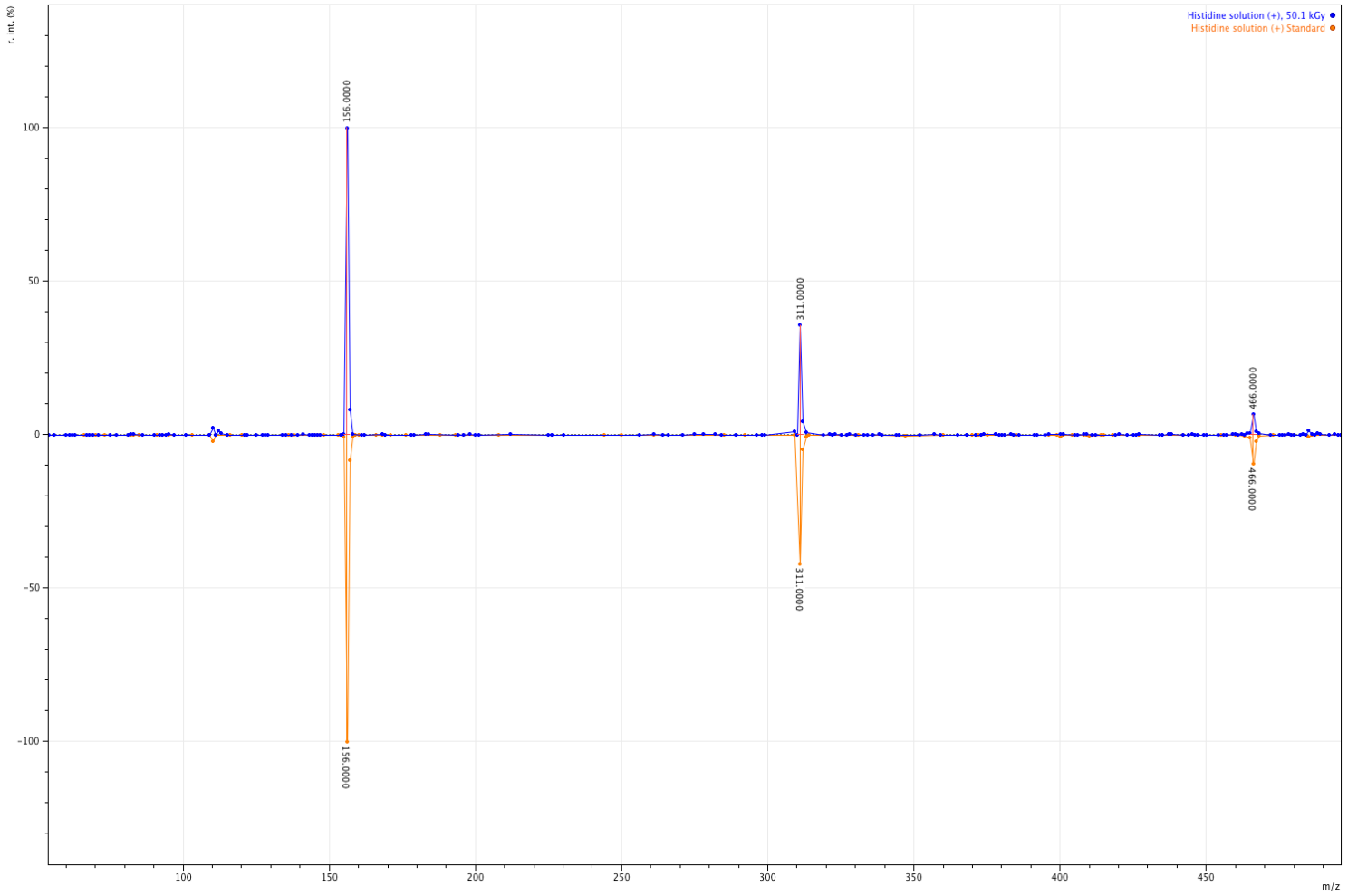

Figure A.59. ESI-MS spectrum of histidine in aqueous solution for control and irradiated 50kGy samples: positive mode

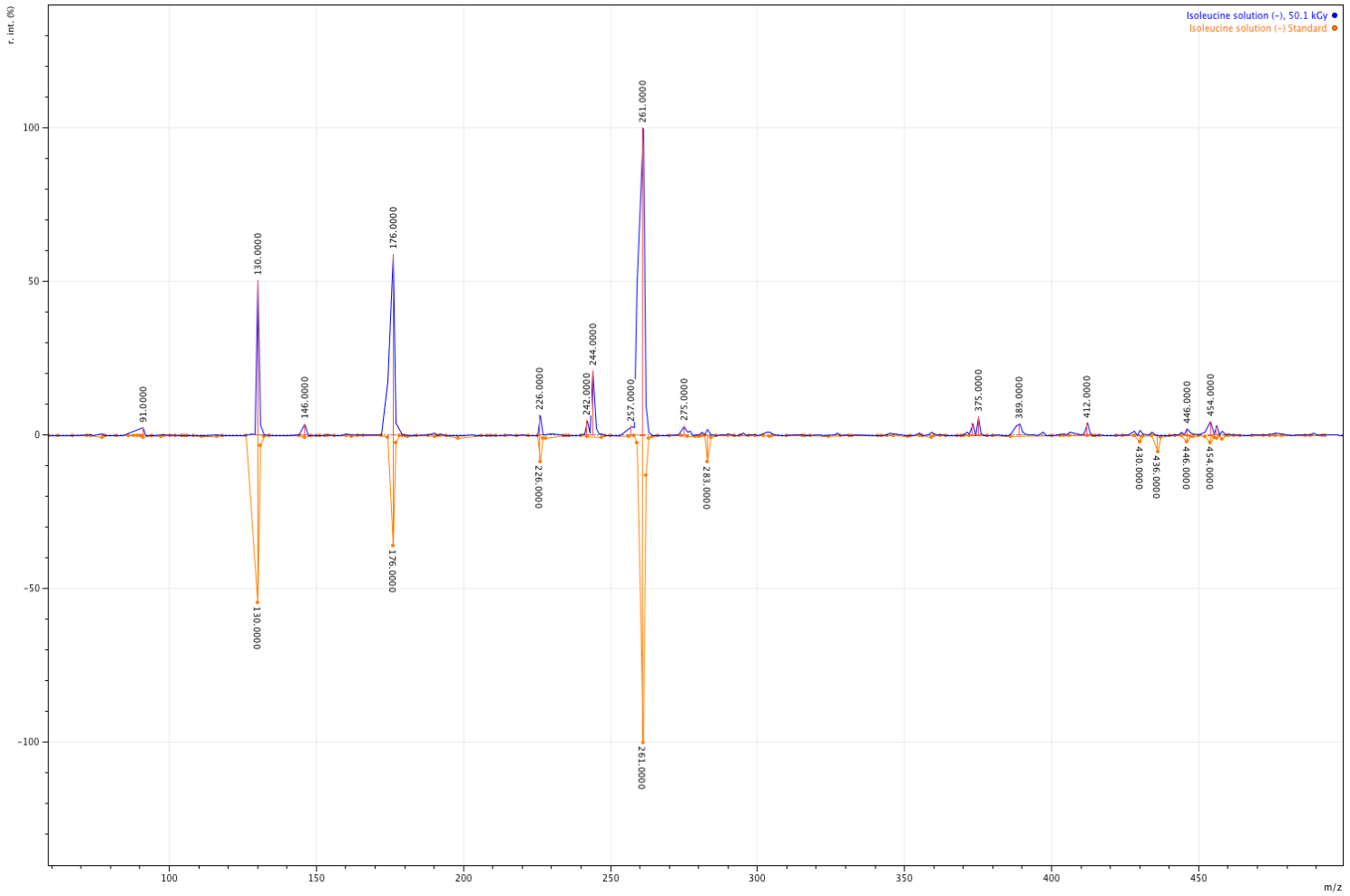

Figure A.60. ESI-MS spectrum of isoleucine in aqueous solution for control and irradiated 50kGy samples: negative mode

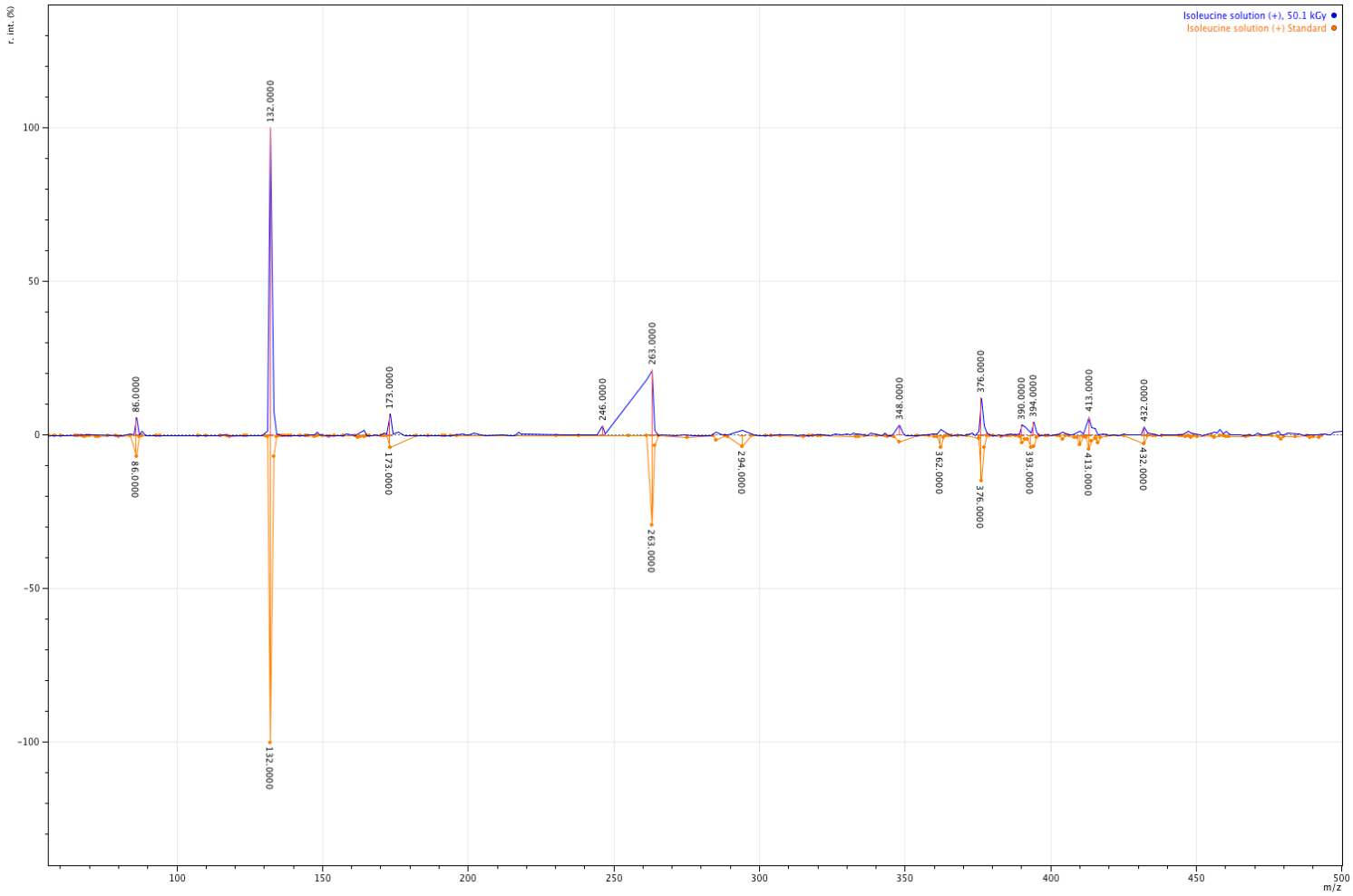

Figure A.61. ESI-MS spectrum of isoleucine in aqueous solution for control and irradiated 50kGy samples:positive mode

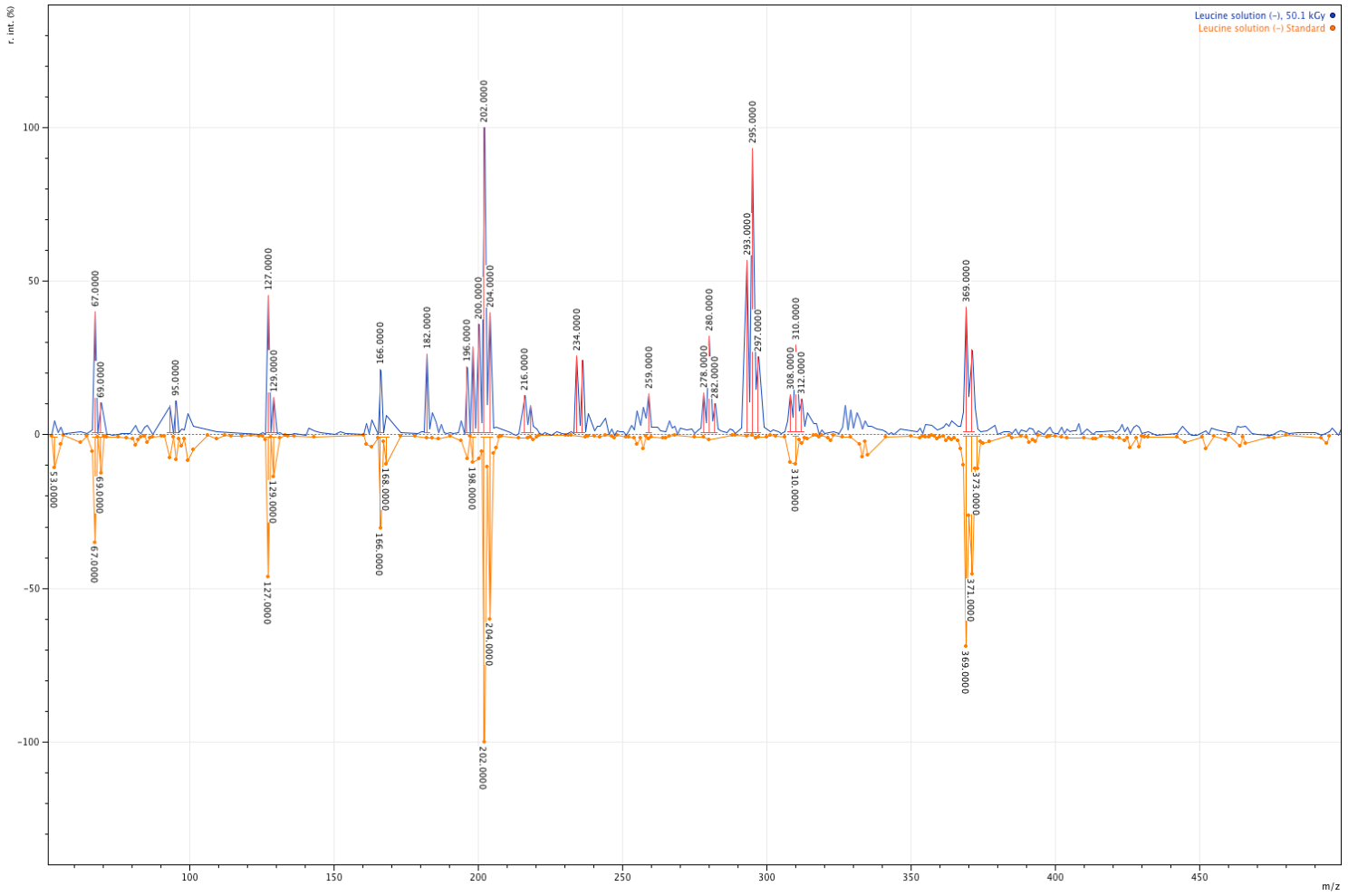

Figure A.62. ESI-MS spectrum of leucine in aqueous solution for control and irradiated 50kGy samples: negative mode

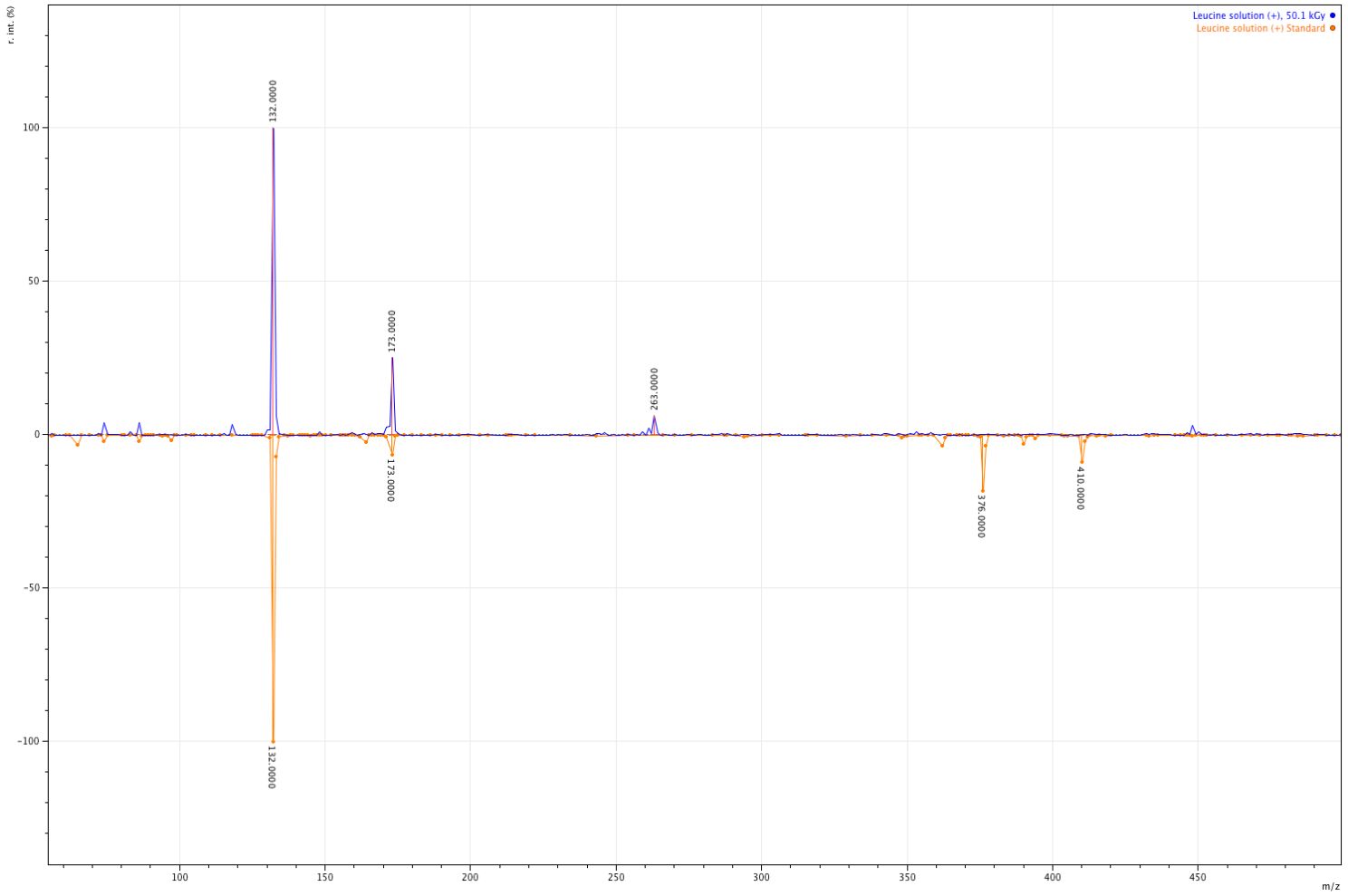

Figure A.63. ESI-MS spectrum of leucine in aqueous solution for control and irradiated 50kGy samples: positive mode

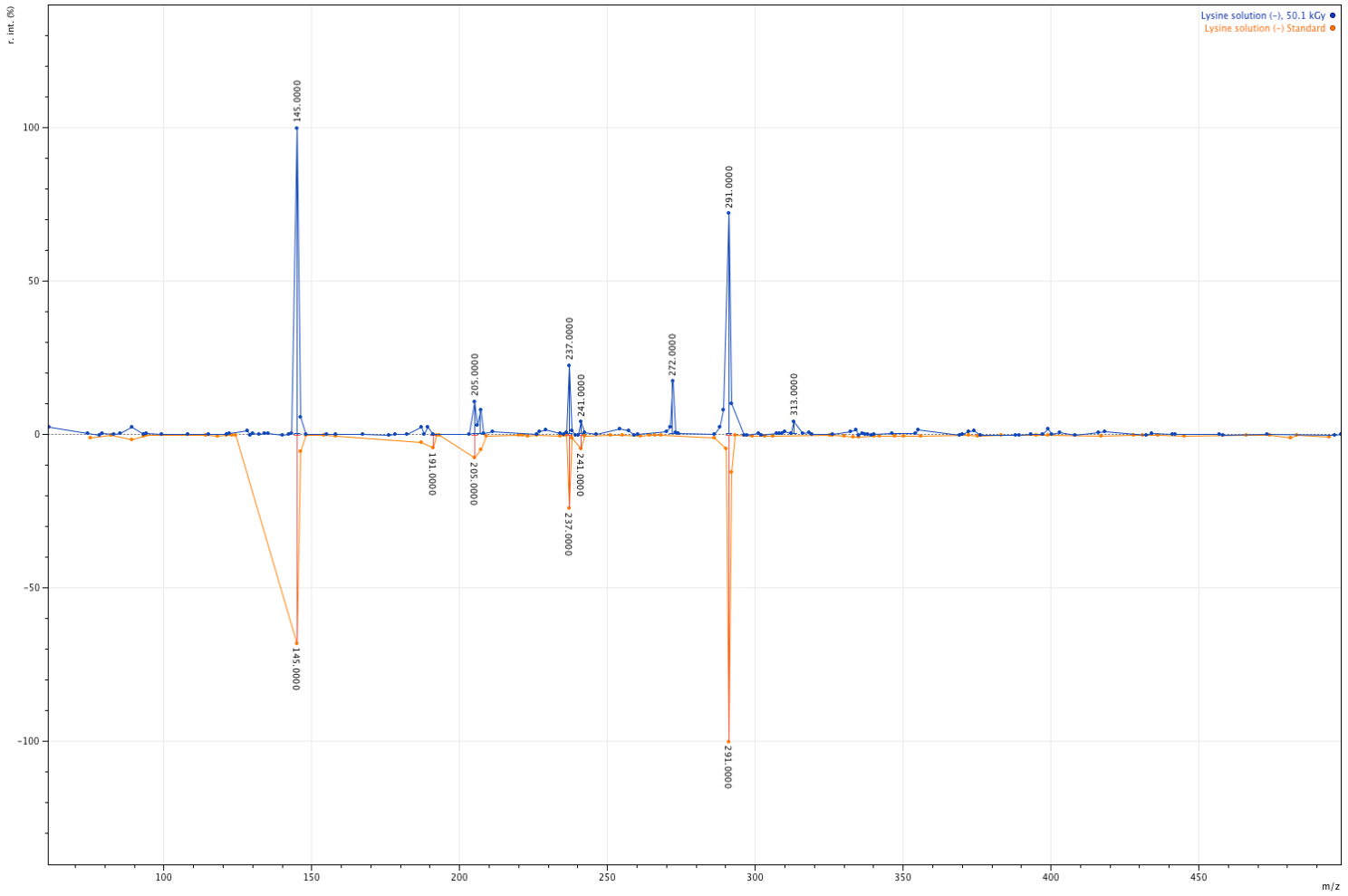

Figure A.64. ESI-MS spectrum of lysine in aqueous solution for control and irradiated 50kGy samples: negative mode

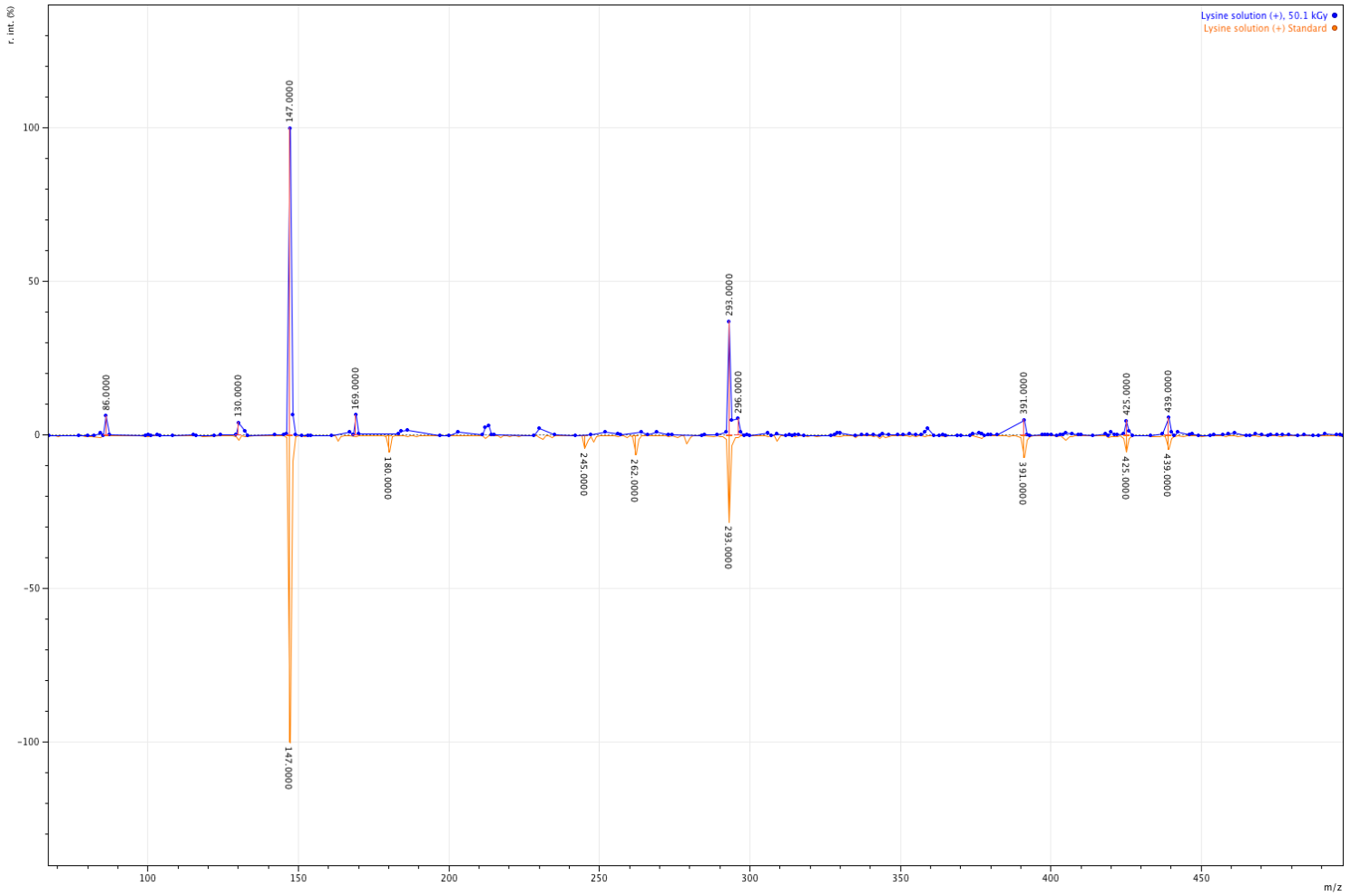

Figure A.65. ESI-MS spectrum of lysine in aqueous solution for control and irradiated 50kGy samples: positive mode

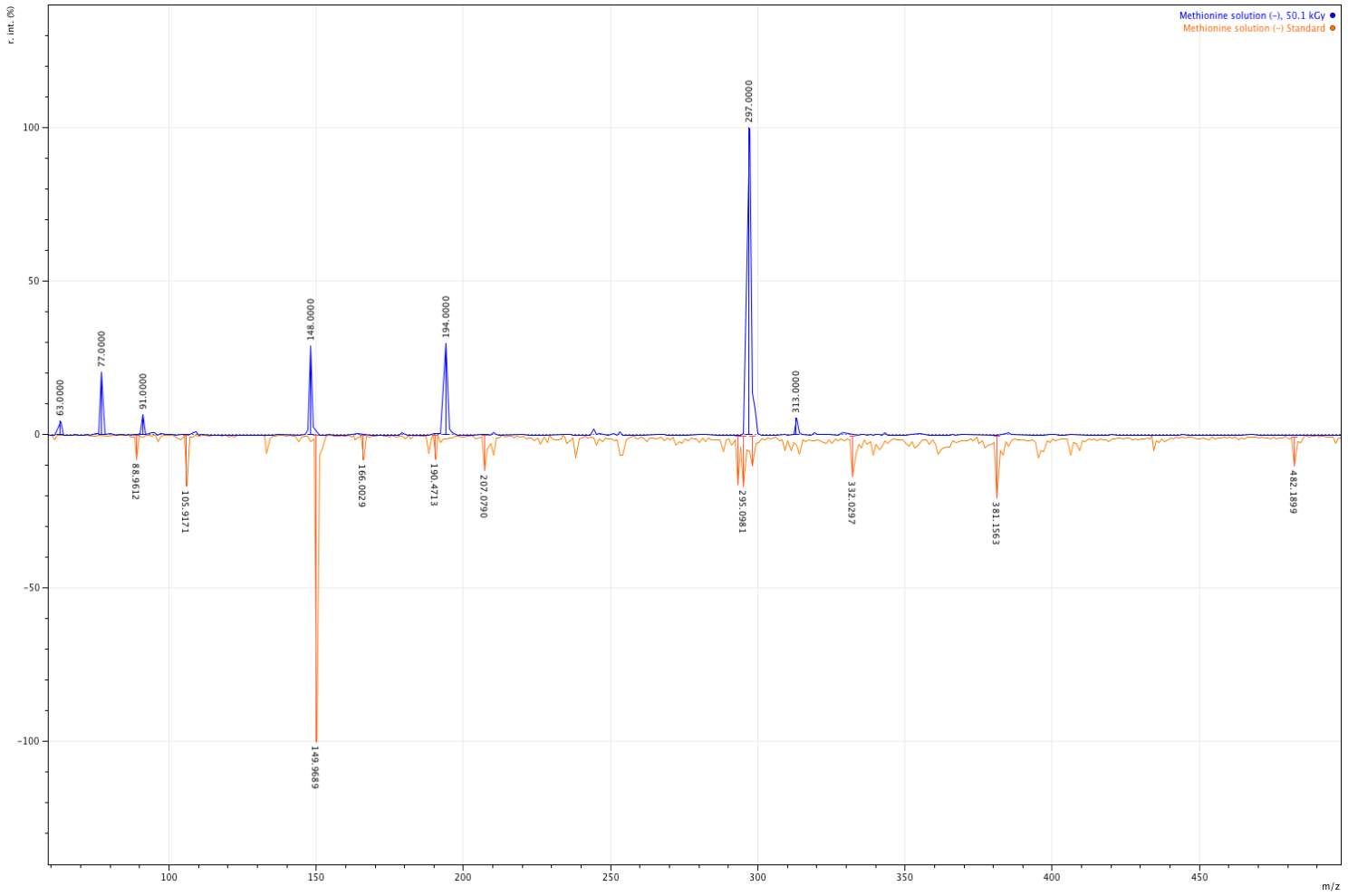

Figure A.66. ESI-MS spectrum of methionine in aqueous solution for control and irradiated 50kGy samples: negative mode

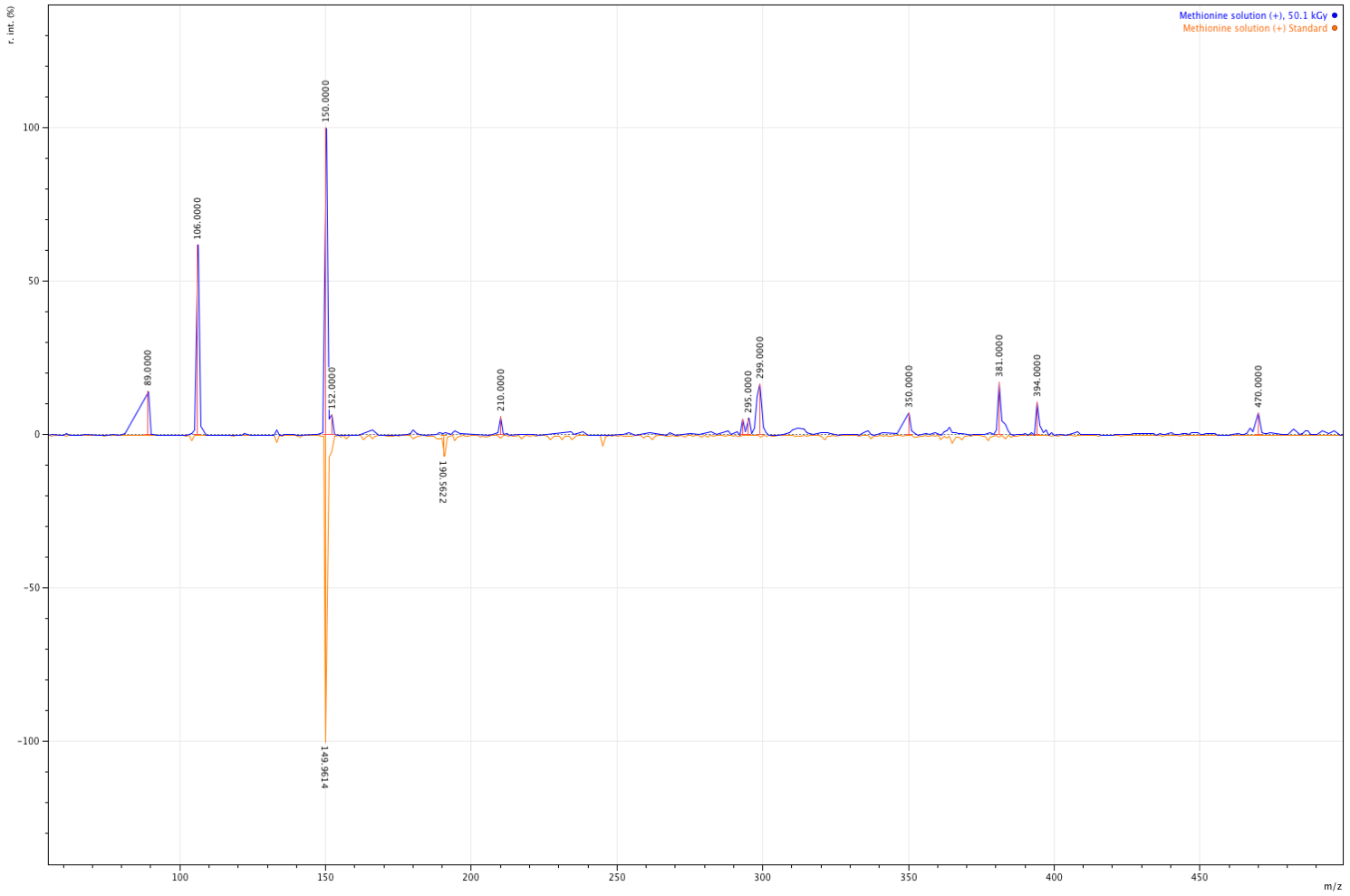

Figure A.67. ESI-MS spectrum of methionine in aqueous solution for control and irradiated 50kGy samples: positive mode

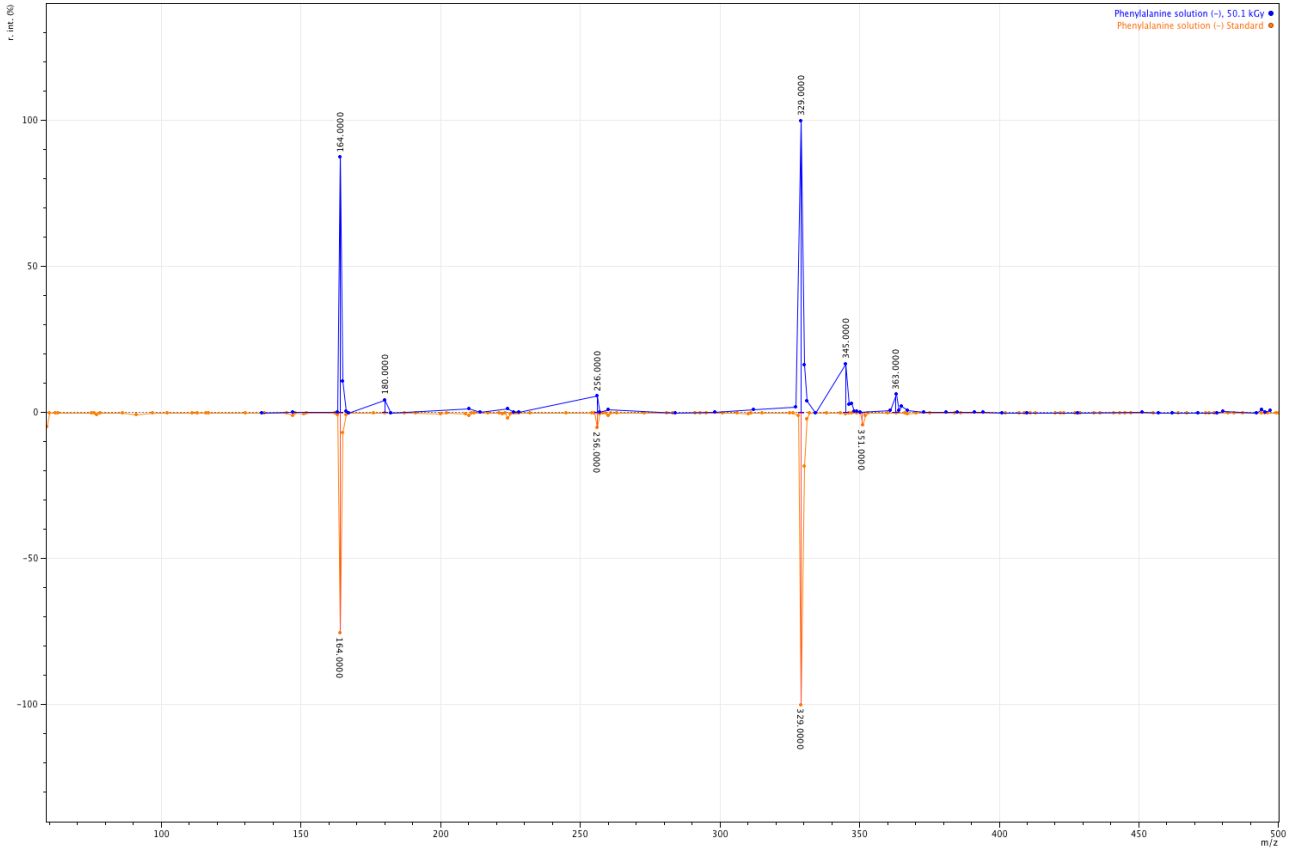

Figure A.68. ESI-MS spectrum of phenylalanine in aqueous solution for control and irradiated 50kGy samples: negative mode

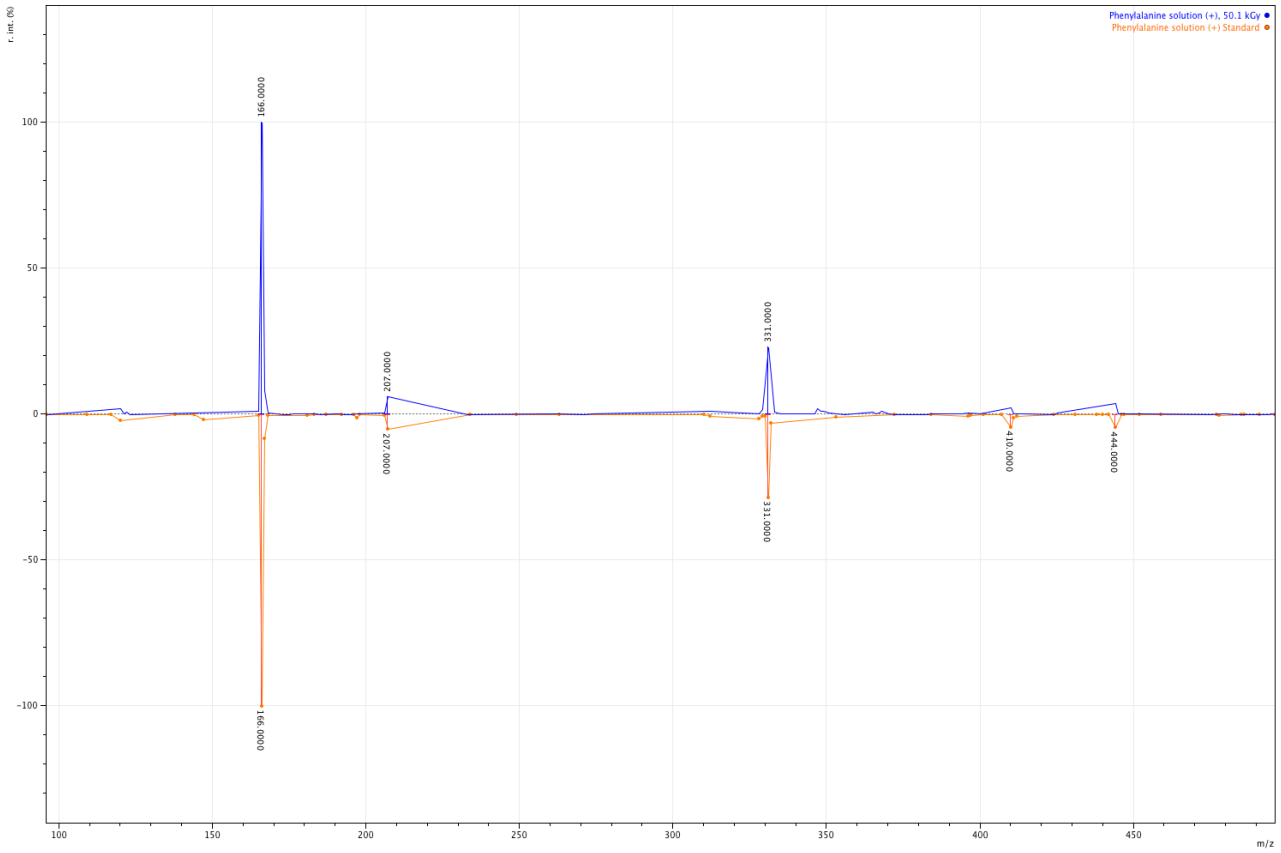

Figure A.69. ESI-MS spectrum of phenylalanine in aqueous solution for control and irradiated 50kGy samples: positive mode

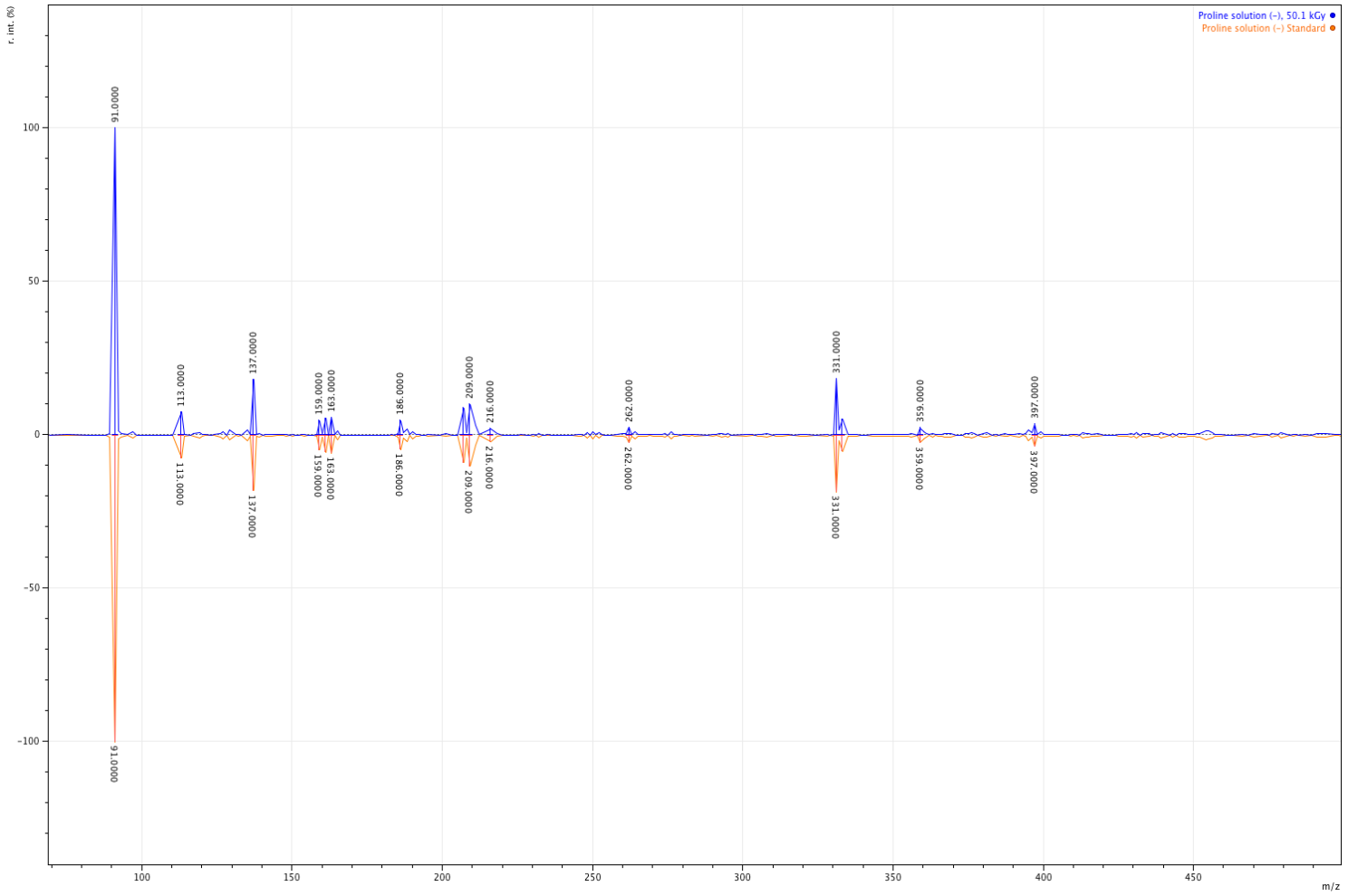

Figure A.70. ESI-MS spectrum of proline in aqueous solution for control and irradiated 50kGy samples: negative mode

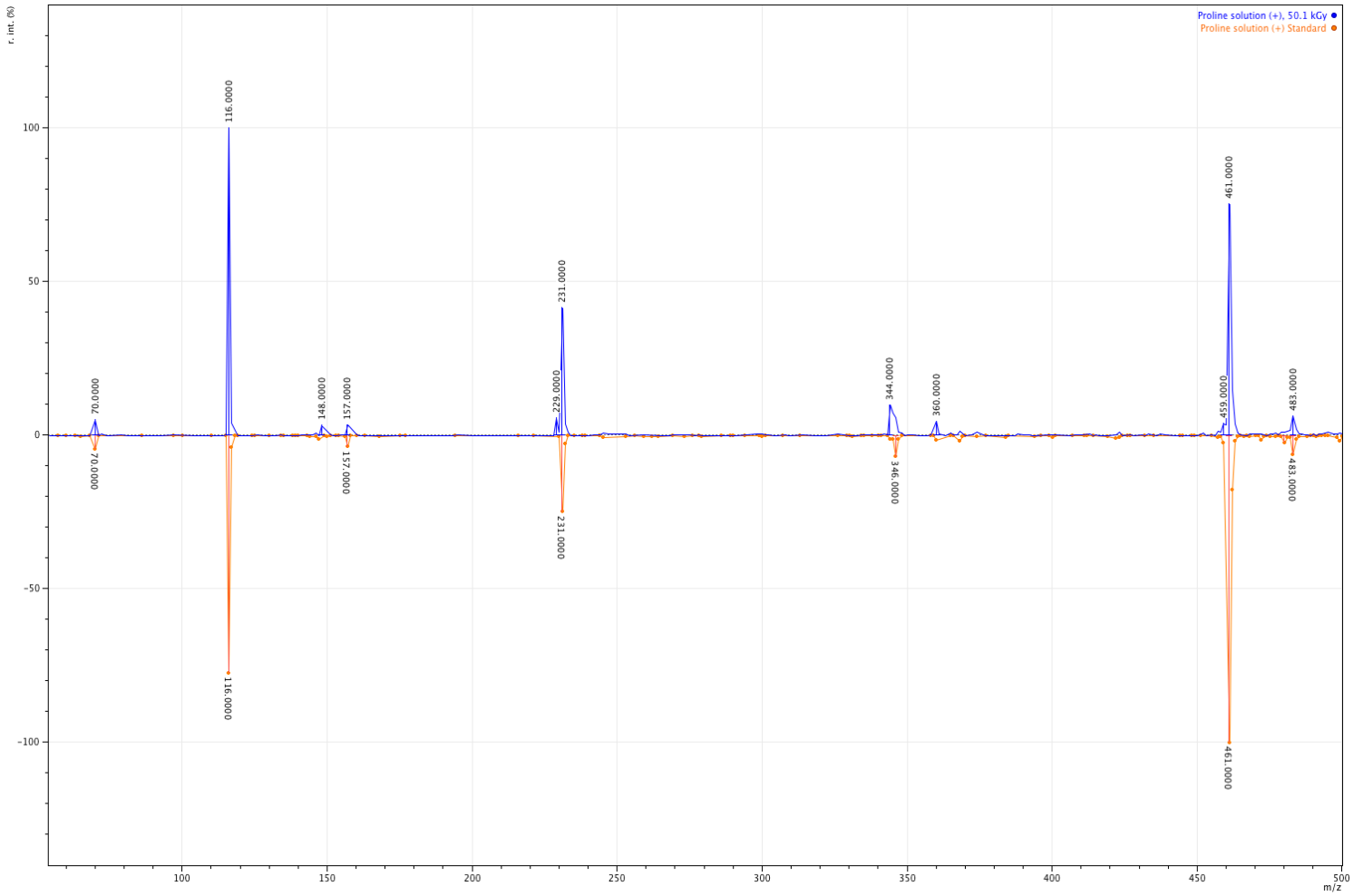

Figure A.71. ESI-MS spectrum of proline in aqueous solution for control and irradiated 50kGy samples: positive mode

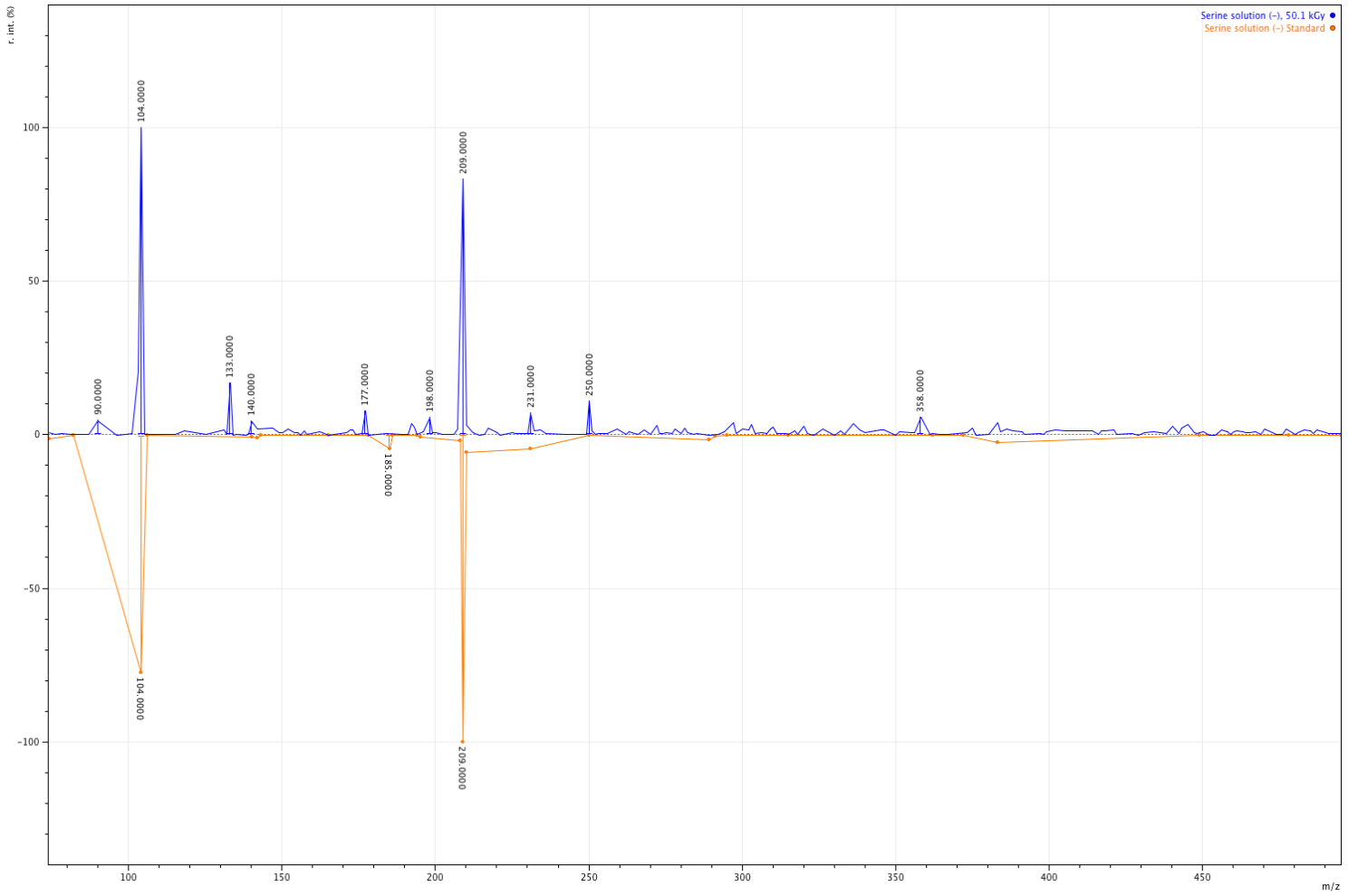

Figure A.72. ESI-MS spectrum of serine in aqueous solution for control and irradiated 50kGy samples: negative mode

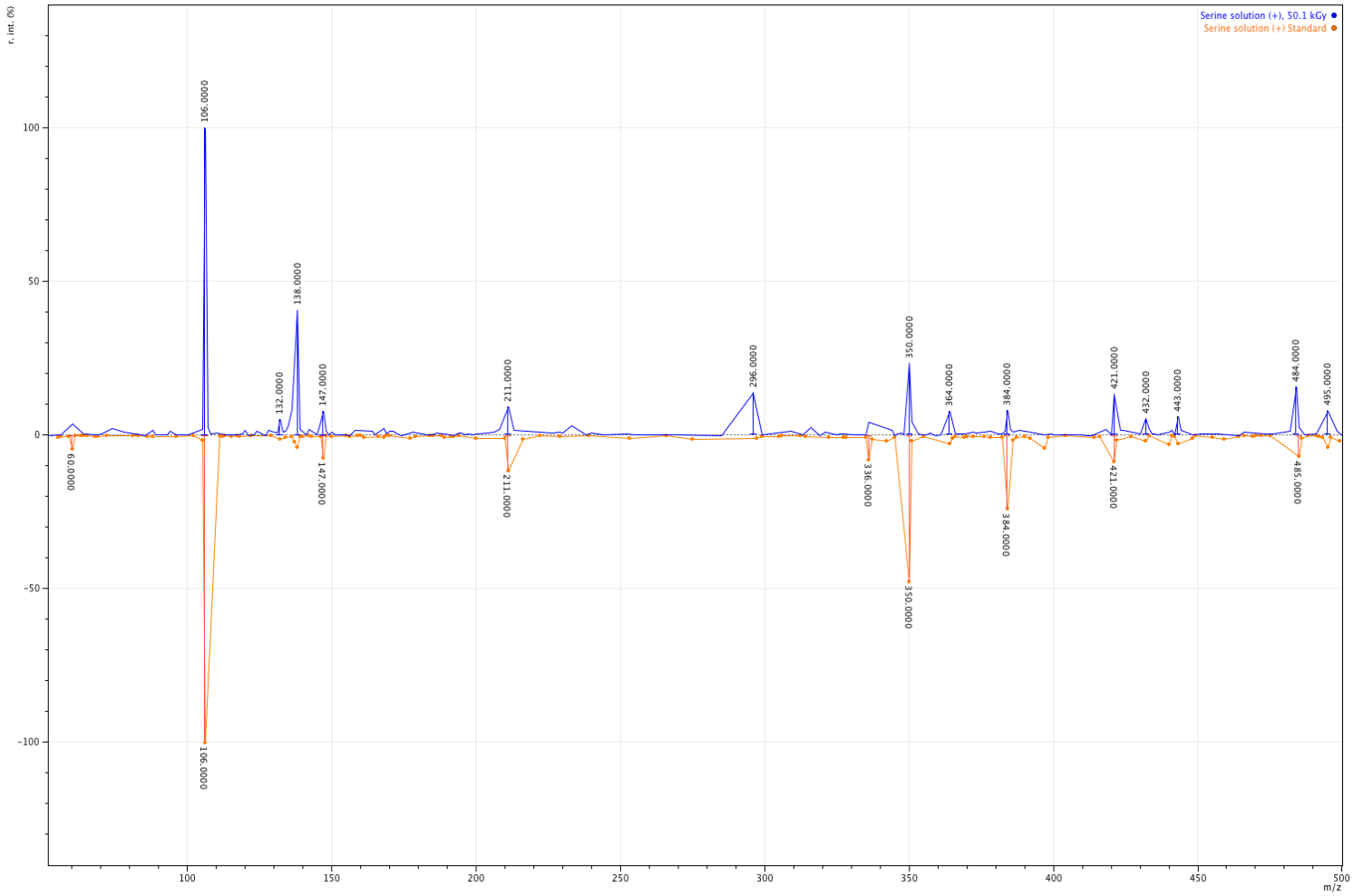

Figure A.73. ESI-MS spectrum of serine in aqueous solution for control and irradiated 50kGy samples: positive mode

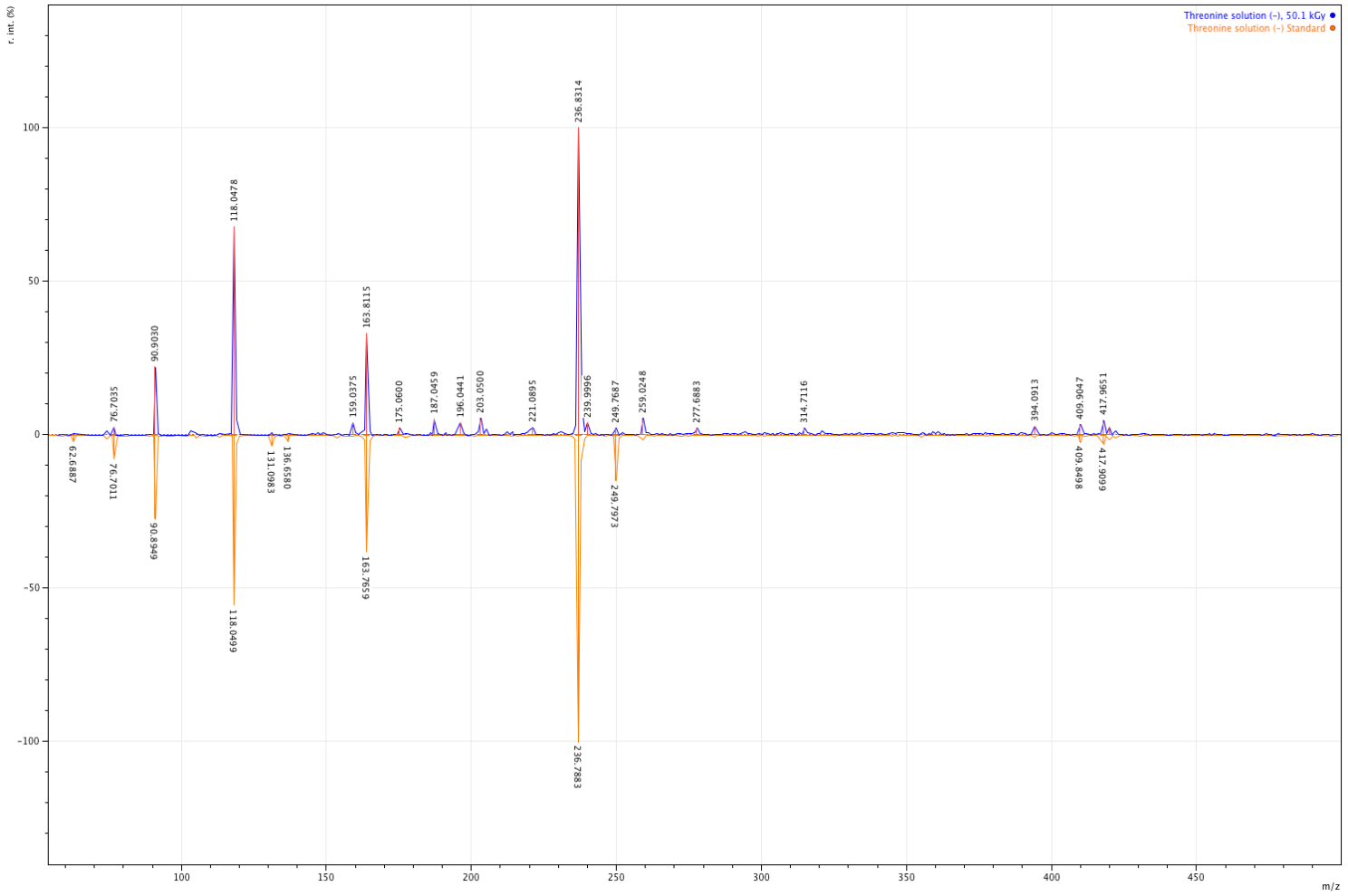

Figure A.74. ESI-MS spectrum of threonine in aqueous solution for control and irradiated 50kGy samples: negative mode

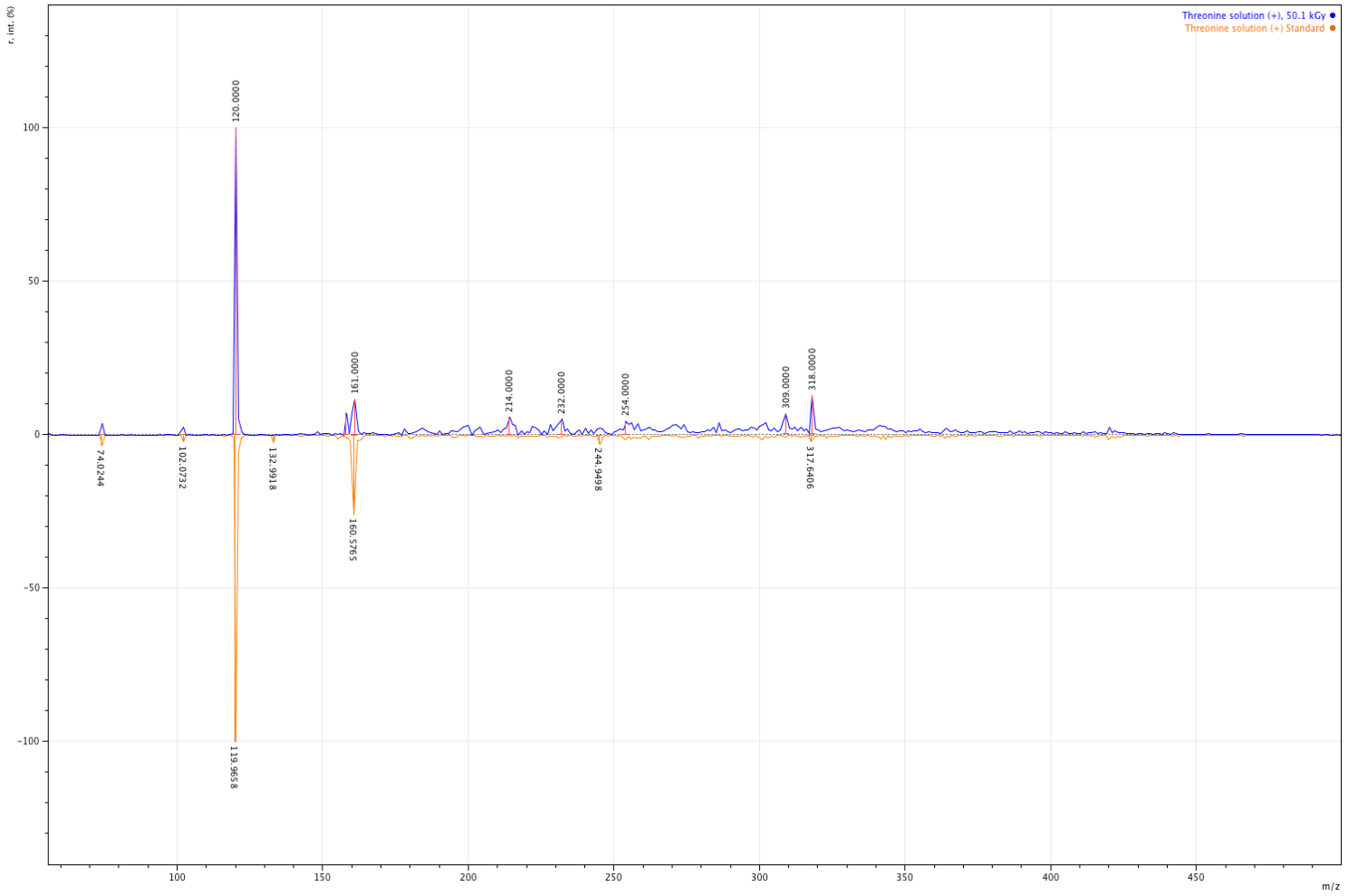

Figure A.75. ESI-MS spectrum of threonine in aqueous solution for control and irradiated 50kGy samples: positive mode

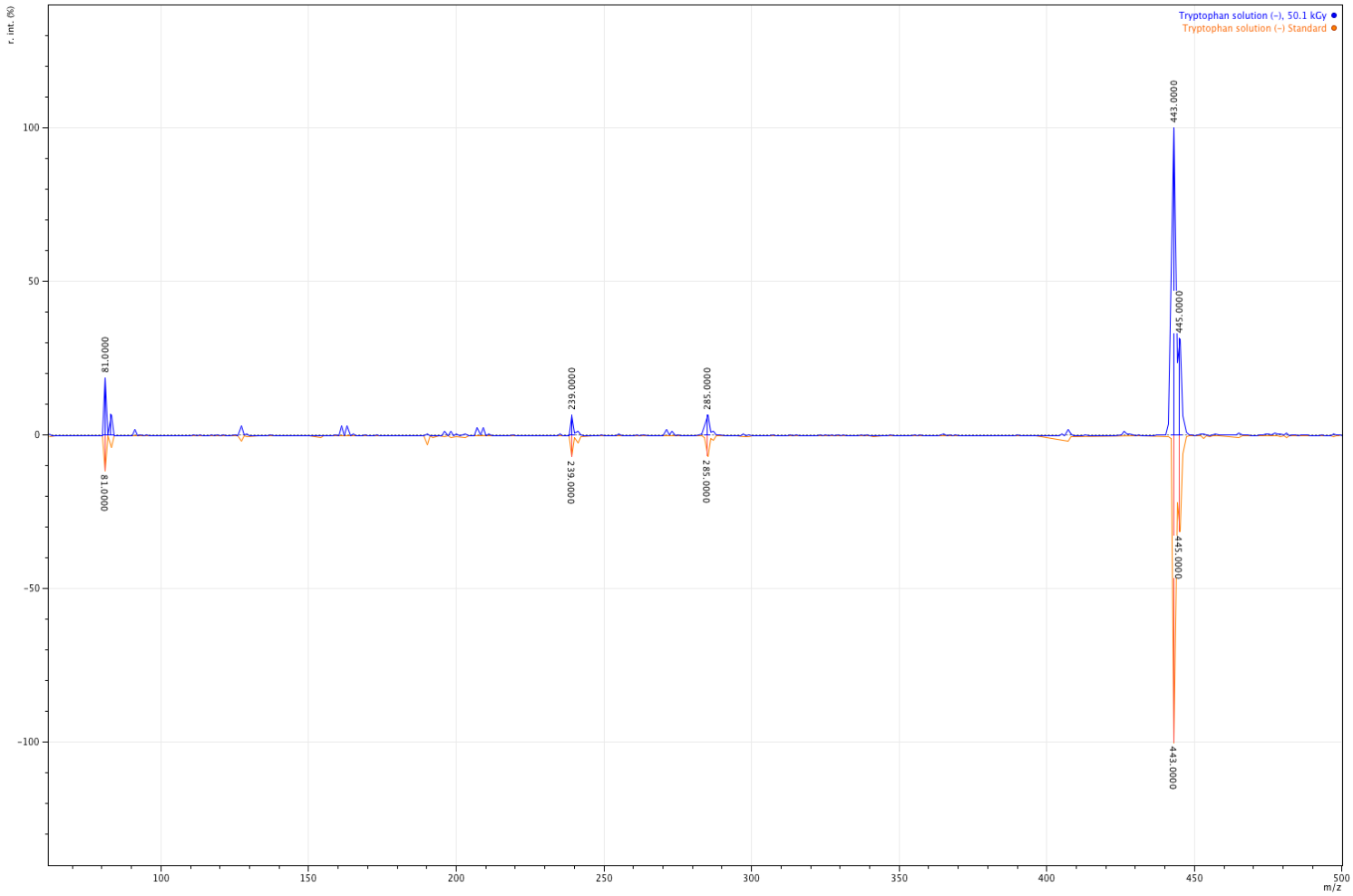

Figure A.76. ESI-MS spectrum of tryptophan in aqueous solution for control and irradiated 50kGy samples: negative mode

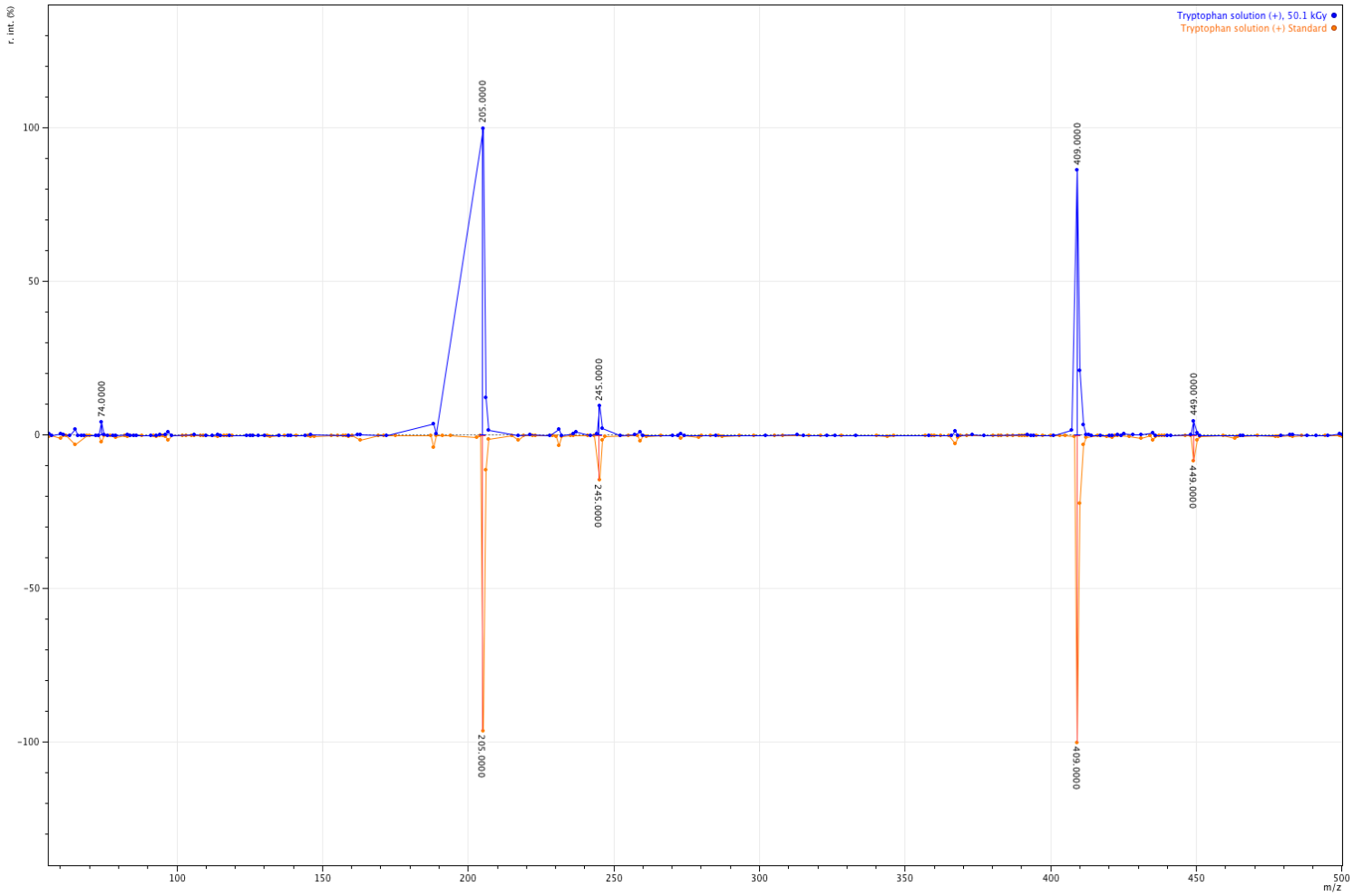

Figure A.77. ESI-MS spectrum of tryptophan in aqueous solution for control and irradiated 50kGy samples: positive mode

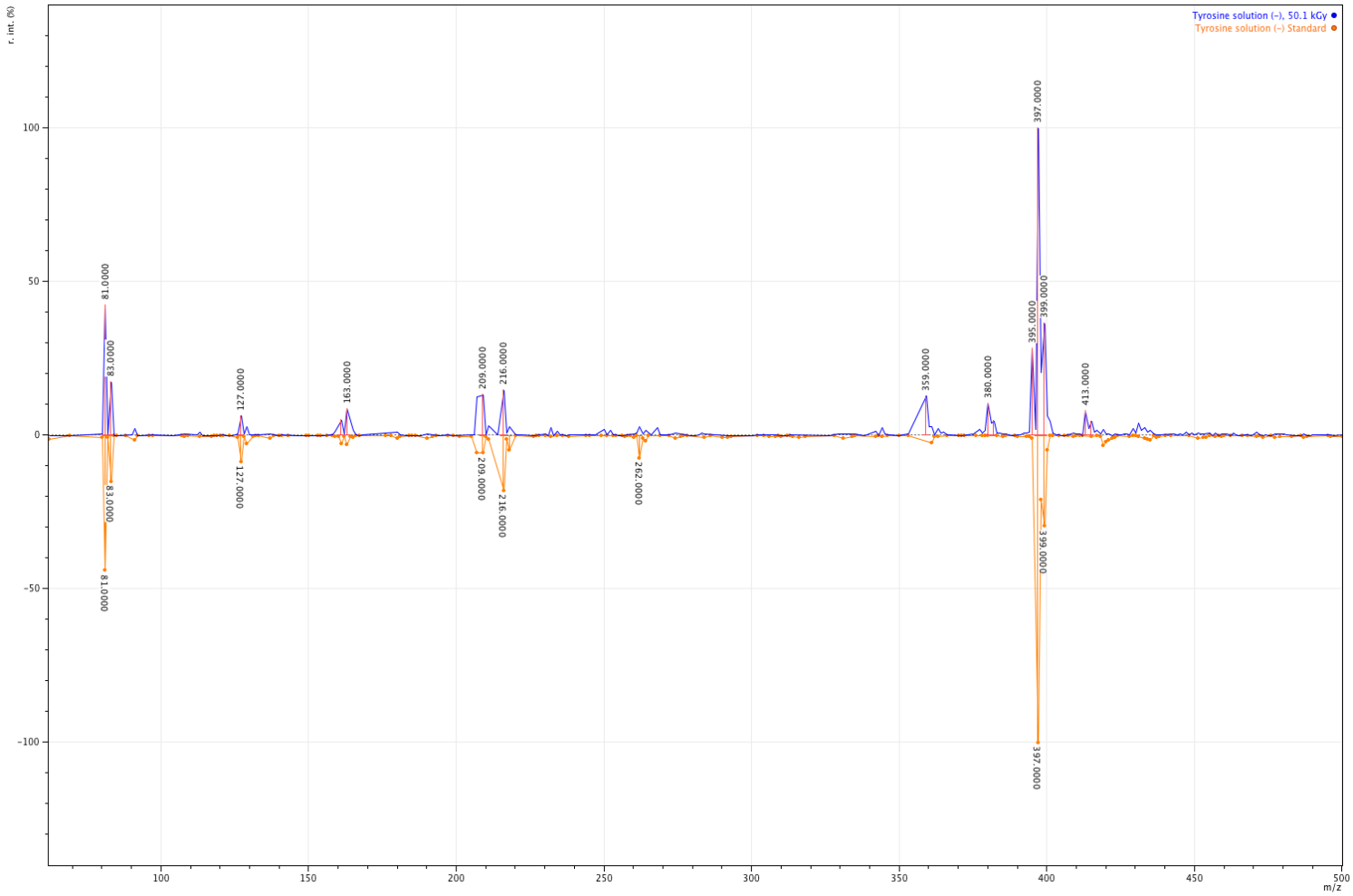

Figure A.78. ESI-MS spectrum of tyrosine in aqueous solution for control and irradiated 50kGy samples: negative mode

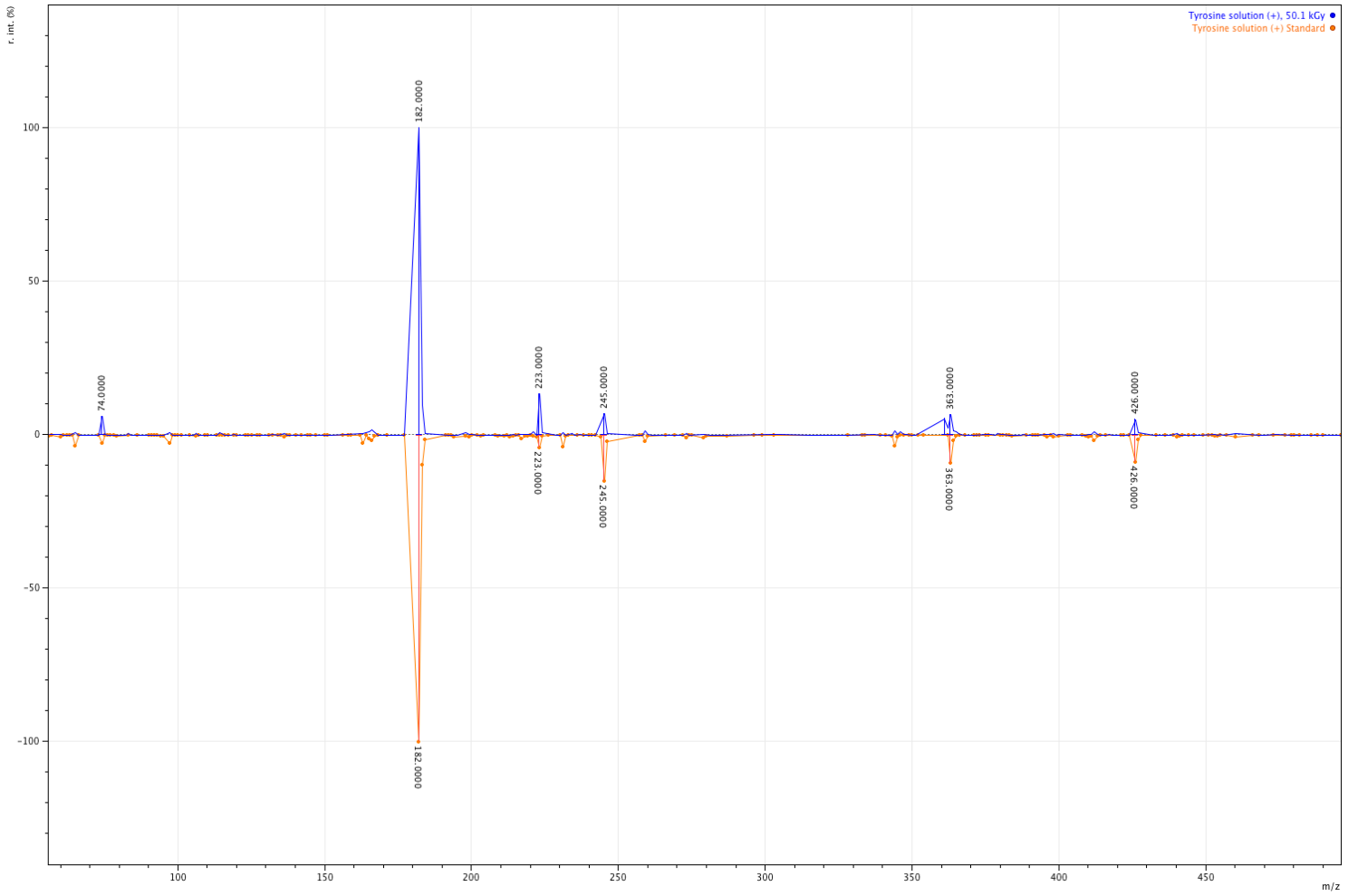

Figure A.79. ESI-MS spectrum of tyrosine in aqueous solution for control and irradiated 50kGy samples: positive mode

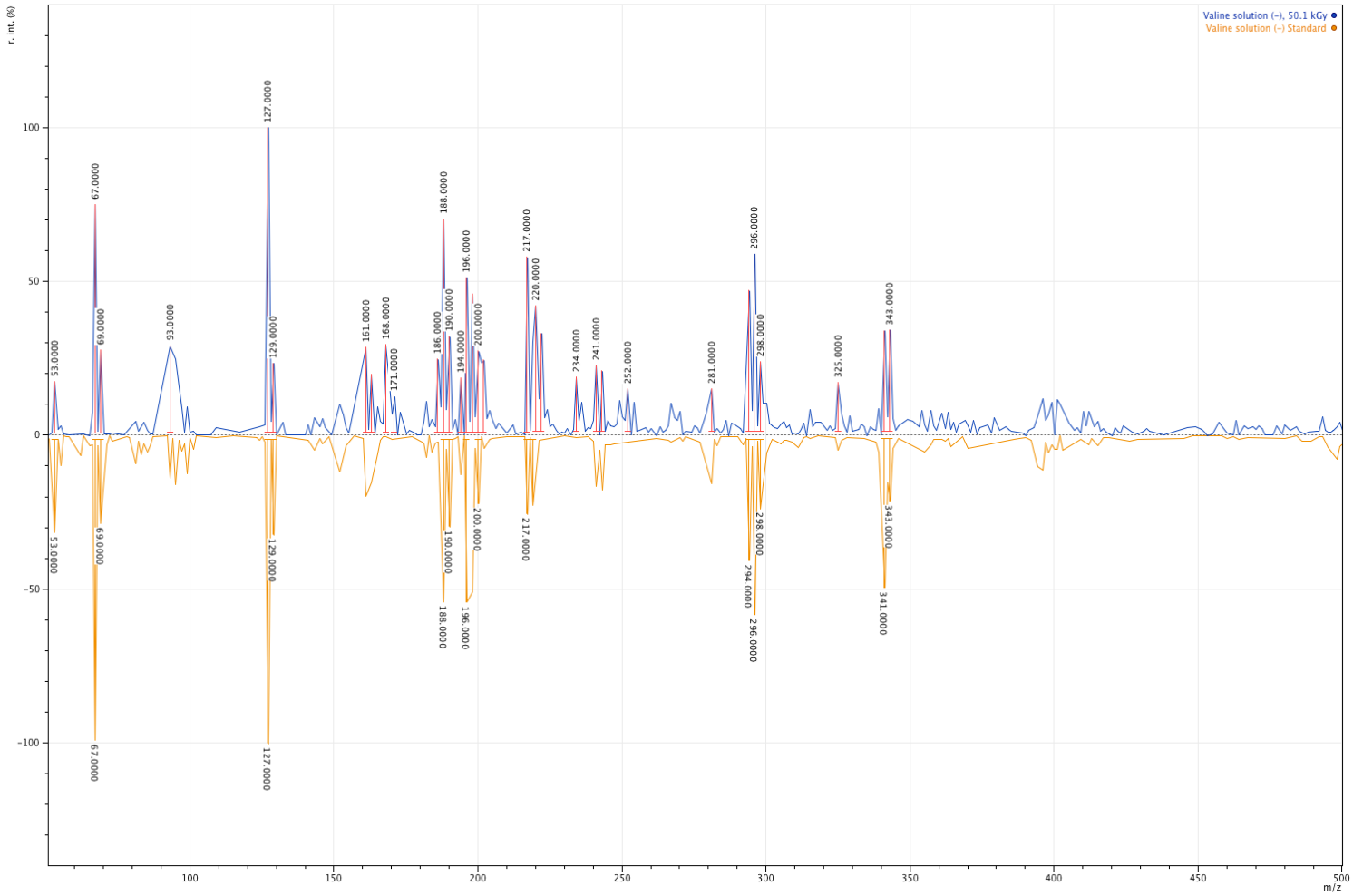

Figure A.80. ESI-MS spectrum of valine in aqueous solution for control and irradiated 50kGy samples: negative mode

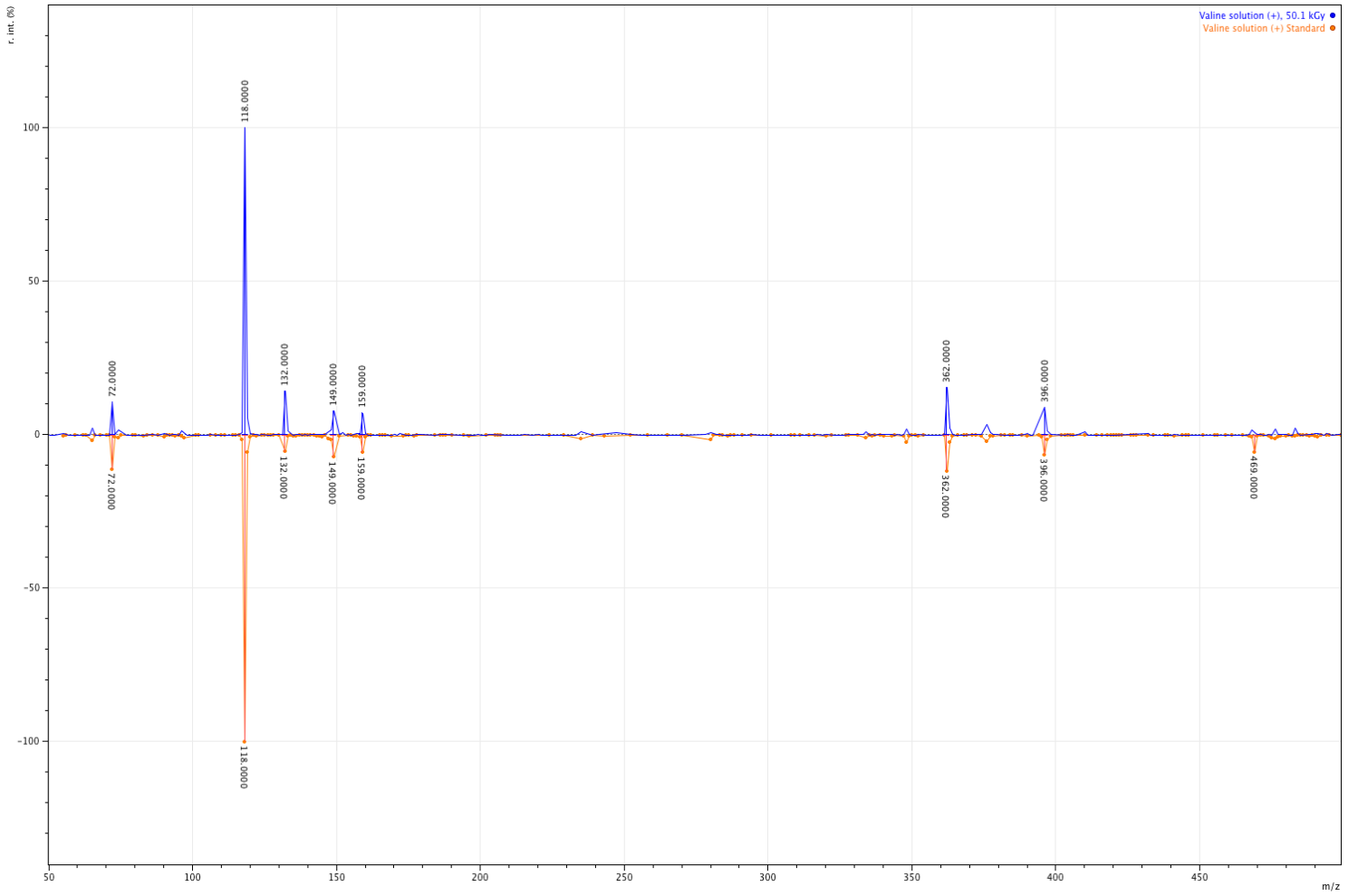

Figure A.81. ESI-MS spectrum of valine in aqueous solution for control and irradiated 50kGy samples: positive mode